Englacial stratigraphy, debris entrainment and ice sheet stability of Horseshoe Valley, West Antarctica

Kate Winter

Ph. D.

2016

Englacial stratigraphy, debris entrainment and ice sheet stability of Horseshoe Valley, West Antarctica

Kate Winter

A thesis submitted in partial fulfilment of the requirements of the University of Northumbria at Newcastle for the degree of Doctor of Philosophy

Research undertaken in the Faculty of Engineering and the Environment

October 2016

ABSTRACT

Despite the importance of ice streaming to the evaluation of West Antarctic Ice Sheet (WAIS) stability, we know little about mid-to long term changes in grounding line migration, ice streaming and ice accumulation in the upper Institute Ice Stream (IIS) catchment. In this thesis ground penetrating radar (GPR) and airborne radio-echo sounding (RES) methods have been employed to investigate the subglacial topography, internal stratigraphy and Holocene flow regime of the upper IIS catchment, in and around Horseshoe Valley. High resolution step-and-collect mode GPR was employed to assess the continuity of a Blue Ice Area (BIA) horizontal ice core climate record at Patriot Hills, where analysis has revealed two unconformities in the otherwise conformable 30,000 year climate sequence. By combining these data with airborne RES returns and pre-existing ice sheet models it is suggested that these unconformities represent periods of erosion, occurring as the former ice surface was scoured by katabatic winds in front of Liberty and Mable Hills. *Snow_Blow* simulations suggest that katabatic winds have scoured the leeward slopes of these mountain ranges for over 10,000 years. This temporal stability can account for the large volume of BI moraine deposits in Horseshoe Valley, where compressive BI flows promote glacial erosion and near-surface debris entrainment through freeze-on processes at the ice/bed interface and compressive thrust faulting. By investigating thicker ice flows in the upper IIS catchment and the Evans Ice Stream, this thesis has also analysed debris entrainment mechanisms at depth, where clasts are incorporated into the ice flow by englacial stratigraphic folding and shearing at the glacial thermal boundary, governed by spatial and temporal changes in ice flow, ice temperature and sediment availability. Mid-to long term changes in ice flow in the wider IIS catchment have been investigated from airborne RES transects, revealing internal layer buckling, and therefore former enhanced ice-sheet flow in three distinct tributaries of the IIS. Buckled ice layers throughout the slow flowing ice in the Independence Trough and the fast-flowing ice in the Ellsworth Trough suggest that enhanced ice flow through these topographically confined regions was the source of ice streaming and ice-flow reconfiguration during the mid-to-late Holocene. Although buckled layers also exist within the slow-flowing ice of Horseshoe Valley, a thicker sequence of surface-conformable layers in the upper ice column suggests slowdown more than 4000 years ago, indicating that enhanced flow switch off here cannot be attributed to late-Holocene ice flow reorganisation. The dynamic nature of ice flow in the IIS and its tributaries suggests that ice stream switching and mass change may have been regular during the Holocene, and that these changes may characterise the decline of the WAIS in this area. These results have important implications for our understanding of ice-sheet dynamics and the response of the ice sheet to climate change and provides explanations for fluctuations in debris entrainment and transportation processes in Antarctica.

TABLE OF CONTENTS

List of figures VII
List of Tables X
Abbreviations XI
Acknowledgements XIII
Declaration XIV

Section I: Introduction, Background and Methodological approach

Chapter 1
INTRODUCTION AND BACKGROUND 1
1.1 Introduction and project rationale 1
1.2 Research aims and objectives 2
1.3 Thesis structure 6

Chapter 2
ICE FLOW AND ICE SHEET STABILITY 7
2.1 Introduction 7
2.2 Ice Sheets 7
2.3 Antarctic Ice Sheet 10
2.4 Stability of the West Antarctic Ice Sheet 10
2.5 Ice Sheet flow 15
2.5.1 Internal deformation 15
2.5.2 Basal sliding 19
2.5.3 Bed deformation 19
2.5.4 Flow velocity 21
2.5.5 Compressive and extensional flow 21
2.5.6 Ice flow in Blue Ice Areas 23
2.5.7 Flow instability - surging glaciers 27
2.6 Ice Streaming 29
2.6.1 Topographic focussing 31
2.6.2 Subglacial till deformation 31
2.6.3 Basal hydrology 32
2.7 Debris in the glacial system 37
2.7.1 Debris sources 38

2.7.2 Debris entrainment mechanisms 38
2.7.3 Controls on debris entrainment 42
2.7.4 Debris transport through the glacial system 43
2.7.5 Significance of debris in the glacial system 46
2.8 Detecting past and present ice flow regimes 48
2.8.1 Detecting basal features 51
2.8.2 Analysing internal stratigraphy 52
2.9 Summary 54

Chapter 3
STUDY SITE 56
3.1 Institute Ice Stream 56
3.2 Ellsworth Mountains 58
3.2.1 Glaciological history of the Ellsworth Mountains 58
3.3 Ice flows in and around the Heritage Range 62
3.4 Horseshoe Valley 64
3.5 Marble, Independence and Patriot Hills 64
3.6 Blue Ice Areas in and around Horseshoe Valley 66
3.6.1 Patriot Hills Blue Ice Area 67
3.6.2 Other Blue Ice Areas in Horseshoe Valley 70
3.7 Summary 73

Chapter 4
METHODOLOGY 76
4.1 Introduction to ice penetrating radar 76
4.2 Ground penetrating radar 79
4.2.1 GPR data collection 79
4.2.2 Common-offset step-and-collect mode GPR 79
4.2.3 Continuous common-offset survey mode GPR 82
4.2.4 Post-processing of ground penetrating radar data 82
4.3 Radio-echo sounding 85
4.3.1 RES data collection 86
4.3.2 Post-processing of RES data 88
4.4 Analysis of radar-detected internal layering 88
4.5 Surface velocity data 92
4.6 Summary 93

Section II: Results and interpretations

Chapter 5

GROUND PENETRATING RADAR 94

5.1 Introduction 94

5.2 Results 96

5.2.1 Ground penetrating radar 96

5.2.2 Ice-sheet model simulations 105

5.2.3 Internal Layer Continuity Index plots 105

5.3 Discussion 108

5.4 Summary 111

Chapter 6

RADIO-ECHO SOUNDING 112

6.1 Introduction 112

6.2 Results 114

6.2.1 Basal topography discrepancies 114

6.2.2 Basal topography of the upper Institute Ice Stream Catchment 119

6.2.3 Internal stratigraphy 124

6.2.4 Surface velocity and surface features 132

6.3 Discussion 133

6.3.1 Current configuration of the Institute Ice Stream and its tributaries 133

6.3.2 Evidence for former enhanced ice flow 135

6.3.3 Evidence for ice flow reorganisation 135

6.3.4 Former ice-sheet configuration, with respect to the Bungenstock Ice Rise 136

6.4 Summary 139

Chapter 7

RADAR DETECTED ENGLACIAL DEBRIS 140

7.1 Introduction 140

7.2 Results 141

7.2.1 Airborne radio-echo sounding of Horseshoe Valley 141

7.2.2 Ground penetrating radar surveys of Horseshoe Valley 148

7.2.3 Other geophysical surveys 152

7.3 Interpretation 155

7.3.1 Englacial reflectors 155

7.3.2 Approximating englacial debris in and around Horseshoe Valley 157

7.4 Discussion 160
7.4.1 Near-surface debris entrainment 160
7.4.2 Debris entrainment at depth 163
7.4.3 Debris transport 164
7.5 Summary 167

Chapter 8
SNOW DRIFT MODELLING FOR BLUE ICE AREAS 169
8.1 Introduction 169
8.2 Methodology 173
8.2.1 *Snow_Blow* model specifications 173
8.2.2 Digital elevation model selection 177
8.2.3 Site specific inputs 181
8.3 Results 181
8.3.1 Model validation 181
8.3.2 Changing prevailing wind direction 184
8.3.3 Historic ice surface elevation 185
8.4 Discussion 191
8.4.1 Model validation 191
8.4.2 Changing meteorological conditions 192
8.4.3 Past snow drift conditions 193
8.5 Summary 196

Section III: Discussion and Conclusions

Chapter 9
DISCUSSION 198
9.1 Introduction 198
9.2 Historic ice flow conditions in and around Horseseshoe Valley 198
9.3 Stability of the upper Institute Ice Stream catchment 202
9.4 Significance of englacial debris detection 204
9.5 Reviewing the *Snow_Blow* model 206
9.5.1 Advantages of the *Snow_Blow* model 206
9.5.2 Disadvantages of the *Snow_Blow* model 208
9.5.3 Considerations for fututre investigations 208
9.6 Summary 209

Chapter 10

CONCLUSIONS 210
10.1 Introduction 210
10.2 Main findings 210
10.3 Reviewing objectives introduced in Chapter 1 211
10.4 Ice flow and ice sheet stability in and around Horseshoe Valley 214
10.5 Limitations of this research 216
10.6 Suggestions for further work 217

REFERENCES 219
APPENDICES 240

List of Figures

Chapter 2 – Ice flow and ice sheet stability

Figure 2.1 Interaction of ice sheets with the climate system and ocean circulation 8
Figure 2.2 Global mean temperature graph 9
Figure 2.3 Map of Antarctica 11
Figure 2.4 Collapse of the West Antarctic Ice Sheet 12
Figure 2.5 Changes in Antarctic ice shelf thickness between 2003-2008 14
Figure 2.6 Elevation change rate of the Antarctic Ice Sheet between 1993-2003 16
Figure 2.7 Schematic diagram of glacier flow 17
Figure 2.8 Velocity distribution within a glacier 18
Figure 2.9 Driving and resisting stresses operating on a block of ice 22
Figure 2.10 Compressive and extending flow in glaciers 24
Figure 2.11 Schematic representation of a closed type Antarctic Blue Ice Area 25
Figure 2.12 Location of Antarctic Blue Ice Areas 26
Figure 2.13 An example of surge events from Búarjökull Glacier, Iceland 28
Figure 2.14 Ice streams in Antarctica 30
Figure 2.15 Schematic ice sheet hydrology 33
Figure 2.16 Map of subglacial lakes in Antarctica 36
Figure 2.17 Mechanisms of debris entrainment in ice sheets 39
Figure 2.18 Englacial layer folding terminology 41
Figure 2.19 Influence of the basal thermal regime on processes of glacial erosion 44
Figure 2.20 Debris transport pathwats through a typical valley glacier 45
Figure 2.21 A numerical model of landform development by glacial erosion 49
Figure 2.22 Methods of radar acquisition over ice 50
Figure 2.23 Ice sheet change in the Institute and Möller Ice Streams 53

Chapter 3 – Study site

Figure 3.1 MODIS and LIMA mosaic of Antarctica 57
Figure 3.2 Map of the Sentinel and Heritage Range in the Ellsworth Mountains 59
Figure 3.3 A reconstruction of ice sheet configurations surrounding Marble Hills 61
Figure 3.4 Satellite imagery, flow speed and bed elevation of the Institute Ice Stream 63
Figure 3.5 Horseshoe Glacier field site 65
Figure 3.6 Patriot Hills Blue Ice Area extent between 1996 and 2008 68
Figure 3.7 Photograph of Patriot Hills Blue Ice Area 69
Figure 3.8 Schematic transect of moraine and debris bands in front of Patriot Hills 71

Figure 3.9 Change detection mapping of blue ice moraines in front of Patriot Hills 72
Figure 3.10 Blue Ice moraine sequences in front of Independence Hills 74

Chapter 4 - Methodology

Figure 4.1 Schematic GPR transect 77
Figure 4.2 GPR collection in Horseshoe Valley 81
Figure 4.3 Flow diagram detailing the processing of ground penetrating radar data..... 84
Figure 4.4 Integration of ice penetrating radar onto long-range aircraft..... 87
Figure 4.5 Comparisons between various airborne RES processing steps 89
Figure 4.6 Ice penetrating radar internal reflection terminology 91

Chapter 5 – Ground penetrating radar

Figure 5.1 Location of GPR transects in Horseshoe Valley 95
Figure 5.2 Three-dimensional transect along Patriot Hills Blue Ice Area 97
Figure 5.3 GPR transect A 98
Figure 5.4 Visual comparisons between GPR returns and the deuterium isotope record..... 100
Figure 5.5 Snow-mobile towed GPR grid..... 101
Figure 5.6 Snow-mobile towed GPR cross lines Y1-Y4 102
Figure 5.7 Snow-mobile towed GPR cross lines Y5-Y8 103
Figure 5.8 Simulated regional ice flux from Parallel Ice-Sheet Model simulations 106
Figure 5.9 Internal Layer Continuity Index plots across Horseshoe Valley 107
Figure 5.10 Inferred ice flow path from Horseshoe Valley head to Patriot Hills 110

Chapter 6 – Radio-echo sounding

Figure 6.1 Location of airborne RES transects 113
Figure 6.2 Site map and airborne RES flight lines..... 115
Figure 6.3 RES flight line across Horseshoe Valley and Patriot Hills..... 116
Figure 6.4 RES transect across Patriot and Independence Hills 117
Figure 6.5 Estimated uncertainty form the bed elevation grid published by Bedmap2 118
Figure 6.6 RES cross section of Horseshoe Valley Trough..... 120
Figure 6.7 RES cross section of Independence and Ellsworth Troughs 121
Figure 6.8 Radio-echo sounding of the Pirrit Lowlands..... 123
Figure 6.9 Internal features in radargrams 125
Figure 6.10 Three-dimensional schematic of Independence and Ellsworth Troughs 126
Figure 6.11 Three-dimensional schematic of all troughs..... 127
Figure 6.12 Full depth Internal Layer Continuity Index plots 129
Figure 6.13 Internal Layer Continuity Index plots partitioned by depth ranges 130

Figure 6.14 Schematic model of ice sheet change 138

Chapter 7 – Radar detected englacial debris

Figure 7.1 Geophysical transect lines examined in this chapter 142
Figure 7.2 Englacial reflectors in Horseshoe Valley 143
Figure 7.3 Englacial reflectors in front of Patriot Hills 144
Figure 7.4 Airborne RES of distinct englacial features 145
Figure 7.5 Detailed investigrations of englacial reflector R5 in 2D radargrams 147
Figure 7.6 GPR transects across Patriot Hills main embayment..... 149
Figure 7.7 GPR transect P1, collected in front of Patriot Hills main embayment 150
Figure 7.8 GPR line IH3, surveyed across Independence Hills moraine..... 151
Figure 7.9 Ground RES transect line A1, surveyed across Horseshoe Valley..... 153
Figure 7.10 Ground RES profile A2, collected in front of Patriot Hills 154
Figure 7.11 Airborne RES of the Evans Ice Stream 156
Figure 7.12 Airborne RES transect annotated to show debris reflector bands 158
Figure 7.13 Possible debris entrainment mechanisms in ice sheets..... 162
Figure 7.14 Investigations of debris entrainment at the glacial thermal boundary 165
Figure 7.15 Extension and compression of ice layers and associated debris..... 166

Chapter 8 – Snow drift modelling for Blue Ice Areas

Figure 8.1 Surface airflow over Antarctica..... 170
Figure 8.2 Antarctic snow accumulation 172
Figure 8.3 Blue Ice Areas in Horseshoe Valley..... 174
Figure 8.4 Schematic diagram to show modified wind deflection for individual cells..... 175
Figure 8.5 Comparisons between three widely-used multiple-flow routing methods 178
Figure 8.6 Methods to remove peaks in a 30 m resolution ASTER DEM..... 179
Figure 8.7 Comparisions between an ASTER and SPOT DEM of Horseshoe Valley 180
Figure 8.8 Iterative path applied to the *Snow_Blow* model 182
Figure 8.9 *Snow-Blow* model outputs from SPOT DEM..... 183
Figure 8.10 Wind-driven snow erosion simulations 186
Figure 8.11 Original and modified SPOT DEMs..... 187
Figure 8.12 Quantified changes in snow drift conditions from present day 189
Figure 8.13 Quantified changes in snow drift conditions – stepped changes 190
Figure 8.14 Schematic illustration of BIA decline during increasing ice thickness 194

Chapter 9 - Discussion

Figure 9.1 Known sources and spatial variability of iron delivery to the Southern Ocean .. 205
Figure 9.2 Detecting sediments from continental source to Southern Ocean delivery 207

LIST OF TABLES

Chapter 2 – Ice flow and ice sheet stability

Table 2.1 Boulder shape, character and texture as a function of glacial transport..... 47

Chapter 4 – Methodology

Table 4.1 Specifications of Northumbria Universities GPR system..... 80
Table 4.2 Specifications of the British Antarctic Surveys RES system..... 86

Chapter 7 – Radar detected englacial debris

Table 7.1 Englacial debris calculations..... 159

Chapter 9 – Discussion

Table 9.1 A summary of ice flow conditions in and around Horseshoe Valley 199

ABREVIATIONS

a.s.l.	Above Sea Level
ASTER	Advanced Spaceborne Thermal Emission and Reflection Radiometer
AWS	Automatic Weather Station
BIA	Blue Ice Area
BioFe	Bio-available Iron
BIR	Bungenstock Ice Rise
DEM	Digital Elevation Model
DGPS	Differential Global Positioning System
EAIS	East Antarctic Ice Sheet
FRIS	Filchner-Ronne Ice Shelf
GPR	Ground Penetrating Radar
GPS	Global Positioning System
Hz	Hertz
IIS	Institute Ice Stream
ILCI	Internal Layer Continuity Index
ka	Unit of time equal to one thousand years
LIMA	Landsat Image Mosaic of Antarctica
LGM	Last Glacial Maximum
MHz	One million hertz
MIS	Möller Ice Stream
MODIS	Moderate Resolution Imaging Spectroradiometer

PASIN	Polarimetric-radar Airborne Science Instrument
PISM	Parallel Ice Sheet Model
RADARSAT	RADAR SATellite
RES	Radio-Echo Sounding
RMS	Root-Mean Square
SAR	Synthetic Aperture Radar
SPOT	Satellite Pour l'Obeservation de la Terre
TWTT	Two-Way Travel Time
WAIS	West Antarctic Ice Sheet
WGS84	1984 World Geodetic System

ACKNOWLEDGEMENTS

The front page of this thesis only shows one name, but many people have contributed to this work, through their inspiration, discussion and encouragement.

First of all, I would like to express my appreciation and thanks to my principal supervisor, Prof. John Woodward, for making this PhD and associated field work possible. I am extremely grateful for all of his advice, knowledge and encouragement. I would also like to thank my other supervisors; Dr. Stuart Dunning, Dr. Leanne Wake and Dr. Neil Ross (Newcastle University) for all of their support and guidance throughout the past three years.

I am indebted to Northumbria University for supporting my research through the Research Development Fund and a Faculty of Engineering and Environment fellowship. My field trip to Antarctica was an incredible and unforgettable experience, and for that I wish to thank the British Antarctic Survey for their logistical support and the field support provided by Scott Webster and Phil Stevens. I would also like to acknowledge the financial support from the UK Natural Environment Research Council who provided standard grants NE/I027576/1, NE/I025840/1, NE/I024194/1 and NE/I025263/1, which made this field work possible.

During my PhD I have been fortunate to be part of a large research group. I am grateful to have worked with Prof. David Sugden, Dr. Andrew Hein, Dr. Shasta Marrero and Dr. Matthew Westoby, who have provided valuable support and discussions. I would also like to thank Prof. Martin Siegert and Dr. Neil Ross for allowing me to analyse airborne geophysical data collected during a NERC Antarctic Funding Initiative grant (NE/G013071/1), which was pre-processed by Dr. Hugh Corr of the British Antarctic Survey. Thanks are also due to Prof. Chris Turney and Dr. Chris Fogwill who provided climate records across Patriot Hills Blue Ice Area, Dr. Robert Bingham who created Internal Layer Continuity Index plots, Dr. Nichols Golledge who provided PISM perturbations of Institute Ice Sream, Dr. Andrés Rivera who supplied ground radio-echo soundings of Horseshoe Valley and Dr. David Ashmore who allowed me to examine a radargram across the Evans Ice Stream. Investigations of katabatic wind scour and BIAs were only made possible with the support of Dr. Anne Le Brocq and Dr. Stephanie Mills.

Lastly, I must say a heartfelt thank you to all of my family. I am especially grateful for the love and encouragement from my parents, grandparents and husband, who have always believed in me and encouraged me to follow my dream of going to Antarctica and studying all things ice related. Particular thanks must also go to my mum who proof read this thesis.

DECLARATION

I declare that the work contained in this thesis has not been submitted for any other award and that it is all my own work. I also confirm that this work fully acknowledges opinions, ideas and contributions from the work of others.

Any ethical clearance for the research presented in this thesis has been approved. Approval has been sought and granted by the Faculty Ethics Committee on the 1st December 2014.

I declare that the word count of this thesis is 38,861 words

Name: Kate Winter

Signature: 

Date: 10.02.2017

CHAPTER 1

Introduction and background

1.1 Introduction and project rationale

The West Antarctic Ice sheet (WAIS) is a marine based ice sheet with its centre situated on bedrock well below sea level, where the deepest known ice rests up to 2555 m below eustatic sea level [*Fretwell et al*., 2013], which introduces potential instabilities that could lead to its rapid collapse [*Weertman*, 1974; *Mercer*, 1978]. The risk is that the volume of ice held in West Antarctica, if lost, would be sufficient to raise eustatic sea level by 5 m if all the ice disappeared or by 3.3 m if ice caps remained on the main mountain blocks [*Bamber et al*., 2009; *Hein et al.*, 2016a]. Draining a combined area of 218,000 km^2 [*Joughin and Bamber*, 2005] (~11% of the WAIS total), the Institute Ice Stream (IIS) and Möller Ice Stream (MIS) are major outlets of the WAIS, where ice and entrained sediment accumulations drain from the WAIS dome into the Filchner-Ronne Ice Shelf (FRIS) and ultimately, the Weddell Sea. Both IIS and MIS have steep reverse bed slopes (where the bed slopes downwards inland of the grounding line) and areas of low basal roughness which could make them susceptible to unstable grounding line retreat [*Ross et al*., 2012; *Wright et al*., 2014]. However, despite IIS being critical to our evaluation of WAIS stability and the likelihood of future sea level change from ice sheet loss [*Bentley et al*., 2010], dynamic former changes in ice flow within the ice stream's upper catchment area are poorly constrained.

Although recent advances in cosmogenic nuclide analysis [*Fogwill et al*., 2012; *Hein et al*., 2016a, 2016b], horizontal climate record interpretations [*Turney et al*., 2013] and ice sheet model simulations [*Golledge at al*., 2013] have helped to improve our understanding of past ice sheet thickness and climate in the Weddell Sea sector of West Antarctica many assumptions have been made. These include Holocene ice flow trajectories, debris availability and entrainment, meteorological conditions (including the frequency of katabatic winds and snow accumulation) and the stability of local Blue Ice Areas (BIAs). Until geophysical data have been collected, analysed and modelled these climate record interpretations and model simulations

will remain un-justified. Combined with fears of ice sheet instability, it is now more important than ever to investigate the past and present behaviour of the WAIS, particularly in the upper IIS catchment.

In order to appreciate past and present ice sheet conditions it is necessary to determine basal topography, ice sheet thickness, flow direction and extent [*Campbell et al.*, 2013]. This can be achieved through the analysis of geophysical data, where radargrams from ice penetrating radar surveys can reveal information about the bed topography, ice sheet surface and internal stratigraphy of the ice at a variety of scales. As recent airborne ice penetrating radar surveys have focussed on the main trunk of the IIS and MIS (near the FRIS grounding line), where investigations by *Siegert et al*. [2013] and *Bingham et al*. [2015] have recorded the basal topography and internal stratigraphy along the main arteries of the ice streams, where Holocene ice flow reconfigurations were recognised near the local FRIS grounding line, this thesis will investigate the englacial stratigraphy, debris entrainment processes and ice sheet stability of ice flowing in and around the Ellsworth Mountains, in the upper IIS catchment. Findings will be compared to local climate records and cosmogenic nuclide derived ice sheet retreat dates to determine the timings of any changes, whilst numerical models will be consulted to determine the stability of the ice sheet in and around Horseshoe Valley. Ice penetrating radar will also be used to assess the availability of debris and debris entrainment mechanisms in and around the Ellsworth Mountains. This work will provide the first detailed account of volume fluxes and debris entrainment processes beneath the thick Antarctic ice sheet.

1.2 Research aims and objectives

The overall aim of this PhD project is to:

Investigate the past and present behaviour of the West Antarctic Ice Sheet in and around Horseshoe Valley and the upper Institute Ice Stream catchment in order to determine changes in ice flow and debris entrainment due to grounding line migration, ice streaming and ice accumulation under a changing climate.

In order to fulfil this aim, a number of research objectives have been identified.

Objective 1: **Analyse englacial stratigraphy within the Blue Ice Area at Patriot Hills to determine historic changes in ice flow and/or accumulation**

High precision GPR collected by the Northumbria PulseEKKO system in 2013/2014 will be used to determine the englacial stratigraphy within the BIA at Patriot Hills. Data will be processed in ReflexW (version 6.1.1) and analysed in MATLAB (R2013a) and Opendtect (2015) to highlight prominent internal GPR reflectors within the BIA in both 2D and 3D. The imagery will be analysed systematically to separate conformable internal layering (indicative of stable firn/ice accumulation) to discontinuous englacial layers (which reveal instability in the accumulation or flow). By combining a variety of datasets from the Heritage Range (e.g. ice elevation data [*Fretwell et al*., 2013], ice velocity measurements [*Rignot et al*., 2011], climate records [*Turney et al*., 2013], Parallel Ice Sheet model simulations [*Fogwill et al*., 2014] and cosmogenic nuclide derived ice thickness measurements [*Hein et al*., 2016a, 2016b]) with the GPR record it will be possible to establish the cause of any changes in ice flow during the Holocene. Results will also be used to improve high precision climate reconstructions in the area, deduced from the analysis of surface deuterium isotope samples collected along Patriot Hills BIA by *Turney et al*. [2013] in 2012.

Objective 2: **Determine the internal structure of the West Antarctic Ice Sheet in the upper Institute Ice Stream catchment to establish historic changes in regional ice streaming**

Airborne RES data collected in and around the Ellsworth Mountains by Dr. Neil Ross (Newcastle University) and collaborators during an aero geophysical investigation of IIS and MIS in 2011/2012 will be processed in ReflexW and analysed in 2D and 3D (in MATLAB and Opendtect respectively) to determine the internal structure of the WAIS in and around Horseshoe Valley. Published RES radargrams from the Weddell Sea sector of West Antarctica (e.g. *Siegert et al*. [2013]) have already revealed strong bed horizons and complex internal layering in this region, where a variety of internal and subglacial features have been identified.

These features include conformable layering, discontinuities, folding, fracturing and crevassing. Analysis of similar internal features in the airborne RES dataset will allow Holocene flow regimes in the upper IIS to be determined. These findings will indicate whether the Horseshoe Valley Trough, the Independence Trough and the Ellsworth Trough were important tributaries of the IIS, both in its current configuration and in the Holocene configurations hypothesised by *Siegert et al*. [2013]. These results are critical for the ice sheet modelling community, where findings will help to determine the historic and future stability of the WAIS in the Weddell Sea sector.

***Objective 3*: Investigate debris entrainment mechanisms in the Weddell Sea sector of the West Antarctic Ice Sheet**

In order to constrain the location and form of debris bands in the ice flows surrounding Horseshoe Valley in the upper IIS, strong and often steeply dipping englacial features within previously analysed GPR and RES transects (collected to fulfil objective 1 and 2) will be mapped and analysed in 2D and 3D using ReflexW and Opendtect respectively. Controls on sediment availability and debris entrainment mechanisms in Antarctica will be considered before site specific processes are discussed. Comparisons will be made to wider ground RES surveys across Horseshoe Valley, supplied by Dr. Andrés Rivera (Centro de Estudios Científicos) as well as an airborne RES flight line across the Evans Ice Stream, supplied by Dr. David Ashmore (Aberystwyth University). By calculating approximate volumes of debris in the glacial system it will be possible to better understand erosive rates in Antarctica, landform development and the transport of debris from the continent to the Southern Ocean. Suggestions will be made regarding the significance of these findings in relation to ice streaming and ice sheet stability.

***Objective 4:* Model the transport of snow by wind in Horseshoe Valley and compile a sensitivity analysis to determine the conditions necessary to initiate and maintain Blue Ice Areas in front of the Patriot, Independence and Marble Hills**

Ross Purves' snow drift model which was recently coded as an ArcGIS (Python) script by Dr. Stephanie Mills at the University of Plymouth and Dr. Anne Le Brocq at the University of Exeter for paleoglaciological reconstructions will be used to improve the understanding of blue ice erosion and snow-drift accumulation in Horseshoe Valley. A 40 m resolution SPOT digital elevation model (DEM) will form the primary input, along with automatic weather station data from Patriot Hills and field observations. Results will be compared to satellite imagery to validate the *Snow_Blow* model. In order to establish how thick the ice needs to be to maintain katabatic wind flow (necessary for blue ice formation), ice elevation data will be altered in subsequent model runs. Ice sheet elevations will be provided by Dr. Andrew Hein from the University of Edinburgh, who used cosmogenic nuclide analysis to date the exposure ages a number of boulders at a variety of elevations along Patriot and Independence Hills. Deuterium isotope measurements from Dr. Chris Turney's (University of New South Wales) climate core will also be used to confine palaeo ice surfaces. These findings will define the current state of erosion and ice flow in front of Patriot and Independence Hills, enhance our understanding of former ice sheet conditions and improve optimal forecasts through sensitivity testing using precise ice sheet surfaces.

Achieving the objectives outlined above will allow the past and present behaviour of the WAIS in and around Horseshoe Valley and the upper IIS to be determined. This will fulfil the overall aim of this thesis. Each data set will first be considered separately, to identify ice flow processes operating at different scales, before the data sets are combined with ice velocity data, climate records, cosmogenic nuclide data and model simulations to determine the controls on ice flow and debris entrainment in and around Horseshoe Valley. This research will provide firm constrains to the scientific communities concerned with Antarctic ice sheet evolution, where results will be particularly relevant to the ice sheet modelling, climate and sea level communities.

1.3 Thesis structure

The structure of this thesis is summarised below:

SECTION I: Relevant background for the thesis will be summarised in Section 1. *Chapter 2* will review our current understanding of ice flow and ice sheet stability. *Chapter 3* will provide a detailed study site description of the Horseshoe Valley and the upper Institute Ice Stream Catchment in the Weddell Sea Sector of West Antarctica. *Chapter 4* will describe the methods used in this thesis, by introducing the relevant background theory for ice penetrating radar data collection and data processing as well as ice velocity data acquisition.

SECTION II: This section will present results and interpretations of data collected from the upper Institute Ice Stream catchment. *Chapter 5* will determine historical ice sheet flow in Horseshoe Valley by presenting results, interpretations and discussions from ground penetrating radar transects collected across Patriot Hills Blue Ice Area, while *Chapter 6* will present results and discussions from regional airborne radio-echo sounding of the upper Institute Ice Stream. Englacial debris recorded in ground penetrating radar and radio-echo sounding transects will be examined in *Chapter 7*, where debris sources in and around Horseshoe Valley will be discussed along with debris entrainment mechanisms in Antarctica. Simulations of katabatic wind flow and snow drift will then be presented in *Chapter 8*, in order to investigate the controls on Blue Ice Area formation and evolution.

SECTION III: This section will discuss the major findings of the study and will synthesise the interpretations discussed in section II. *Chapter 9* will provide a synthesis of the evolution of ice sheet flow in and around Horseshoe Valley whilst *Chapter 10* will summarise key findings and conclusions from the thesis, where suggestions for further work will also be made.

CHAPTER 2

Ice flow and ice sheet stability

This chapter will review the current understanding of ice flow and ice streaming in ice sheets. Potential instabilities in ice sheets, driven by internal and external forces will be discussed, along with techniques capable of detecting past and present ice sheet conditions.

2.1 Introduction

Large ice sheets form an integral part of the Earth's climate system [*Solomon et al*., 2007], where they exert a strong control over atmospheric circulation patterns [*Roe and Lindzen*, 2001], ocean overturning [*Hemming*, 2004] and global sea level (Figure 2.1). It is for this reason that recent, dramatic examples of mass loss from the Greenland [*Kahn et al., 2015*] and Antarctic Ice Sheets [*Shepherd et al., 2010; 2012*] have heightened concern for unprecedented and irreversible global change. Although this fear stemmed from measured atmospheric and oceanic warming, where subsequent climate simulations and predictive ice sheet models have heightened concerns for unprecedented change in the future [*Collins et al.*, 2013] (Figure 2.2), many of the observed mass-loss processes are not driven directly by ice surface melting, but instead they involve the flow of ice, and as such, this is the primary focus of this literature review.

2.2 Ice Sheets

Only two large, kilometres-thick continental ice sheets exist on Earth today; in Greenland and Antarctica, where they differ from smaller scale versions, termed ice caps, which can be found in the Canadian, Norwegian and Russian Arctic, as well as some small islands in the Southern Ocean, and much more abundant steeper mountain glaciers, where ice flow is controlled by bedrock topography. Ice sheets in Greenland and Antarctica are maintained by cold surface temperatures which are largely a function of their high latitude and elevation, which has allowed the ice sheets to sustain a net accumulation of snow at their centre for hundreds of annual

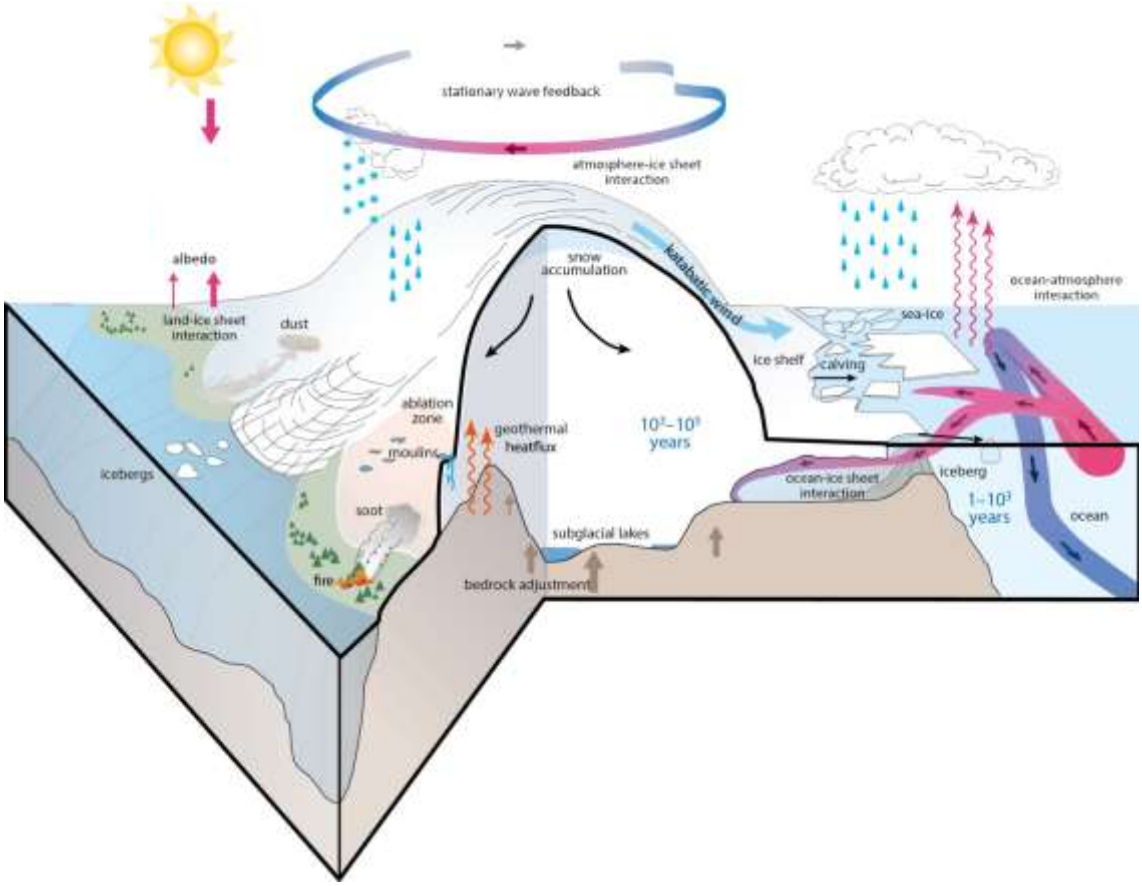

Figure 2.1. The interaction of ice sheets with the climate system and ocean circulation. This schematic figure was obtained from IPCC AR5 (Figure 1 in box 5.2) [*Masson-Delmotte et al*., 2013].

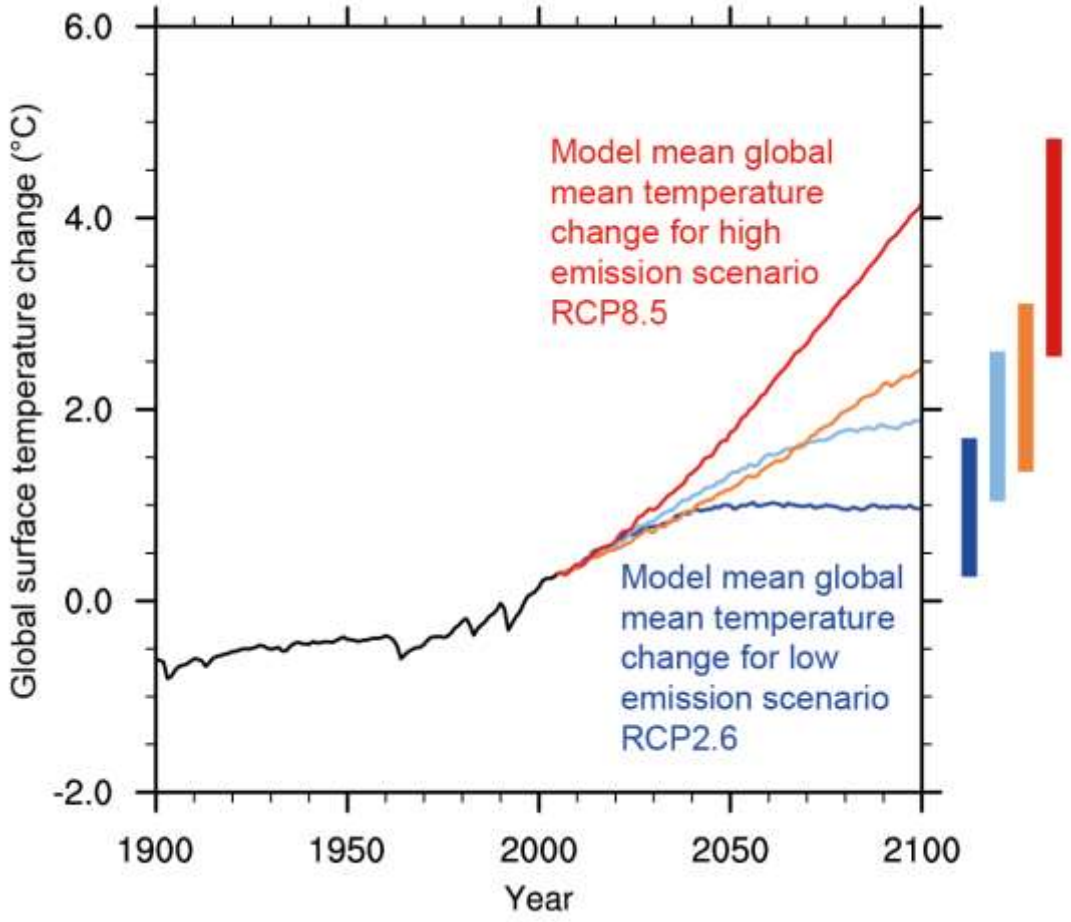

Figure 2.2. Global mean temperature change averaged across all Coupled Model Intercomparison Project Phase 5 (CMIP5) models (relative to 1986–2005) for the four Representative Concentration Pathway (RCP) scenarios: RCP2.6 (dark blue), RCP4.5 (light blue), RCP6.0 (orange) and RCP8.5 (red); 32, 42, 25 and 39 models were used respectively for these 4 scenarios. Likely ranges for global temperature change by the end of the 21st century are indicated by vertical bars. Note that these ranges apply to the difference between two 20-year means, 2081–2100 relative to 1986–2005, which accounts for the bars being centred at a smaller value than the end point of the annual trajectories. For the highest (RCP8.5) and lowest (RCP2.6) scenario, illustrative maps of surface temperature change at the end of the 21st century (2081–2100 relative to 1986–2005) are shown for two CMIP5 models. These models are chosen to show a rather broad range of response, but this particular set is not representative of any measure of model response uncertainty. This graph was obtained from IPCC AR5 (FAQ 12.1, Figure 1) [*Collins et al*., 2013].

climate cycles. Lower surface elevations and sometimes lower latitudes can lead to warmer surface temperatures near the ice-sheet margins, where mass loss may occur as a function of significant marginal melting (typical of the south-western Greenland Ice Sheet [*Fettweis et al*., 2011]) or ice-berg calving, when ice spreads to the continent margins and begins to float at the grounding line (characteristic of the Antarctic Ice Sheet).

2.3 Antarctic Ice Sheet

The Antarctic Ice Sheet (Figure 2.3) covers an area of ~13.5 million km^2 and contains a total ice volume of 25.4 million km^3 (including ice shelves) [*Benn and Evans*, 2010]. This makes the Antarctic Ice Sheet the largest freshwater ice mass on the globe, where *Bennett and Glasser* [2009] have estimated that it could store approximately 70% of the entire world's fresh water, which would contribute a change in eustatic sea level of ~57 m, should the ice sheet melt completely [*Lythe et al*., 2001]. It is for this reason that an understanding if ice-flow dynamics in Antarctica is urgently needed, as even a modest change in ice-sheet volume would impact sea level around the globe and increase freshwater flux to the oceans [*Lemke et al*., 2007].

The Antarctic Ice Sheet can be divided into two major ice sheets: the East Antarctic Ice Sheet (EAIS), which has a grounded ice volume of 21.7 million km^3 and the West Antarctic Ice Sheet (WAIS), which has a total grounded ice volume of 3 million km^3 [*Benn and Evans*, 2010] (Figure 2.3). The two ice sheets are divided by the Transantarctic Mountains (Figure 2.3). The EAIS rests on a large land mass, while the majority of the smaller WAIS is grounded below sea level, where ice flows into two large ice shelves (the Filchner-Ronne Ice Shelf and the Ross Ice Shelf) or through several smaller outlet glaciers.

2.4 Stability of the West Antarctic Ice Sheet

Potential instabilities in the WAIS were first proposed in the late 20th century by *Weertman* [1974] and *Mercer* [1978] (Figure 2.4), who recognised the urgent need to study and understand the stability of marine based ice sheets, particularly under a changing climate. These pioneering

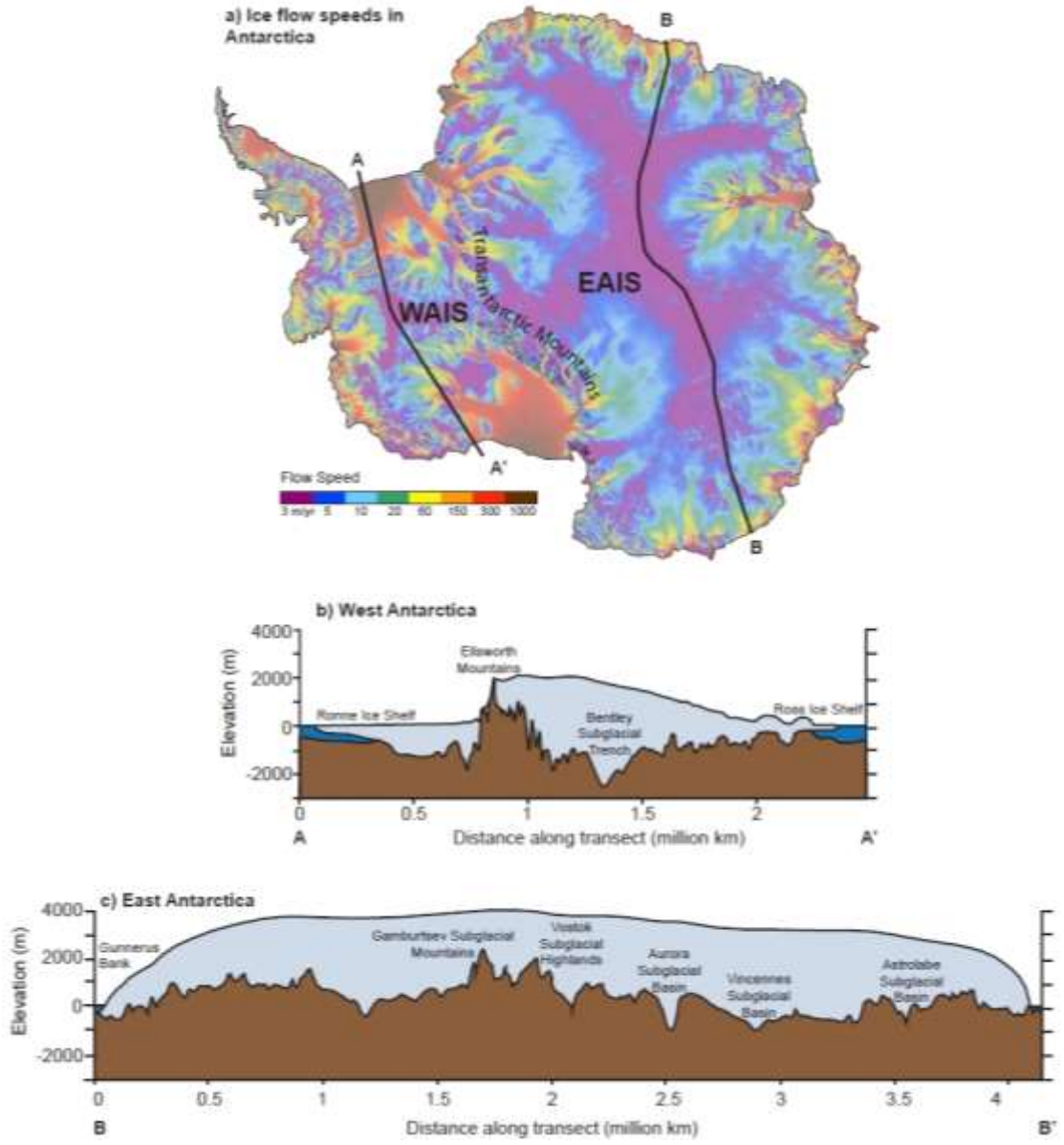

Figure 2.3. Map of Antarctica showing a) Surface velocities in Antarctica, generated from *Rignot et al*., [2011a], where the channelised structure of ice-stream flow is clearly visible in both the West Antarctic Ice Sheet (WAIS) and the East Antarctic Ice Sheet (EAIS), which are largely separated by the Transantarctic Mountains, b) Cross section through West Antarctica, as shown by the line A-A' in (a), where the ice sheet bed is mostly situated below sea level and c) Cross-section of the EAIS, from B-B', where the majority of the ice sheet rests on land above sea level.

Figure 2.4. A comparison of the area of the Antarctic Ice Sheet calculated to survive after a collapse of the West Antarctic Ice Sheet in studies by (A) *Mercer* [1978] and (B) *Bamber et al*. [2009], (from *Bamber et al*. [2009]).

studies proposed that the removal of floating ice shelves would result in a rapid and irreversible inland migration of the grounding line. It was hypothesised that such a retreat would encourage progressively thicker ice at the ice sheet margin, which would lead to higher ice mass loss and further grounding line retreat [*Rignot and Jacobs*, 2002; *Schoof*, 2007]. In addition, rising sea level would allow more ice at the margin of the ice sheet to float, producing instabilities in the ice shelf, which would cause the ice to flow more rapidly into the oceans.

The risk of this instability was quantified in the early 21st century when it was determined that the volume of ice held in the WAIS, if lost, would be sufficient to raise sea level by 5 m if all the ice disappeared, or by 3.3 m if icecaps remained on the main mountain blocks [*Lythe et al*., 2001; *Bindschadler*, 2006; *Bamber et al*., 2009]. Although entire ice sheet loss is thought to be a high risk, low probability event [*Bamber et al*., 2009] there is evidence that the WAIS was substantially larger than today [*Bentley et al*., 2010] and that the WAIS was smaller during past interglacials [*Hein et al*., 2016a]. It is also worth noting that several ice sheets of similar sizes, such as the North American Laurentide Ice Sheet (estimated volume of 18-35 million km^3 [*Fisher et al*., 1985; *Hughes et al*., 1981]) have completely disintegrated in the past.

As the last three decades on the Earth's surface have been successively warmer than any preceding decade since 1850, global climate change currently poses the greatest threat to ice sheet stability [*Collins*, 2013]. Although globally averaged land and ocean surface temperatures show a warming of 0.65°C – 1.06°C over the period 1880 to 2012, some areas like the Antarctic Peninsula have experienced even greater rapid regional warming, where temperatures have risen by nearly 3°C since 1951 [*Meredeth and King*, 2005]. Here, measured atmospheric and oceanic warming (Figure 2.5) has led to increased concern over the stability of high-latitude, ocean-terminating glaciers in Antarctica. This includes Pine Island glacier and Thwaites glacier which are situated on the East Pacific side of West Antarctica, where recent studies have suggested that full collapse of the main trunk of Pine Island glacier could occur in the next 100-200 years [*Gladstone et al*., 2012]. Unlike ice flows draining into the Weddell Sea or Ross Sea, Pine

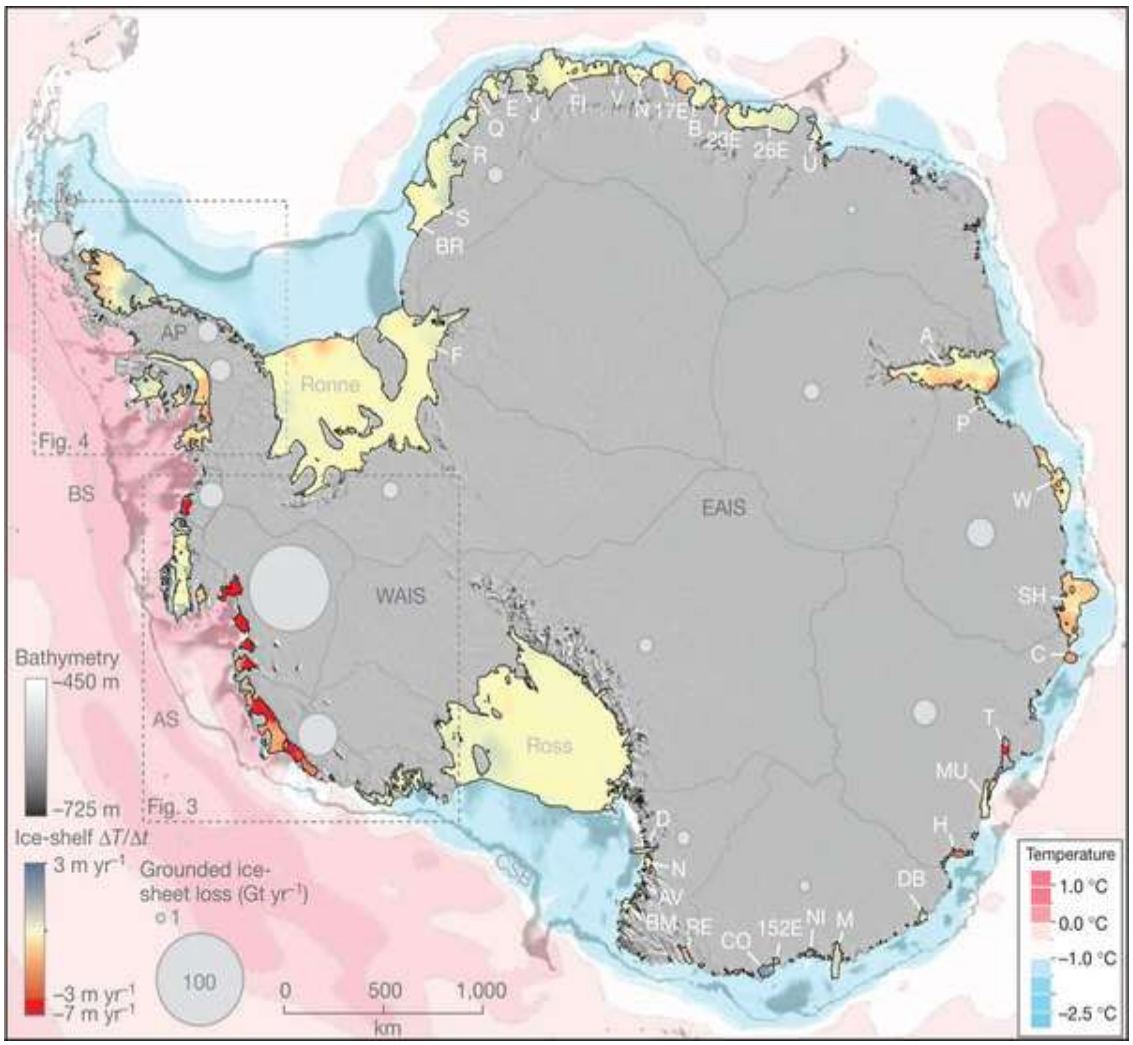

Figure 2.5. Antarctic ice shelf ice thickness change rate between 2003-2008 from *Pritchard et al*. [2012]. Average sea floor potential temperatures - acquired from the World Ocean Circulation Experiment Southern Ocean Atlas are also plotted. Grey circles show relative ice losses for ice-sheet drainage basins (outlined in grey) that lost mass between 1992 and 2006.

Island and Thwaites glaciers do not have large ice shelves to shield their grounding lines from external influences. Instead, these glaciers, which are currently the fastest flowing ice streams in West Antarctica, with grounding line speeds of nearly 4000 m yr^{-1} [*Joughin et al*., 2010] drain into much smaller ice shelves, which are only a few tens of kilometres wide. As the drainage basins of both ice streams overlie deep subglacial depressions with reverse bedrock slopes, these ice streams are thought to be the most vulnerable part of the WAIS to climate and sea level changes. Studies have already recorded thinning (Figure 2.6) [*Wingham et al.*, 2009] and grounding line retreat here [*Rignot et al.,* 2014] – both of which are believed to have occurred in response to increased ocean temperatures [*Shepherd et al*., 2004]. By investigating the flow of ice in areas vulnerable to change, it may be possible to predict how the ice sheet could evolve in the future, particularly under a changing climate.

2.5 Ice Sheet Flow

In large ice sheets snow and ice is transferred from the interior ice sheet to the ice sheet margins by ice flow, which can occur through plastic or brittle deformation (Figure 2.7). This is typically facilitated by deformation of the ice, basal sliding or deformation of the glacier bed. Under one or more of these processes, the ice can move through the landscape, delivering snow and ice to areas where ablation exceeds accumulation, and eventually to the ice sheet margins, where meltwater and icebergs can exit the system [*Benn and Evans*, 2010]. Due to the importance of each mechanism with respect to ice sheet flow, the processes of internal deformation, basal sliding, deformation of the glacial bed and ice flow velocity have been detailed below, and accounted for visually in Figure 2.8.

2.5.1 Internal deformation

Internal ice deformation is the most dominant ice flow process, occurring in virtually all moving ice when gravity and the weight of overlying firn and ice cause ice crystals at depth to move in response to stress. In most locations, the crystals orientate themselves in parallel layers which

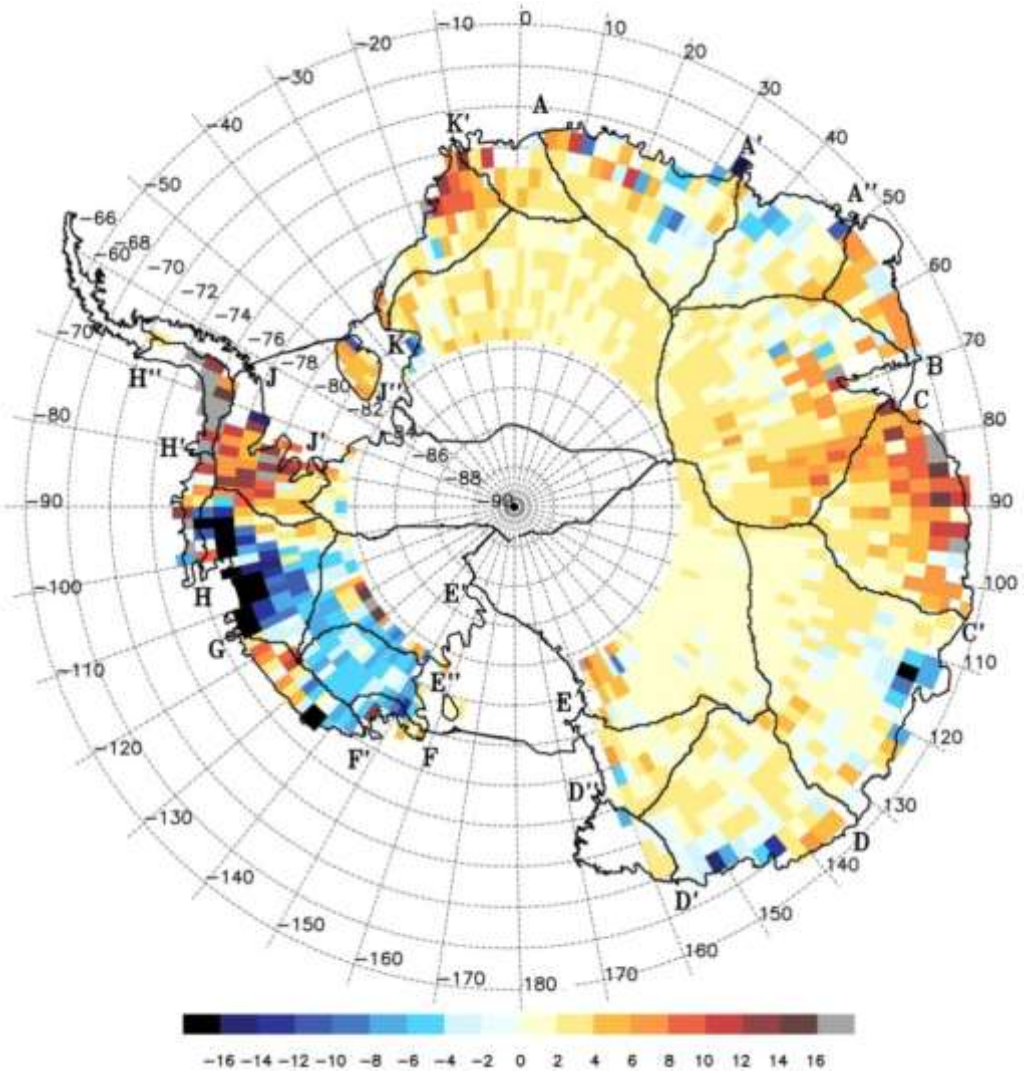

Figure 2.6. Elevation change rate (cm/year) from 1992 to 2003 for 8.5 x 10^6 km^2 of the grounded Antarctic Ice Sheet interior as measured by *Davis et al*. [2005].

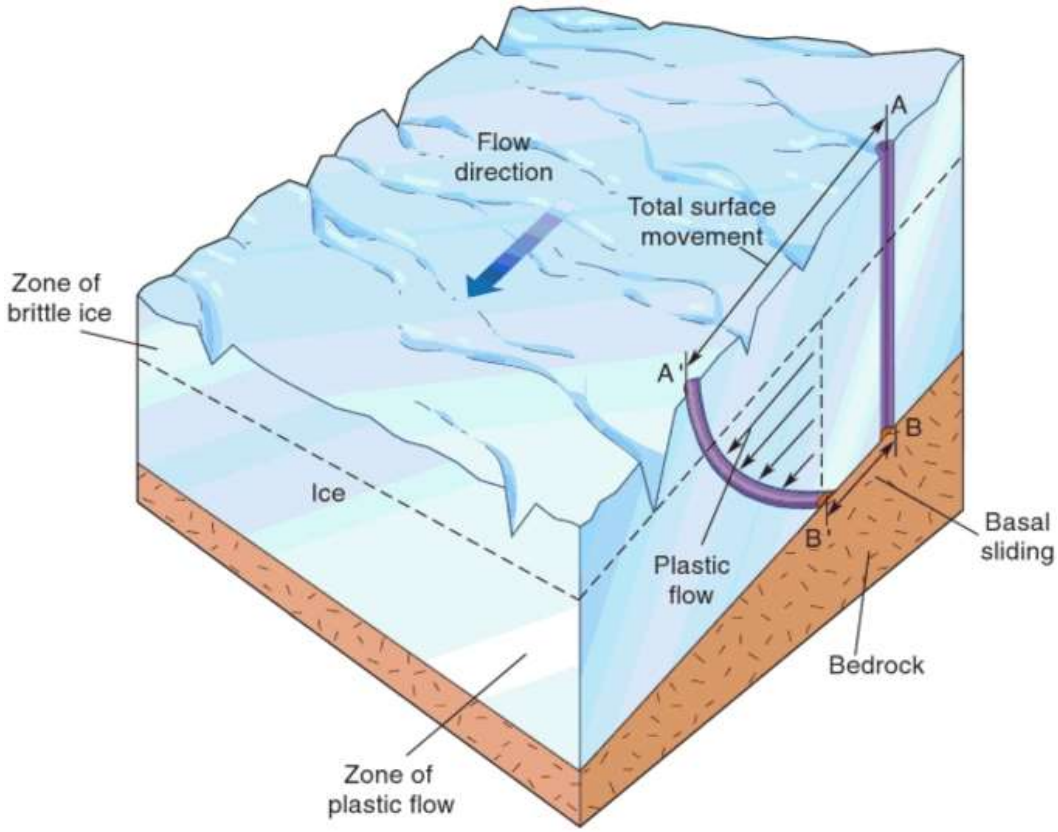

Figure 2.7. Schematic diagram of glacier flow from *Gabler et al*. [2009]. The weight of overlying snow and ice allows most movement to occur by plastic deformation, although basal sliding is possible if meltwater is available at the bed. The entire ice column moves at the same velocity during basal sliding (B-B') but velocity is greatest at the glacier's surface (A-A') when plastic flow dominates. This is a result of pressure; pressure is greater lower in the ice column but plastic flow is cumulative upwards so that flow deeper in the ice column carries along overlying ice layers, like the zone of brittle ice.

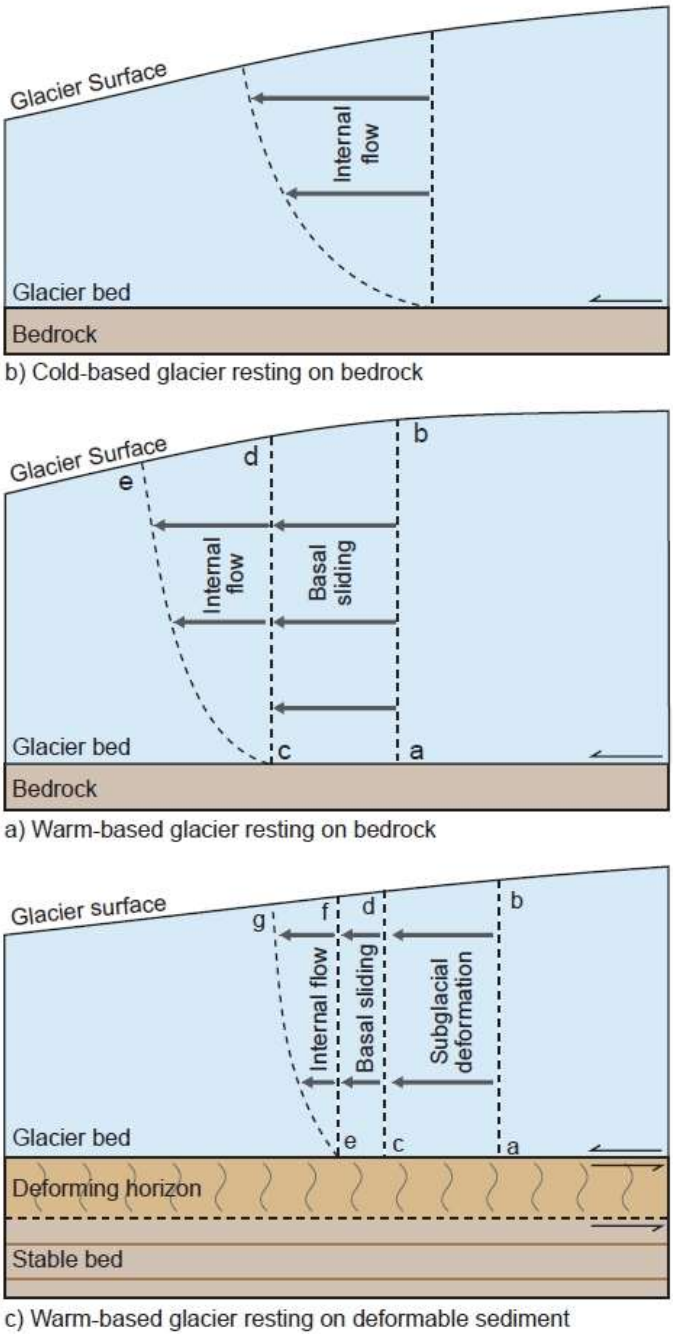

Figure 2.8. The velocity distribution within three glaciers of different basal thermal regimes resting on bedrock and deforming substrates. A vertical line a-b inserted in the glacier would be displaced as follows: a) cold-based glacier resting on hard bedrock: movement is by internal deformation alone, b) warm-based glacier resting on hard bedrock: the vertical line a-b is displaced from c-d by basal sliding and e-g by internal deformation, and c) warm-based glacier resting on deformable sediment: the line a-b is displaced to c-d by subglacial sediment deformation, to e-f by basal sliding and e-g by internal deformation. This figure has been modified from *Boulton* [1993].

can glide over each other, but this only happens when a threshold pressure from the overlying ice mass is exceeded. This typically occurs when the ice is at least 30 m thick [*Cuffey and Patterson*, 2010]. Although internal deformation is a dominant ice flow process, rates of creep typically decrease with depth when a glacier flows through internal deformation alone, as high resistive stresses at the glacial bed and valley side walls allow ice to flow much faster near the surface of the glacier [*Jiskoot*, 2011].

2.5.2 Basal sliding

When glaciers are not frozen to the substrate (bedrock or sediments), internal deformation at depth may occur through enhanced basal creep and/or regelation processes, which can promote ice flow through basal sliding [*Jiskoot*, 2001] (Figure 2.8). Although basal creep and regelation both occur when local increases in pressure on the upstream side of a bedrock bump lower the melting point of ice, which forces it to melt and move towards the leeward side of the bump (where pressure is lower and where refreezing occurs [*Jiskoot*, 2001]), enhanced basal creep is more efficient for large bedrock obstacles (>1 m wide [*Boulton*, 1972]), whilst regelation is much more efficient round smaller obstacles (which are generally < 1 m wide [*Boulton*, 1972]). Whilst both of these processes can occur without bed separation, a thin layer of water at the ice-rock interface can reduce basal friction and hydrostatic pressure, and enhance basal sliding. This allows the ice to slide forwards, often at an increased velocity [*Alley*, 1993].

2.5.3 Bed deformation

In addition to internal deformation processes, Figure 2.8 details how ice flow can also be promoted by the deformation of soft sediment or weak rock beneath a glacier. This type of deformation typically occurs in temperate ice flows, when high water pressure in the pores or spaces between fine basal sediments like clay or sand reduces the resistance between individual grains, which allows the sediment to move or flow relative to one another as a slurry-like mass [*Jiskoot*, 2011]. Provided that the basal shear stress imposed by the overriding glacier is greater

than the yield strength of the till, some, or all of this shear stress can be accommodated by bed deformation - as the slurry of sediment forms a continuously deforming layer on which the glacier moves [*Jiskoot*, 2011]. As bed deformation is primarily controlled by the mechanical and hydrological properties of the sediment below, rather than properties of the ice, ice flow through bed deformation is controlled by the yield strength of the sediment, which is highly dependent on the grain size distribution, the fractional water content and the water pressure within the till. as well as its deformation history [*Jiskoot*, 2011], where the amount of bed deformation is dependent on till thickness, till composition and water pressure. As subglacial till is a highly heterogeneous material, where yield strength and bed deformation can vary spatially and temporally there are no standard constitutive relationships or general flow laws for soft bed deformation. Although most soft bed deformation laws assume an average till deformability based on field measurements [*Boulton and Hindmarsh*, 1987], laboratory experiments [*Iverson et al.*, 1998] or mathematical understanding of till physics [*Fowler*, 2003], a number of studies (e.g. *Iverson et al*. [1988] and *Tulaczyk et al*. [2000]) have recognised that till deformation rate is dependent on the amount of shear stress. As till behaves like a plastic material, a quasi-viscous flow law (equation 2.1) is often used [*Hooke*, 2005].

$$\dot{\varepsilon} = A_2 \frac{\tau}{e^{b\tau_0}} \tag{2.1}$$

Where $\dot{\varepsilon}$ is direct strain, A2 is a constant related to a reference strain rate, b a constant that is dependent on pre-consolidation stresses and texture of till, and τ_0 the stress taken at a reference shear strain (larger than the Mohr-Coulomb yield strength) [*Hooke*, 2005]. This relationship implies that small increases in shear stress should result in large increases in till deformation (which accounts for unstable runaway flow of glaciers over soft deformable beds, which in extreme cases could result in surges – see section 2.5.7) [*Jiskoot*, 2011].

2.5.4 Flow velocity

As deformational ice flow velocity depends on the local balance between the driving forces (largely controlled by gravitational acceleration downslope) and resisting forces which slow the ice down (e.g. drag at the bed and at the margins of the glacier) (Figure 2.9), the rates and patterns of glacier motion vary enormously from one location to another. However, ice velocity is ultimately controlled by four processes: temperature, ice thickness, bedrock and gradient. In general, warmer temperate and polythermal glaciers can flow faster than cold, polar glaciers as the ice can deform more readily, whilst the re-routing of surface meltwater can allow the basal ice to slip, thereby greatly increasing velocity [*Bennett and Glasser*, 2009]. The thickness of the ice sheet (a function of climate and resultant mass balance conditions) is also very important, as thicker ice can exert more pressure on the bed, which will promote deformation and basal slip. The amount of deformation and sliding is then largely dependent on bedrock composition and topography, as more rapid movement can occur over loose sediment or easily deformable rock like clay or shale, whilst harder bedrock like sandstone or granite creates greater friction [*Boulton*, 1972]. In terms of topography, ice flowing over steep gradients will also experience high surface gradients, which can greatly increase gravitational acceleration downslope [*Benn and Evans*, 2010]. Combined, each of these processes can alter ice flow velocity both spatially and temporally. These variations can occur over a variety of scales, both between neighbouring ice flows and within large ice sheets, ice caps or smaller glaciers. For example, in individual ice flows velocity tends to be greatest near the equilibrium line (where accumulation equals ablation over a 1-year period) where the ice is relatively thick, whilst reduced ice flow velocities are recorded along the ice margins where flow is retarded by friction. In most ice masses these spatial changes in velocity occur in response to compressive and extensional flow.

2.5.5 Compressive and extensional flow

Although the majority of an ice flow experiences plastic deformation, the upper surface of a glacier is often dominated by brittle ice which is carried along by movements in the underlying

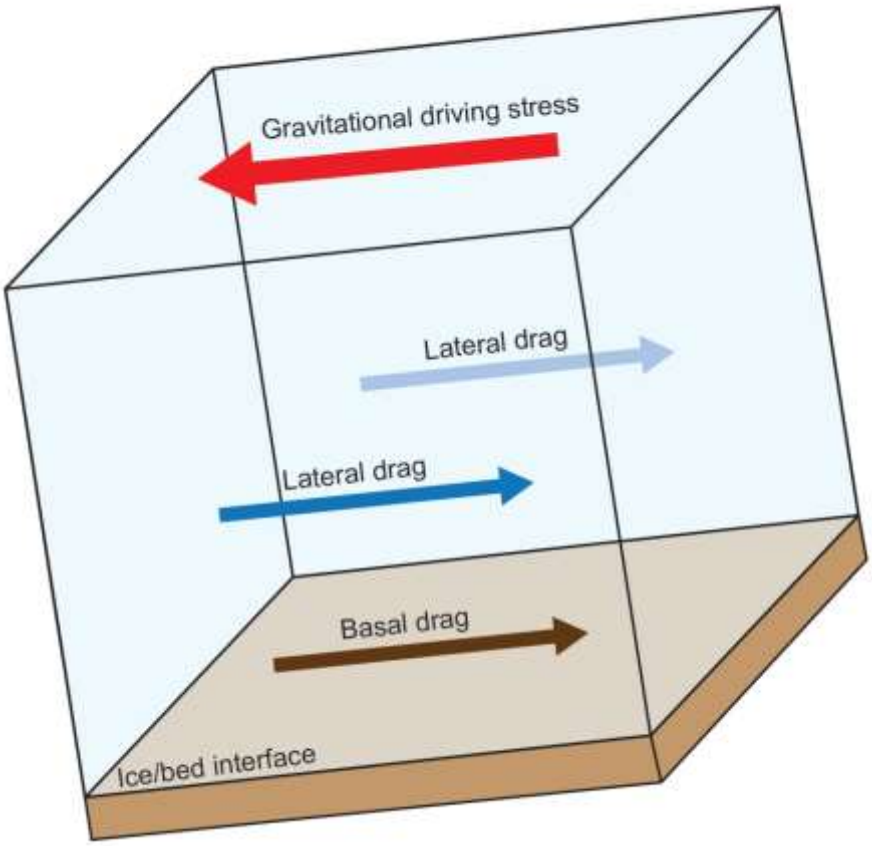

Figure 2.9. Driving and resisting stresses operating on a block of ice on an inclined slope.

plastic deformation zone (Figure 2.7). As the mid-lower ice column flows, the glacier surface can often experience tensional stress as it become stretched, which can create large cracks and fractures in the surface, called crevasses. These extensional crevasses typically form when ice flows over steep subsurface gradients, or when the ice flow becomes less confined (Figure 2.10). This allows the glacier to accelerate and thin. However, compressional crevasses can also form when the opposite occurs, i.e. when there is a reduction in subsurface gradient which forces the ice flow to slow down, or when the ice flow becomes confined (Figure 2.10). Although surface gradient largely controls the flow regime of an ice mass, this literature review demonstrates that subglacial topography can also impose compressive and extensional flow regimes, particularly in areas of high topographic relief.

2.5.6 Ice flow in Blue Ice Areas

Blue Ice Areas (BIAs) represent regions of exposed ice with a relatively low surface albedo [*Bintanja,* 1999], where katabatic wind-driven snow erosion and enhanced sublimation of the ice surface [*Jonsson*, 1990; *Van den Broeke and Bintanja*, 1995, *Casassa et al*., 1998] create a negative surface mass balance which is counteracted by emerging ice as a result of compressive flow (Figure 2.11). This local ice flow phenomenon is unique to the Antarctic continent, where BIAs cover approximately 0.8 – 1.6 % of the entire ice sheet surface (Figure 2.12) and vary in size from a few hundred square metres to thousands of square kilometres [*Winther et al*., 2001]. BIAs typically materialise in the vicinity of mountain ranges and nunataks, where the exposed bedrock highs and subglacial bedrock ridges tend to slow down or dam ice flow. Combined with surface ablation from katabatic wind scour and flow around the mountain range, this compression forces older ice to rise towards the surface where it is exposed in the typically rippled blue ice surface [*Bintanja,* 1999; *Fogwill et al*., 2012]. This flow phenomenon enables ice at the surface to range from zero to hundreds of thousands of years old [*Fogwill et al*., 2012; *Turney et al*., 2013], which creates a unique opportunity for investigating past climate [*Orheim and Lucchitta,* 1990]. The collection of ice surface samples across a horizontal BIA climate

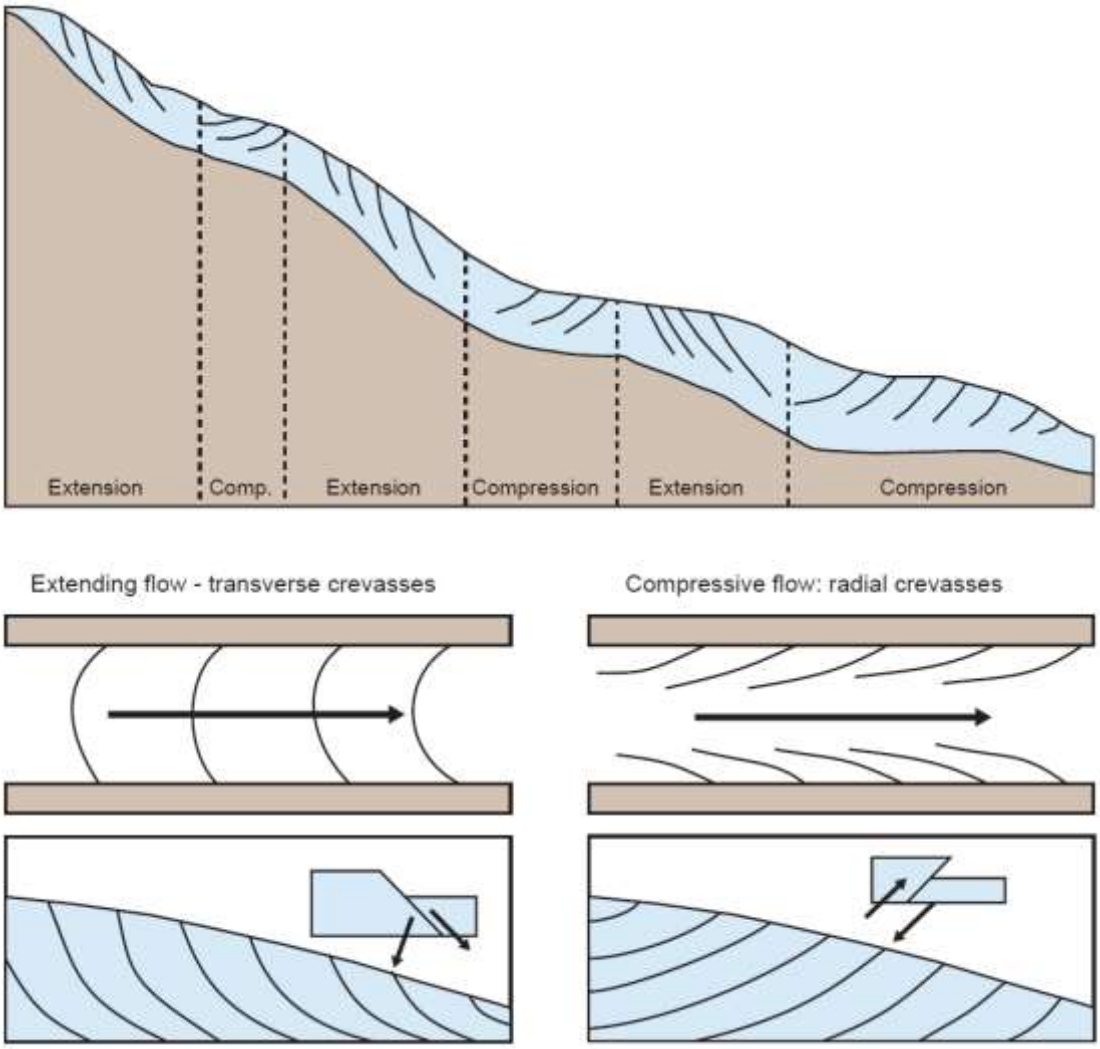

Figure 2.10. Compressive and extending flow in glaciers. Compressive flow is associated with a decrease in subglacial slope and angle or a change from warm-based ice to cold-based ice, while extending flow is encountered where the glacier bed steepens or with a cold-based to warm-based thermal boundary. Note that the pattern of surface crevasses differs between the two flow types. This figure has been modified from *Bennett and Glasser* [2009].

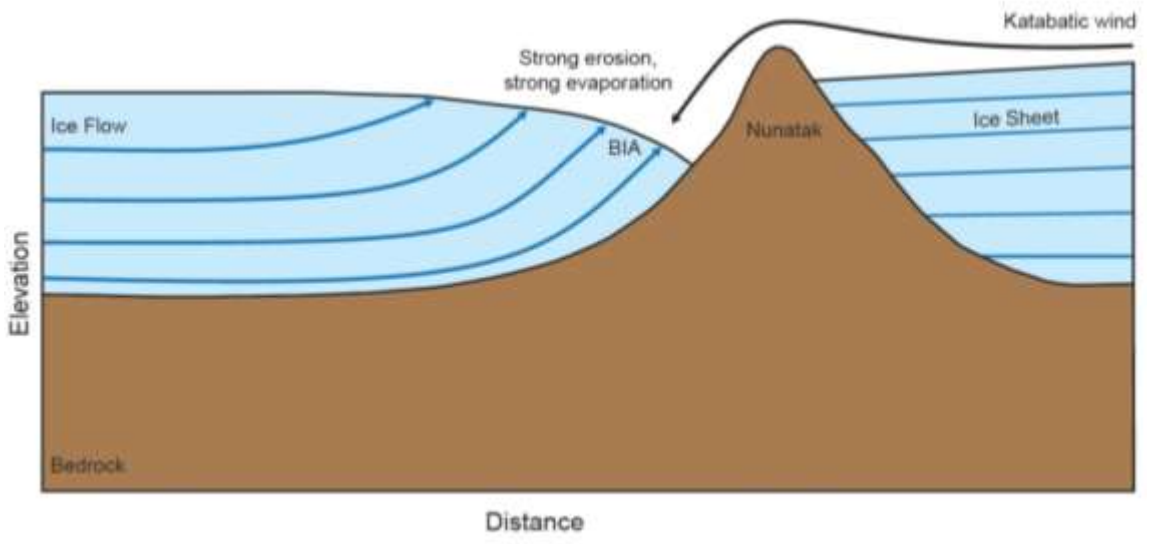

Figure 2.11. Schematic representation of a closed type Antarctic Blue Ice Area (BIA). The isochrones represent individual annual layers which flow up to the BIA surface as a result of strong erosion from katabatic winds which flow from the ice sheet interior. The oldest isochronal layers are exposed near the nunatak. This figure has been modified from *Van Den Broeke and Bintanja* [1995].

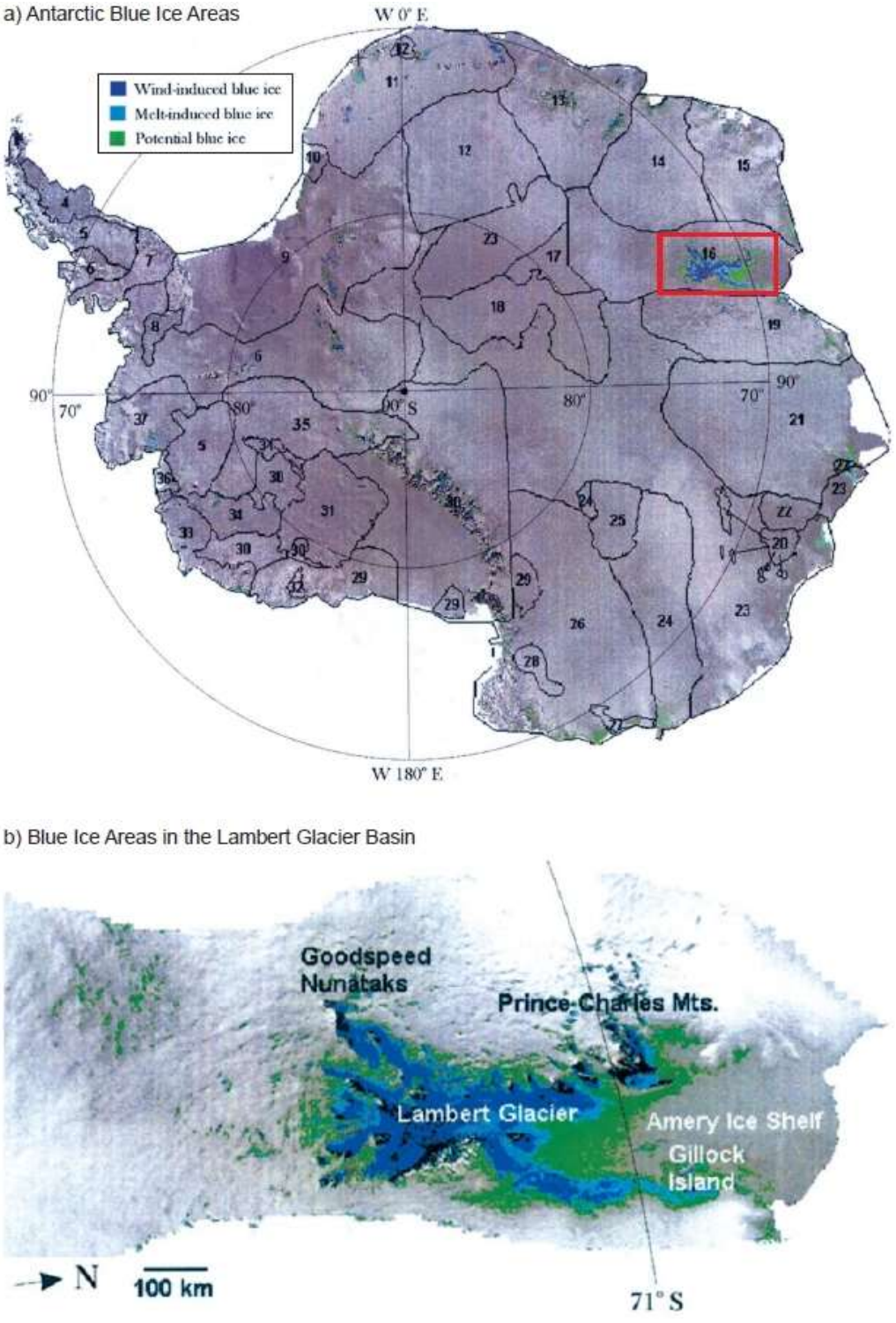

Figure 2.12. a) Location of Antarctic Blue Ice Areas (BIAs), superimposed onto NOAA AVHRR mosaic image of Antarctica, red box shows location of Lambert Glacier Basin. b) Zoom in of the largest BIAs in the Antarctic continent, located in the Lambert Glacier Basin. In both a) and b) wind-induced and melt induced BIAs have been mapped, along with potential BIA locations, where the occurrence of blue ice is uncertain. These figures have been adapted from *Winther et al*. [2001].

transect offers a much cheaper alternative to traditional vertical ice core drilling, as large samples of old ice can be collected from remote, mountainous locations to measure trapped gases and gas isotopes [*Sinisalo and Moore*, 2010]. Their potential to indicate mass balance has also been recognised by *Yu* [2011], who found that BIAs can show the highest correlations between the rate of surface elevation change and the percent rate of change in blue ice extent.

2.5.7 Flow instability – surging glaciers

Although all glaciers flow, the way in which they flow can vary, and as a result, some ice flows are more unstable than others. This is particularly evident in surging glaciers, where ice is subject to cyclical flow instabilities. Surging glaciers typically have long periods of quiescence, with thinning, melting and down wasting - with some forward motion, followed by short periods of rapid ice flow velocity where the glacier can advance dramatically. For example, when Brúarjökull in eastern Iceland surged in 1963, the glacier front advanced 8 km over its forefield, with a daily rate in excess of 100 m [*Thorarinsson*, 2011] (Figure 2.13). Although timings vary both regionally and by individual glacier, in Svalbard the quiescent phase of a surging glacier tends to exist for approximately 100 years, whilst the high-velocity period can last anywhere between a few months and 5 years [*Hagen et al*., 1993]. Although the precise mechanism of surging is still debated, most studies agree that changes in the glacier thermal regime are often responsible. For example, *Sevestre et al*. [2015] noticed that the subglacial hydrological regime and/or the strength and availability of subglacial till is often altered as a result of feedbacks associated with changes in the glacial thermal regime (these are often related to ice thickness fluctuations). These alterations can then have an important impact on ice flow, as changes in the subglacial hydrology and/or subglacial till properties can modify subglacial friction and the basal shear stress of the glacier, which will ultimately promote or suppress high velocity ice flow.

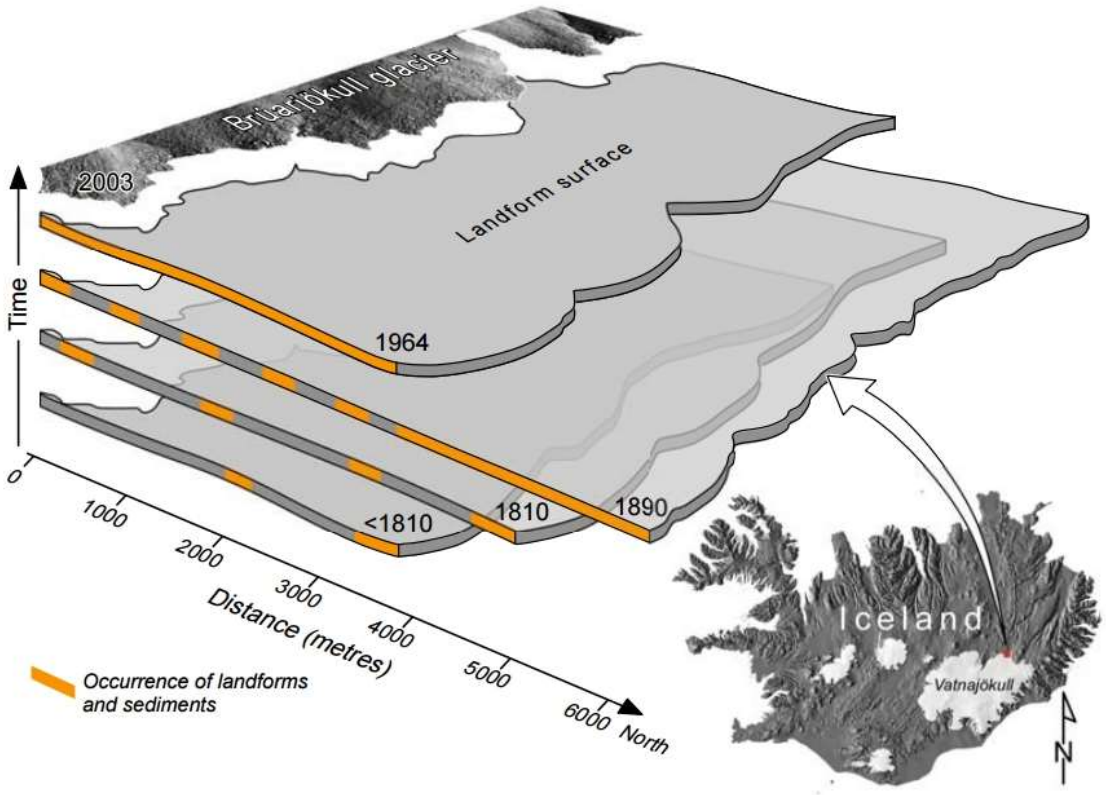

Figure 2.13. An example of surge events from Brúarjökull Glacier, Iceland [*Kjær et al*., 2008]. This figure shows that the present terrain surface is the cumulated result of at least four surge events: pre-1810, 1810, 1890 and 1964.

2.6 Ice Streaming

Although this literature review has accounted for large scale ice sheet flow and local ice flow phenomena such as surging glaciers and compressive blue ice areas, faster stream flow has yet to be accounted for. In comparison to slow-moving ice sheet flow (which typically occurs within the dome areas of the interior ice sheet), faster stream flow, namely through ice streams, can move approximately 10-100 times faster than the adjacent non-streaming ice sheet [*Bindschadler and Scambos*, 1991; *Whillans and van der Veen*, 1993]. The Antarctic Ice Sheets are drained by a number of these fast flowing ice streams, which are typically hundreds of kilometres long and tens of kilometres wide [*Bennett*, 2003] (Figure 2.14). These ice streams were first recognised in the mid-20th century, where they were soon defined by *Swithinbank* [1954] as "part of an inland ice sheet in which the ice flows more rapidly than, and not necessarily in the same direction as, the surrounding ice". This definition points to the two main features which define ice streams: (1) ice streams are surrounded by ice (if they were surrounded by rock, they would be considered outlet glaciers), and (2), the ice remains part of the inland ice sheet, and thus, it is not floating. It should also be noted here that the exact area at which the ice changes from sheet flow to streaming flow is referred to as the "onset zone" [*Bindschadler et al*., 2001].

Controls on the formation and location of ice streams followed their initial discovery; a review of creep instability in glaciers and ice sheets by *Clarke et al*. [1977] pulled together theories, models and field work studies to conclude that all ice sheets will inherently stream as a result of thermomechanical feedbacks. Subsequent numerical modelling experiments revealed that on a uniform bed the development and location of ice streams will tend towards uniformity, with a self-organised, radial flow regime [*Payne and Dongelmans*, 1997; *Hulton and Mineter*, 2000; *Boulton et al*., 2003; *Hindmarsh*, 2009]. However, as observations of some contemporary ice sheets indicated non-regularity in ice streaming, it was soon noted that their exact location must be governed by a variety of factors such as topographic focussing, subglacial till deformation and basal hydrology [*Winsborrow et al*., 2010]. These factors are detailed below.

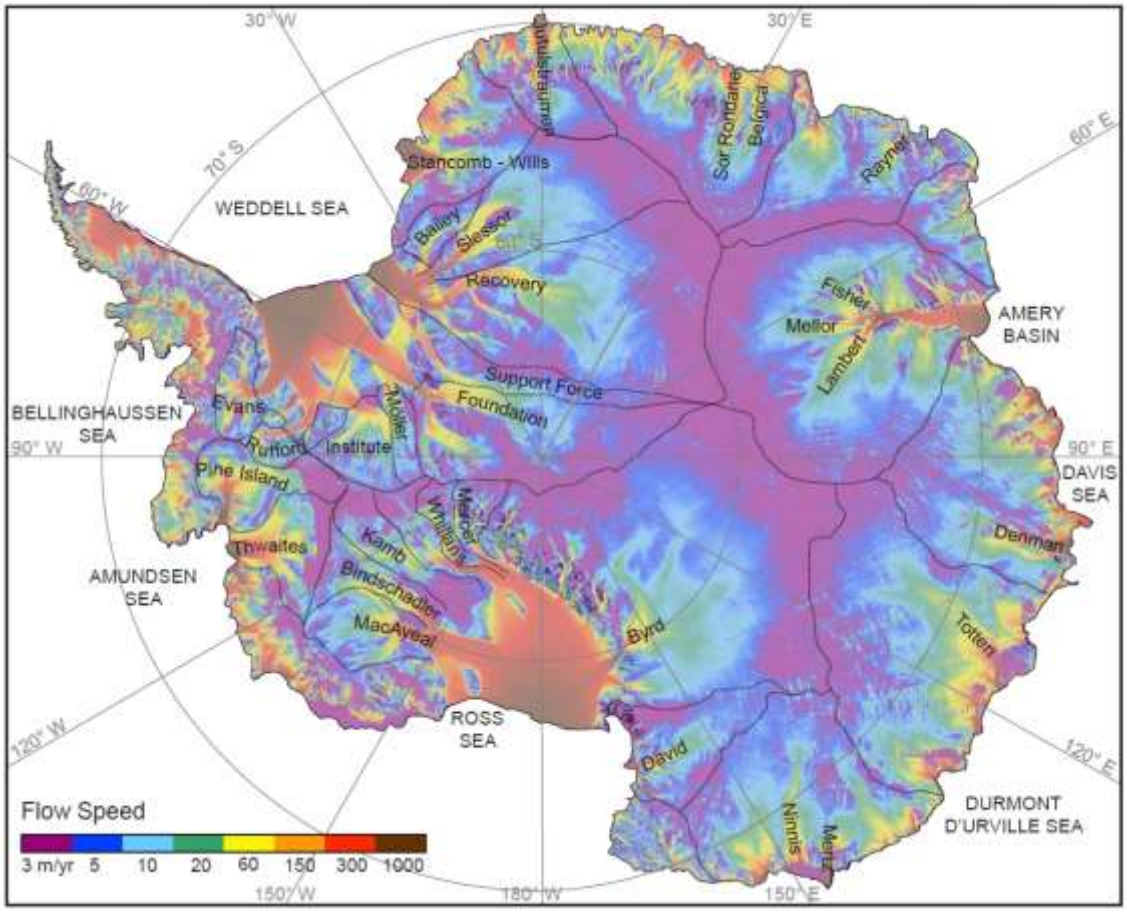

Figure 2.14. Satellite-derived surface ice flow velocities of the Antarctic Ice Sheets from MEaSUREs [*Rignot et al*., 2011], superimposed over MODIS satellite imagery [*Haran et al*., 2006] and annotated to show dominant ice streams and their catchment areas.

2.6.1 Topographic focussing

As most ice streams flow along troughs in the bed, basal topography was thought to be the obvious control governing ice stream location when research began in earnest during the mid-20th century. Many studies realised that deep trough systems could support large ice masses and sustain considerable driving stresses, capable of impelling large ice fluxes into and through deep topographic channels. This was exemplified by *McIntyre* [1985] who recognised that ice velocities tended to increase when ice was channelised through troughs in the subglacial topography, although the study also recognised that larger driving stresses were required when troughs were narrow, as marginal drag along the valley walls provided resistance to flow. Although topographic focussing remains one of the main controls on ice streaming, *Shabtaie and Bentley* [1987], amongst others, quickly recognised that it was not a necessary condition for ice streaming and that subglacial till deformation could support ice streaming in areas with low topographic constraints.

2.6.2 Subglacial till deformation

Ice streams located in areas with little to no topographic constraints are often termed 'pure ice streams' [*Bennett,* 2003]. These ice streams are extremely rare, and at present can only be found along the Siple Coast region of Antarctica (Figure 2.14) where unconfined ice flows stream from the central dome of the WAIS towards the coast, draining ~40% of the WAIS [*Price et al*., 2001]. Following the identification of a thick, saturated and possibly deforming till beneath the Whillans Ice Stream, in the Siple Coast in the 1980's, many studies such as those by *Alley et al.* [1986], *Blankenship et al*. [1986], *Alley et al*. [1987] and *Blankenship et al*. [1987] suggested that these unconfined 'pure ice streams' could flow as a result of subglacial till deformation. Field work investigations followed, where the inherent instability of pure ice streams was discovered. Borehole investigations of the Kamb Ice Stream in the Siple Coast revealed that a change in subglacial hydrological routing ~150 years ago caused the ice stream to slow down considerably and eventually 'switch-off' as the debris-rich basal ice began to freeze to the bed,

preventing streaming flow above [*Retzlaff and Bentley*, 1993]. GPS measurements across the Whillans Ice Stream have also revealed more recent changes in the Siple Coast. Here, *Joughin et al*. [2005] realised that the Whillans Ice Stream is currently decelerating at a rate of 0.6%/yr^2, as a result of increasing till strength. An extrapolation of this deceleration trend suggests that the ice stream could stagnate in the next 100-200 years as the basal sediment approaches the driving stress of the ice stream, preventing significant horizontal-plane shearing in the ice [*Joughin et al*., 2005]. Combined, these studies have confirmed that ice streaming can be promoted, and indeed controlled by the deformation of a subglacial till layer (see section 2.5.3) [*Anandakrishnan et al*., 1998; *Bell et al*., 1998]. However, it should be re-enforced here that this mechanism of ice streaming is inherently unstable. The lack of topographic control in pure ice streams allows subglacial sediment, water and overlying ice to re-route over timescales of a few years or less [*Smith et al*., 2007], which can dramatically alter properties of the subglacial till, and therefore the flow of overlying ice [*Alley et al*., 1994; *Tulaczyk et al*., 2000].

2.6.3 Basal hydrology

Although the importance of water-saturated sediments at the base of an ice sheet have been explored in this chapter, it is also important to discuss the controls that water alone exerts on ice sheets and ice streams. Like water saturated sediments, the presence of basal water beneath an ice sheet can lower the basal strength of an ice mass to below the driving stress, causing stress to shift from the bed to the lateral shear margins. This typically increases basal slip and promotes faster ice flow. In order to appreciate ice flow fully it is therefore critical to assess the hydrology of ice sheets and ice streams in Antarctica.

Hydrological sources

Effective lubrication of the glacier bed can arrive from surface, englacial and basal melt as well as groundwater sources (Figure 2.15). Like ice flow, the availability of water from each of these sources depends upon the climatic regime at the ice surface, the thermal regime of the ice, ice

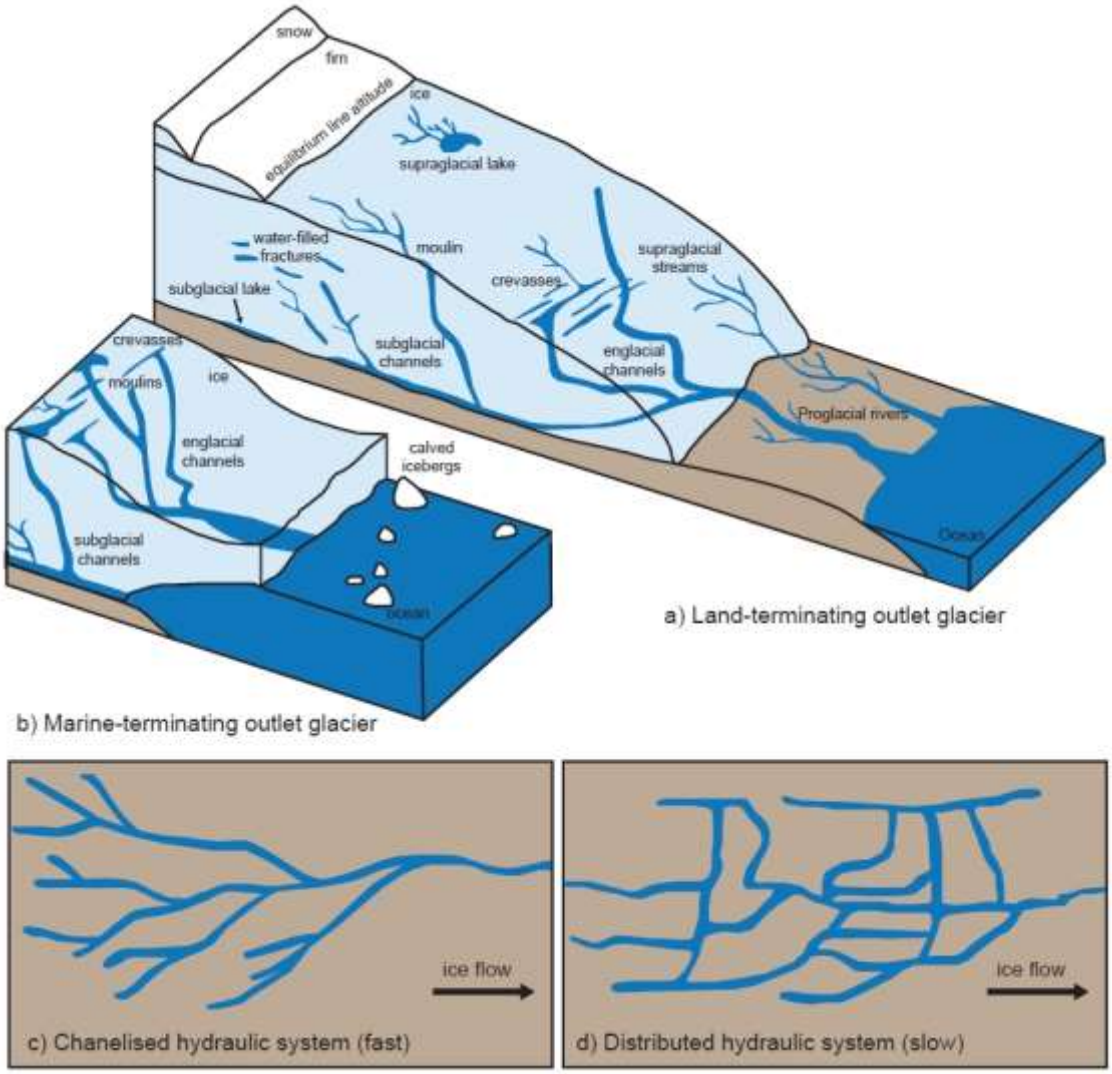

Figure 2.15. Schematic ice sheet hydrology of a land-terminating outlet glacier (a) and a marine-terminating outlet glacier (b), both modified from *Cuffey and Paterson* [2010]. c) and d) represent plan views of channelised and distributed hydraulic systems (adapted from *Benn and Evans* [2010]).

flow dynamics and the nature of the bed [*Sharp*, 2005]. Although surface melt is the dominant source of water on high latitude, low elevation glaciers, these types of glaciers are largely limited in Antarctica to a few glaciers along the Antarctic Peninsula. As such, basal melting provides the majority of hydrological sources in Antarctica. This melt is generated as temperatures near the bed reach the pressure melting point, as a result of pressure from the thick overlying ice sheet. Frictional heating from fast flowing ice can also generate water within the glacial system, as a result of englacial melt (e.g. Jakobshavn Isbrae, Greenland [*Harrington et al*., 2015]). Although ground water inputs are poorly resolved in large ice sheets [*Christofferson et al*., 2014], they can also provide another important hydrological source for glacial systems, particularly when they relate to aquifers below the surface (e.g Trapridge Glacier in Canada [*Flowers and Clarke*, 2002] or the Vatnajökull ice cap in Iceland [*Flowers et al*., 2005]).

Channelised and distributed drainage systems

Once water has entered the glacial system it can be moved, retained or stored in response to water inputs, glacier geometry, thermal regimes and ice flow dynamics [*Sharp*, 2005; *Chu*, 2013]. The movement of water through the glacial system is often facilitated by channelised or distributed subglacial drainage systems (Figure 2.15). Channelised systems, where water is confined to relatively narrow conduits are generally the most efficient pathways for water flow beneath or through ice, where well-formed channels permit rapid flow. In contrast, distributed systems, which often extend over large proportions of the bed, are generally less efficient. As these systems can change over time (as a function of water supply and temperature changes) these drainage systems can exert a strong control over glacier dynamics over both short and long time periods, by controlling the distribution of stored water and altering frictional resistance at the bed [*Benn and Evans*, 2010].

The advancement of ice penetrating radar collection and processing has allowed numerous drainage systems to be identified beneath the Antarctic Ice Sheets. For example, *King et al.* [2004] provided seismic evidence for water flow through small channels in the subglacial

sedimentary substrate beneath the Rutford Ice Steam in West Antarctica; while more distributed flow has been recorded near the Gamburtsev Subglacial Mountains in East Antarctica. In the Gamburtsev Subglacial Mountains distributed networks dominate alpine overdeepenings (created during the early growth phase of the EAIS [*Wolovick et al*., 2013]), where water flows downhill or uphill depending on the ice surface gradient [*Ashmore and Bingham*, 2014]. This type of drainage imposes spatially variable flow velocities in the overlying ice, as the ice mass can flow rapidly over subglacial channels but not over surrounding bedrock, where friction is increased.

Subglacial lakes

In areas where water is available but drainage is prevented by ice, sediment or rock, water can be stored in supraglacial, englacial, subglacial or proglacial environments. In Antarctica, the storage of water in supraglacial, englacial and proglacial environments is limited as a function of low surface temperatures and, as such, water is more typically stored in subglacial lakes. These lakes are usually found in regions with low hydraulic gradients [*Bindschadler and Choi*, 2007; *Carter et al*., 2007] which include ice divides, ice stream onset zones and prominent subglacial troughs [*Benn and Evans*, 2010]. Since their discovery in the 1970's by *Robin et al*. [1970], an ever increasing number of lakes have been identified beneath the Antarctic Ice Sheets using airborne radio echo sounding and satellite laser altimetry. Although the first continent-wide inventory by *Siegert et al.* [2005a] recorded 145 lakes beneath the ice sheet, recent technological advances and new radar flight lines have allowed a further 234 lakes to be identified, bringing the latest total of subglacial lakes in Antarctica to 379 [*Wright and Siegert*, 2012] (Figure 2.16). Of the initial 145 subglacial lakes identified by *Siegert et al.* [2005a], 124 were found to be 'active' between 2003 and 2008 [*Smith et al*., 2009]. This 'activity' is defined as any water accumulation and/or discharge over the measured time period. The high activity record suggests that the lakes are capable of providing or withdrawing water from the hydraulic

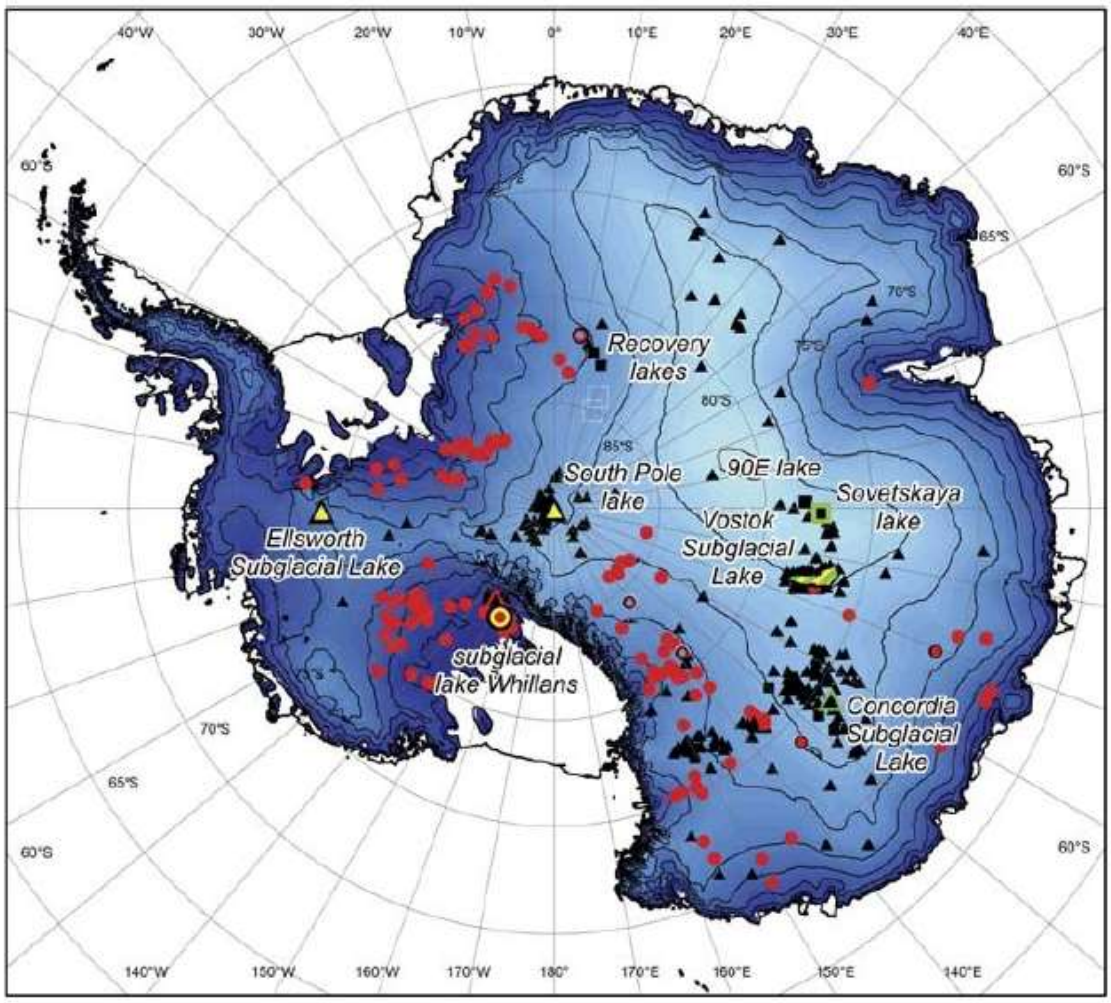

Figure 2.16. Map of subglacial lakes in Antarctica from *Wright and Siegert* [2012]. Colours/shapes indicate the type of investigations undertaken at each site: Black triangle = radio echo sounding, yellow triangle = seismic sounding, green triangle = gravitational field mapping, red circle = surface height change measurement, square = shape identified from ice surface feature. Vostok Subglacial Lake is shown with an outline.

systems that lubricate glacier flow, and, as such, it is highly likely that these subglacial reservoirs could force rapid temporal changes in glacier velocity [*Smith et al*., 2009].

With an estimated volume of 5400 km^3 [*Studinger et al*., 2004], Lake Vostok in the centre of the EAIS is the largest subglacial lake to be identified. The lake represents a closed hydrological system where melting occurs at the northern end of the lake where the overlying ice is thicker and at the pressure melting point, whilst freezing dominates the southern end of the lake where the ice is thinner. However, as *Smith et al*. [2009] stress, most lakes in Antarctica represent much more open systems than that of Lake Vostok. For example, the water body volume of 1.37 km^3 in subglacial Lake Ellsworth in West Antarctica [*Woodward et al*., 2010] is unlikely to be produced solely by local melt; instead it is more likely delivered via subglacial drainage [*Vaughan et al*., 2007]. Again, this promotes instabilities in ice flow as episodic drainage/fill events are known to create short-term speedups of both land-terminating portions of an ice sheet [*Bartholomew et al*., 2010; *Palmer et al*., 2011; *Zwally et al*., 2002] and fast-moving marine terminating outlet glaciers [*Andersen et al*., 2011; *Joughin et al*., 2008; *Shepherd et al*., 2009]. This has important implications for the stability of ice sheets and ice streams over short to long time-periods.

2.7 Debris in the glacial system

As ice travels to the coast by slow-moving sheet flow or faster ice stream flow, sediment from subglacial or extraglacial sources can be picked up, entrained and transported. During entrainment and transportation, glaciers can shape the landscape by scouring broad areas clear of debris or through trough excavation. These features make glaciers among the most effective agents of erosion on Earth [*Benn and Evans*, 2010]. As debris can shape the subglacial landscape and alter ice flow this section of the literature review will focus on debris sources, entrainment mechanisms and debris transport processes through the glacial system, where particular emphasis will be placed on the relationship between debris and ice flow.

2.7.1 Debris sources

Potential debris sources can be grouped into two categories: extraglacial or subglacial, although englacial transportation and mass movement processes can move debris from one end member to the other. Extraglacial debris is typically supplied by rockfalls, avalanches, and/or valley-side regolith, whilst subglacial debris is sourced from loose sediments or material eroded from the bed. Like all ice flow processes, the amount of available material is related to hydrology, glacial thermal regimes and ice flow dynamics, although in this case, geology also plays an important role as softer bedrock is more easily eroded than hard bedrock and cohesive sediments are much more difficult to pick up than loose sediments [*Boulton*, 1972]. It should also be noted here that past glaciations and glacial history can also play an important role in the availability of sediment, as marine ingression can supply sediment, whilst long periods of glaciation are known to exhaust sediment supplies [*Bennett and Glasser*, 2009].

2.7.2 Debris entrainment mechanisms

Once debris has been sourced, it can be incorporated into the ice flow by a variety of processes linked to internal ice deformation. This includes thrusting, folding, regelation (freeze-on), and crevasse-filling. As each of these processes is intrinsically linked to ice flow and glacial structures each of these entrainment mechanisms are detailed below and outlined in Figure 2.17.

Thrusting

Thrusts can develop under longitudinal compression where there is a thermal transition from warm to cold based ice (e.g. a downstream transition from a sliding bed to a frozen bed). In most ice flows this occurs when ice flows against a reverse bedrock slope, but in surging glaciers longitudinal compression can also develop as the compressive surge front moves down glacier [*Sevestre et al*., 2015] (see section 2.5.7). In each of these situations stress builds up until it is released by failure along a thrust plane which can either propagate to the ice surface, or

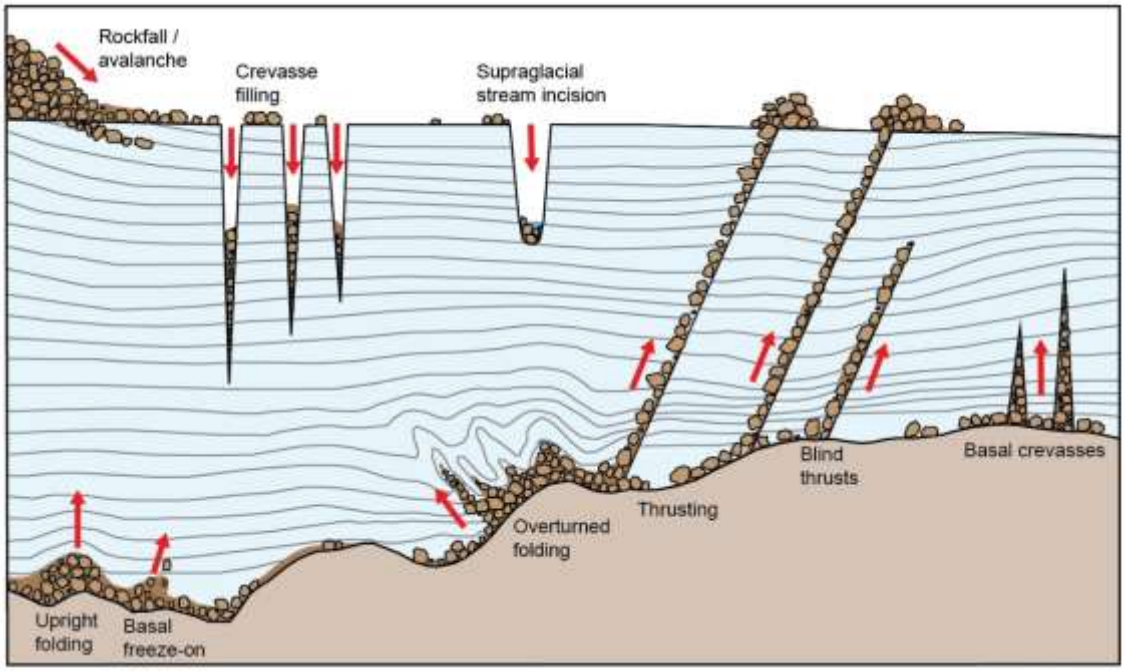

Figure 2.17. Possible debris entrainment mechanisms in ice sheets. Supraglacial debris can be incorporated into ice flows through successive snow deposition in the accumulation zone, through crevasse filling or supraglacial stream incision. Basal debris can be entrained through a variety of processes linked to internal ice deformation. This includes folding, thrusting, freeze-on and crevasse-filling.

terminate within the ice mass as a blind thrust (Figure 2.17). Sediment can be incorporated in the initial fault event or injected through brine infiltration at a later date [*Hambrey and Glasser*, 2011].

Folding

When ice passes through local zones of compression as the glacier flows against obstructions in the bed or valley walls principal stresses near to the horizontal can cause the ice to fold, producing "open-folds" with gently sloping limbs in low stress regimes, and "isoclinal folds" with parallel limbs in areas subject to high longitudinal compression (Figure 2.18). It has been suggested that this can induce folding in soft subglacial and basal sediments of the same geometry (although this has not yet been observed) [*Hambrey and Glasser*, 2011]. The amount of folding is subject to several geometric factors: the tightness of the fold, the orientation of the axial plane relative to the horizontal and the thickness of the fold.

Regelation (freeze-on)

Net freezing of melt-water can occur when ice moves from warm to cold based, making the pore-water pressure in the subglacial sediment less than the ice pressure [*Weertman*, 1961]. Although this mechanism requires water to re-freeze around all entrained clasts, and thus, the rate of freeze-on will only decrease with increasing debris thickness [*Boulton*, 1972], *Alley et al.* [1997] suggest that regelation can allow debris sources to be lifted to relatively high levels of englacial transport, several tens of metres above the bed.

Crevasse filling

Crevasse filling is common in areas of complex stress regimes, where ice undergoes both extensional and compressional flow (typical of surging glaciers – see section 2.5.7). When the basal crevasse opens, saturated and deformable till is squeezed under pressure into the crevasses, creating 'crevasse squeezes' [*Woodward et al.*, 2003a]. This allows sediment to enter

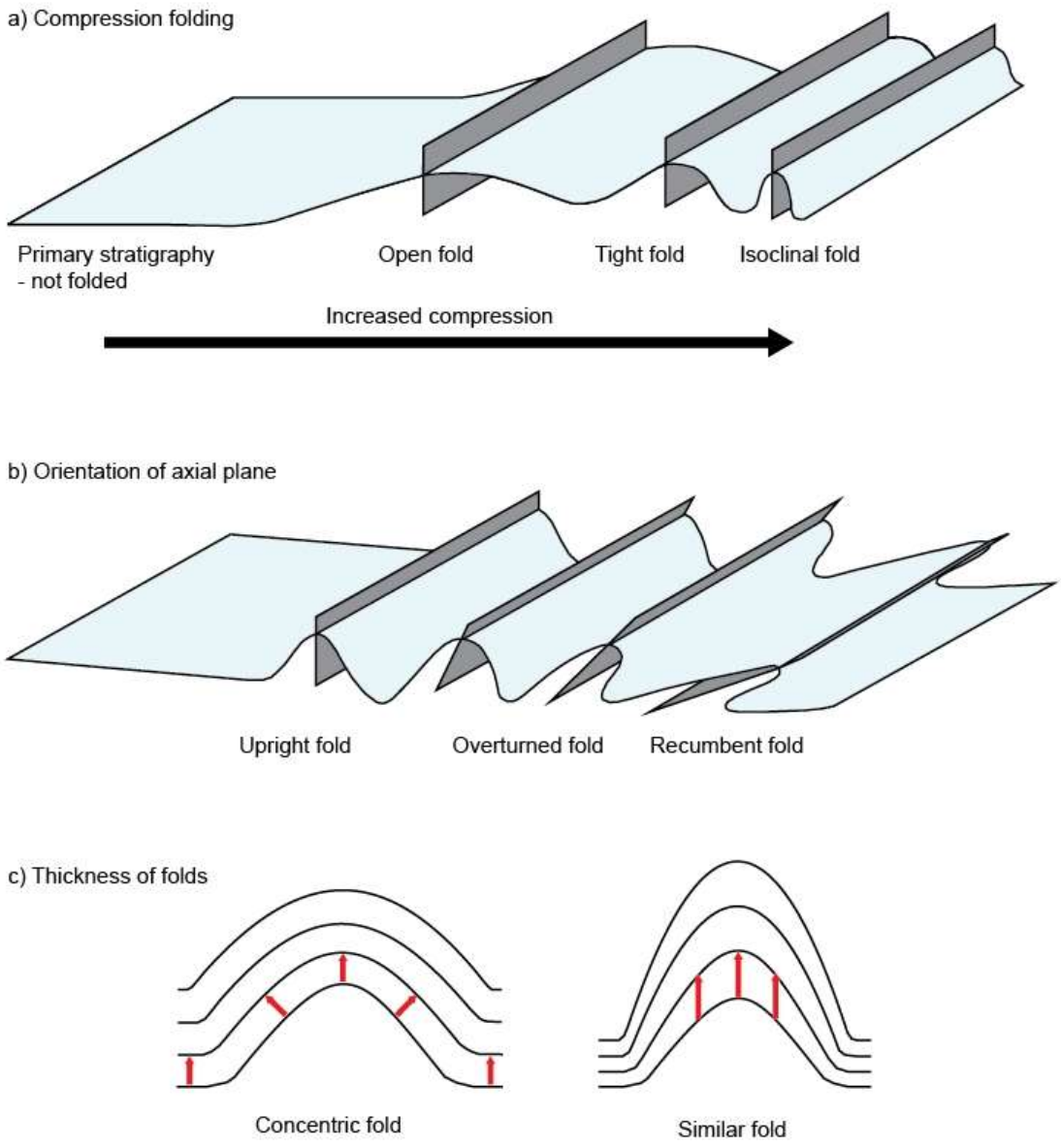

Figure 2.18. Englacial layer folding terminology, a) compression folding, b) orientation of axial plane and c) thickness of folds (modified from *Fossen* [2010]).

the glacial system, or even emerge supraglacially during full depth bottom-up crevassing, although *Rea and Evans* [2011] stress that full-depth bottom-up crevassing is rare, and only occurs when ice thicknesses are in in excess of ~200 m, with basal water pressures in excess of 80-90% flotation.

2.7.3 Controls on debris entrainment

Each of the debris entrainment mechanisms detailed above can only occur under specific circumstances, which broadly rely on sediment availability, ice flow and ice temperature. Each of these controls has been detailed below.

Sediment availability

First of all, debris can only be entrained in ice if sediment is available for entrainment. This is a complex control, as the location and amount of available debris is a function of glacial history (e.g. trough excavation and/or marine ingression), basal geology, basal topography, local erosion rates and ice flow velocity [*Dunning et al*., 2015]. If sediment is made available through the erosion or deposition of clasts, it could be incorporated into the ice flow if conditions allow, though it should be noted that this entrainment will inevitably cease once the sediment source is exhausted.

Ice flow

Once sediment is made available, the likelihood of debris entrainment is then a function of ice flow [*Jennings et al*., 2014], where the stress regime of a glacier can limit or permit debris entrainment through thrusting, crevasse formation and folding. Again, these types of entrainment mechanisms will only incorporate large volumes of sediment if they migrate over time and/or space.

Ice temperature

Ice temperature is controlled by a number of factors including the local weather and climate, ice thickness, ice velocity and geothermal heat flux [*Sugden*, 1977]. As these factors vary over space and time, ice temperature can have a variable control on debris entrainment. Although debris excavation occurs when ice moves from warm to cold based [Boulton, 1972] (figure 2.19), spatial and temporal changes in the thermal regime will inevitably alter the precise location of debris entrainment.

2.7.4 Debris transport through the glacial system

Once incorporated, debris can be moved through the glacial system supraglacially, englacially and/or subglacially [*Boulton*, 1993] (Figure 2.20). As initial transportation modes are largely controlled by source location and glacial flow characteristics, a distinction is sometimes made between high-level (passive transport) where the material remains in the supraglacial or englacial zones and low-level (active) transport where debris is brought into contact with the bed. High-level transport is frequently encountered when debris is made available at the ice surface through rockfall activity: in the accumulation area, rockfall and/or avalanche material is often buried by subsequent snow and firn deposits, which force clasts to take an englacial transport path [*Berthling et al*., 2000]. Here debris transport follows the flow lines of the ice from the accumulation area through to the ablation zone [*Degenhardt and Giardino,* 2003; *Monnier et al*., 2008; *Degenhardt*, 2009]. However, high-level transport can also occur when debris falls onto the ice surface close to the equilibrium line, where limited snow accumulation allows debris to follow a more shallow englacial path, where the debris will likely emerge a short distance down glacier [*Hambrey and Glasser*, 2011] (Figure 2.19). Finally, when debris falls in the ablation zone, it is often draped over the glacier surface and passively transported down glacier (as limited snowfall makes it unlikely for clasts to be fully incorporated into the ice flow [*Knight*, 1999]).

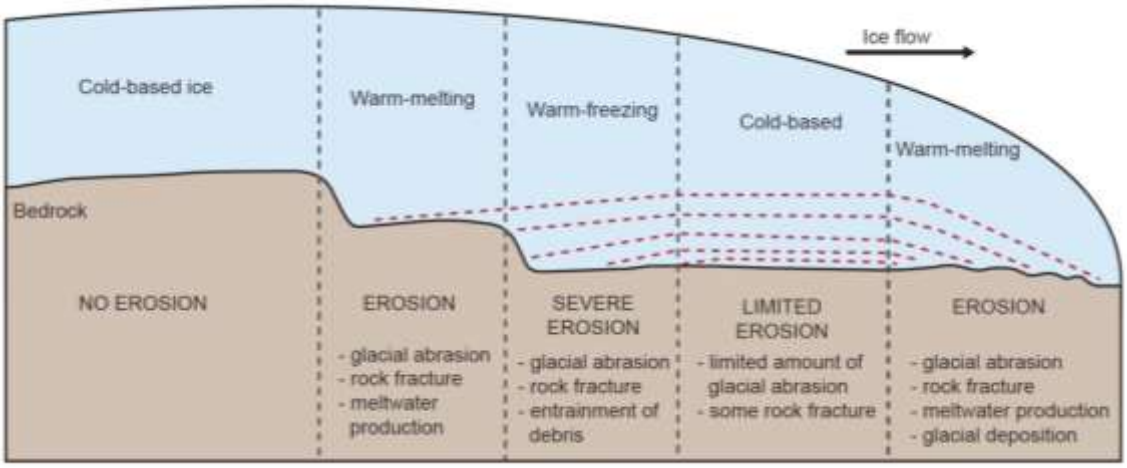

Figure 2.19. Schematic cross-section through an ice sheet showing the influence of the basal thermal regime on processes of glacial erosion. This figure has been modified from *Bennett and Glasser* [2009].

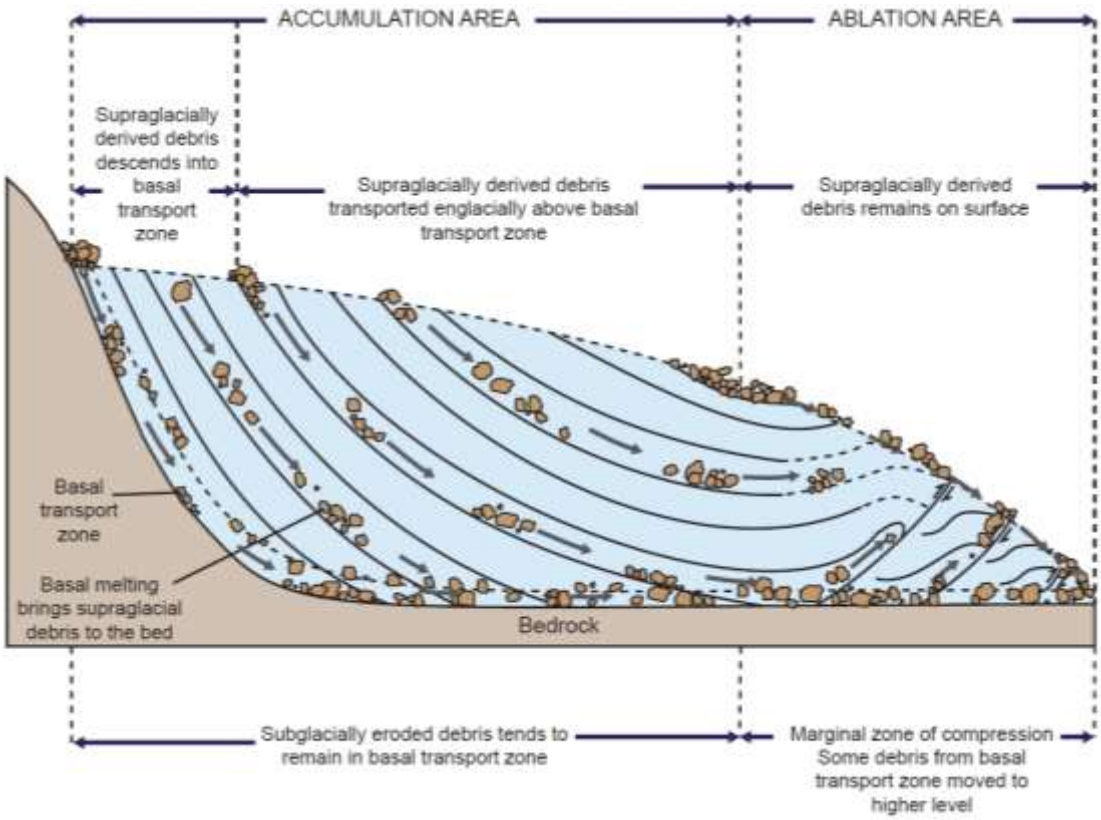

Figure 2.20. Debris transport pathways through a typical valley glacier. Two transport pathways can be identified 1) a high-level pathway in which the debris does not come into contact with the bed and 2) a low-level pathway in which the debris is in contact with the bed. This figure has been modified from *Boulton* [1993].

As low level transport is defined as transport where debris is brought into contact with the bed, sediment which reaches the bed is typically sourced near the glacial bed or high up in the accumulation zone, where it takes time for the debris to be brought to the bed by ice flow. Once debris comes into contact with bedrock it often becomes eroded and scratched, producing rounded clasts with several directions of striations [*Boulton*, 1978] (Table 2.1). However, when basal debris is embedded in lodgement till, striations tend to develop parallel to glacier flow, where they often exhibit truncated distal extremities (rather like a roche mountonnée) [*Boulton*, 1978] (Table 2.1). Although each of these examples show that the location of entrainment is a key factor for debris transportation, the speed of conveyance and path of transport can again depend on internal and external factors such as hydrology, ice dynamics (extending vs compressive flow), thermal regimes and basal topography.

2.7.5 Significance of debris in the glacial system

Although this literature review has already demonstrated the importance of basal topography and sediment availability in terms of ice flow and ice streaming, the significance of quantifying debris sources and determining debris incorporation still needs to be addressed. In Antarctica it has been very difficult to quantify supraglacial debris accumulations, as the primary source - rockfall deposits are relatively short-lived on glacial surfaces (as snow accumulation quickly buries deposits [*Berthling et al*., 2000] – see section 2.7.4). However, a recent study of rock avalanche deposit sequestration by *Dunning et al*. [2015] has suggested the possibility of detecting landslide deposits englacially, with the use of ice penetrating radar. As rockfall deposits could increase in the future (as ice sheets respond to feedbacks associated with global warming and de-stabilise exposed rock headwalls and valley sides [*Deline et al*., 2014]) ice penetrating radar surveys open up new possibilities for detecting englacial debris deposits and improving magnitude/frequency curves for rockfall events in Antarctica. These methods can also be applied to detect englacial debris sources, and debris entrainment mechanisms at depth, where sources and processes of debris entrainment can provide insight into the local thermal,

Transport zone	Boulder shape	Boulder character	Texture
Supraglacial	Angular	No striations	High level transport type
Supraglacial or englacial	Sub-rounded to rounded	Several striae directions	Tractional type (often strong secondary modification
Basal or glacier bed	Rounded	Parallel striae, distal truncation	Tractional type (might have secondary modification)
Glacier bed	Sub-rounded to rounded	Often water warn	Tractional type (often strong secondary modification)

Table 2.1. Boulder shape, character and texture as a function of glacial transportation. Table adapted from *Boulton* [1978].

hydrological and/or stress regime [*Boulton*, 1972]. This is particularly important in Antarctica where in-situ measurements of ice temperature, englacial stress and hydraulic regimes are limited as a function of accessibility and cost. On a longer timescale, englacial debris can also have an important influence on the nature of the subglacial topography and ice sheet conditions [*Harbor et al*., 1998]. As glacially eroded and entrained sediment can help to wear down valley side walls over time (Figure 2.21), debris accumulations can eventually alter ice flow directions [*Harbor et al*., [1988], ice velocity [*Bell et al*., 1998] and debris transport pathways, where ice flow can potentially transport large quantities of sediment and essential nutrients from continental sources to Southern Ocean deposition [*Death et al*., 2014; *Hawkings et al*., 2014].

2.8 Detecting past and present ice flow regimes

Although this literature review has highlighted examples of ice flow regimes, the precise mechanisms for detecting ice flow and indeed changes in ice flow have yet to be fully addressed. The principal method for detecting englacial and subglacial features in large ice masses is ice penetrating radar, which can be split into two distinct methods; radio-echo sounding (RES) and ground penetrating radar (GPR) (figure 2.22), which operate at different scales and frequencies. Both methods require a transmitter that emits electromagnetic waves and a receiver that records reflections (or 'echoes') from any surfaces where there is a contrast in dielectric properties [*Bingham and Siegert*, 2007]. Over ice sheets and ice caps, the most common reflectors constitute the ice surface, the basal interface, and englacial (internal) layers; although additional features such as subglacial lakes, subsurface crevasses, thermal boundaries and debris can also be discerned [*Bingham and Siegert*, 2007]. As basal conditions have been found to exert a strong control on ice flow, hydrology and debris availability, methods to detect basal conditions will be examined before systems for detecting and analysing internal ice sheet stratigraphy are explored.

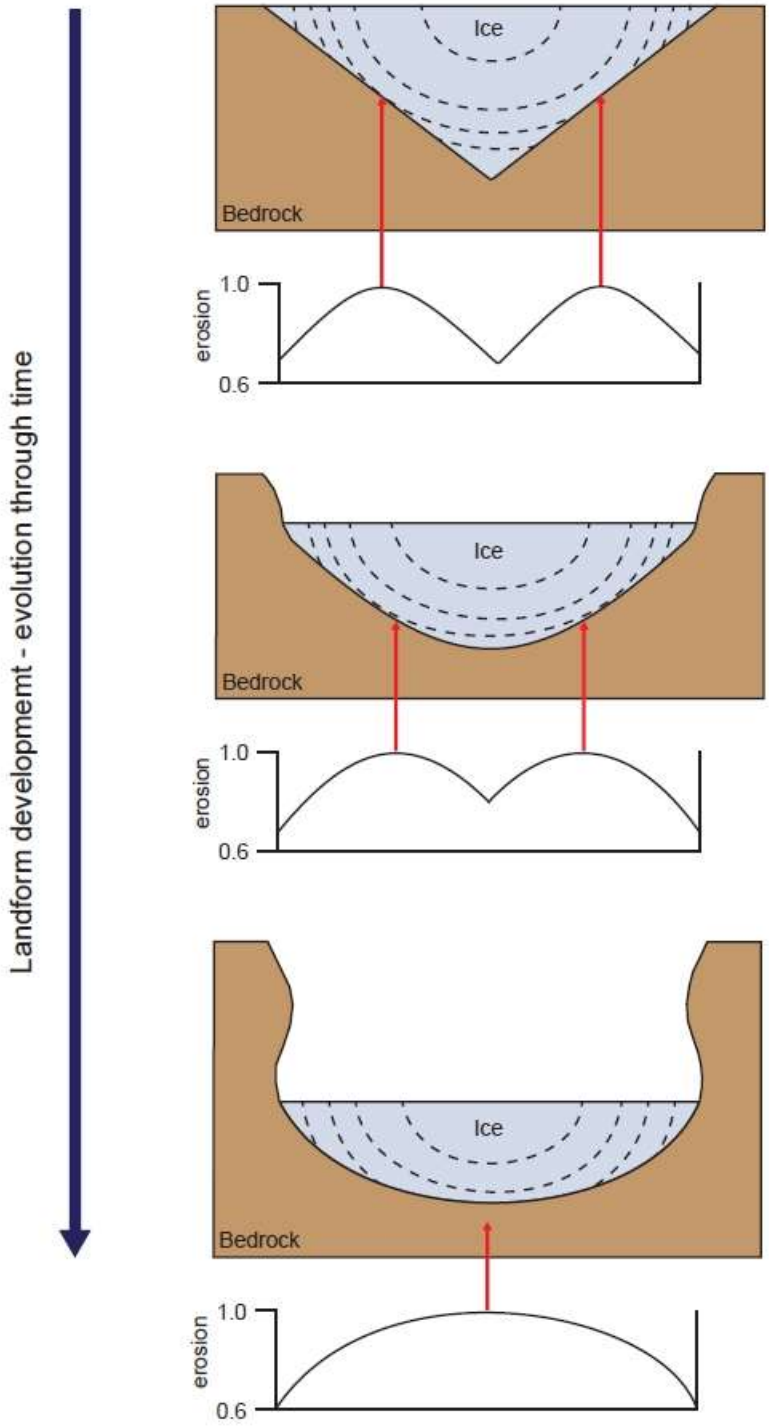

Figure 2.21. A numerical model of landform development by glacial erosion through time. Figure modified from *Harbor et al*. [1988].

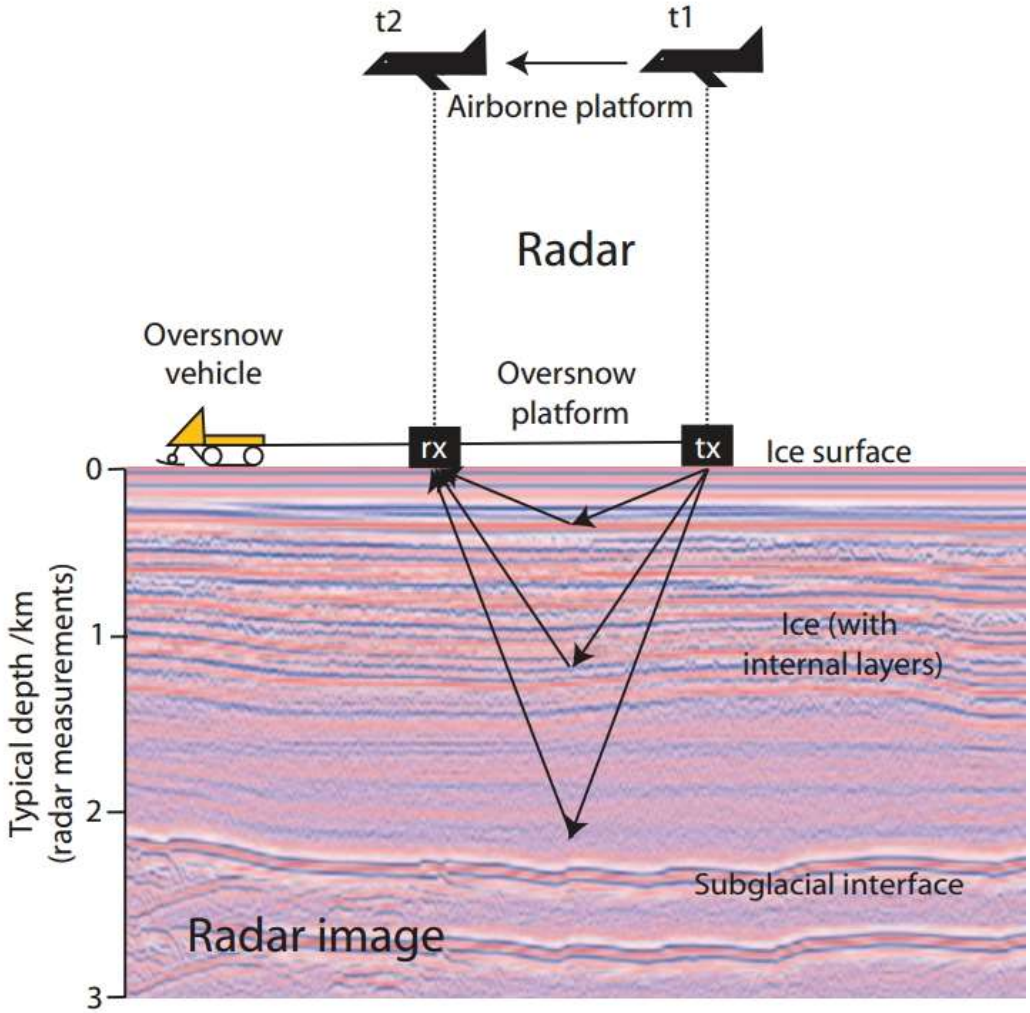

Figure 2.22. Schematic diagram from *Bingham et al.* [2010] showing methods of radar acquisition over ice from airborne and over snow platforms. Both systems require a transmitter (tx) that emits electromagnetic waves and a receiver (rx) that records reflections in the subsurface.

2.8.1 Detecting basal features

Developed in the 1960s as a method for locating the bed beneath ice sheets in order to constrain subglacial topography for the determination of ice sheet thickness, RES remains the principal method for investigating subsurface properties of the polar ice sheets and ice caps. One of the most obvious subsurface features is the bed, as sediment and/or rock provides a highly reflective interface which is easily discernible from even the thickest overlying ice sheets in radar returns. Although RES has been widely employed in Antarctica since its invention, the first continent-wide account of subglacial topography in Antarctica was provided in 2001 by the Bedmap consortium [*Lythe et al*., 2001]. This unique dataset, having recently been updated to form Bedmap2 [*Fretwell et al*., 2013], has revealed the spatial variability of basal conditions in Antarctica, by mapping out numerous subglacial mountain ranges and deep trough systems.

By employing more detailed analysis of specific RES lines, a number of studies have also investigated regional basal features which have included subglacial sediments, basal water and subglacial lakes, where each new finding has helped to improve the understanding of flow mechanisms, discussed in earlier sections of this literature review. Repeat surveys have also been employed to analyse temporal changes in the bed, where a number of studies, e.g., *Vaughan et al*. [2003], *Smith*, [2006] and *Murray et al.* [2008] have indicated rapid change over measured time periods. For example, repeat imaging of the bed of the Rutford Ice Stream has revealed rapidly changing bed forms, probably in the form of mega-scale glacial lineations or drumlins [*Smith et al*., 2007; *King et al*., 2007, 2009, 2016].

2.8.2 Analysing internal stratigraphy

In order to determine past and present ice flow regimes in Antarctica it is necessary to analyse the internal stratigraphy within the thick EAIS and WAIS. Primary stratification accounts for the majority of internal features within the upper reaches of an ice sheet. This type of stratification develops when surface snow accumulations are compacted and buried by subsequent snowfall, eventually producing stratigraphic layers within the ice sheet. As each

layer has a unique dielectric property, geophysical methods can be used to detect and trace the individual layers, or more commonly, packets of layers within the ice sheet (e.g. Figure 2.22), where their shape and form can reveal information about past and present ice flow. However, this type of undisturbed primary stratification is only found in slow moving sheet flow, typically in upland areas of the ice sheet where snow accumulation dominates. Here, regional GPR and RES can often detect the conformable, isochronal layers (i.e. layers of the same age) [*Fujita et al*., 1999; *Parrenin and Hindmarsh*, 2007] for several tens of km [*Siegert*, 2003; *Siegert and Payne*, 2004; *Cavitte et al*., 2013], where the relative thickness of each layer can be used to infer past accumulation rates [*Fahnestock et al*., 2001; *Woodward and King*, 2009] or to constrain layer ages from ice cores [*Waddington et al*., 2007].

As the ice flow changes from sheet flow to more channelised streaming flow, this primary stratification can become buckled and disrupted as the ice adapts to changes in the local strain rate. As previously discussed in sections 2.5 and 2.6, these changes frequently occur in ice as a result of fluctuations in the basal topography, basal flow conditions, basal melting, surface accumulation and/or converging or diverging ice flow [*Siegert et al*., 2004]. By examining the exact shape and form of buckles and disrupted layers along with their spatial context it is therefore possible to infer both past and present ice flow regimes. This technique has helped to reveal temporal changes in the location and velocity of ice streams throughout Greenland and Antarctica. For example, *Siegert et al*. [2013] recently detected ice deformed by former enhanced flow beneath un-deformed, very slow flowing ice in the Weddell Sea sector of West Antarctica by airborne RES (Figure 2.23). Through detailed analysis, these findings reveal an adjustment to the flow path of the Institute Ice Stream ~4000 – ~400 years ago (Figure 2.23).

Despite the glaciological insights that are possible from the study of ice penetrating radar returns, their use has been largely limited because of the lack of data availability [*Siegert et al*., 2005b]. This review highlights the need for more geophysical surveys, in order to detect and understand ice flow mechanisms, past ice sheet conditions and overall ice sheet stability. Outputs are critical for the development and validation of numerical and predictive ice sheet

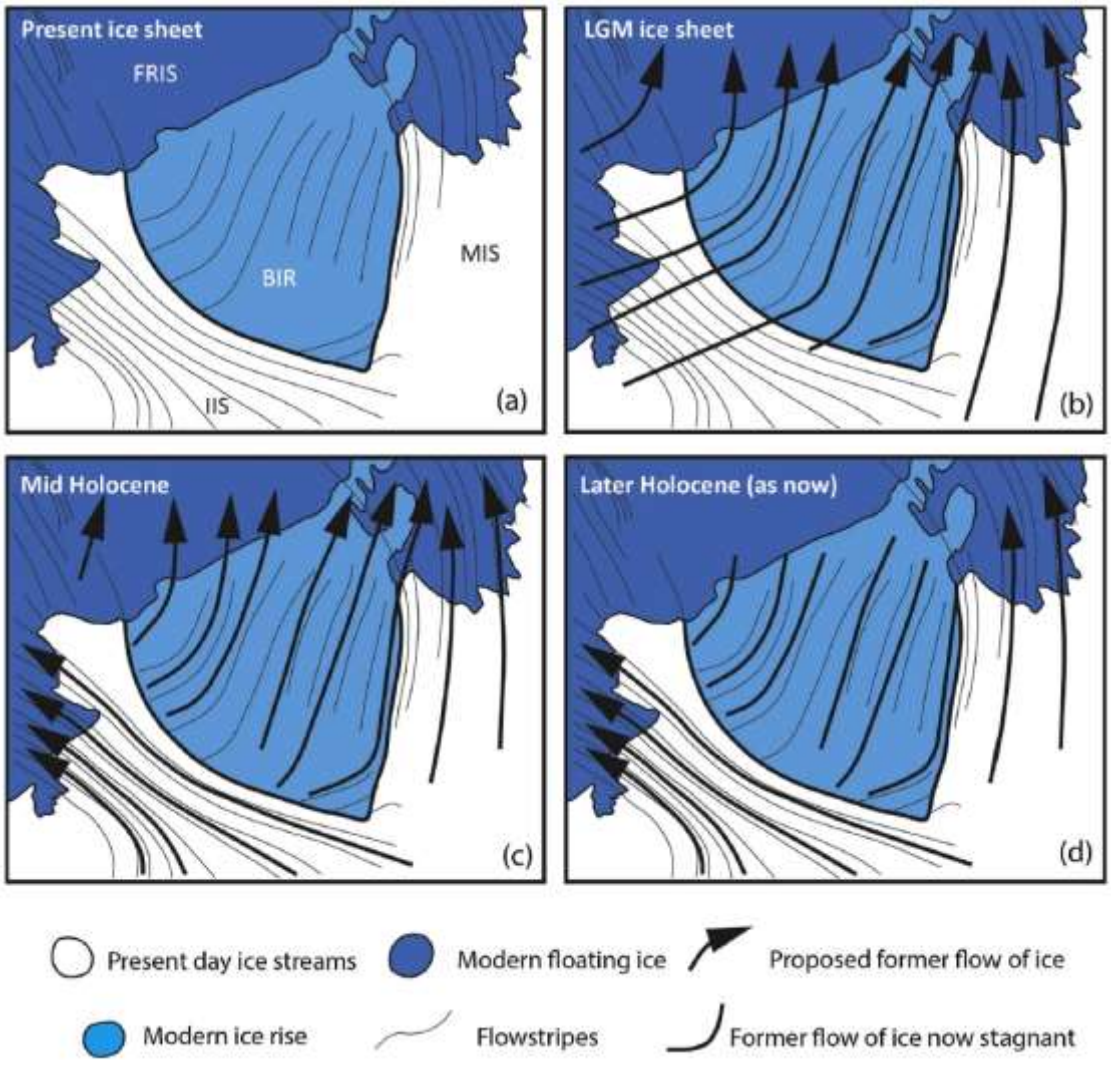

Figure 2.23. Schematic description of ice sheet change in the Institute and Möller Ice Streams (IIS and MIS), West Antarctica [*Siegert et al*., 2013]. (a) The current glaciological situation, with respect to the Bungenstock Ice Rise (BIR) with ice flow stripes from the BIR noted. (b) Proposed ice flow during the Last Glacial Maximum (LGM), when northward ice flow from the WAIS interior cross-cuts the present day trunk of the IIS. (c) Mid Holocene, post-LGM situation, where the IIS becomes active to the south of the BIR. (d) Later Holocene ice configuration, in which ice over the BIR becomes stagnant, thus leading to the present day ice sheet configurations.

models (e.g. *Conway et al*. [1999]; *Siegert et al*. [2003]; *Martin et al*. [2006], [2009]; *Waddington et al*. [2007]; *Eisen* [2008]; *Sime et al*. [2011]).

2.9 Summary

Recent changes in the global climate have heightened concerns for rapid irreversible ice sheet loss, with resultant implications for atmospheric circulation patterns [*Roe and Lindzen*, 2001], ocean overturning [*Hemming*, 2004] and global sea level. As Antarctica stores ~70% of the entire world's fresh water [*Bennett and Glasser*, 2009], making it capable of raising sea levels by ~57 m should the ice sheet melt completely [*Lythe et al*., 2001], it is critical to understand both past and present ice-flow dynamics in Antarctica, as even a modest change in ice-sheet volume will strongly affect future sea level and freshwater flux to the oceans [*Lemke et al*., 2007].

This literature review has highlighted the importance of understanding ice flow in Antarctica, particularly in areas which are deemed to be unstable, or vulnerable to change. These areas include, but are not limited to ice sheets resting on bedrock well below sea level and ice streams which flow over water or thick subglacial sediments, where ice flow is acutely sensitive to a number of internal and external factors. Although some of these factors can be triggered, and to some extent paced by external forcing (atmospheric and oceanic), this literature review demonstrates that each ice stream is unique and that a multitude of factors can modulate their location and flow regime, as well as the precise rate and timings of any change in ice flow dynamics [*Livingstone et al.,* 2012].

As a result of this literature review, this thesis will use ice penetrating radar to address the controls on ice flow and internal stratigraphy in the upper IIS catchment, in the climate sensitive WAIS. The geological and glaciological features of this study site, in and around Horseshoe Valley in the Ellsworth Mountains will be discussed in *Chapter 3*, while *Chapter 4* will introduce methodologies used in this thesis. *Chapter 5* will investigate the internal stratigraphy of Patriot Hills BIA, *Chapter 6* will examine the complex basal topography and ice

sheet flows of the Ellsworth subglacial highlands using airborne RES and *Chapter 7* will detail debris sources and entrainment mechanisms in Horseshoe Valley. Analysis of katabatic winds and other controls on BIAs will be then be discussed in *Chapter 8*, in order to investigate past and present flow regimes. All of this work will be combined to create a site wide discussion chapter (*Chapter 9*) as well as a conclusion chapter (*Chapter 10*) where limitations of the study will be discussed, along with suggestions for future work.

Chapter 3

Study site

3.1 Institute Ice Stream

Ice streams, accounting for approximately 90% of the total discharge of the WAIS, retain evidence of former flow conditions that make them suitable for investigating past and present ice flow conditions (see chapter 2). One of the largest ice stream basins in West Antarctica is the Institute Ice Steam (IIS) which captures a total drainage area of 151,000 km^2, where ice flow is drained from the central WAIS dome to its release at the Filchner-Ronne Ice Shelf (FRIS) in the Weddell Sea (Figure 3.1). The IIS catchment borders the southern lobe of the Pine Island Glacier drainage system, the southern catchment of the Rutford Ice Stream, the northern extent of the Möller Ice Stream (MIS) and the uppermost part of the Kamb Ice Stream basin. In the upper catchment two distinct flow units are recognised; one is ice that comes from the broad catchment that adjoins the Siple Coast ice streams, and the second, which is the main focus of this thesis, comprises a series of tributaries around and west of the Ellsworth Mountains (Figure 3.1).

As 60% of the IIS catchment lies well below sea level (Figure 3.1c, 3.1d), where recent analyses of airborne geophysical surveys revealed that the basal topography is characterised by steep reverse bed slopes, deep trough systems and low basal roughness, a number of studies (e.g. *Ross et al*. [2012]; *Wright et al*. [2014] and *Siegert et al*. [2016]) have recently voiced concern for potential widespread instability in this sector of West Antarctica. These fears were recently compounded in a study by *Ross et al.* [2014] who recognised that there is little small-scale topography that could act as a pinning point to delay any future retreat of the IIS's grounding line. As investigations by *Hein et al*. [2011, 2016a] and *Golledge et al*. [2013] have discovered that the FRIS grounding line comprises an area sensitive to changes in ice thickness in the Weddell Sea sector of Antarctica, it is more than possible that the grounding line could retreat in the future, particularly if forecasted climate change scenarios come to fruition (see chapter 2). *Ross et al.* [2014] suggested that even a slight retreat of the grounding line could

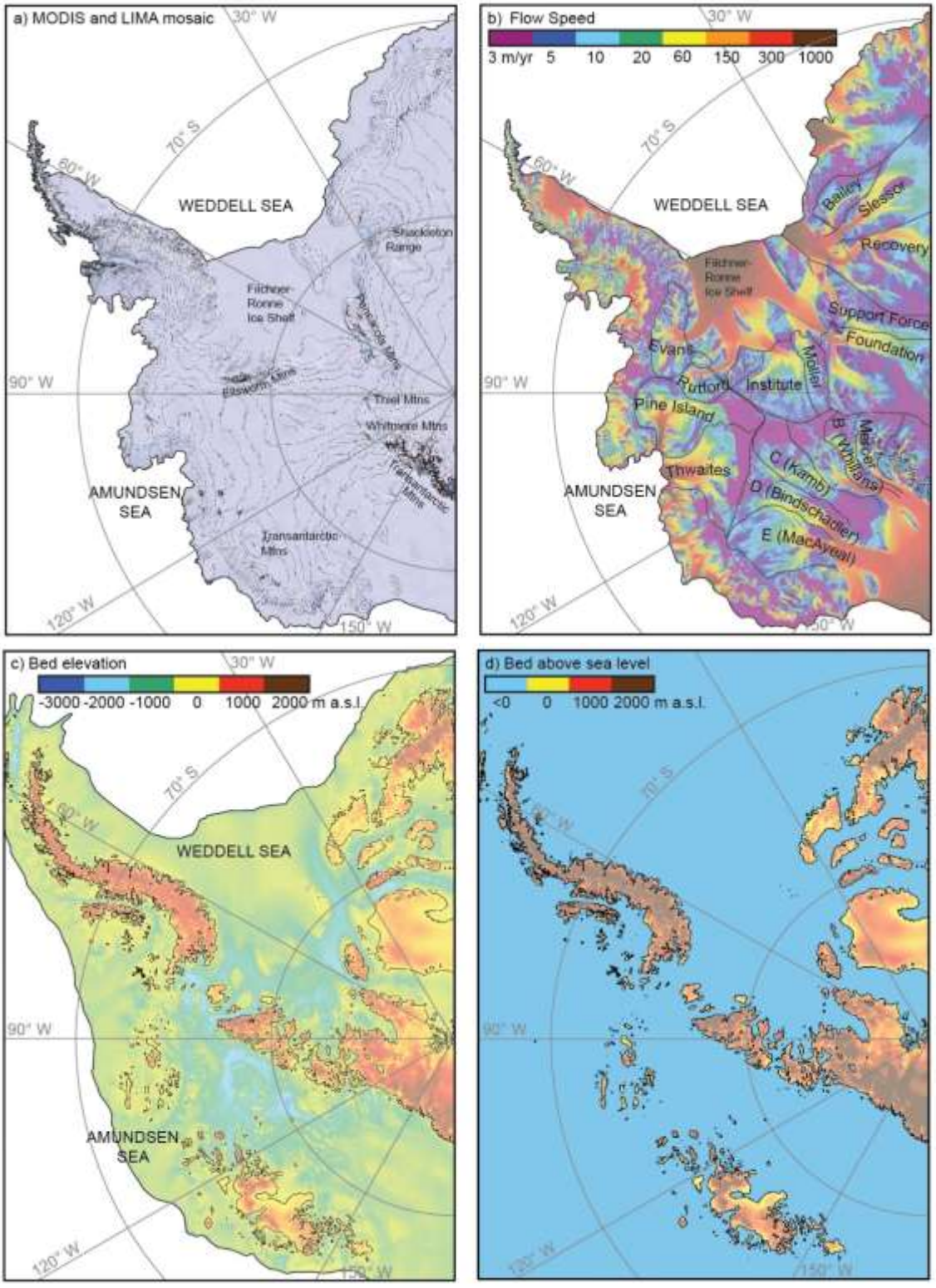

Figure 3.1. a) MODIS and LIMA mosaic of Antarctica with prominent geographical features labelled, thin black lines indicate 500 m elevation contours, b) Satellite-derived surface ice flow velocities from MEaSUREs [*Rignot et al*., 2011a], superimposed over MODIS satellite imagery [*Haran et al*., 2006] and annotated to show dominant ice streams and their catchment areas, c) map of subglacial topography, thin black lines indicate 0 m elevation, d) subglacial topography map with bedrock shading to show areas above present sea-level (blue).

quickly transform the IIS tributaries into discrete ice stream outlets, capable of generating enhanced ice flow from the main WAIS divide. The study stressed that this enhanced flow could increase the potential for more widespread and possibly irreversible ice sheet drawdown [*Ross et al*., 2014]. As large proportions of the upper IIS catchment flow above subglacial beds which are often situated well below sea level (particularly in areas around the Ellsworth Mountains) it is critical to better understand the past and present ice flow regime in this region.

3.2 Ellsworth Mountains

The Ellsworth Mountains comprise a 350 km long and 80 km wide isolated mountain block, built of a conformable sequence of folded Cambrian to Permian sediments, which can be differentiated into two distinct units; the Sentinel and Heritage Range (Figure 3.2). The Sentinel range is composed of younger quartzites which support high mountainous peaks, like Mount Vinson, which stands at 4892 m a.s.l. (making it the highest point in Antarctica) (Figure 3.2), whilst the Heritage range, to the south-west is defined by a number of lower elevation ridges and peaks, comprised of older limestone and quartzite conglomerates [*Webers et al*., 1992]. Although geologically distinct, both ranges are defined by a series of high amplitude basement faults and geological folds running north-west to south-east [*Jordan et al.*, 2013] which define tectonically-controlled sub-basins which are often more than 300 km long and up to ~2500 m deep.

3.2.1 Glaciological history of the Ellsworth Mountains

Fluvial regimes, alpine glaciation and wide-spread ice sheet ingress have helped to shape the unique topography of the Ellsworth Mountains in West Antarctica over millions of years. Many pioneering studies, like that by *Rutford* [1972] suggested that rivers would have initially sculpted the dendritic pattern of the valleys and rolling hills (which are preserved around Mt. Vinson in the Sentinel Range), whilst alpine glacier systems, most likely associated with a

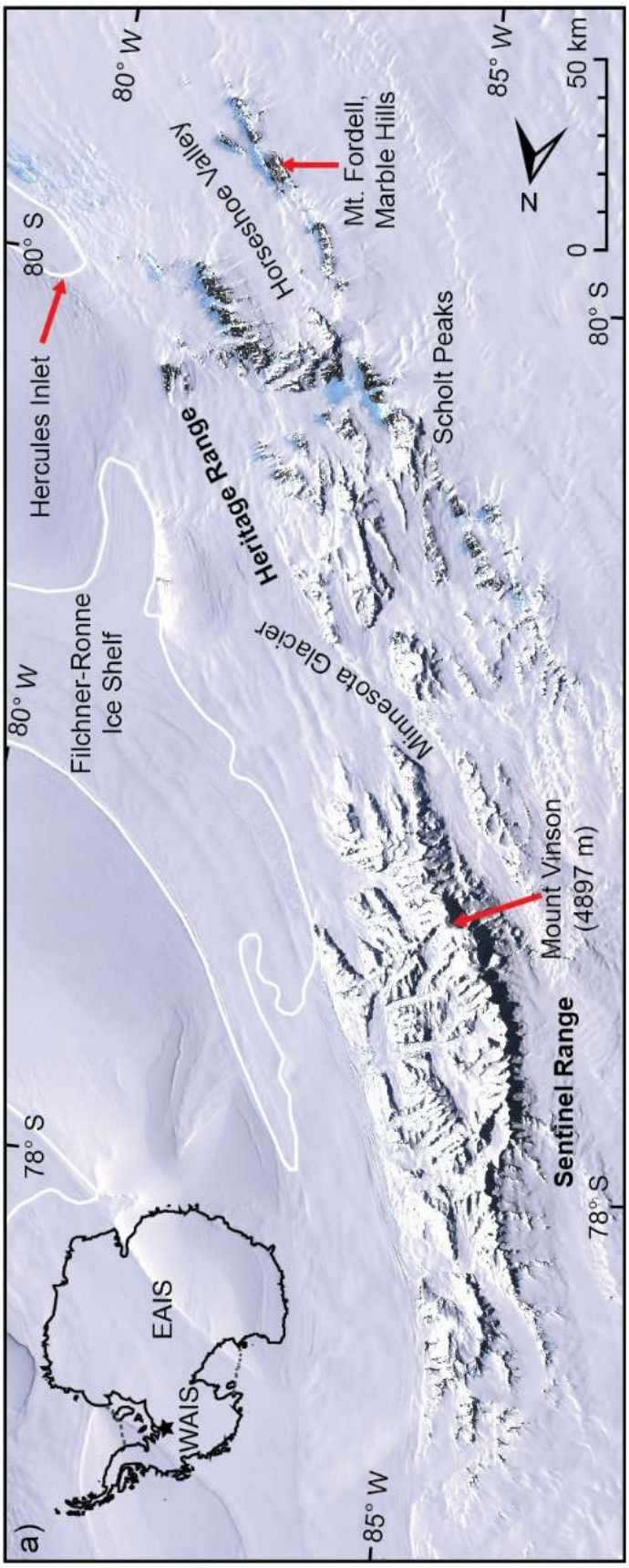

Figure 3.2. Map of the Sentinel and Heritage Range in the Ellsworth Mountains, West Antarctica.

predominantly maritime climate [*Ross et al.,* 2014] would have formed the arêtes, horns and sharp spurs that dominate the lower Heritage Range [*Denton et al*., 1992].

Although recent cosmogenic nuclide dating of bedrock and boulders along the southern Heritage Range has revealed continuous ice sheet conditions for at least 1.4 Ma, *Hein et al*. [2016a] stress that there have been distinct fluctuations in ice sheet thickness in the Weddell Sea sector of Antarctica during this time. For example, it is possible that a regional ice sheet could have dominated the highland areas in and around the Ellsworth Mountains during the Pleistocene, where oscillations in ice thickness would have occurred in response to Pleistocene sea level fluctuations [*Hein et al*., 2016a]. A conceptual reconstruction of this time period, focussed on Marble Hills in the Southern Heritage Range (Figure 3.2) can be seen in Figure 3.3. This figure also details probable ice sheet conditions during the early Last Glacial Maximum (LGM) - a period conventionally defined as the most recent interval in history when global ice sheets reached their maximum integrated volume. *Clark et al.* [2009] suggest that this would have occurred sometime between 29 and 33 ka ago in West Antarctica. A number of studies (e.g. *Bentley et al*. [2010]; *Fogwill et al*. [2012]; *Hein et al*. [2016a, 2016b]) have provided evidence for a long-term trajectory of ice surface lowering in and around the Southern Heritage Range since the LGM. This overall thinning trend (interspersed with slight increases in ice sheet thickness) is expected to have occurred in response to quaternary glacial-interglacial climate and sea level cycles, the most recent of which is expected to have occurred sometime between 6.5 and 3.5 ka ago [*Hein et al*., 2016b]. During this time period it is anticipated that marine downdraw would have instigated a rapid pulse of ice sheet thinning in the Weddell Sea sector of West Antarctica, causing the ice surface in Horseshoe Valley in the southern Heritage Range to drop by ~400 m, to almost present day conditions [*Hein et al*., 2016b]. These conditions are simulated in Figure 3.3c.

Dynamic changes in the ice sheet are expected to have occurred both before, during and after this rapid pulse of thinning, where it is expected that the ice flow regime ~3.5 ka ago would have been different to that of today [*Larter et al*., 2012]. Parallel surface lineations on the

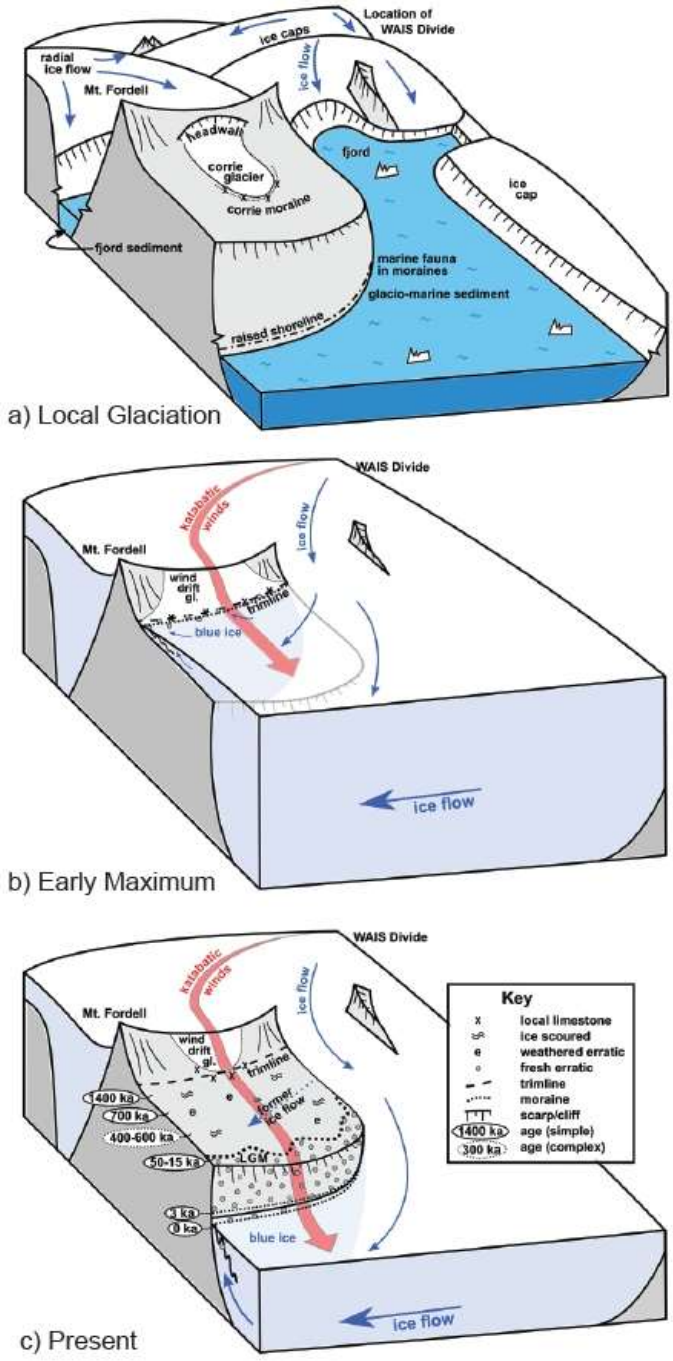

Figure 3.3. A conceptual reconstruction of ice sheet configurations surrounding Marble Hills in the southern Heritage Range, a) shows features that would accompany local glaciation (which could have occurred during the Pleistocene), b) details past maximum blue-ice relationships and c) shows the present minimum. This figure has been adapted from *Hein et al*. [2016a].

Bungenstock Ice Rise (BIR), running at a significantly different angle to modern ice flow have provided the first potential evidence to support these assertions [*Siegert et al*., 2013] (See Chapter 2, section 2.8.2). Assuming that the lineations represent flow stripes, they could epitomise former IIS drainage conditions approximately 0.4 - 4 ka ago, where their orientation suggests that ice flow used to stream over the region now covered by the BIR [*Siegert et al*., 2013]. These findings imply that the prevailing flow regime of the IIS could be very recent, and that local ice stream dynamics have been subjected to significant alterations since the LGM.

Focussing on much more recent periods of time, since the exploration of Antarctica through ground and satellite observations, a variety of measurements have determined that the ice elevation in and around the southern Heritage Range is in a near steady state (e.g. *Casassa et al*. [2004]). However, ablation stake surveys of Horseshoe Glacier, in Horseshoe Valley (southern Heritage Range) since 2000 have recognised a slight but significant ice elevation increase. This ice thickening is likely to be a function of the sheltered nature of the valley, which is fed by sustained accumulation rates of approximately 0.2 – 0.3 m w.e. a^{-1} [*Genthon and Braun*, 1995] (where precipitation is delivered by frontal systems originating in the Weddell Sea [*Wendt et al*., 2009]) as well as low mean annual temperatures, which are estimated to be approximately −28°C [*Dahe et al*., 1994]).

3.3 Ice flows in and around the Heritage Range

Three distinct sub-basins have been detected by airborne RES in and around the Heritage Range (Figure 3.4b, 3.4c). These deep trough systems have been named Horseshoe Valley Trough (after "Horseshoe Valley") at its head, Independence Trough, after the Independence Hills which delimit the northern edge of the trough and the Ellsworth Trough, which is described in detail by *Ross et al*. [2014] amongst others, following the discovery of subglacial Lake Ellsworth in 1966 (see section 2.6). Each of these deep trough systems support thick ice flows which are separated by subglacial mountain ranges and nunataks (Figure 3.4c), which allows

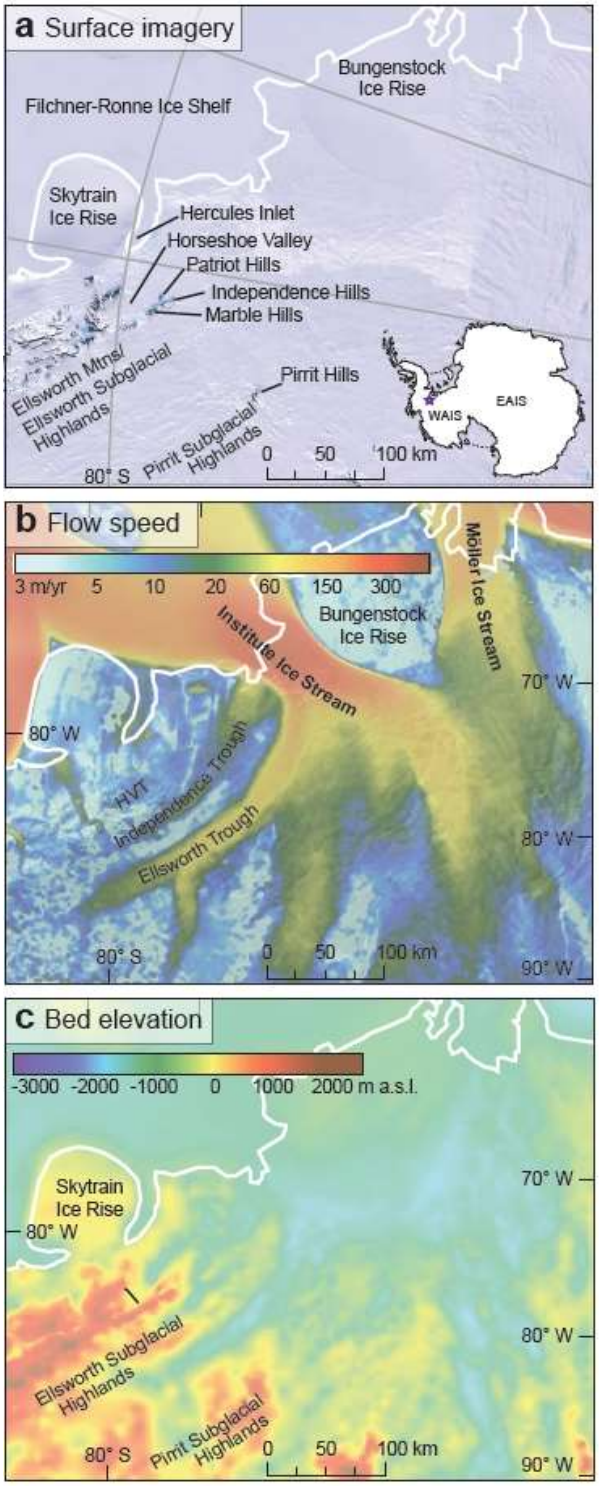

Figure 3.4. Satellite imagery, flow speed and bed elevation of the Institute Ice Stream in the Weddell Sea Sector of the WAIS. Note that the white line indicates the ASAID grounding line [*Bindschadler et al*., 2011]. (a) MODIS and LIMA mosaic, with prominent geographical features labelled (b) Satellite-derived surface ice flow velocities from MEaSUREs [*Rignot et al*., 2011a] superimposed over MODIS satellite imagery [*Haran et al*., 2006] and annotated to show dominant ice streams, the Bungenstock Ice Rise, Horseshoe Valley Trough (HVT), Independence Trough and Ellsworth Trough. (c) Bed elevation, derived from Bedmap2 [*Fretwell et al*., 2013].

interior ice to flow through discrete channels towards the main trunk of the IIS, and ultimately the FRIS in the Weddell Sea (Figure 3.4a).

3.4 Horseshoe Valley

Horseshoe Valley in the Southern Heritage Range (80°018'S, 81°122'W) is situated approximately 300 km from the central WAIS dome and ~45 km from the local grounding line of the FRIS at Hercules Inlet. Ice flows in and around Horseshoe Valley therefore comprise an ideal location to investigate the past and present flow regime of the Weddell Sea sector of the WAIS, in the upper IIS catchment. Horseshoe Valley itself is clearly visible in satellite imagery, where a number of mountains peaks and ridges form a distinct horseshoe shape which disconnects the valley ice flow from other glaciers, like the northward flowing Union Glacier (Figure 3.5). To the north-east the valley is delineated by the Enterprise and Douglas Peaks, whilst the Liberty Marble, Independence and Patriot Hills delimit Horseshoe Valley to the south-west (Figure 3.5). Recent geomorphological analysis and cosmogenic nuclide dating of these massifs suggest that Horseshoe Valley ice flow has remained geologically isolated from the main WAIS, since at least the last glacial cycle [*Fogwill et al*., 2012; *Golledge et al*., 2012; *Hein et al*., 2016a]. This suggests that the ice in Horseshoe Valley is local in origin, where Horseshoe Glacier is fed by in-situ accumulation and ice flow from three main outlet glaciers which pass the Liberty, Marble and Independence Hills [*Genthon and Braun*, 1995]. These glaciers help to drain the inland ice sheet by deflecting flow towards the local FRIS grounding line at Hercules Inlet (Figure 3.4a). A brief description of the Marble, Independence and Patriot Hills has been provided below.

3.5 Marble, Independence and Patriot Hills

The Marble, Independence and Patriot Hills (Figure 3.5) comprise a number of sharp peaks and ridge systems, largely composed of Cambrian limestones that outcrop in grey well-bedded limestones which contain massive marble-like limestones [*Spörli and Craddock*, 1992].

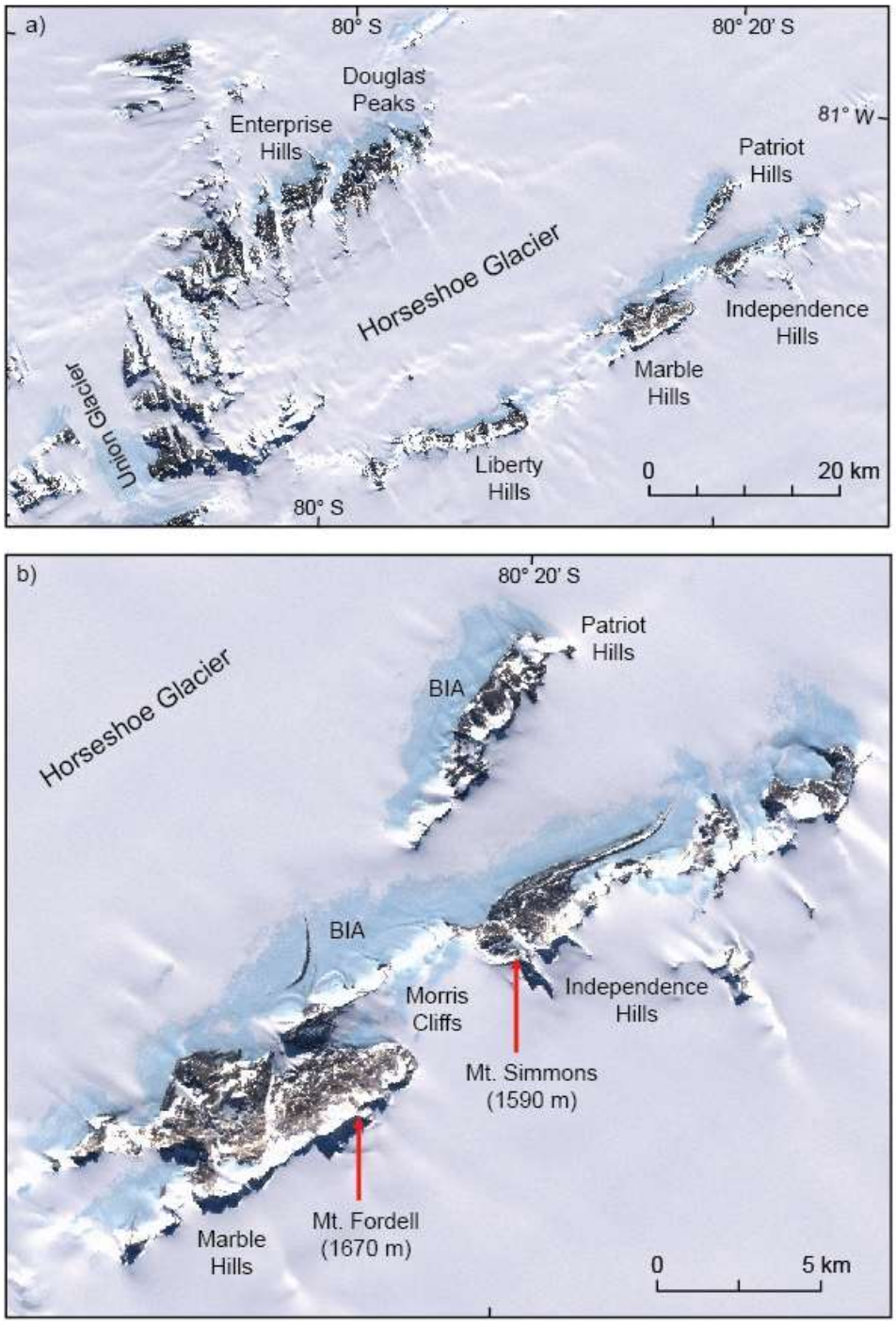

Figure 3.5. MODIS and LIMA mosaic detailing a) Horseshoe Glacier, which is confined by a number of mountain chains which define Horseshoe Valley, and b) a detailed zoom in of the Marble, Independence and Patriot Hills, as well as Morris Cliffs, where large BIAs are recorded on the leeward foreground of each massif.

Conglomerates underlie these limestone systems in Patriot Hills, whilst local limestones, exotic quartzite and basic igneous erratics scatter the surface of the three massifs, at a variety of elevations. Some of these erratics were investigated by *Denton et al*. [1992] during a field campaign of Horseshoe Valley, where geological analysis revealed that several of the more exotic igneous erratics would have derived from the Scholt Peaks, an area some 70 km to the north-north-west of the massifs. Of the three massifs, Marble Hills is the tallest, where the summit of Mount Fordell reaches an elevation of 1670 m above present day sea level. Similarly high peaks are also recorded along Independence Hills, where the tallest peak, Mount Simmons stands at an altitude of 1590 m a.s.l. (Figure 3.5). Morris cliffs is situated between these two ranges, where the steep cliff face separates the high elevation central WAIS flow from the lower elevation Horseshoe Valley ice flow. At the extreme end of Horseshoe Valley and orientated at an angle to the largely linear Liberty, Marble and Independence Hills is Patriot Hills, where ridges reach a maximum elevation of 1246 m a.s.l. These ridge systems are interspersed with a number of bedrock spurs, which constrain large embayments.

3.6 Blue Ice Areas in and around Horseshoe Valley

Although the main ice flow direction in the upper IIS catchment in and around the Ellsworth Mountains is towards the FRIS, some ice flows to the surface to counter-act negative mass balance, caused by katabatic wind scour and enhanced sublimation of the leeward slopes of nunataks which define Horseshoe Valley (see Chapter 2, section 2.5.5 for a full discussion of BIA formation). These strong katabatic winds (estimated to be >30ms^{-1} in Horseshoe Valley [*Carrasco et al*., 2000]) have shaped the local topography of the southern Heritage Range by moving inland snow accumulations to sheltered zones on the stoss sides of the Patriot, Independence, Marble and Liberty Hills, and eroding the leeward slopes of the four massifs. Although prolonged katabatic wind scour has enabled large BIAs to form in front of the massifs [*Hein et al*., 2016a] (Figure 3.5), the exact shape and size of each BIA varies in accordance with local meteorological and ice flow conditions.

3.6.1 Patriot Hills Blue Ice Area

The most widely used and studied BIA in Horseshoe Valley is located in front of Patriot Hills, where the expansive BIA, comprising an area of ~12 km^2 (Figure 3.5), has been accessed as an aircraft runway since 1987. For 25 years, Adventure Network International (later re-branded as Antarctic Logistics and Expeditions) used the ice runway to support commercial and scientific operations, before relocating to nearby Union Glacier (some 60 km to the north-west) a couple of years ago. However, since 1995 Patriot Hills BIA has also been used to support Chile's Antarctic program, where ongoing work has documented the extent of the BIA annually (e.g. *Wendt et al*. [2009] and *Rivera et al*. [2014]). Figure 3.6 shows how these studies have not recorded any significant change in the areal extent of Patriot Hills BIA since measurements began in 1996 - although interannual variability, most likely connected to prevailing meteorological conditions has been recorded [*Wendt et al*., 2009; *Rivera et al*., 2014]. This relative stability encouraged *Turney et al.* [2013] to extract a horizontal climate sequence from Patriot Hills BIA in 2012, where deuterium isotope analysis and cross-correlation revealed a 30,000 year record of climate history. On the whole, these investigations found similar results to more traditional ice core surveys from the continental ice sheet, although two distinct periods of change were noted at ~ ~18 cal ka and ~12 cal ka.

Whilst field work is predominantly focussed on the ice surface of Patriot Hills BIA, some studies have also investigated englacial debris bands and east-west orientated blue ice moraine sequences in front of Patriot Hills (some of these sequences are visible in Figure 3.7). In the late 20^{th} century these deposits were scoured by *Lee et al*. [1998] in search of rare meteorite deposits (which were found to be abundant in other BIAs in Antarctica). However, no meteorites were found during this expedition and indeed, only one meteorite has been collected in front of Patriot Hills to date, when *Grossman and Zipfel* [2001] identified a small meteorite in a moraine band in 2001. These moraine bands lie approximately parallel to the present-day ice sheet margin, where debris accumulates in large embayments, contained by bedrock spurs (like the one visible in Figure 3.7). Several ridge and trough systems can be recognised within the moraine systems, where the bands reach heights of ~20 m and extend for over 4 km down

Figure 3.6. Patriot Hills BIA extent between 1996 and 2008, derived from field GPS measurements and manual digitisation of ASTER images. The Antarctic and Logistic Expeditions (ALE) camp and aircraft runway (L) are marked, as well as a moraine band (M). Background imagery was acquired from ASTER. White arrows indicate dominant ice flow directions. Image and associated data from *Rivera et al*. [2014].

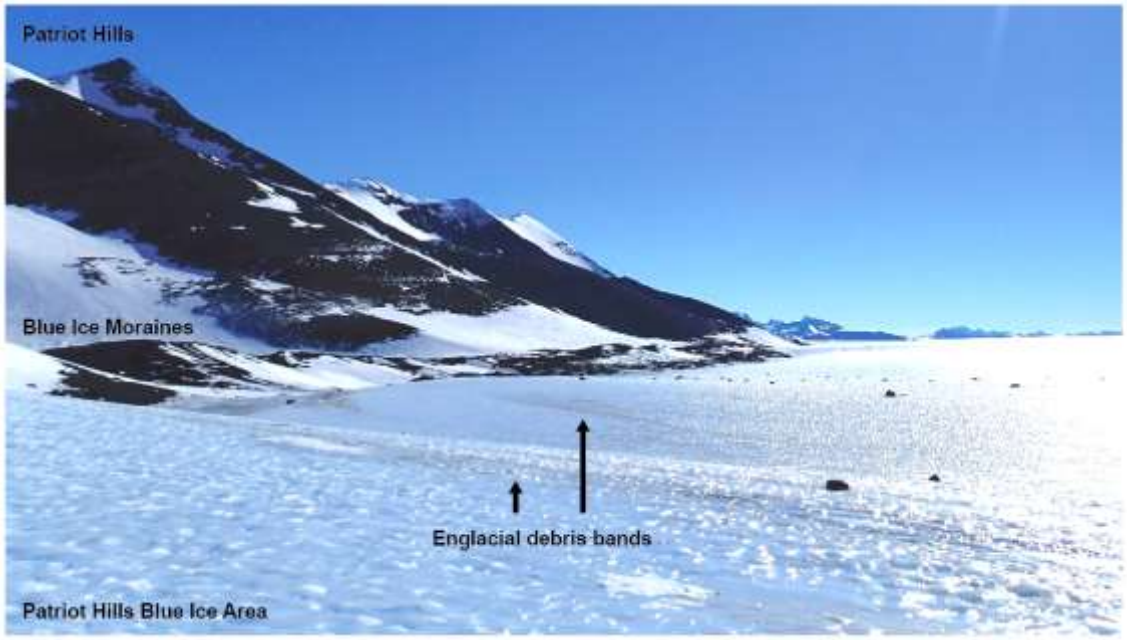

Figure 3.7. Photograph of Patriot Hills BIA, showing the location of blue ice moraines along the mountain range and in the main embayment as well as englacial debris bands and ice surface deposits.

valley, with widths of up to 200 m. Since 2011, three field campaigns, detailed by *Fogwill et al*. [2012] and *Westoby et al*. [2015, 2016] have focussed on researching the geomorphology, geology and history of the moraine sequences in front of Patriot Hills using a variety of techniques including cosmogenic nuclide dating, terrestrial-laser-scanning, structure-from-motion photogrammetry and through the analysis of aerial photos from an unmanned aerial vehicle. A cross section through the blue ice moraine and ice sequence, collected by *Fogwill et al*. [2012] (recorded in Figure 3.8) shows the complexity of the system by detailing the hummocky moraine terraces that sit above the sloping surfaces of Patriot Hills as well as boulder moraine ridges, ice patches, thermokast melt pools, moraine ridges and troughs, folded englacial debris bands (where clasts emerge at the rippled blue ice surface), local and exotic boulders and the elevated firn deposits, which mark the transition between compressional blue ice flow and conventional valley ice flow. By analysing the moraine clasts in detail *Fogwill et al.* [2012] discovered that the moraine ridges are often just one clast thick and although the majority (~80%) of clasts comprise of local lithologies, some other lithologies like sandstone and quartzite (which are exotic to the massif) were also recognised. Recent techniques in Digital Elevation Model (DEM) differencing, applied by *Westoby et al*. [2016] have revealed activity in these blue ice moraine systems, where analysis of data collected over two field seasons has revealed a net uplift and lateral movement of the moraine crest. This movement, which is forced by local ice flow, has been documented in Figure 3.9, where the study by *Westoby et al.* [2016] revealed a mean uplift of 0.10 m over a three month period in the austral summer of 2012/2013, and 0.70 m over a 13 month time period (between two field seasons), ending in February 2014.

3.6.2 Other Blue Ice Areas in Horseshoe Valley

Although Patriot Hills BIA is the most intensively studied BIA in Horseshoe Valley (as a result of its relatively easy accessibility - in terms of aircraft landing), several other BIAs have also been documented in the southern Heritage Range. For example, a number of studies (e.g. *Doake* [1981], *Casassa et al*. [1998], *Bentley et al*. [2010] and *Fogwill et al*. [2012]) have detailed the distinct hooked blue ice moraine sequences in front of Independence Hills, which can be seen in

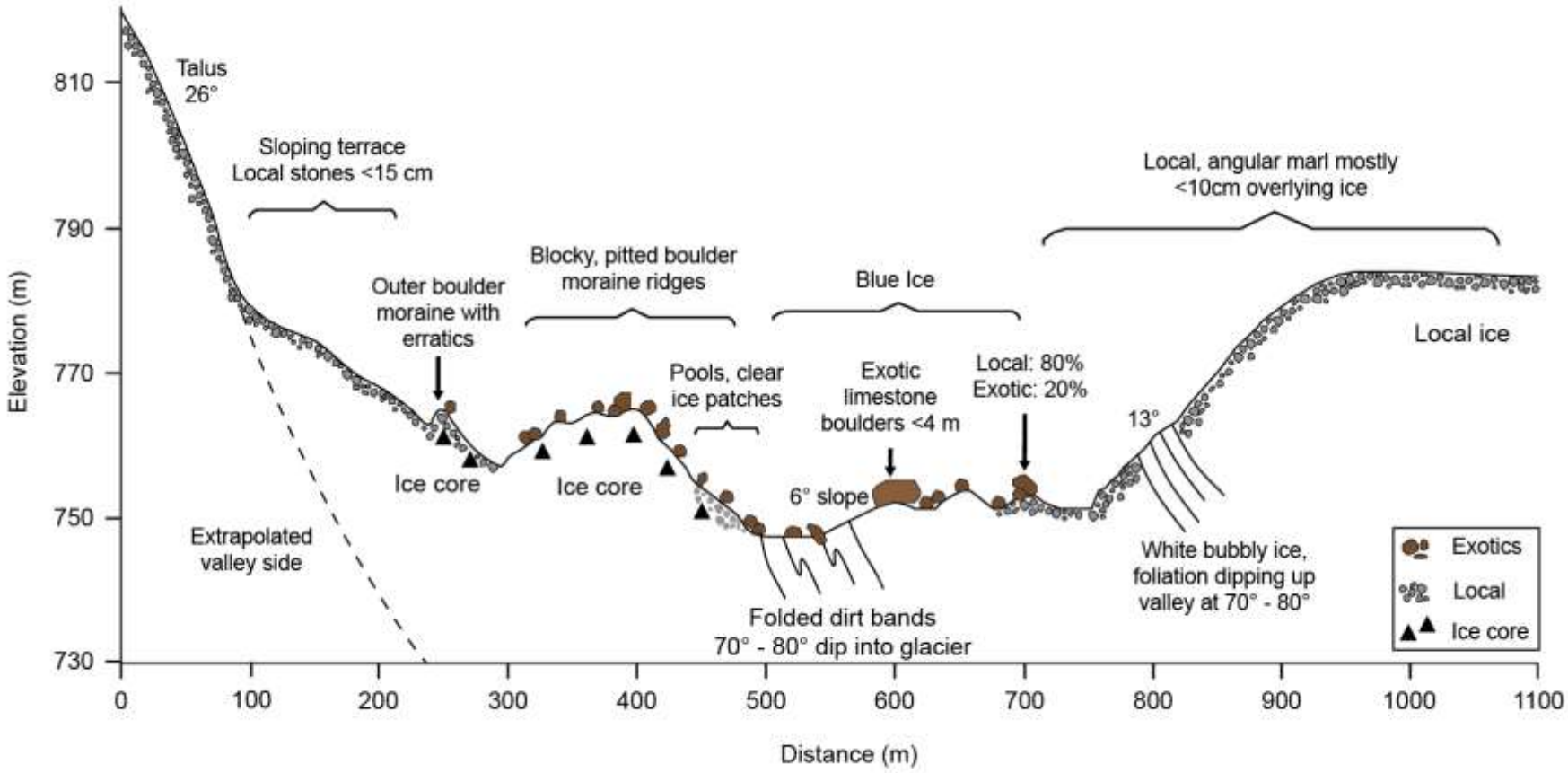

Figure 3.8. Schematic transect of moraine and debris sequences extending from Patriot Hills main embayment. Local talus slopes stretch across the valley side, before more exotic boulders and moraine ridges are encountered, often above ice cored moraines. Folded dirt bands can be seen in the blue ice area before angular marl clasts are recorded above local ice. This figure has been adapted from *Fogwill et al.* [2012].

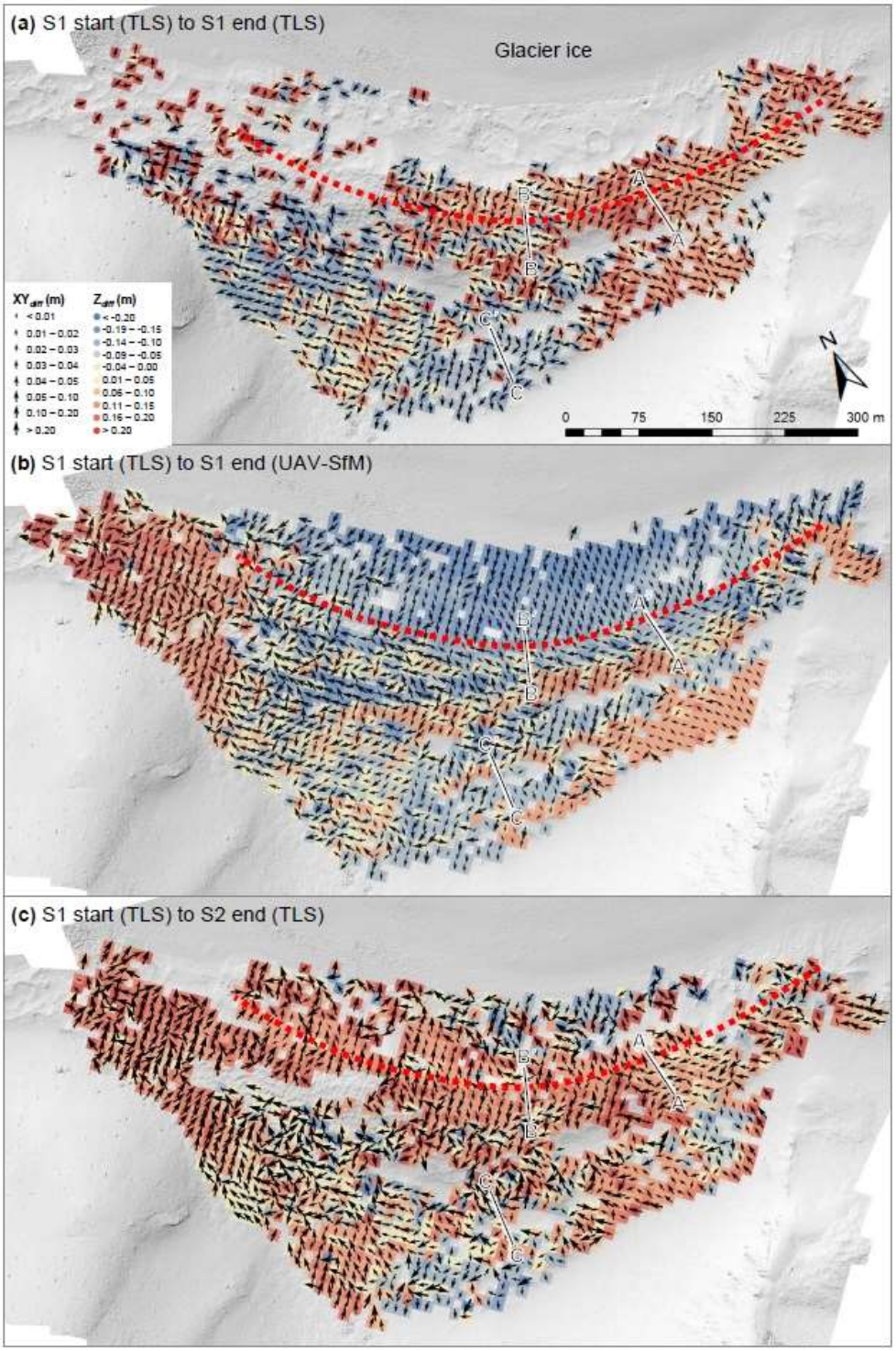

Figure 3.9. Change detection mapping of blue ice moraines in front of Patriot Hills main embayment using a) terrestrial laser scanning data collected at the start and end of season 1 (defining a 3-month period), b) terrestrial laser scanning and unmanned aerial vehicle Structure-from-Motion surveying over the same 3-month period and c) terrestrial laser scanning returns, compared between the start of season 1 and the end of season 2 (defining a 13-month period, ending in February 2014). Horizontal difference vectors (XYdiff) are detailed with black arrows (orientated according to the direction of change) while vertical change (Zdiff) is coloured in the background. Red dashes on all panels shows the approximate location of primary moraine ridge crest, where mean uplift is recorded. This figure has been extracted from *Westoby et al*. [2016].

satellite imagery in Figure 3.5b. These moraine sequences (photographed in Figure 3.10) have recently been described by *Westoby et al*. [2016] who detailed 10 closely spaced parallel moraines (comprising a maximum elevation of 10 km, a length of ~4 km and a width of a few tens of metres) at the foot of a 500 m escarpment (Figure 3.10). Further investigations by *Westoby et al*. [2016] revealed that the lithologic composition of these moraines varies down valley and across ridges as a result of the along-strike variation in the geology of the Independence Hills. Although there are no direct measurements of the shape or size of Independence Hills BIA in the past, the large moraine sequences in the foreground of the mountain chain suggest prolonged katabatic wind scour and sublimation. Similar hypothesis are formed further up valley, where comparably large BIAs and BI moraine systems dominate the leeward slopes of elevated nunataks (including Morris Cliffs, Marble Hills and Liberty Hills) (Figure 3.5).

3.7 Summary

The potential for widespread instability in the Weddell Sea sector of West Antarctica has been highlighted in a number of studies in recent years, where investigations by *Ross et al.* [2014]; *Wright et al*. [2014] and *Siegert et al*. [2016] have stressed that even a slight retreat of the local grounding line between the over-land flowing IIS and the floating FRIS could increase the potential for widespread and possibly irreversible ice sheet drawdown. This fear has been compounded by airborne geophysical RES analysis, which has revealed that 60% of the large IIS catchment lies well below sea level, where there is little small scale topography to act as a pinning point for grounding line retreat. It is therefore imperative to improve our understanding the flow of ice in the upper IIS catchment in and around the Ellsworth Mountains, where IIS tributaries flow through deep trough systems which lie well below sea level.

The range of sites and relatively easy access makes Horseshoe Valley and the surrounding area an ideal site for investigating the past and present ice flow regime of the upper IIS catchment. A variety of local and contemporary studies in the region which focus on climate, mass balance and geology will help to provide a back drop for investigating ice sheet

Figure 3.10. Blue Ice moraine sequences in front of Independence Hills. Photograph courtesy of Dr Shasta Marrero (University of Edinburgh).

dynamics and ice flow history of the upper IIS catchment in and around the Ellsworth Mountains. Geophysical investigations of BIAs and debris entrainment in and around Horseshoe Valley will also help to complete our understanding of local ice flow phenomenon and continent wide debris entrainment mechanisms.

CHAPTER 4

Methodology

This chapter will present a brief background on the uses and capabilities of ice penetrating radar in glaciology. The collection and processing methodologies of GPR and RES data from Horseshoe Valley and the upper Institute Ice Stream catchment will be detailed, along with methods for data analysis, which include manual and automatic classification of radargram features as well as comparisons to recent ice velocity data.

4.1 Introduction to ice penetrating radar

Ice or ground penetrating radar techniques use electromagnetic waves to detect a variety of subsurface features, such as rock, soil and ice, as well as man-made structures like pavements. In cryospheric research, ice penetrating radar has been used since the early 20th century to image ice thickness, to investigate changes in ice flow [*Siegert et al*., 2004a; *Rippin et al*. 2006], to calculate past accumulation rates [*Fahnestock et al*., 2001a], in ice-flow modelling studies [*Conway et al*., 1999; *Siegert et al*., 2003; *Martin et al*., 2006, 2009; *Waddington et al.*, 2007; *Eisen,* 2008] and to constrain layer ages from ice cores [*Waddington et al.*, 2007]. In each case, the radar system is composed of three main components: a transmitting unit, a receiving unit and a control unit, which typically contains a display unit. Both the transmitter and receiver are equipped with similar antennae, which typically contain dipoles. The transmitter's primary function is to generate a pulse of electromagnetic radar waves that penetrate the subsurface, commonly at frequencies between 1 and 1,000 MHz [*Daniels et al*., 1988; *Hubbard and Glasser*, 2005], whilst the receiver is designed to detect both the direct signal travelling straight from the transmitter (the 'airwave') and the components of the transmitted signal that are reflected within the ice body [*Hubbard and Glasser*, 2005] (Figure 4.1). These signal components vary as radar waves are preferentially absorbed or reflected by internal surfaces. The frequency output of the system will depend upon the lengths of the dipole antennae and the

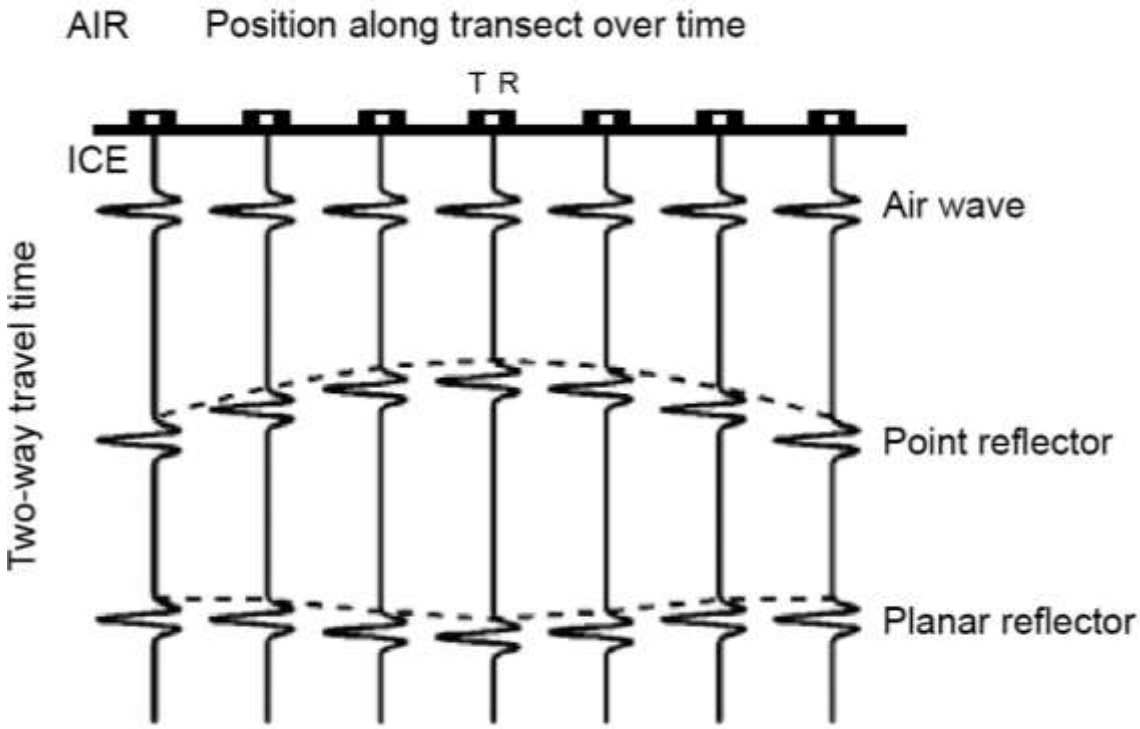

Figure 4.1. Schematic GPR transect showing a transmitter (T) and receiver (R) with a fixed antenna separation on the ice surface. The resultant radar waves are also shown. This Figure has been extracted from *Davis and Annan*, [1989].

material into which the waves are propagated. High frequency antennae, producing short wavelengths, will allow thin layers to be resolved, relative to low frequency antennae which produce longer wavelengths. In essence, the lower the antennae frequency is (i.e. the longer the wavelength), the greater the penetration depth that can be achieved. There is therefore a trade-off between resolution (the thickness of a layer which can be imaged [*Davis and Annan*, 1989]) and penetration depth. The energy received is typically displayed as a plot of signal amplitude against two-way travel time (TWTT) (Figure 4.1). This produces an image of the subsurface beneath the transect line, which includes off-line reflective components.

In glaciological applications, radar wave propagation through ice is principally controlled by two material properties: i) permittivity, and ii) conductivity. Permittivity refers to the capacity of ice to store an electrical charge. This effectively impedes the flow of an applied electrical current. Electrical permittivity is therefore normally described relative to that in free space, and, as such, it should more accurately be referred to as relative permittivity, which is commonly called the dielectric constant [*Hubbard and Glasser*, 2005]. Electrical conductivity on the other hand describes the ability of a material to conduct an electrical current. In ice this is controlled by its ionic or impurity content. *Kulessa* [2007] describes how electrical conduction through ice with high impurity content occurs principally at grain boundaries and triple junctions within the ice, whilst networks of impurities at grain boundaries are more important in ice which has moderate impurity content. Finally, *Kulessa* [2007] also states that electrical conduction through low-impurity ice occurs principally through the movement of protonic point defects. Although the precise effects of impurity characteristics, density and temperature on electrical conductivity are poorly understood *Stillman et al.* [2013] note that electrical conduction through meteoric polar ice is principally controlled by subtle impurities that originate mostly from volcanic eruptions, sea salt and biomass burning. As such, natural polar ice tends to be more conductive than natural temperate ice, where fewer impurities are found [*Hubbard and Glasser*, 2005]. Relative permittivity and electrical conductivity are both important factors to consider when detecting and analysing radar waves, as both can strongly influence radar wave velocity, power loss, resolution and detectability.

Further information on the history of ice penetrating radar, methodological approaches and applications are beyond the scope of this PhD, but can be found in reviews by *Bingham and Siegert* [2007], *Daniels* [1996, 2004] and *Jol* [2009], amongst others.

4.2 Ground penetrating radar

4.2.1 GPR data collection

Several GPR transects have been collected and analysed for this thesis. During each survey Differential Global Positioning System (DGPS) measurements were collected at the same time as GPR returns, in order to locate and topographically correct transect lines. DGPS measurements were collected using a handheld or snowmobile-mounted Trimble GPS unit, linked to a local base station installed above bedrock, at the edge of Patriot Hills. Each GPR line was collected using Northumbria University's PulseEKKO 1000 GPR system. Specifications of this system are detailed in Table 4.1. During GPR collection, in the austral summers of 2012/2013 and 2014 the PulseEKKO system was attached to a wooden sledge, to ensure that the co-polarised antennae consistently maintained a fixed separation distance of 1 m, with their broadsides parallel to each other (Figure 4.2). Once installed, the sledge mounted GPR system was pulled along transect lines in one of two modes depending on the coverage and resolution required; i) common-offset in step-and-collect mode or ii) continuous common-offset survey mode. Each of these methods is described below.

4.2.2 Common-offset step-and-collect mode GPR

Continuous step-and-collect mode surveying was used to record high resolution 200 MHz GPR profiles across Patriot and Independence Hills BIAs and their associated moraine sequences in the austral summer of 2012/2013 (Figure 4.2). In order to resolve detailed subsurface features within BIAs and ice-cored moraines the GPR system was slowly towed or 'stepped' along transect lines, between survey points at 0.1 m intervals, where the GPR could 'collect' data. This method allows GPR location to be precisely controlled, allowing surface features to be

GPR SPECIFICATIONS	
Manufacturer	Sensors and Software Inc., Canada
System	PulseEKKO 1000
System performance	162 dB
Programmable time window	32 – 32767 ns
Programmable sampling interval	10ps - 20000ps in 2ps steps
Programmable stacking	1 – 2048 stacks
Transmitter output voltage	1000 V
Transmitter power	2.1A @ 12V DC
Antennae frequency	225, 450, 900, 1200 MHz

Table 4.1. Specifications of Northumbria Universities GPR system.

Figure 4.2. GPR data collection in Horseshoe Valley, a) shows the Pulse EKKO 1000 system, employed in common-offset step-and-collect mode, where the system records subsurface properties at pre-defined intervals whilst b) shows the set-up of continuous common-offset survey mode data collection, where the sledge-mounted GPR system is towed by a snow-mobile equipped with a DGPS rover.

linked to exact sub-surface radar returns. During data collection a constant time window of 7000 ns was selected, along with an in-field stack of 8. This established but time-intensive method is described in more detail by *Woodward et al.* [2003b].

4.2.3 Continuous common-offset survey mode GPR

Continuous common-offset surveying was employed in 2014 to investigate regional GPR returns, particularly across the BIA/firn margin at Patriot Hills (Figure 4.2). In comparison to step-and-collect mode GPR, this method allows faster data collection, albeit at a reduced resolution. During data collection the sledge-mounted PulseEKKO system was towed by snowmobile at approximately 12 km/hr, with no in-field stacking.

4.2.4 Post-processing of GPR data

Following data collection all GPR surveys were imported into ReflexW radar processing software (version 6.1.1) [*Sandmeier Scientific Software*, 2012] to sharpen the signal waveform by improving the signal to noise ratio [*Reynolds*, 2011]. Standard processing steps [*Welch and Jacobel*, 2005; *Woodward and King*, 2009; *King*, 2011] were applied in order to produce a cross-section of the subsurface electrical properties in terms of two-way wave travel time (TWTT), and then, depth or elevation in m (see figure 4.3). Processing steps to optimise the data series included time-zero correction; high pass frequency filtering (Dewow); bandpass filtering; background removal and diffraction-stack migration. An energy-decay gain was also applied. A brief description of these processing steps is provided below.

Time-zero correction: As it takes a short time for the fibre optic cables to connect the antennae to the computer during a GPR survey, a delay is frequently recorded in the arrival time of the first wave-form (the airwave) from the transmitter. This delay does not remain constant as the

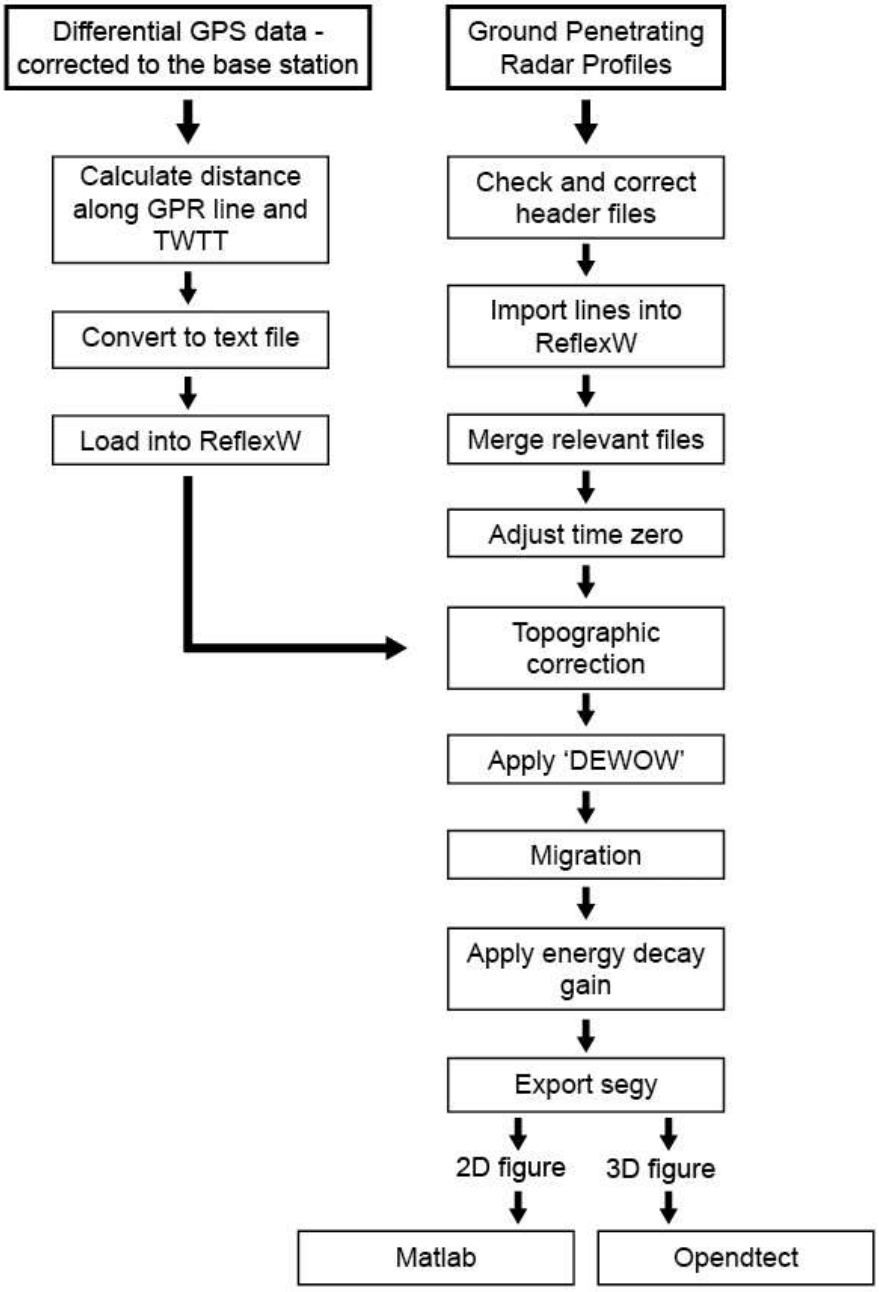

Figure 4.3. Flow diagram detailing the processing sequence applied to GPR profiles. Various processing steps are applied in ReflexW (Sandemeir Scientific Software) to produce the final migrated, topographically corrected GPR reflection profiles displayed throughout this thesis (this chart has been adapted from *Neal* [2004]).

GPR unit warms up to its optimal operating temperature as a survey progresses – creating drift in the arrival time. Time-zero correction removes this drift by aligning the air wave arrival on the radargram.

High pass frequency filtering (Dewow): Low frequency noise (<1 MHz) caused by saturation of the GPR electronics from large amplitude air and direct waves can often obscure real data at higher frequencies [*Jol,* 2009]. *Daniels* [2004] suggest that the exact frequency of this noise, or wow, is a function of the distance between the antennae, the antenna-to-ground coupling and the electrical state of the near surface medium. High pass frequency filtering can be used to eliminate this low frequency part (dewow) by passing frequencies above a specified high pass frequency in the time domain.

Band-pass filtering: This filter acts on each trace independently, to remove unwanted noise at the high and low end of the amplitude spectrum, in the frequency domain [*Woodward et al*., 2003b]. Four frequency values are set to define an upper and lower plateau before a constant-phase filter is applied. This filter prevents events shifting in time, which would result in depth calculation errors.

Background removal: Repetitive noise signals across a whole profile, created by a slight ringing in the antennae can often produce coherent banding effects in a radargram, parallel to the surface wave [*Woodward et al*., 2003b]. To remove these bands of consistent noise background removal can be applied. This processing step performs a subtracting of an averaged trace, which effectively removes the banding without degrading information within the trace [*Woodward et al*., 2003b]. In order to keep real linear events in the profile, such as the air and surface wave, the window at which the filter operates must be specified.

Diffraction-stack migration: Time migration is used to trace reflections and diffraction energy back to their true position or source, using a velocity function [*Daniels*, 2004]. This processing step contracts strong reflectors to a minimum and allows more useful interpretations of the radargram to be made.

Energy-decay gain: This processing step can be applied to compensate for damping or geometric spreading losses in the radargram [*Daniels*, 2004]. By activating this option, a gain curve in the y (time) direction is applied to the complete profile (based on the mean amplitude in the decay curve, which is determined from all existing traces).

Final display: For display purposes depth and topographic corrections were also applied using base-station corrected DGPS data and a standard ice velocity of 0.168 m ns^{-1}. Applying this standard velocity underestimates the depth of firn layers away from the mountains and their associated BIAs. Once processed, all radargrams were plotted in 2D in ReflexW (version 6.1.1) or Matlab (R2013a) (depending on the resolution required), whilst Opendtect seismic interpretation software (2015) was used to plot radargrams in real-space using base-station corrected GPS co-ordinates, to enable three-dimensional analysis of the radargrams.

4.3 Radio-echo sounding

4.3.1 RES data collection

Airborne RES data, collected by the British Antarctic Survey Polarimetric-radar Airborne Science Instrument (PASIN) ice-sounding radar [*Corr et al*., 2007] will also be analysed in this thesis to determine the subglacial topography and englacial stratigraphy of the upper IIS catchment (specifications of this system are detailed in Table 4.2). These data were collected during a traverse of the IIS and MIS during the austral summer of 2010/2011, when the PASIN system was installed on a ski-equipped Twin Otter aircraft (Figure 4.4). Flights were flown in a stepped pattern to optimise the acquisition of gravity data [*Ross et al*., 2012], whilst radar/laser

RES SPECIFICATIONS	
Manufacturer	British Antarctic Survey
System	PASIN
Type	Coherent 2 pulse
Carrier Frequency	150 MHz
Bandwidth	10 MHz
Resolution	0.1 m along track / 8 m depth

Table 4.2. Specifications of the British Antarctic Survey's RES system.

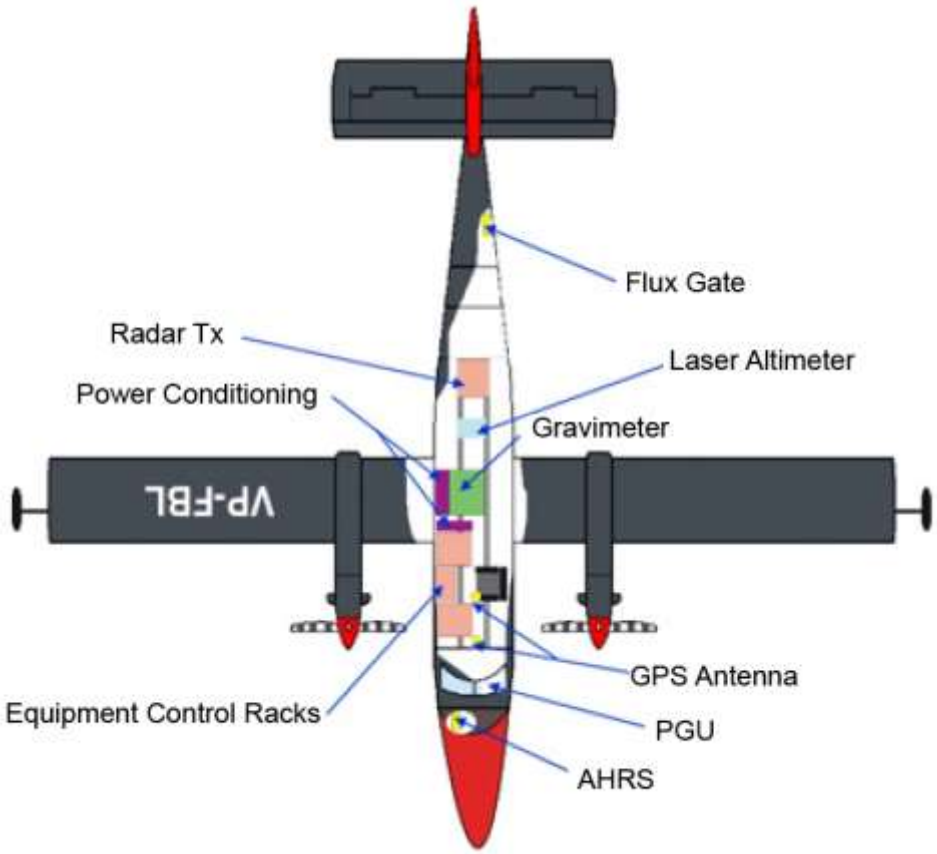

Figure 4.4. Integration of ice penetrating radar onto long-range British Antarctic Survey aircraft. Figure acquired from the British Antarctic Survey.

altimeter terrain-clearance measurements compensated for flight altitude. Aircraft position was obtained from DGPS. During each flight the radar system was operated at a frequency of 150 MHz and a bandwidth of 12 MHz, with a pulse-coded waveform acquisition rate of 312.5 Hz. All RES data were initially pre-processed using Doppler (SAR) processing which was 2D focused. As this processing step is designed to enhance basal features, the uppermost ~150 m of SAR-processed radargrams is often poorly resolved (e.g. Figure 4.5). In order to investigate near-surface reflections, most RES lines were also subject to Chirp and Pulse processing (e.g. Figure 4.5). A visual comparison of these airborne RES processing steps is provided in Figure 4.5. More technical details of the PASIN system are available in *Corr et al*. [2007], and additional details on the acquisition of the airborne RES data are provided in *Ross et al*. [2012].

4.3.2 Post-processing of RES data

Post-processing of RES data was provided by the British Antarctic Survey, who migrated radar-scattering hyperbolae in the along-track direction of flight lines before a natural logarithm was applied to enhance weaker reflections. Conversion of time to depth was achieved by application of a constant two-way travel time of 0.168 m ns^{-1}, offset by a nominal value of 10 m to correct for the firn layer [*Ross et al*., 2012]. Once processed, radargrams were plotted in 2D and 3D using Matlab and Opendtect seismic interpretation software (set in real-space using DGPS data) respectively. Based on crossover analysis of the entire survey, RMS differences of 1.44 m were found in ice surface elevation and 18.29 m in ice thickness measurements, although an RMS error of 20.58 m was obtained for the upper parts of the gridded survey area, which is in part caused by the roughness of the underlying topography [*Ross et al*., 2012]. Further information on processing steps employed by the British Antarctic Survey is provided in *Ross et al*. [2012].

4.4 Analysis of radar-detected internal layering

Following discussions on the formation of englacial layering in Chapter 2 and methods used to collect geophysical data in sections 4.2 and 4.3, this section will now detail conventions for

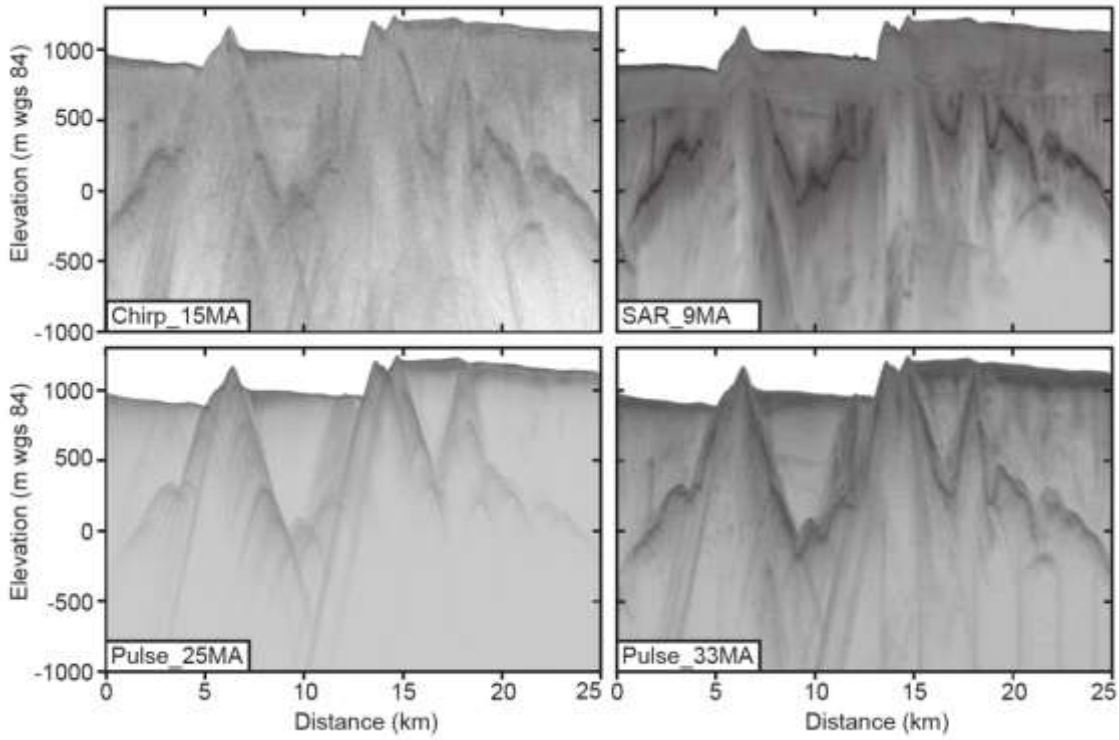

Figure 4.5. Comparisons between various airborne RES processing steps: Chirp (15 MA), SAR (9MA), Pulse (25MA) and Pulse (33MA). It is worth noting that each MA value relates to the number of radar shots that were coherently integrated with a moving average window. Although each processing step creates a visually distinct output (focussing on the bed or surface etc.), in each case, RES returns detect the surface, basal topography and strong englacial features.

analysing ice penetrating radar detected englacial stratigraphy. To begin with, it is widely agreed that all englacial features resolved by geophysical means should be described in terms of their reflection continuity, dip angle and relationship to other reflections (e.g. *Neal* [2004]) (Figure 4.6). Once described, internal layers can then be classified into one of two broad categories; continuous or discontinuous layering. These terms are frequently used in geophysical surveys (e.g. *Rippin et al*. [2003]; *Siegert et al*. [2003]; *Bingham et al*. [2007] and *Karlsson et al*. [2009]) to define either continuous, well-defined layering, which comprises of internal layers which predominantly follow the surface and/or bed topography or discontinuous, buckled or disrupted layering which denotes internal-layer geometries that substantially diverge from the bed and/or surface. Continuous layering is primarily located in regions which currently experience or have experienced slow-flowing ice, which is defined here, in the upper IIS catchment as ice flow $\leq$30 m a^{-1} which has undergone little motion. In contrast, disrupted layering is often coincident with areas that have previously encountered, or are currently experiencing enhanced flow (defined here as >30 m a^{-1}), or at the boundary between areas of slow and enhanced flow [*Karlsson et al*., 2009]. In this thesis, the term "enhanced flow" is distinct from the term "fast flow" because the latter term is often equated with more extreme ice speeds in ice streams. However, previous studies (e.g. *Bingham et al*. [2007]) have shown that even the more modest speeds attained by ice-stream tributaries are all that is required to produce disruptions to internal layering.

In this thesis, interpretations of ice penetrating radar detected internal stratigraphy will follow two established approaches, which work at different scales: 1) manual, qualitative interpretations will be used for detailed analysis of local ice penetrating radar data whilst 2) automated, quantitative interpretations will be used to examine more regional airborne RES returns. The first approach highlights internal stratigraphy through manual digitisation of radargrams, where obvious features are marked by continuous black lines, whilst less discernible features are highlighted by dashed lines. The second approach uses a faster, automated Internal Layering Continuity Index (ILCI) to characterise regions of apparently

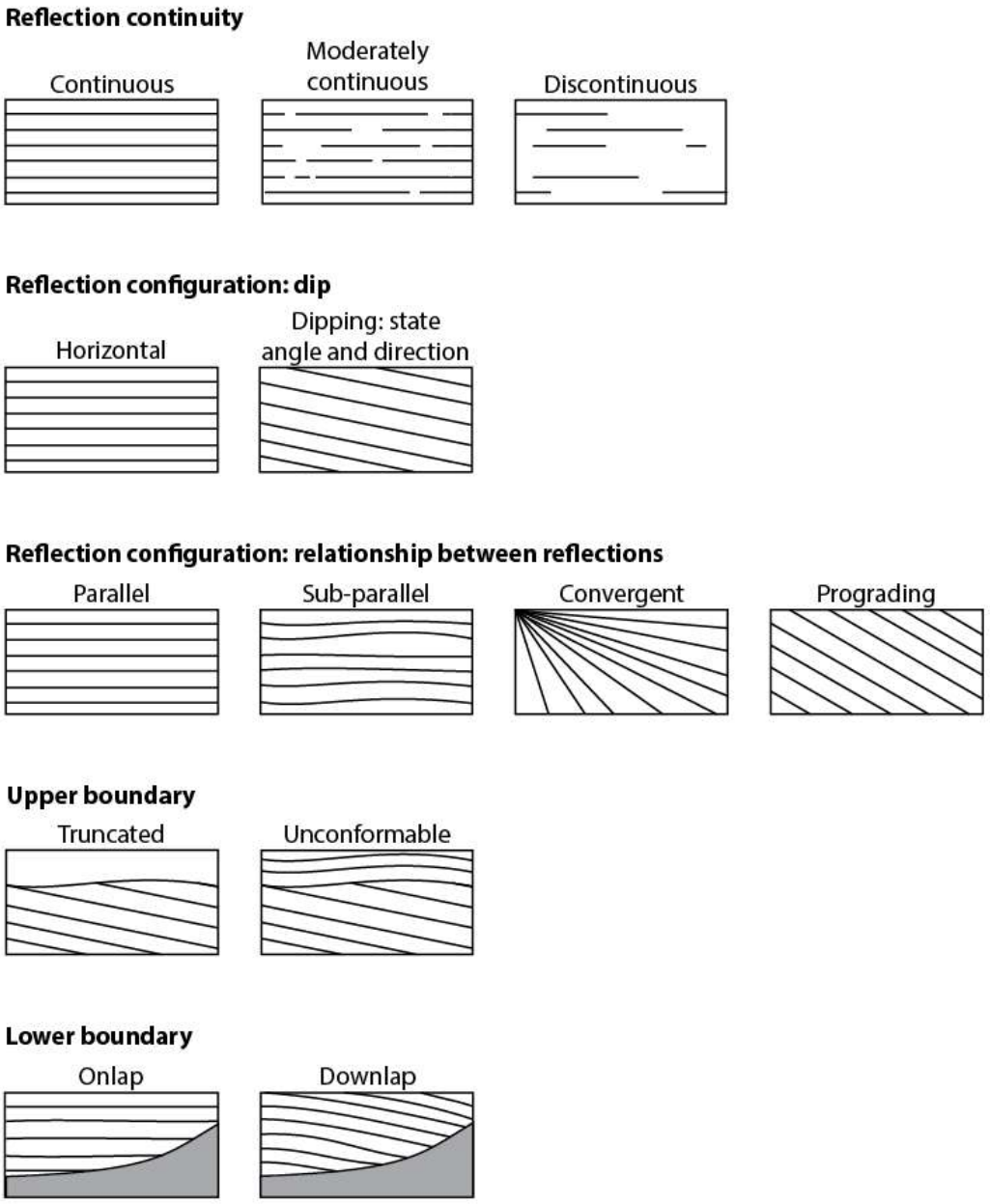

Figure 4.6. Ice penetrating radar internal reflection terminology, modified from *Neal* [2004].

continuous versus disrupted internal layering from large-scale RES data sets. The ILCI, developed by *Karlsson et al*. [2012], and recently applied to the wider catchments of IIS and MIS by *Bingham et al*. [2015], uses A-scope plots of each RES trace (each trace representing a stack of ten consecutive raw traces to minimise noise [*Karlsson et al*., 2012]) to record peaks of high reflected relative power, bounded by values of lower reflected relative power. Using the relative changes in power (uniform in value across all study sites) the continuity of internal layers can be determined at a full-depth profile scale, or percentage layer scale, as areas with clear internal layers will return a high continuity index (0.06 - 0.10), whilst A-scopes interrogated where layering is absent will return a low continuity index (0 - 0.03). This leaves disrupted internal layering to return an intermediate value (0.03 - 0.06), where low and intermediate values have been interpreted to represent present or previously enhanced flow, which is characterised by disrupted layer packages interspersed with regions of little to no layering.

4.5 Surface velocity data

Surface velocity data, acquired from the MEaSUREs InSAR-based Antarctica Ice Velocity Map [*Rignot et al*., 2011a] will also be used throughout this thesis to compare radar returns to current ice flow velocities. The digital mosaic was created by *Rignot et al.* [2011b] using ALOS PALSAR, RADARSAT-1, RADARSAT-2, ERS-1, ERS-2 and Envisat Advanced Synthetic Aperture radar sensors which each covered discrete areas of Antarctica from 1996 – 2009. Nominal errors, associated with the precision of ice flow mapping do exist, and vary within the digital mosaic depending on data collection methods, the type of instrument used, the geographic location, the time period and repeat cycle of the instrument, as well as the amount of data stacking. Using the error map form *Rignot et al*. [2011b] the precision of ice flow mapping in the upper IIS catchment is estimated to be 4.2 m a^{-1}.

4.6 Summary

In this thesis a variety of ice penetrating radar surveys will be collected and analysed to investigate ice flow and englacial debris entrainment in and around Horseshoe Valley. Methods of data collection and analysis follow well-established approaches, used by all geophysical researchers in cryospheric settings. As GPR and RES operate at different scales and frequencies, radargrams acquired from each method will be discussed and analysed individually in 2D and 3D, before datasets are combined with ice velocity data for regional and historic analysis.

CHAPTER 5

Ground penetrating radar

Several high-resolution GPR transects will be investigated in this chapter to assess the continuity of a BIA horizontal climate record from Patriot Hills published by *Turney et al*. [2013]. Results are combined with PISM model simulations and RES-derived ILCI plots to determine the evolution of ice sheet flow in Horseshoe Valley over the last 30,000 years. This chapter includes and expands upon work published by *Winter et al*., [2016].

Ground penetrating radar objective

Analyse englacial stratigraphy within the Blue Ice Area at Patriot Hills to determine historic changes in ice flow and/or accumulation.

Research questions

1) Can ground penetrating radar be used to examine BIA?
2) Is the BIA horizontal climate record at Patriot Hills continuous?
3) Can the climate record at Patriot Hills be relied upon?
4) Is there evidence for growth and/or stabilisation of Patriot Hills BIA?

5.1 Introduction

This chapter uses high-resolution GPR transects to record the internal stratigraphy of Patriot Hills BIA in Horseshoe Valley. In 2013 a 900 m long central BIA transect (transect A), extending perpendicular from Patriot Hills (Figure 5.1) was surveyed using GPR in continuous step-and-collect mode to examine the continuity of an 800 m long climate transect published by *Turney et al*. [2013]. Three 100 m long crosslines were also surveyed in continuous step-and-collect mode during this period, intersecting transect A at 200 m, 500 m and 800 m along the

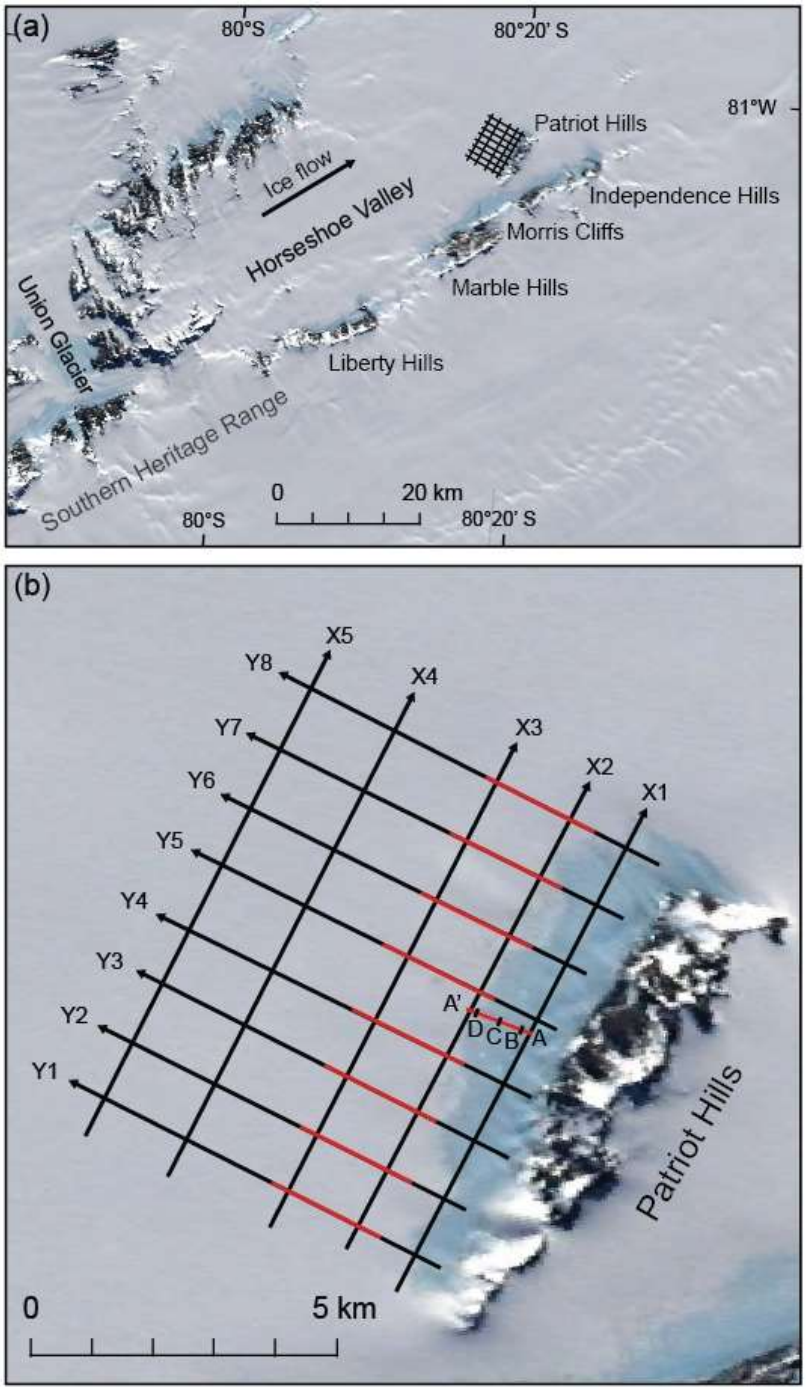

Figure 5.1. (a) MODIS mosaic [*Haran et al*., 2006] showing the location of GPR transects in front of Patriot Hills, Horseshoe Valley. Ice flows from the head of the Horseshoe Valley towards Patriot Hills. (b) Zoom in of the nested ground penetrating radar grid (X1-X5, Y1-Y8) and the climate transect (A), with cross lines (B-D). Red lines show the location and extent of ground penetrating radar profiles displayed in 2D in this chapter. Arrows show the direction of data collection away from the mountains (A, Y1-Y8) and down valley (X1-X5, B-D).

profile (Figure 5.2). In 2014 snowmobile-towed common-offset surveying was also employed for wider analysis of Patriot Hills BIA and firn. These surveys provided a nested grid of high frequency lines (approximately 7 x 9 km with 1 km x 1.5 km grid cells) extending from the BIA moraine margin towards the centre of Horseshoe Valley (Figure 5.1). All GPR surveys have been analysed in conjunction with pre-existing Parallel Ice-Sheet Model simulations and ILCI plots at pre-defined depth intervals of 0-20% (uppermost ice column), 40-60% and 80-100% ice thickness, to place GPR findings into an historical context.

5.2 Results

5.2.1 Ground penetrating radar

Returns from GPR transect A, surveyed along Patriot Hills BIA are displayed in 3D in figure 5.2. This figure is annotated to show the beginning of the 800 m long climate transect, which starts 100 m along the GPR profile, as well as the intersection of crosslines B, C and D. Figure 5.2b shows each of these crosslines in detail, where internal horizons representing former ice sheet surfaces are recorded throughout the 250 m deep profile, although, like inline A, reflection strength decreases with depth (as a function of radar attenuation) which limits the analysis of deep internal layers. In order to investigate the detailed internal structure of transect A, and indeed Patriot Hills BIA, Figure 5.3 focusses on the uppermost 50 m of the transect, along the 800 m long climate line. This figure reveals a number of steeply dipping isochrones which are punctuated by shallow (2 m) ice core sites at 100 and 200 m along the transect where *Turney et al.* [2013] extracted ice for climate analysis. Ignoring the reflections from the boreholes, it is clear that continuous, conformable, steeply dipping (inclined by 24° - 45° towards Patriot Hills) isochrones dominate the radargram, where they are recorded from 0 m – 246 m, 249 m – 359 m and 362 m – 800 m. Here, the internal reflectors strike from the lower ice column up towards the BIA surface. However, at 247 m and 360 m there are discontinuities in the isochrone layers (highlighted in red and labelled D1 and D2 in Figure 5.3), where divergent isochrones represent significant changes in isochrone dip angle. Figure 5.3b focusses on these features, where the

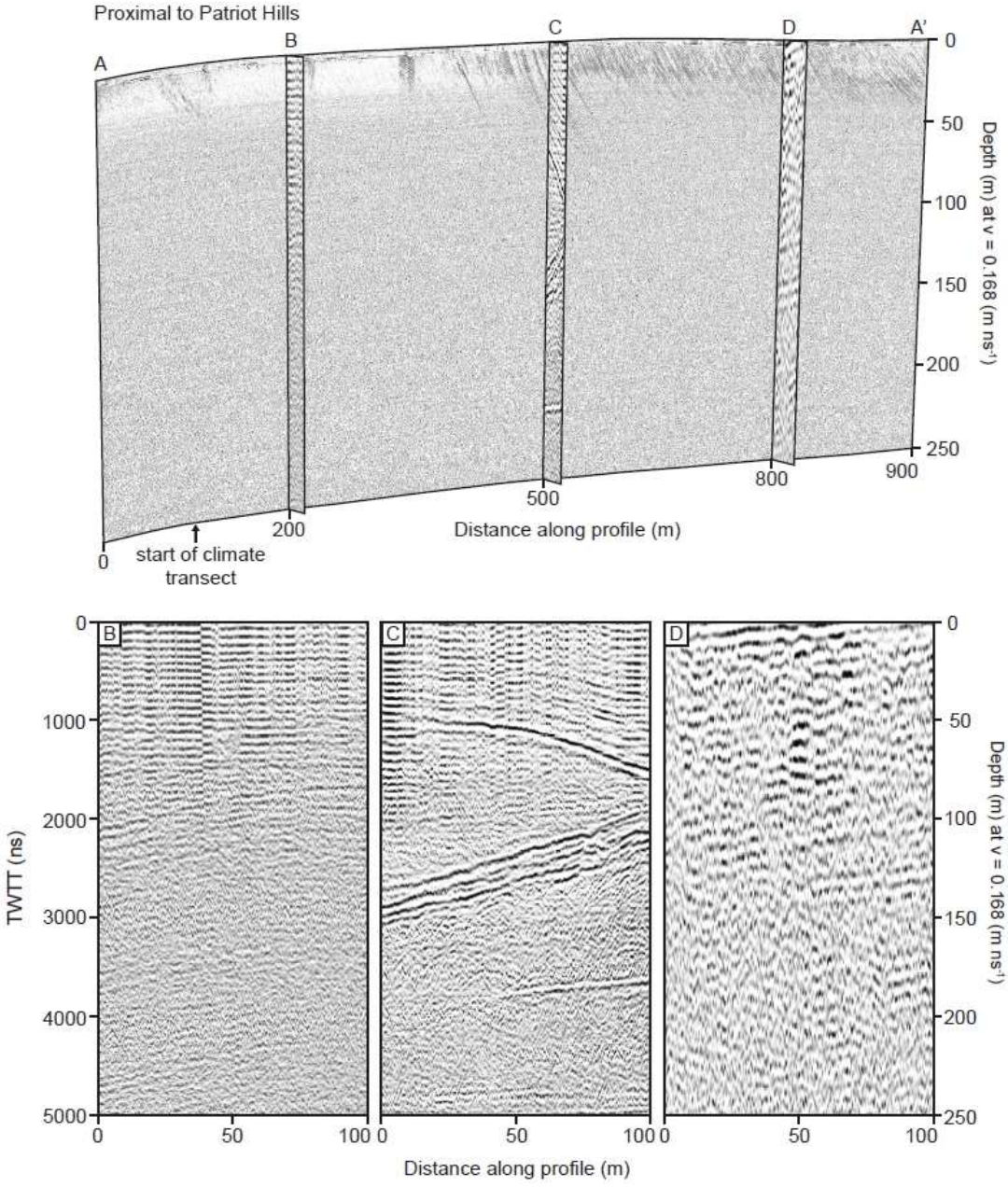

Figure 5.2. Three-dimensional transect along Patriot Hills Blue Ice Area showing the intersection between transect A and cross lines B, C, D which are shown in detail in the lower panel. The start of the 9800 m long climate transect, beginning at 100 m along transect A is also highlighted.

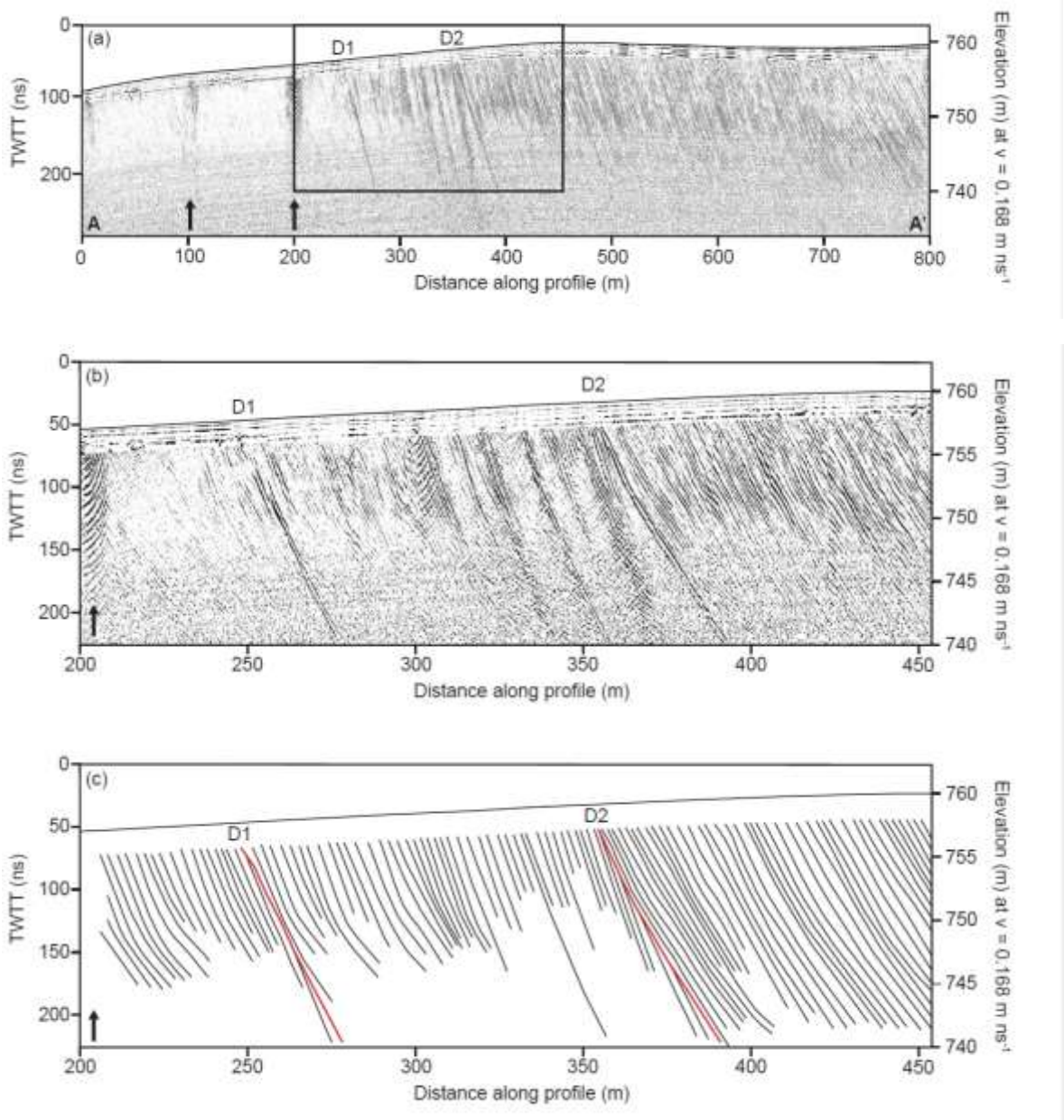

Figure 5.3. (a) Ground penetrating radar transect A, collected along Patriot Hills Blue Ice Area climate line. The black box represents the spatial extent of (b) and (c) which focus on two discontinuities (D1 and D2) that show changes in dip in an otherwise conformable englacial sequence. Both discontinuities are associated with the truncation of isochrones. D1 is located 247 m along the radar profile, whilst D2 is situated 360 m along the transect.

radargram and digitised transect (Figure 5.3b and 5.3c) reveal that D1 and D2 are associated with the truncation of isochrones.

By comparing GPR transect A with the climate record published by *Turney et al.* [2013] in Figure 5.4, it is evident that discontinuities D1 and D2 correlate to rapid changes in the trend of the deuterium isotopic record (δD) at approximately 18 cal ka and 12 cal ka [*Turney et al*., 2013]. These rapid changes had previously been highlighted by *Turney et al*. [2013], in the form of shaded bands B1 and B2 (Figure 5.4 d) where B1 marks the transition from a low average δD rate to a rising trend in δD concentrations (where δD increases from -380 to -254‰), whilst B2 marks a very rapid rise in δD concentrations (from -300 to -254‰), after which a higher average ratio continues for the remainder of the profile. Combined with a third band, B3 *Turney et al.* [2013] suggested that these zones could reflect significant fluctuations in temperature and/or precipitation during both the late Pleistocene and Holocene. However, unlike B1 and B2, further analysis of GPR transect A reveals no evidence of divergent or truncated isochrones at any other location along the profile, even at B3 (~ 8 cal ka), where a depletion in deuterium isotope content is recorded.

Examples from the snowmobile-towed GPR grid, collected for wider analysis of the BIA and firn, are displayed as a three-dimensional grid in Figure 5.5 and in two-dimensional inline transects (surveyed perpendicular to Patriot Hills) in Figure 5.6 and 5.7. Compared to GPR in step-and collect mode this method is much faster, allowing a larger area to be surveyed, albeit at a decreased resolution (see chapter 4, section 4.22 and 4.23). As such, the snowmobile-towed GPR can only resolve distinct features in Patriot Hills BIA, where there is a sharp dielectric contrast. In the BIA, these features are largely limited to D1 and D2, which are clearly recorded in inline profiles Y1-Y8 (e.g. Profile Y1, Figure 5.5) as well as the ice/bed interface which is reflected at the beginning of each inline profile (Figure 5.5).

Although the BIA is poorly resolved by the snowmobile towed GPR, numerous internal horizons can be identified at the BIA/firn margin, and indeed well into the firn zone, as the inline transects extend towards the centre of Horseshoe Valley. At the margin, internal reflectors

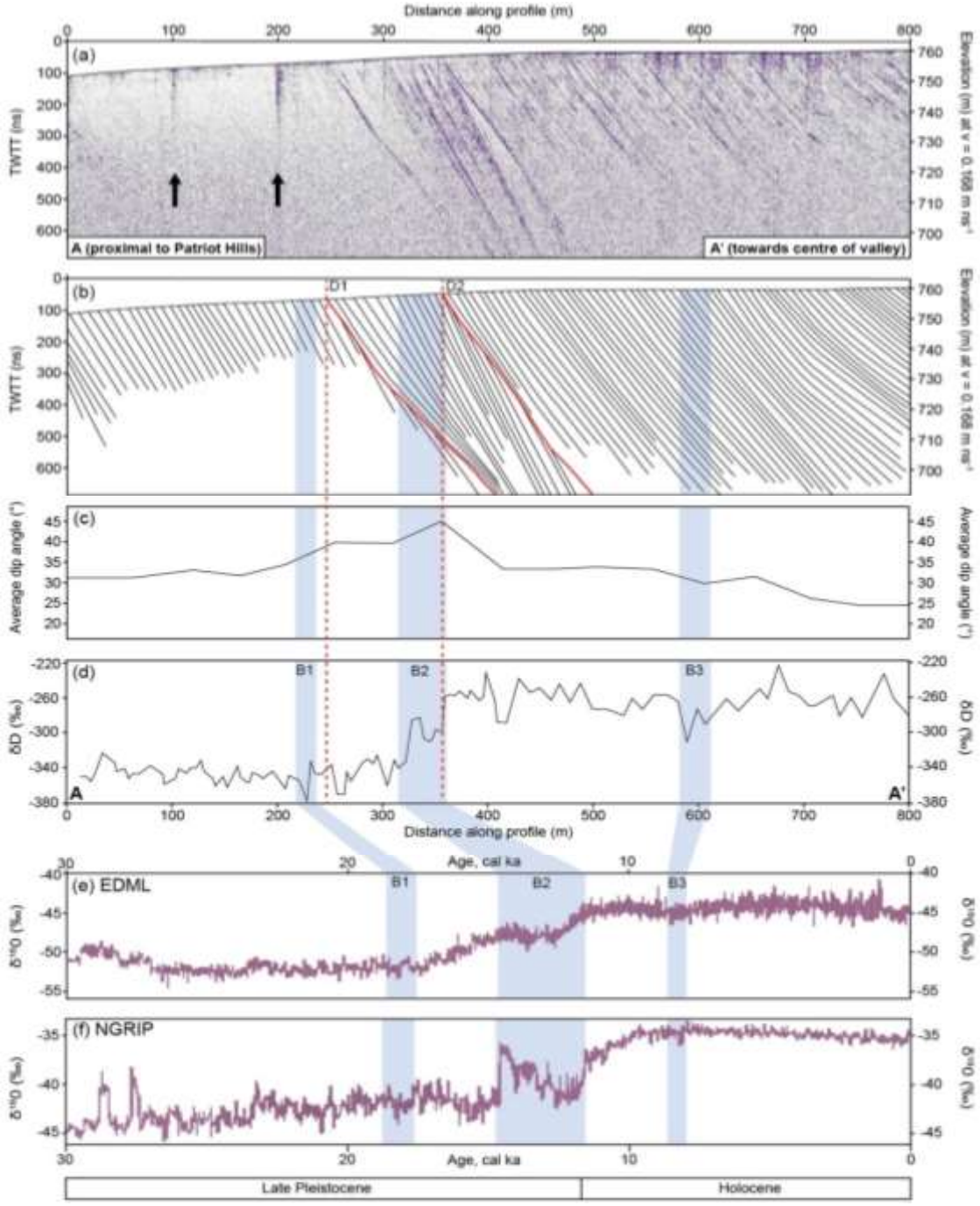

Figure 5.4. Visual comparisons between GPR returns and deuterium isotope records along a central BIA transect, extending from Patriot Hills (a) Ground penetrating radar transect A records the subsurface internal layer structure of Patriot Hills BIA (arrows indicate vertical noise from boreholes). (b) Picked, prominent internal GPR reflectors showing two locations where the internal reflectors are disturbed, i.e. showing changes in dip and discontinuity. D1 is at 247 m and D2 at 360 m along the transect. (c) Spatial variability of internal reflector dip angles in the along-line direction (averaged over 20 m intervals), and (d) Patriot Hills deuterium isotope record (δD) collected by *Turney et al*. [2013] in 2012. Shaded bands B1, B2 and B3 are inferred points of correlation with (e) the EPICA EDML δ18 O record [*EPICA*, 2006] (on the GICC05 timescale) and (f) the North Greenland ice core δ18 O [*Rasmussen et al*., 2006] as shown in Figure 4 of *Turney et al*. [2013].

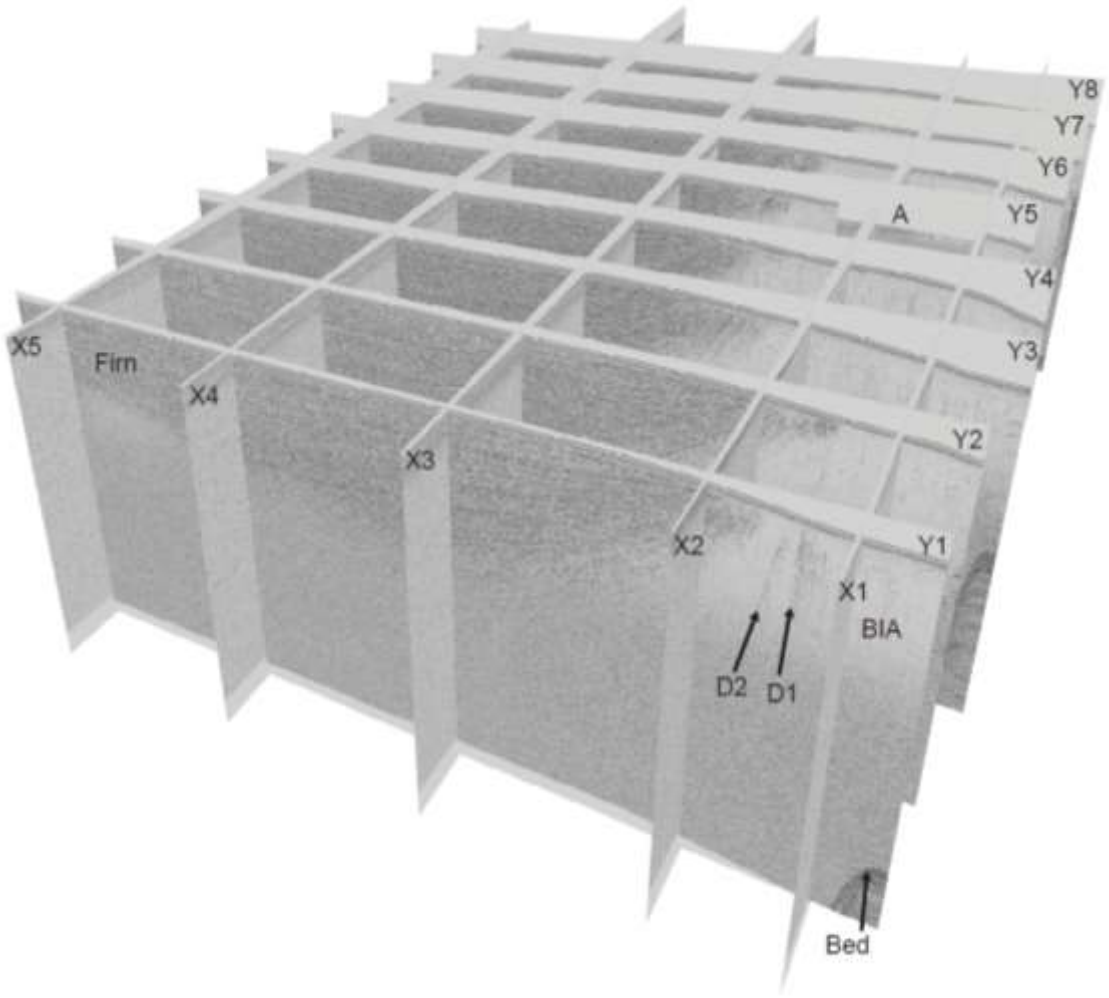

Figure 5.5. Snow-mobile towed GPR returns reveal poorly-resolved englacial stratigraphy in the dense BIA of Patriot Hills, although prominent reflectors, including D1, D2 and the bed are visible in most inline transects. The detailed firn sequences, digitised in 2D in figures 5.6 and 5.7 are well-resolved in 3D, in both inlines and cross lines.

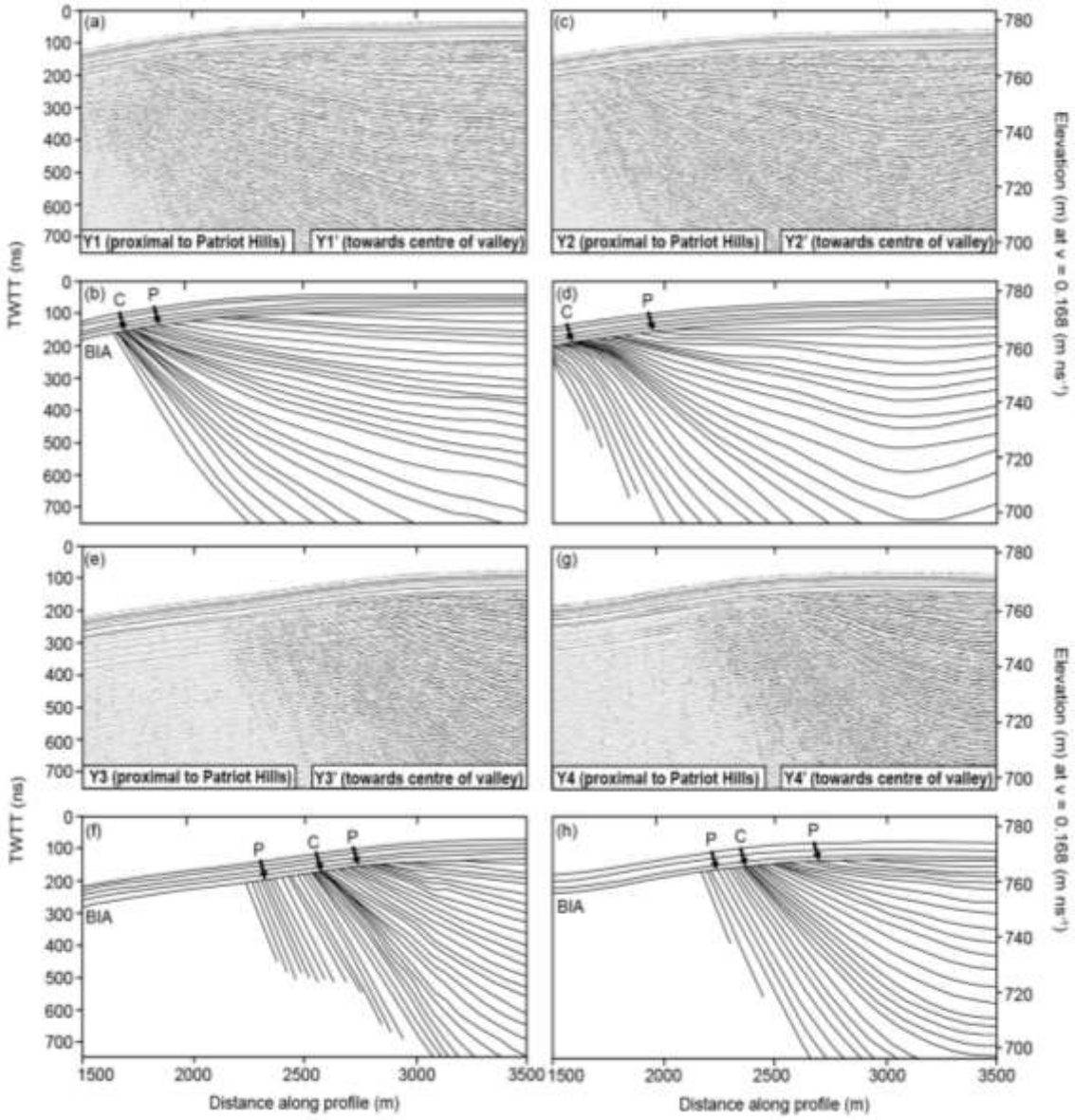

Figure 5.6. Snowmobile-towed 200 MHz ground penetrating radar cross lines. (a), (c), (e) and (g) all display elevation-corrected GPR profiles, where prominent internal reflectors have been picked and digitised to form (b), (d), (f) and (g), where prograding (P) and convergent (C) isochrone sequences are clearly visible.

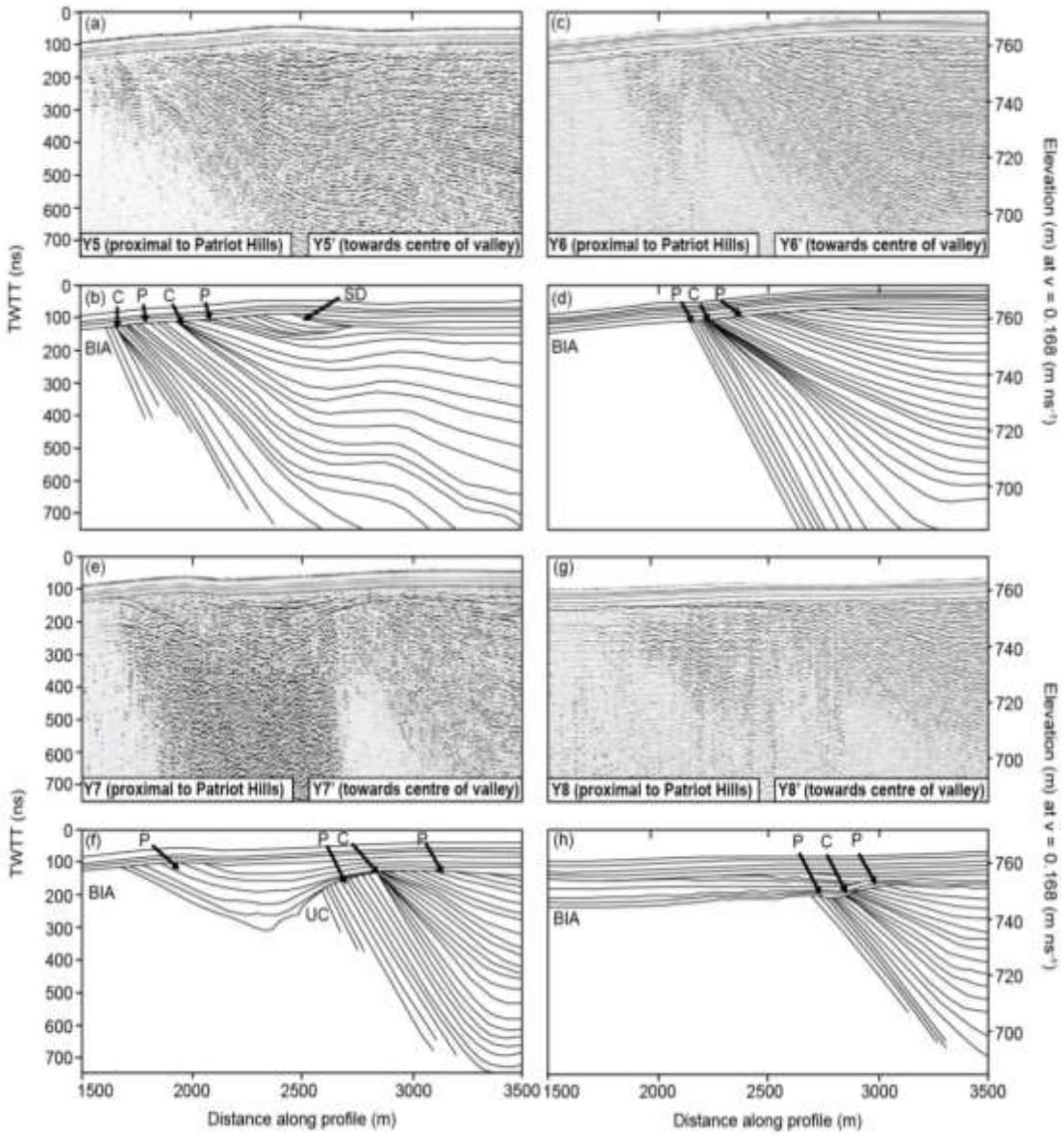

Figure 5.7. More snowmobile-towed 200 MHz ground penetrating radar cross lines. Like figure 5.6, (a), (c), (e) and (g) all display elevation-corrected GPR profiles, where prominent internal reflectors have been picked and digitised to form (b), (d), (f) and (g), where prograding (P) and convergent (C) isochrone sequences are clearly visible in each transect. Profiles Y5 and Y7 also display unique features; a snow drift (SD) is recorded in profile Y5, whilst a stratigraphic unconformity (UC) can be seen in Y7, where shallow dipping (2° apparent dip towards Patriot Hills) internal reflectors are overlain by younger near - horizontal firn layers.

record a net upward ice flow component, where isochrones are compressed and inclined to a maximum dip angle of 5°. However, as the transect extends away from Patriot Hills and the BIA, the steeply dipping internal reflectors smoothly transition to more horizontal and parallel firn layers which are recorded to a depth of 140 m below the surface, where radar reflection strength meets background noise levels.

The transition between blue ice and firn is recorded and displayed for each inline transect in Figures 5.6 and 5.7. Each of these radargrams reveal a relatively featureless BIA, followed by sequences of convergent and prograding isochrones (see Figure 4.7 for a definition of internal reflection terminology), where englacial layers gently transition from inclined layers to more horizontal layers, as the radargram extends away from Patriot Hills. Although profiles Y1 and Y2 (Figure 5.6) display a similar pattern of englacial stratigraphy, where convergent and then prograding isochrones are recorded immediately after the BIA, profiles Y3 and Y4 (Figure 5.6) exhibit a change to a prograding-convergent-prograding isochrone sequence, which occurs when Patriot Hills BIA increases in size, and extends further into Horseshoe Valley. In profile Y5 a larger convergent-prograding isochrone sequence is recorded, where layers are tightly compacted between the BIA and a shallow snow drift (~9 m thick) which extends 440 m along the former, near horizontal firn surface. Although the next snowmobile-towed GPR line (Y6) is only 1 km down valley from profile Y5, the large snow drift is no longer visible in this inline transect. Instead, profile Y6 displays a prograding-convergent-prograding sequence ~2150 m along the transect line, after the now enlarged and still featureless BIA. The only erosional unconformity to be discovered in the snow-mobile towed GPR grid is revealed in profile Y7 (Figure 5.7) where gently sloping (2° apparent dip towards Patriot Hills) internal horizons reveal a prograding-convergent-prograding sequence overlain by younger, near horizontal firn layers between 2690 m and 3149 m along the transect. These almost horizontal layers more than double in thickness with increasing distance from Patriot Hills. Again, this feature is not recorded 1 km down valley in Profile Y8, where a thicker horizontal firn sequence is recorded above a prograding-convergent-prograding isochrone sequence (Figure 5.7).

5.2.2 Ice-sheet model simulations

In order to place GPR findings into a regional and historic context, simulated regional ice flux models for Horseshoe Valley and the upper IIS catchment (provided by Dr. Nicholas Golledge, Victoria University of Wellington, New Zealand) were consulted (Figure 5.8). These Parallel Ice-Sheet model perturbations help to explain the initial response of the LGM ice sheet to ocean and atmospheric forcing. Although model runs simulate high discharge rates through all major troughs surrounding Horseshoe Valley, each simulation (representing time intervals) shows that no major ice flux or flow direction change is expected to have occurred in Horseshoe Valley since the mid-Holocene. Indeed, the simulations show that even with a rapid increase in ice flux in response to ocean warming and sea level rise (at 15,000 model years) [*Golledge et al*., 2012], modelled ice flowing into the IIS continues to discharge through Rutford Trough (Figure 5.8b), even when flow accelerates at the ice margins. As such, these model runs imply that continued oceanic forcing and grounding line retreat had no direct impact on the flow of ice around Patriot Hills, even when ice discharging into the main trunk of the IIS was diverted in a more east-south-easterly direction towards the Thiel Trough during the mid-to-late-Holocene (Figure 5.8c, lower panel).

5.2.3 Internal Layer Continuity Index (ILCI) plots

Although regional model simulations by Dr. Nicholas Golledge have suggested that no major ice flux or flow direction change occurred in Horseshoe Valley during the mid-Holocene, it is also important to analyse local field evidence, in the form of deep airborne RES transects, collected by Dr. Neil Ross and colleagues. ILCI plots across a central transect line in Horseshoe Valley (Figure 5.9) demonstrate that the uppermost ice in Horseshoe Valley (0-20% of the ice column) is dominated by continuous internal layering, indicative of slow flow, while older ice at 40-60% ice thickness and then 80-100% of the ice column return progressively higher ILCI values. Following methodologies reported in Chapter 4, these high ILCI values, sourced at depth, provide evidence for previously enhanced ice flow in Horseshoe Valley (more

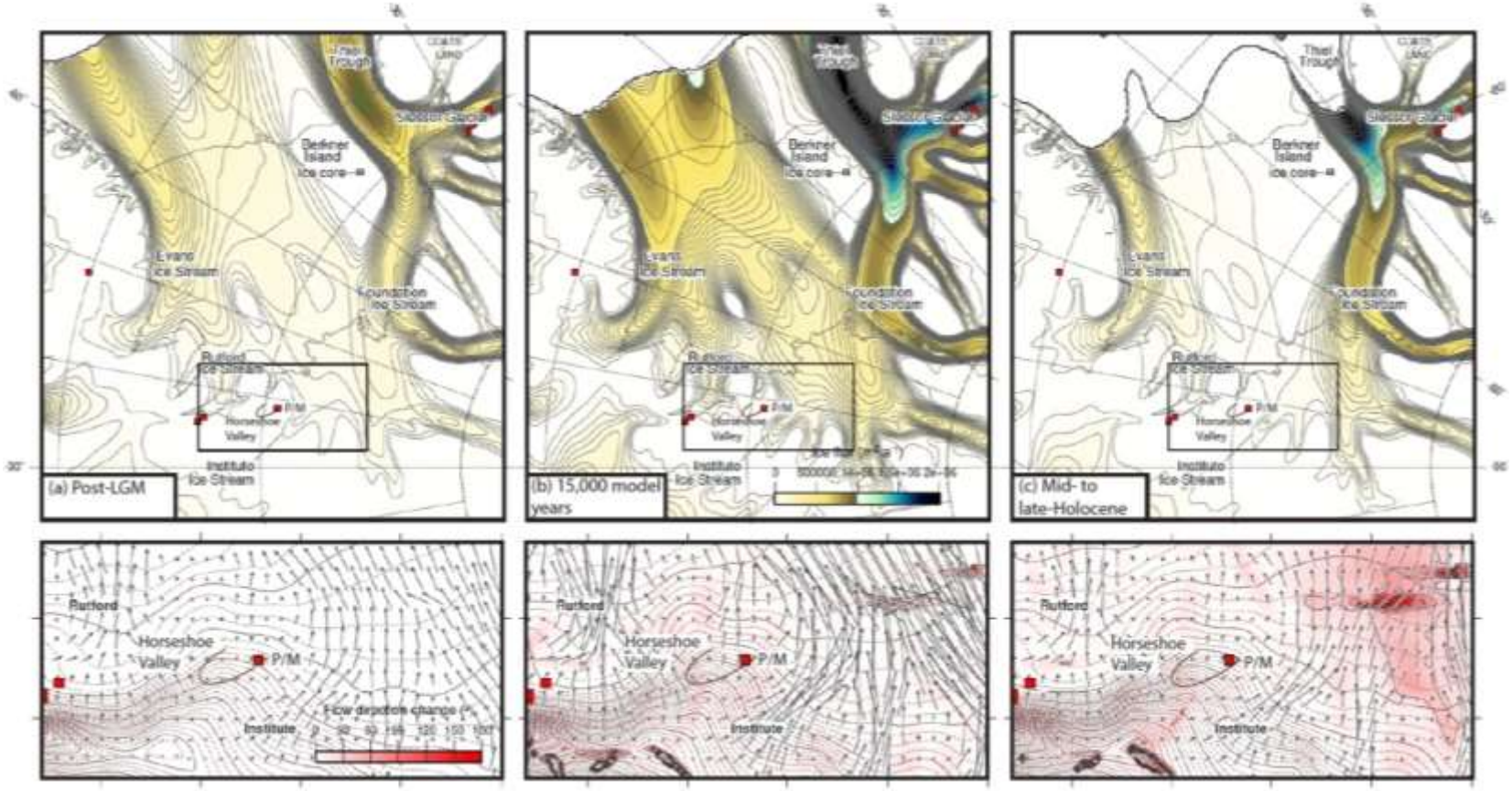

Figure 5.8. Simulated regional ice flux, generated from Parallel Ice-Sheet Model simulations, capturing configurations representative of (a) post-LGM, (b) 15,000 model years and (c) the mid- to late-Holocene response of the ice sheet to ocean and atmospheric forcing. Model results show that continued forcings do not impact the flow direction of ice around Patriot and Marble Hills (P/M), even when ice discharging into Institute Ice Stream is diverted in a more east-south-easterly direction towards Thiel Trough during the mid- to late-Holocene [*Winter et al.*, 2016]

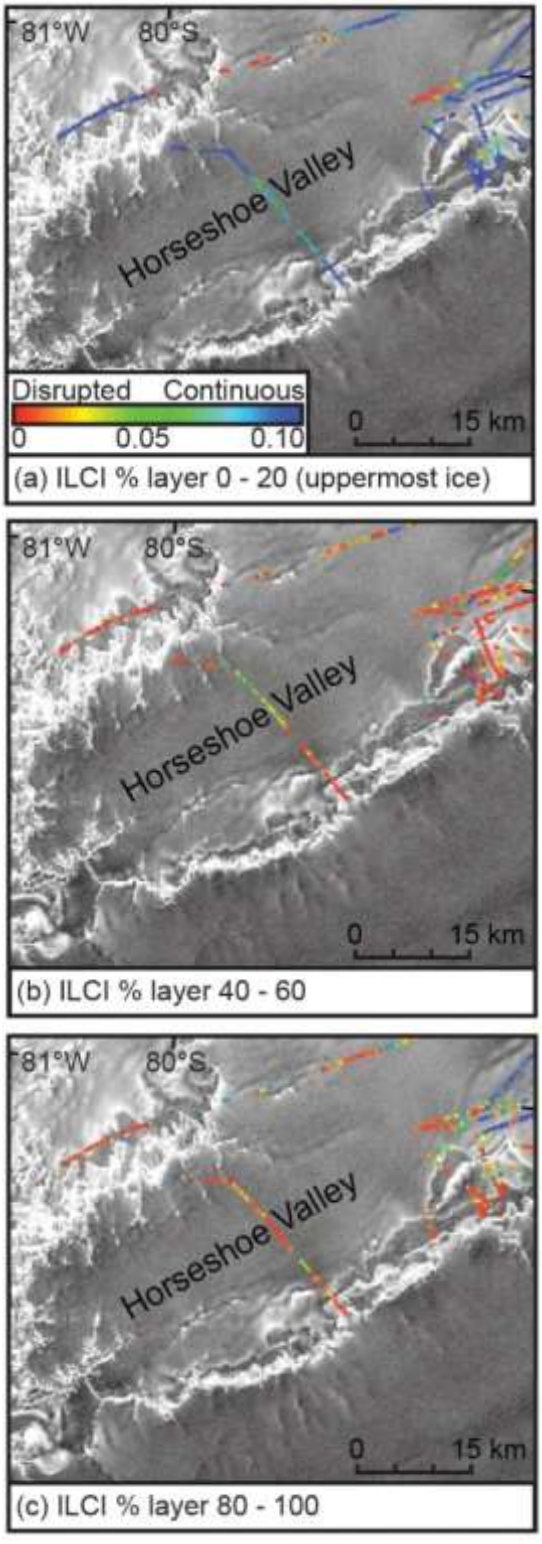

Figure 5.9. ILCI results from airborne RES flight lines across Horseshoe Valley (using 100 trace moving windows) at various depth intervals, (a) % layer 0-20 reveals high ILCI values indicative of continuous layering in the uppermost ice column, (b) % layer 40-60 in the central ice column shows both continuous and disrupted internal layering, while (c) % layer 80-100 shows the most disrupted and discontinuous layering at depth. These plots, superimposed onto a RADARSAT mosaic [*Haran et al*., 2006] reveal that ice flow in Horseshoe Valley has been stable and slow-flowing in recent years.

information is provided in Chapter 6 and the resultant paper – *Winter et al*. [2015]). As this enhanced ice flow is not recorded in any of the mid-Holocene to post-LGM PISM perturbations, it is expected that the disrupted englacial layering recorded deep within Horseshoe Valley ice flow formed near the start of the Holocene period, or possibly, even earlier (depending on the speed of ice excavation).

5.3 Discussion

By combining findings form GPR transects with ice sheet model simulations and ILCI analysis, it has been possible to constrain the evolution of Patriot Hills BIA, and better understand historic ice flow in Horseshoe Valley. The central BIA GPR transect A has revealed a sequence of largely conformable isochrones, which are inclined towards Patriot Hills BIA surface (to compensate for the negative mass balance promoted by katabatic wind scour and enhanced sublimation which create BIAs – see Chapter 2, section 2.5.6). Minor changes in the dip angle of these predominantly parallel internal horizons have been recorded, and are expected as a result of differential snow deposition, burial and subsequent ice flow over time but the pronounced changes in dip angles at D1 and D2 (Figures 5.3 and 5.4) represent larger scale change. These discontinuities, associated with truncated isochrones, correspond to abrupt shifts in the local climate record between ~18 cal ka (B1) and ~12 cal ka (B2) (Figure 5.4) and therefore represent breaks in an otherwise largely unbroken 30,000 year climate record. These breaks, given new context by the unconformities in GPR Transect A, could have formed by one of two mechanisms: (i) changes in ice flowline trajectory, or (ii) by the local interaction of topography, snow accumulation and wind.

As ice-sheet model simulations and ILCI analysis suggest that ice in Horseshoe Valley has not experienced directional change (Figure 5.8) and has remained slow-flowing (Figure 5.9) since the mid-Holocene, the possibility that discontinuities D1 and D2 were formed by changes in ice flow-line trajectory can largely be eliminated. However, these simulations do not rule out significant periods of erosion which could have resulted from the interaction of topography,

snow accumulation and wind as ice flows from the head of Horseshoe Valley towards Patriot Hills (Figure 5.10). It is therefore expected that discontinuities D1 and D2, corresponding to changes in deuterium isotope concentrations at B1 and B2 (Figure 5.4d), were created by localised katabatic wind scour of the former snow and ice surface as ice flowed along its present-day trajectory, through BIAs in front of Liberty and Marble Hills (Figure 5.10). Consequently, it seems probable that deuterium isotope incursions B1 and B2 do not directly represent abrupt climatic changes, but instead reflect breaks in the otherwise conformable climate record. As no other erosional events are found in the GPR record, it is assumed that other inferred depletions in the deuterium isotopes, such as that at B3 (Figure 5.4d), could reflect direct climatic changes during the early Holocene, and indeed may correlate with changes in other ice cores as suggested by *Turney et al*. [2013].

The findings from the extended radar grid are in close agreement with the high resolution BIA transect. Here the inline profiles show more recent periods of BIA stability and instability, reflected by convergent and prograding isochrones in the firn zone. Prograding isochrones in the GPR record (Figures 5.6 – 5.7) are attributed to increased katabatic wind scour, and subsequent BIA expansion since the LGM. This is likely the result of surface lowering in Horseshoe Valley of up to ~400 m since the LGM [*Hein et al.,* 2016b], which would have revealed more of the nunataks in the Southern Heritage Range, capable of promoting stronger katabatic wind scour. In contrast, younger convergent isochrones in the GPR record (Figures 5.6 and 5.7) represent more stable meteorological conditions, where katabatic winds of consistent velocity and direction have produced a transition zone between all annual snowfall to no snowfall scoured. If these transition zones are in the same location annually, convergent layering will result. It should be noted that this phenomenon also requires slow and stable ice flow. The sequences of BIA growth and stabilisation from the larger snowmobile-towed GPR grid combine to identify an evolving BIA over the past ~1,000 years, which is consistent with the previously analysed 30,000 year ice flow records. Like the boreholes recorded in GPR Transect A, the unconformable surface firn in profile Y7 and the snow drift in profile Y5 (Figure 5.7) have anthropogenic origins which, this time, are attributed

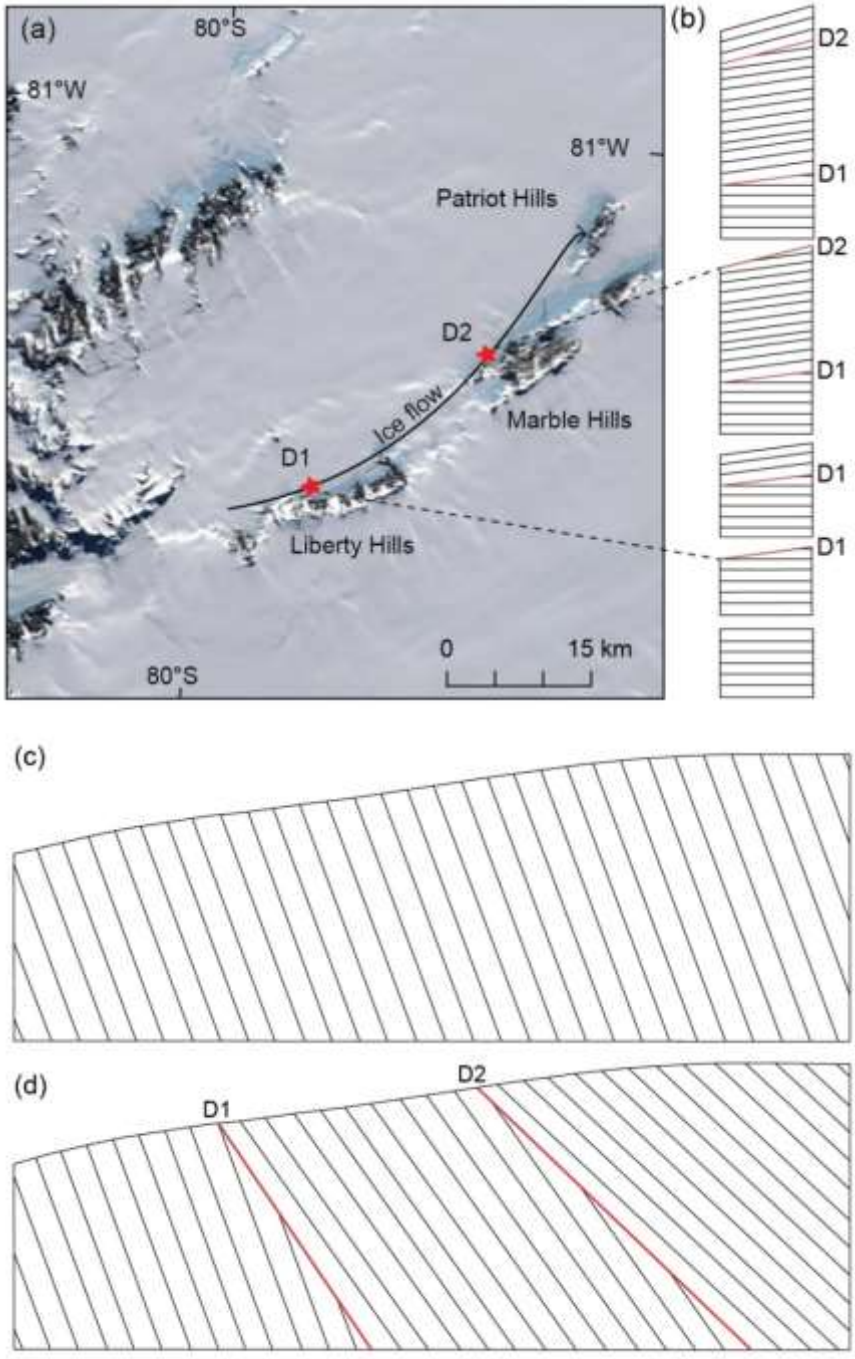

Figure 5.10. (a) Inferred ice flow path from the head of Horseshoe Valley to Patriot Hills (MODIS background image [*Haran et al*., 2006]), where discontinuities D1 and D2 formed as a result of Blue Ice Area wind scour in front of Liberty and Marble Hills, (b) schematic stratigraphic succession, indicating ice accumulation punctuated by two periods of erosion (red lines), (c) lowermost panel of (b) rotated 90 degrees to show an inferred cross section of unbroken snow/firn stratigraphy and, (d) uppermost panel of (b) rotated to show the observed GPR stratigraphic sequence at Patriot Hills BIA, where red lines indicate erosional events D1 and D2.

to the recent movement of snow to create Patriot Hills Antarctic Logistics and Expeditions Base Camp (seasonally occupied between 1987 and 2010).

5.4 Summary

This chapter and associated paper (*Winter et al*. [2016]) provide the first detailed account of the internal structure of BIAs. Radar-detected stratigraphic relationships analysed in conjunction with deuterium isotope records, ice-sheet model simulations and internal layer continuity index analysis at Patriot Hills BIA indicate the following: (1) stable periods of snow accumulation and ice flow have been interrupted by episodes of significant erosion, which have resulted in unconformities within an otherwise conformable stratigraphic record and (2) the current trajectory of ice flowing towards Patriot Hills BIA is, in essence, unchanged over the recent historical record. These findings imply that deuterium isotope records from Patriot Hills BIA reflect conditions in Horseshoe Valley (and the WAIS) over at least the last 30,000 years, though due consideration must be taken around the two periods of differential wind scour.

Importantly, this research also demonstrates the considerable value of using GPR in step-and-collect-mode to interpret ice sheet history from BIAs, as conventional snowmobile towed GPR cannot resolve the detailed internal structure of these ice features. This finding is particularly relevant to the climate community, as low-cost and portable GPR surveys in step-and-collect mode can greatly improve the reliability of relatively easily-accessible horizontal climate records.

CHAPTER 6

Radio-echo sounding

This chapter will use airborne RES to investigate the subglacial topography, internal stratigraphy and Holocene flow regime of the upper IIS catchment. It will include and expand upon the analysis of RES profiles published by *Winter et al*. [2015] in the Journal of Geophysical Research – Earth Surface.

Radio-echo sounding objective

Determine the internal structure of the West Antarctic Ice Sheet in the upper Institute Ice Stream catchment to establish historic changes in regional ice streaming.

Research questions

1) What is the current configuration of the upper Institute Ice Stream catchment and how does it affect ice sheet flow?
2) What was the ice sheet configuration, with respect to the Bungenstock Ice Rise, during the Holocene?
3) Was ice in Horseshoe Valley Trough an important tributary of the Institute Ice Stream in the past, both in its current configuration and in the configuration of *Siegert et al*. [2013]?

6.1 Introduction

Over 25,000 km of airborne RES data, collected during a survey of the IIS in 2010/2011 by Dr. Neil Ross and collaborators has been analysed in this chapter to investigate the internal structure and subglacial topography of the upper IIS catchment (Figure 6.1). Synthetic Aperture Radar (SAR) processed radargrams have been displayed in 2D and 3D, and investigated using manual digitisation of internal features and ILCI analysis. To recap methodologies detailed in Chapter 4, during manual digitisation strongly reflective horizons were marked by black solid lines,

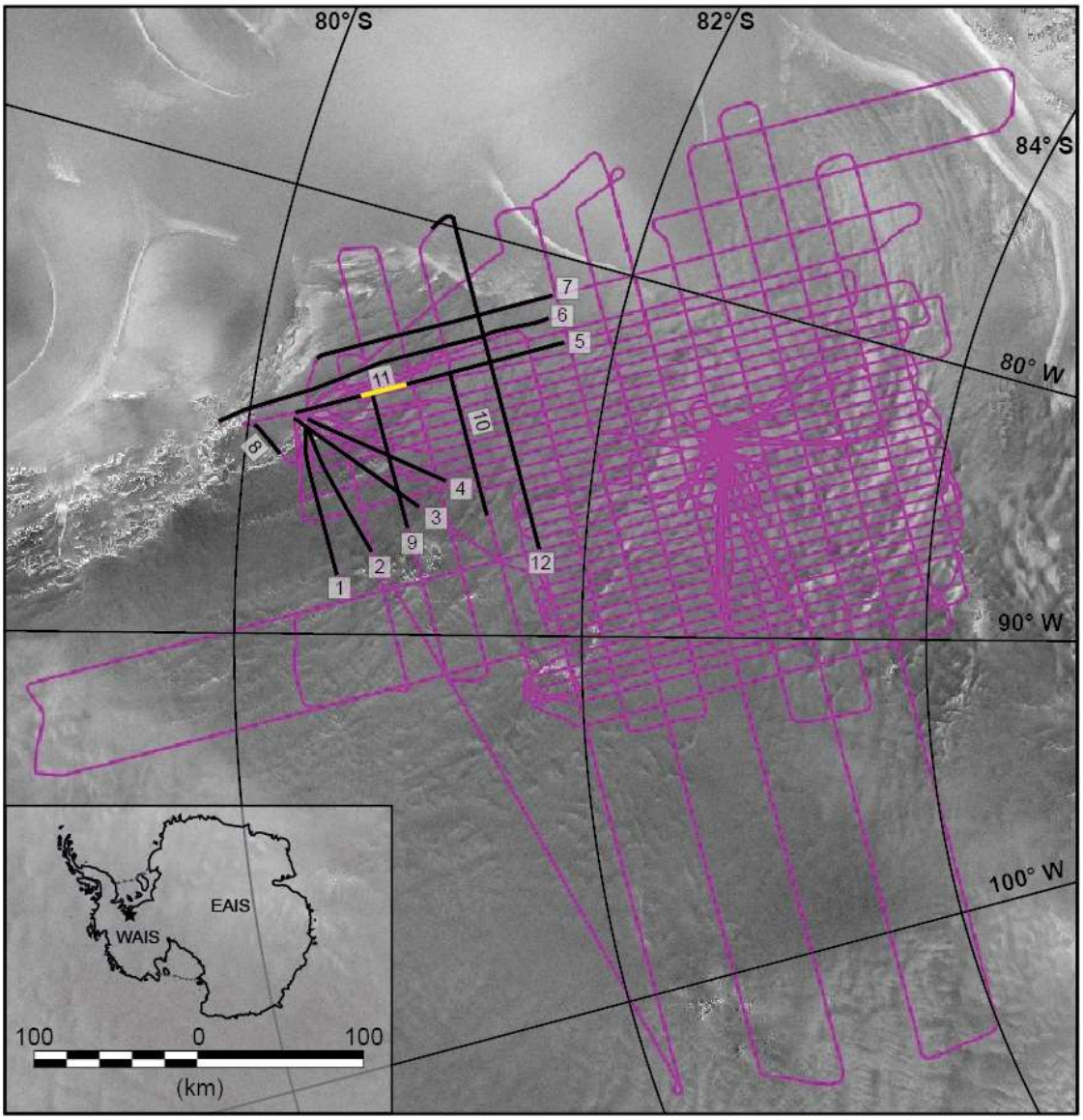

Figure 6.1. Location of airborne radio-echo sounding transects across the Institute and Möller Ice Stream catchments (pink), surveyed by Dr. Neil Ross and collaborators in 2010/2011. The dashed box denotes the extent of airborne radargrams investigated in this thesis whilst black and yellow lines highlight the location of radar profiles displayed in this chapter. Background imagery comprises MODIS mosaic images [*Haran et al*., 2006].

whilst internal features with reduced reflectivity were marked with dashed lines (as their exact form was harder to define). Purple lines were used to extrapolate internal stratigraphic features in areas where radar returns were low. During automatic ILCI classification a high continuity index (0.06 - 0.10) is returned when layers are clear and continuous, intermediate values (0.03 - 0.06) when layer packages are disrupted, with regions of little to no englacial layering, and low values (0 - 0.03) when layering is absent. It should also be noted here that internal layering cannot be resolved within the south-western side of Horseshoe Valley Trough as aircraft took off and/or landed in front of Patriot Hills. The uppermost 200 samples of the ice column (equivalent to ~9070 ns) are also poorly resolved in all radargrams as a function of 2D SAR processing. Once processed and analysed, RES transects were compared to surface velocity data (see Chapter 4) and previously examined surface lineations on the Bungenstock Ice Rise [*Siegert et al*., 2013] (Figure 6.2) to determine past ice sheet configurations and flow dynamics in the upper IIS catchment.

6.2 Results

6.2.1 Basal topography discrepancies

During preliminary analysis of RES radargrams in Horseshoe Valley and the upper IIS catchment large discrepancies were found between RES-detected bed topography and the basal topography data presented in Bedmap2 [*Fretwell et al*., 2013]. In Horseshoe Valley, Bedmap2 plots the basal topography ~1000 m higher than the RES detected bed (Figure 6.3), while discrepancies of up to 500 m are recorded elsewhere in the upper IIS catchment (for example, in the Independence Trough - Figure 6.4). In all cases, the RES-detected bed reveals a lower elevation than the Bedmap2 dataset, and in most cases, Bedmap2 topography is aligned with a strong internal reflector. The errors encountered in the Bedmap2 dataset exceed the uncertainty values provided by *Fretwell et al*. [2013] (mapped in Figure 6.5), suggesting that automatic picking of radar lines in and around Horseshoe Valley incorrectly assigned the strong internal reflector identified in RES figures 6.3 and 6.4 as the bed. As such, all elevations and ice thicknesses cited in this chapter will utilise RES-derived bed topography measurements.

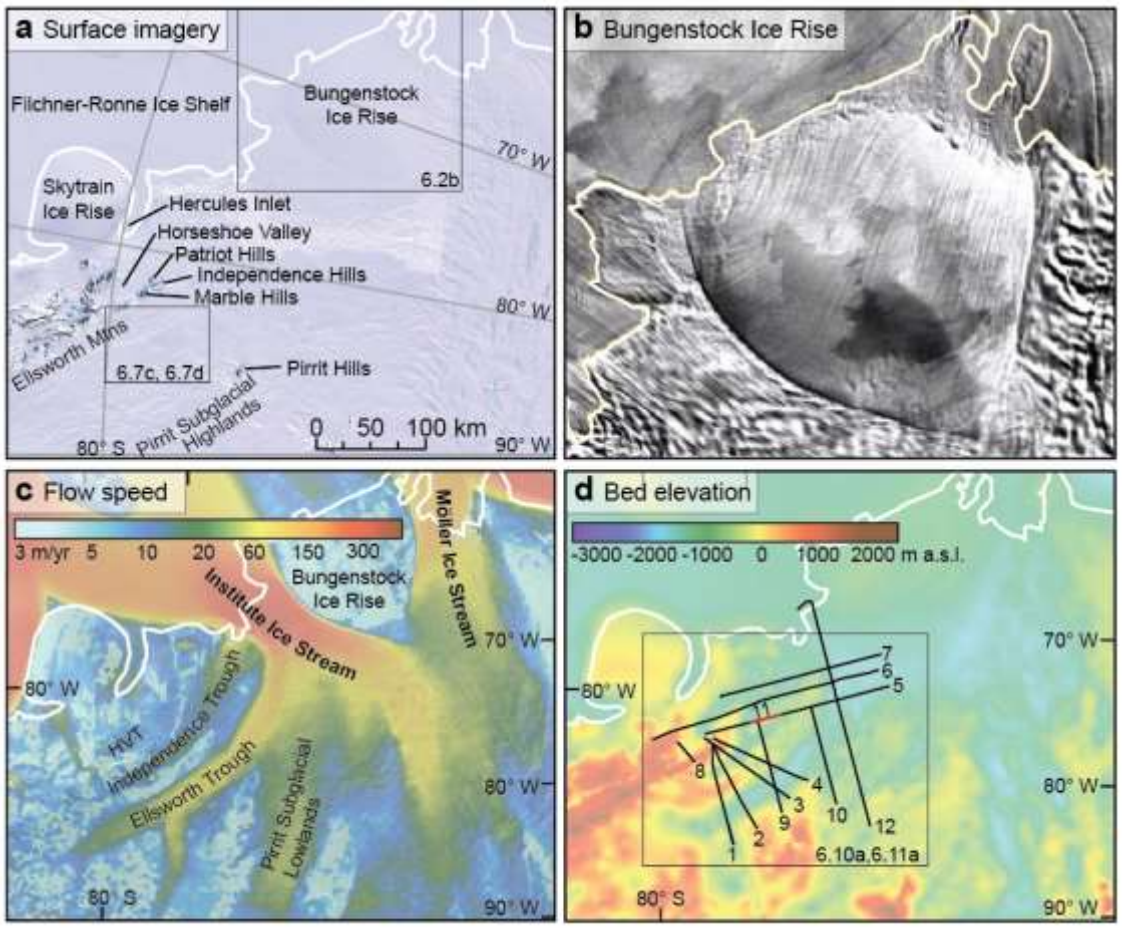

Figure 6.2. (a) Landsat Image Mosaic of Antarctica (LIMA) mosaic with prominent geographical features labelled; the labelled boxes outline the location of Figures 6.2b, 6.7c and 6.7d. The white line in each section indicates the ASAID grounding line [*Bindschadler et al*., 2011]. (b) MODIS mosaic of surface lineations on the Bungenstock Ice Rise [*Haran et al*., 2006]. (c) Satellite-derived surface ice-flow velocities from MEaSUREs [*Rignot et al*., 2011a] superimposed over MODIS satellite imagery [*Haran et al*., 2006] and annotated to show dominant ice streams, the Bungenstock Ice Rise, Horseshoe Valley Trough (HVT), Independence Trough, Ellsworth Trough and Pirrit Subglacial Lowlands. (d) Location of radargram transects imaged in this chapter. Background shows bed elevation from the same area as Figures 6.2a and 6.2c, derived from Bedmap2 [*Fretwell et al*., 2013].

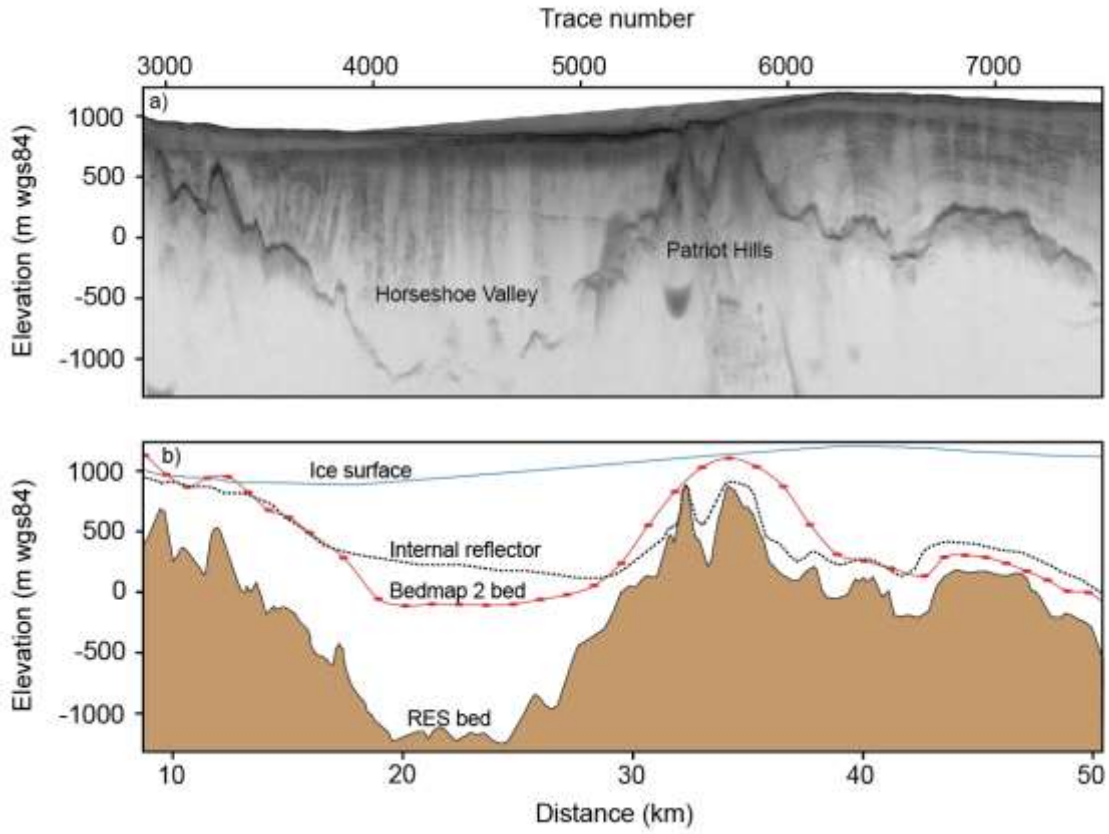

Figure 6.3. (a) RES flight line 8 across Horseshoe Valley and Patriot Hills, where ice flow is into the page. (b) Comparison between radar-detected bed (solid dark line) and the basal topography plotted from Bedmap2 [*Fretwell et al.,* 2013] (red line). It is suspected that automatic picking, applied prior to Bedmap2 compilation could have incorrectly assigned the strong internal reflector, visible in (a) and marked by a black dashed line in (b) as the bed. The ice surface has been marked by a solid blue line.

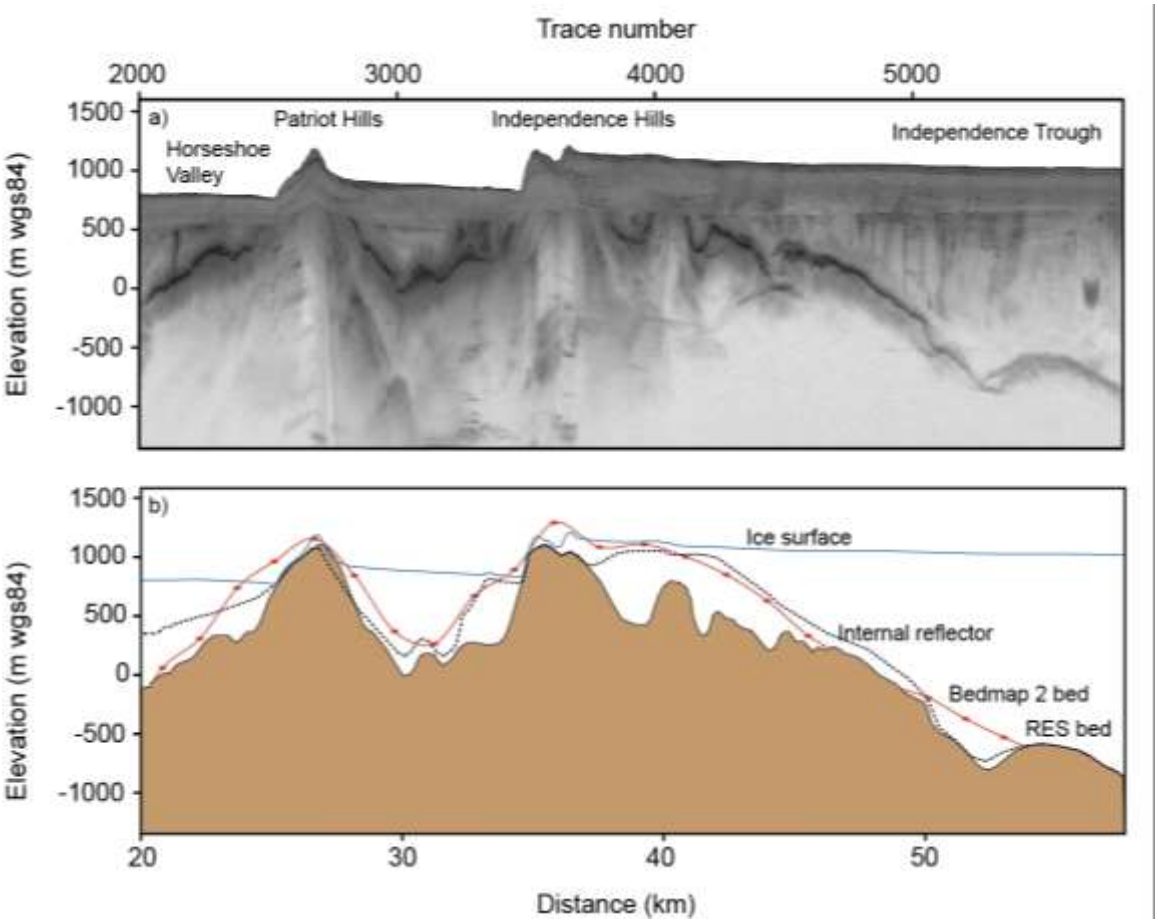

Figure 6.4. (a) RES flight line 3 transects Horseshoe Valley, the trough between Horseshoe Valley and Independence Hills as well as Independence Trough, where ice flow is into the page. (b) Comparisons between RES detected bed topography (solid dark line) and the basal topography derived from Bedmap2 [*Fretwell et al.*, 2013] (red line) reveal more similar bed topography projections, although the basal topography in Bedmap2 often follows a strong internal reflector (marked in (b) by a black dashed line).

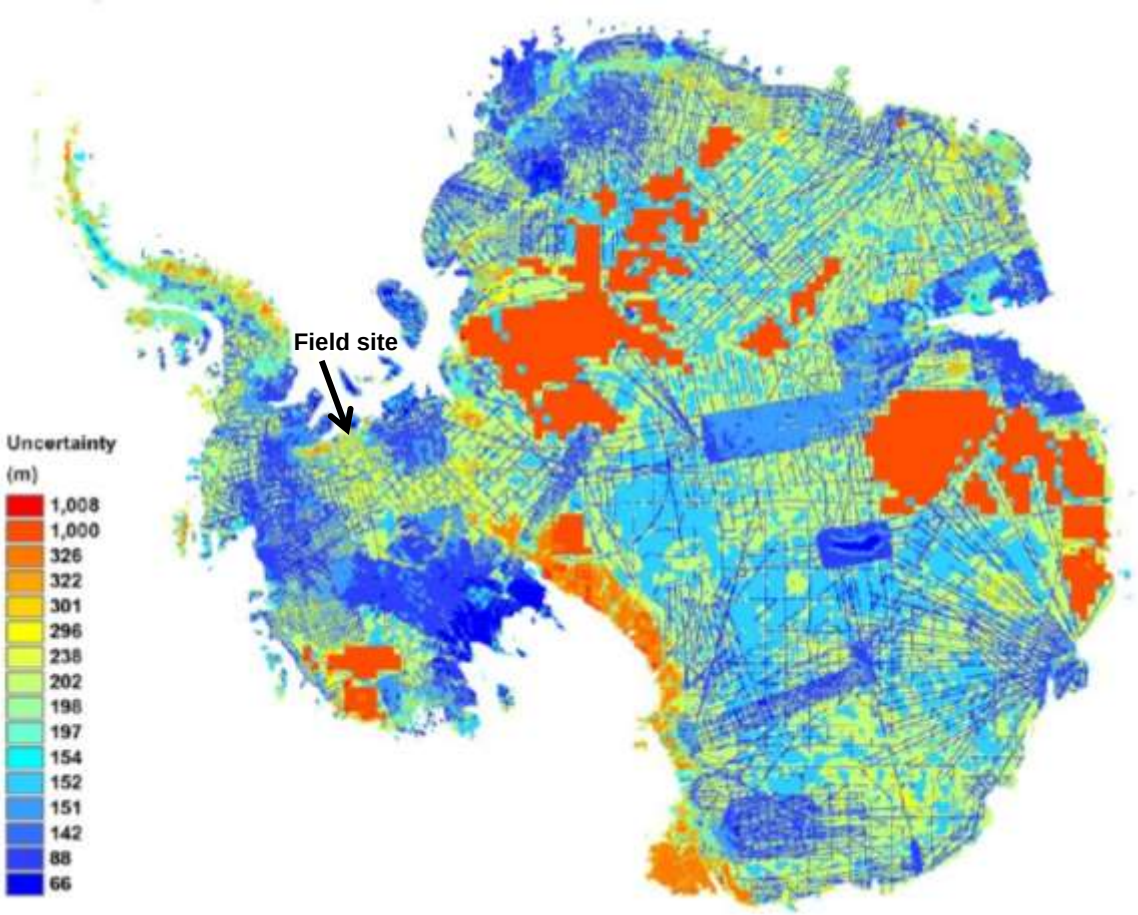

Figure 6.5. Estimated uncertainty from the bed elevation grid published by Bedmap2 [*Fretwell et al*., 2013]. The field site investigated throughout this thesis has been indicated with a black arrow.

6.2.2 Basal topography of the upper Institute Ice Stream catchment

Radar observations of the IIS's upper catchment, in and around the Ellsworth Subglacial Highlands, reveal complex tectonically-controlled basal topography [*Jordan et al*., 2013; *Ross et al*., 2014] with multiple nunataks, buried mountains, highland plateaus, basins and troughs (Figure 6.2d). This chapter focusses on three distinct troughs in the upper IIS catchment; Horseshoe Valley Trough, named after Horseshoe Valley at its head, Independence Trough, named after the adjacent Independence Hills and Ellsworth Trough which was named after the neighbouring Ellsworth Mountains. A distinct subglacial lowland, termed Pirrit Lowlands (after Pirrit Hills in the Pirrit Subglacial Highlands) has also been investigated. Each of these areas have been highlighted in Figure 6.2c.

As a main focus of this thesis, it is important to describe the RES-detected features of Horseshoe Valley Trough, which has been imaged in 2D in Figure 6.6. As briefly mentioned in Chapter 3, the 20 km wide trough is confined in its upper parts by the steep mountains of the Heritage Range. However, RES has also revealed that some of the ice flow is also constricted at the end of the valley, where a subglacial ridge separates the somewhat confined ice flow with the present day trunk of the IIS. With a smooth bed lying 1300 m below sea level, Horseshoe Valley Trough contains an ice column in excess of 2000 m. However, this ice sheet thickness reduces significantly, to just 750 m, as the ice flows out of Horseshoe Valley where it is deflected northwards over the higher elevation terrain towards the main trunk of the IIS (Figure 6.2d).

Lying sub-parallel to Horseshoe Valley Trough, but separated from it by the 1400 m high peaks of Independence Hills, is Independence Trough (Figure 6.7). This 22 km wide trough is delineated to the south by a 20 km wide subglacial mountain range which has a maximum elevation of 770 m above present sea level. Unlike Horseshoe Valley Trough, the Independence Trough has a unique shape, which is characterised by the existence of two 6 km wide plateaus (P1 and P2 in Figure 6.7), which line either sides of the trough. These plateaus break the steep slope from the high nunataks which define Independence Hills and the deep subglacial valley floor, which sits 1100 m below present day sea level. The trough itself remains

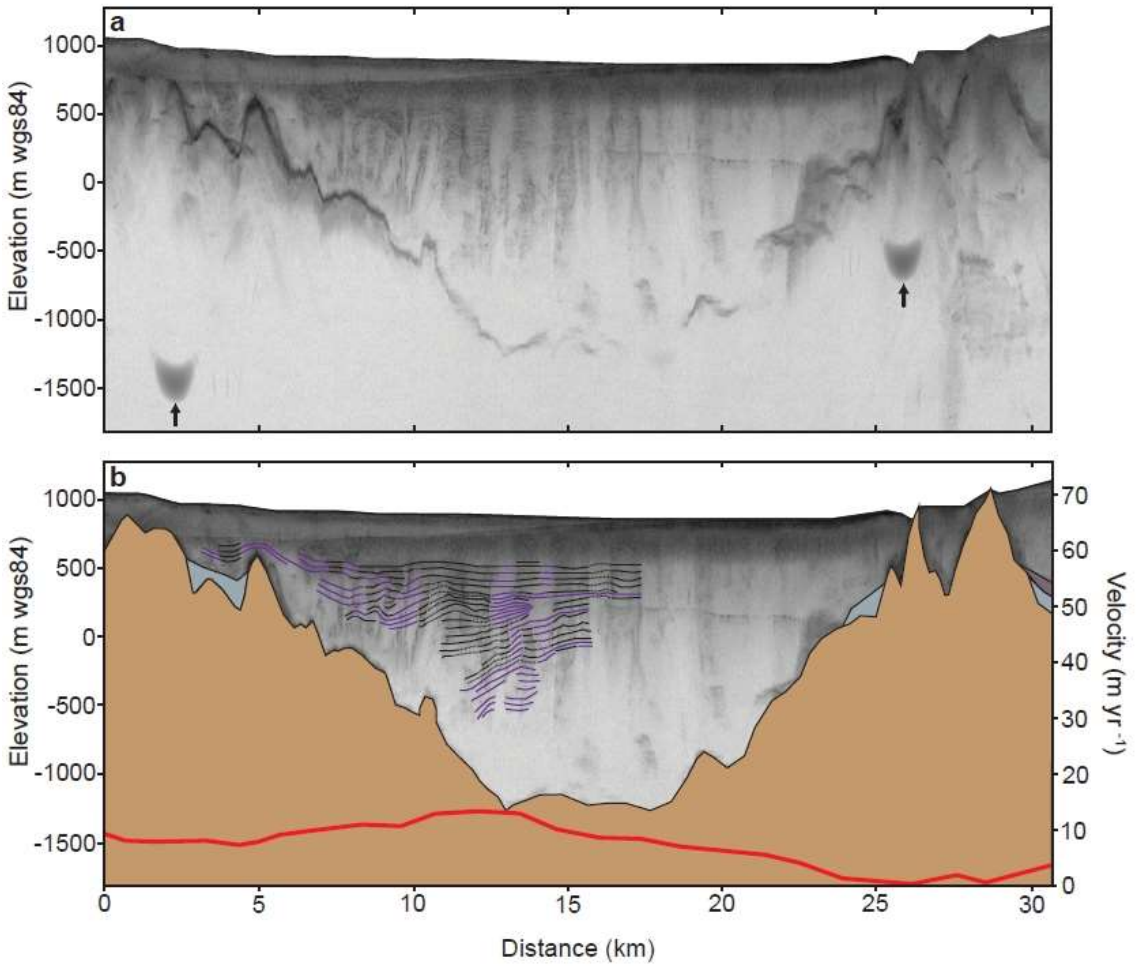

Figure 6.6. (a) Radio-echo sounding cross section of Horseshoe Valley Trough (line 8), where ice flow is into the page; the arrows indicate processing artefacts. (b) Digitised basal topography (brown), lower basal ice unit (blue) and upper basal ice unit (purple) as well as internal stratigraphic features (black for observed, dashed for inferred and purple for best estimate). The secondary axis shows satellite-derived surface ice-flow velocities in red from MEaSUREs [*Rignot et al.*, 2011a].

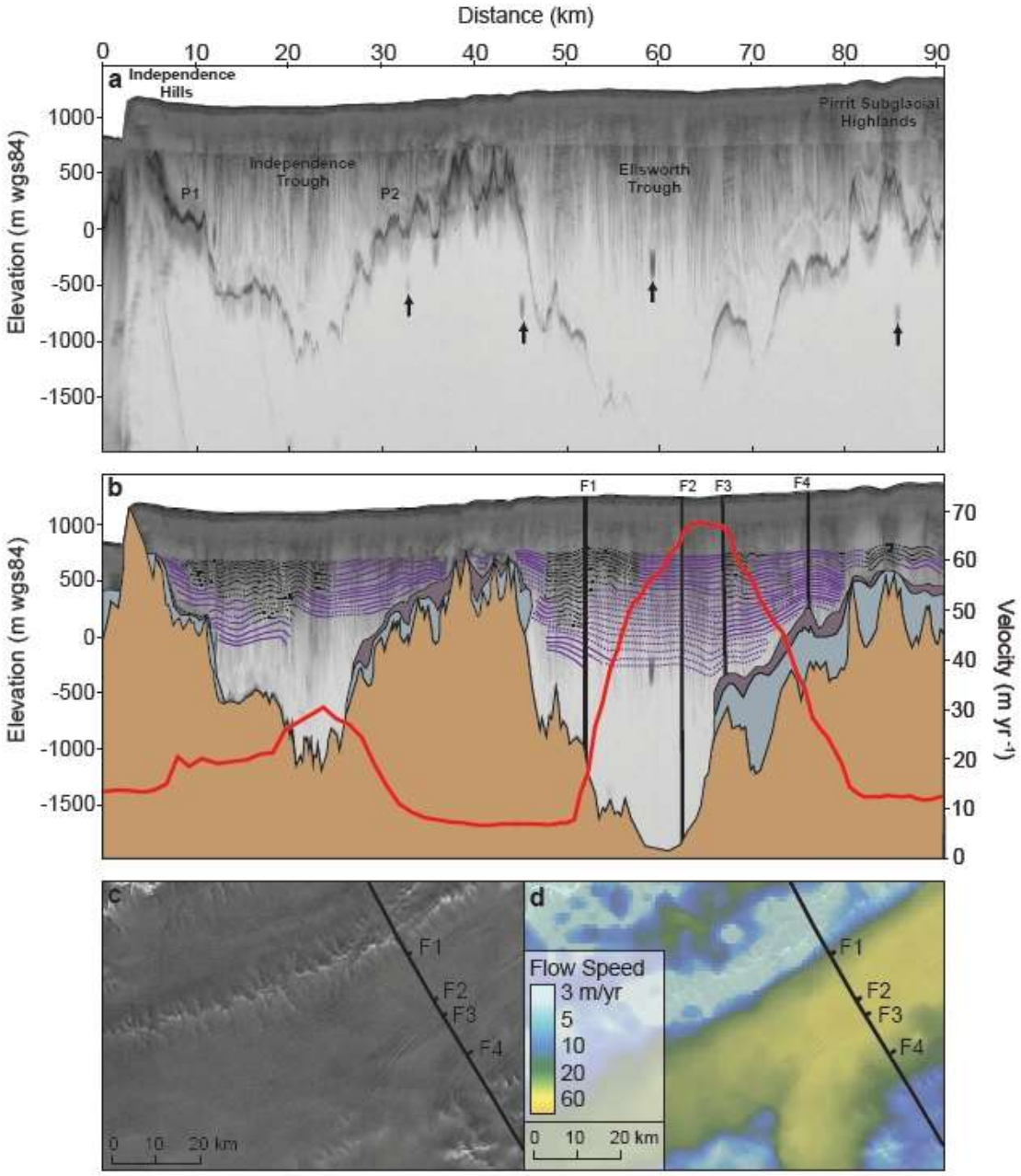

Figure 6.7. (a) Radio-echo sounding cross section of Independence and Ellsworth Troughs (line 2) where ice flow is into the page; the arrows indicate processing artefacts. P1 and P2 indicate plateaus in the basal topography. (b) Digitised basal topography (brown), lower basal ice unit (blue), and upper basal ice unit (purple) as well as internal stratigraphic features (black for observed, dashed for inferred, and purple for best estimate) and the location of surface flow stripes (F1–F4). The secondary axis highlights satellite-derived surface ice-flow velocities in red from MEaSUREs [*Rignot et al*., 2011a]. (c) Flow stripes (F1–F4) annotated from RADARSAT mosaic [*Haran et al.*, 2006]. (d) Flow stripes identified on a satellite-derived surface ice-flow velocity map from MEaSUREs [*Rignot et al*., 2011a].

deep and straight for 54 km until the ice begins to flow in a more northwards direction, where the ice flow widens to 50 km, as the ice flow splays out between high elevation subglacial plateaus, until it reaches the main trunk of the IIS, where the ice crosses the local grounding line (Figure 6.2c).

Described in detail by *Ross et al*. [2014], Ellsworth Trough (Figure 6.7) is the widest (up to 34 km wide) and most extensive valley (at ~260 km long) to be surveyed (Figure 6.2c). Although steep-sided bedrock walls confine the northern flank of the trough, the southern walls feature a more gradual inclination towards a high elevation subglacial plateau (Figure 6.7). This plateau defines mountainous basal topography which is intersected by a number of smaller valleys that are orientated roughly perpendicular to the main trough axis and present day ice flow. Two major tributaries feed Ellsworth Trough at the point where the trough becomes straight and aligned with Independence Trough (Figure 6.2c). Here ice thicknesses of 2100 m - 2620 m are recorded as the ice is funnelled northwards towards the IIS, above bed elevations of 700 m - 1500 m below present day sea level.

Although a distinctive trough morphology is not recorded in the vicinity of the Pirrit Lowlands (Figure 6.2), ice flow from the southern IIS catchment merges and flows between a number of highland plateaus and subglacial lows which define the Pirrit Highlands, as the ice makes its way towards the main trunk of the IIS and the local grounding line. Here, several bedrock obstacles, in the form of ridges, troughs and rough terrain are detected beneath the ~1000 m thick ice flow (Figure 6.8). These obstacles create distinct fluctuations in bed elevation, allowing the basal topography to range from 200 m to 1150 m below present day sea level. However, basal topography is difficult to ascertain in Figure 6.8, at the point where the ice flow meets the Ellsworth Trough. This is largely a function of ice thickness. The basal horizon is also diffuse in the first 40 km of transect line 12, where the radar system identifies water at the base of the FRIS.

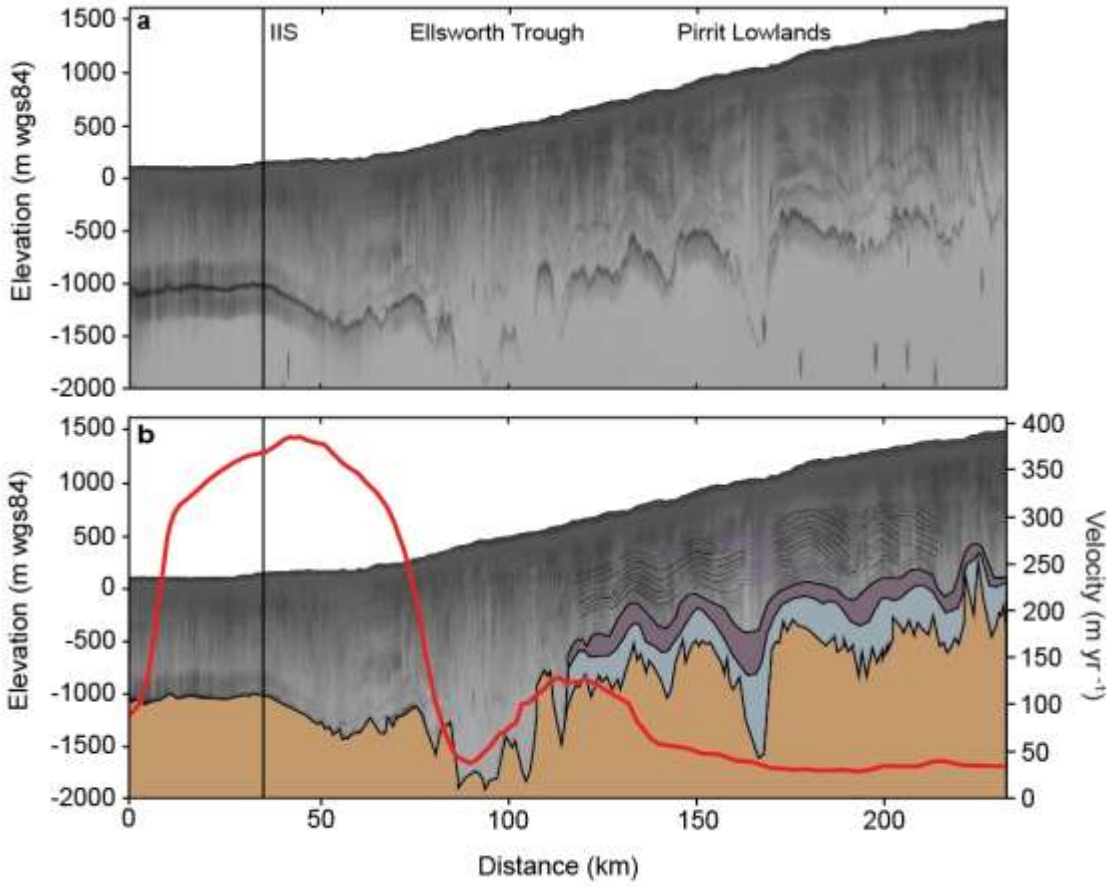

Figure 6.8. (a) Radio-echo sounding line 12 detailing subsurface features across Pirrit Lowlands, the Ellsworth Trough and the Institute Ice Stream (IIS). The horizontal black line in (a) and (b) indicates a turn in the RES flight, where the flight line crosses the local grounding line of the Filchner-Ronne Ice Shelf (b) Digitised basal topography (brown), lower basal ice zone (blue) and upper ice zone (purple) as well as internal stratigraphic features (black for observed, dashed for inferred and purple for best estimate). The secondary axis highlights satellite-derived surface ice flow velocities in red from MEaSUREs [*Rignot et al*., 2011a].

6.2.3 Internal stratigraphy

Although basal topography is clearly detected by the British Antarctic Survey's PASIN system, the airborne RES transects also reveal several englacial features related to ice dynamics. These include basal units lacking evidence for clear internal ice-sheet layering, continuous and discontinuous internal layers, highly disrupted internal layers and low-reflectivity structures which resemble 'whirlwinds' or 'tornados' [*Karlsson et al.,* 2009]. The latter are visible in radargrams throughout the study area, in a variety of radar flight-line orientations. An example of these 'whirlwinds' is shown in Figure 6.9 (although also visible in Figures 6.6, 6.7, 6.10 and 6.11 the larger scales used in these figures, which were chosen for regional analysis, are not appropriate for marking the locations of 'whirlwind features'). In Figure 6.9, and indeed, within numerous other radargrams investigated during this study, englacial layering is disrupted and occasionally obliterated by the 'whirlwinds', which highlight vertical to sub-vertical low-reflectivity zones. These features are believed to represent the complex response of the radar signal to high-amplitude buckling of layers within the ice sheet (i.e. physical ice sheet features that present in the radargrams as whirlwinds [*Holschuh et al*., 2014]). As such, the 'whirlwinds' can be used to identify and map zones of buckled and disrupted layering.

Basal ice units have also been detected above the bed in multiple radargrams (e.g. Figures 6.7, 6.8 and 6.9). These basal units, identified throughout the study area, are clearly distinguishable from the bed and the upper ice column, where they can often be sub-divided vertically into two distinct sub-units, where the boundary between them is marked by an upper reflective interval. Although their formation requires further investigation, *Knight* [1997] and *Bingham et al*. [2015] have suggested that their form could be attributable to changes in ice fabric, or contrasting physical, dielectric properties associated with a glacial/interglacial palaeoclimatic switch.

Horseshoe Valley Trough

Airborne RES transects reveal a number of internal features within Horseshoe Valley ice flow. Figure 6.6 shows that basal ice units up to 450 m thick have been recorded above the subglacial

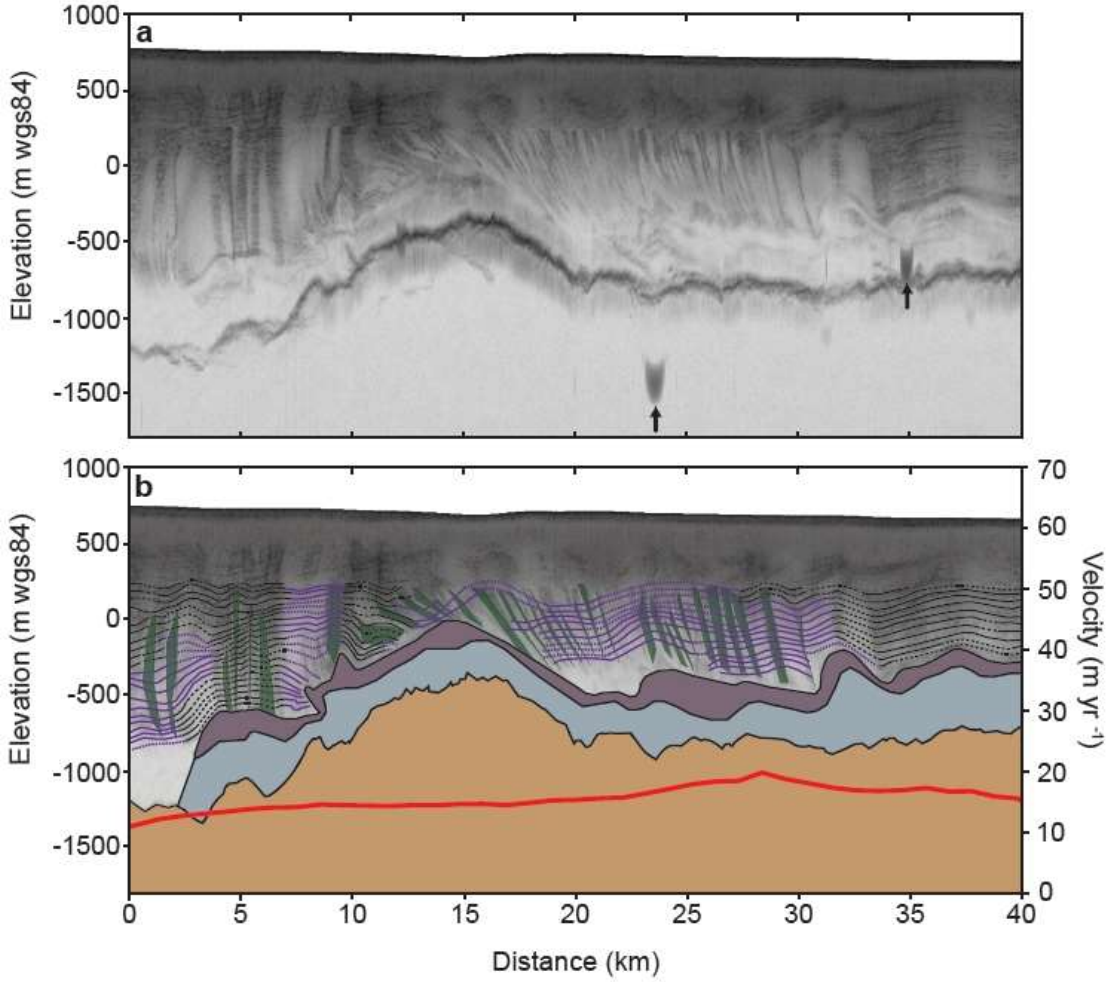

Figure 6.9. (a) Selected internal features in radio echo sounding flight line 11; the arrows indicate a processing artefact. (b) Digitised basal topography (brown), lower basal ice unit (blue), and upper basal ice unit (purple) as well as internal stratigraphic features (black for observed, dashed for inferred, and purple for best estimate); the green polygons show the location of internal whirlwinds. The secondary axis highlights satellite-derived surface ice flow velocities in red from MEaSUREs [*Rignot et al*., 2011a].

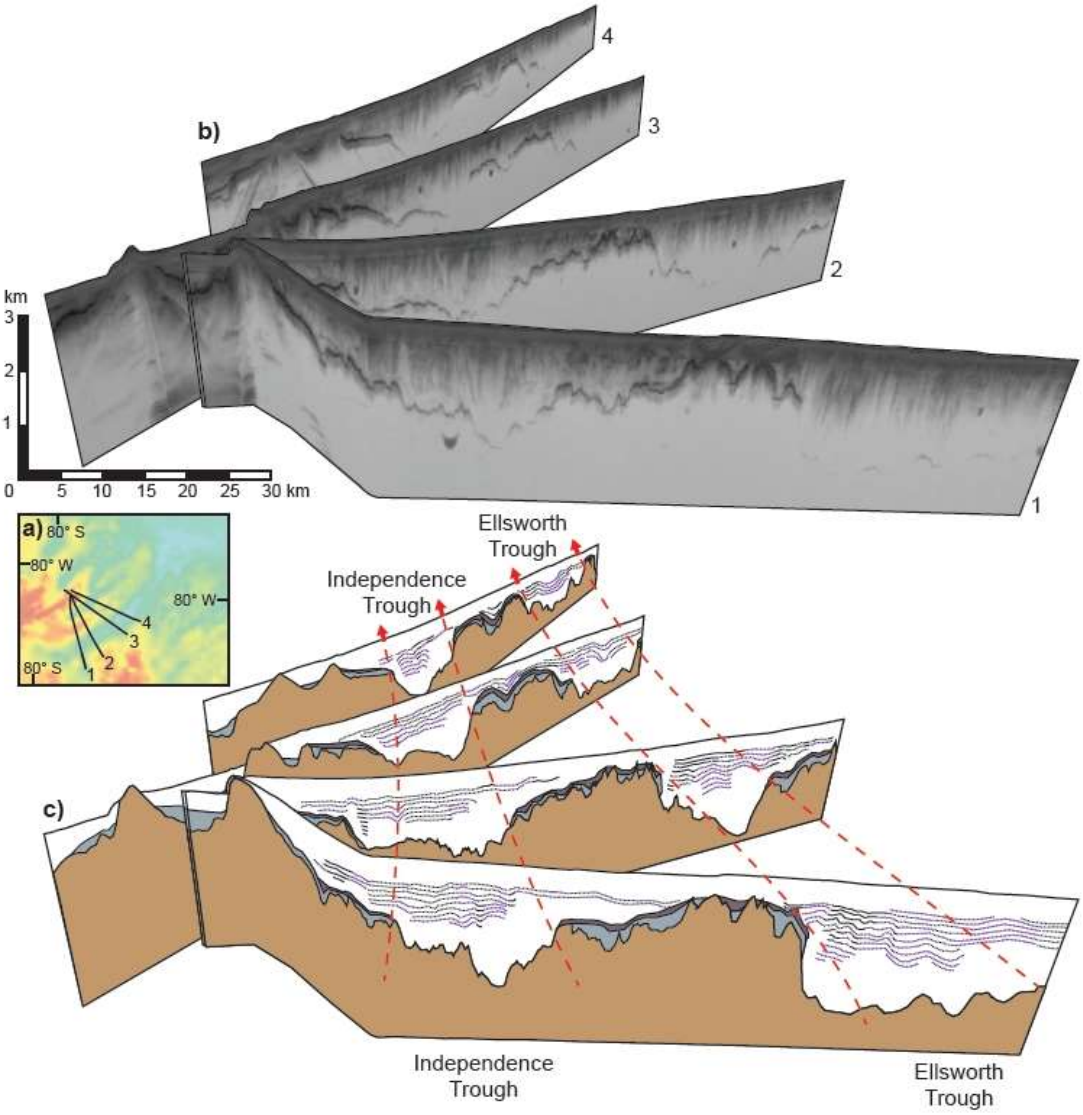

Figure 6.10. (a) Location of lines 1–4 in relation to the bed topography, derived from Bedmap2 [*Fretwell et al.*, 2013]. (b) Three-dimensional schematic diagram placing RES lines into approximate geographic/spatial context to highlight the morphology of Independence and Ellsworth Troughs, as well as the development of internal stratigraphy down flow. (c) Interpreted gross-scale structure of the two troughs approximately marked by red dashed lines and flow direction arrows. Conformable layering is present above the highland plateaus which define the troughs. The gradual inclination in bed elevation from Independence Trough to Independence Hills, coupled with the presence of basal ice zones and a thin ice column, suggests that there has been no recent transfer of ice from Independence Trough into Horseshoe Valley Trough.

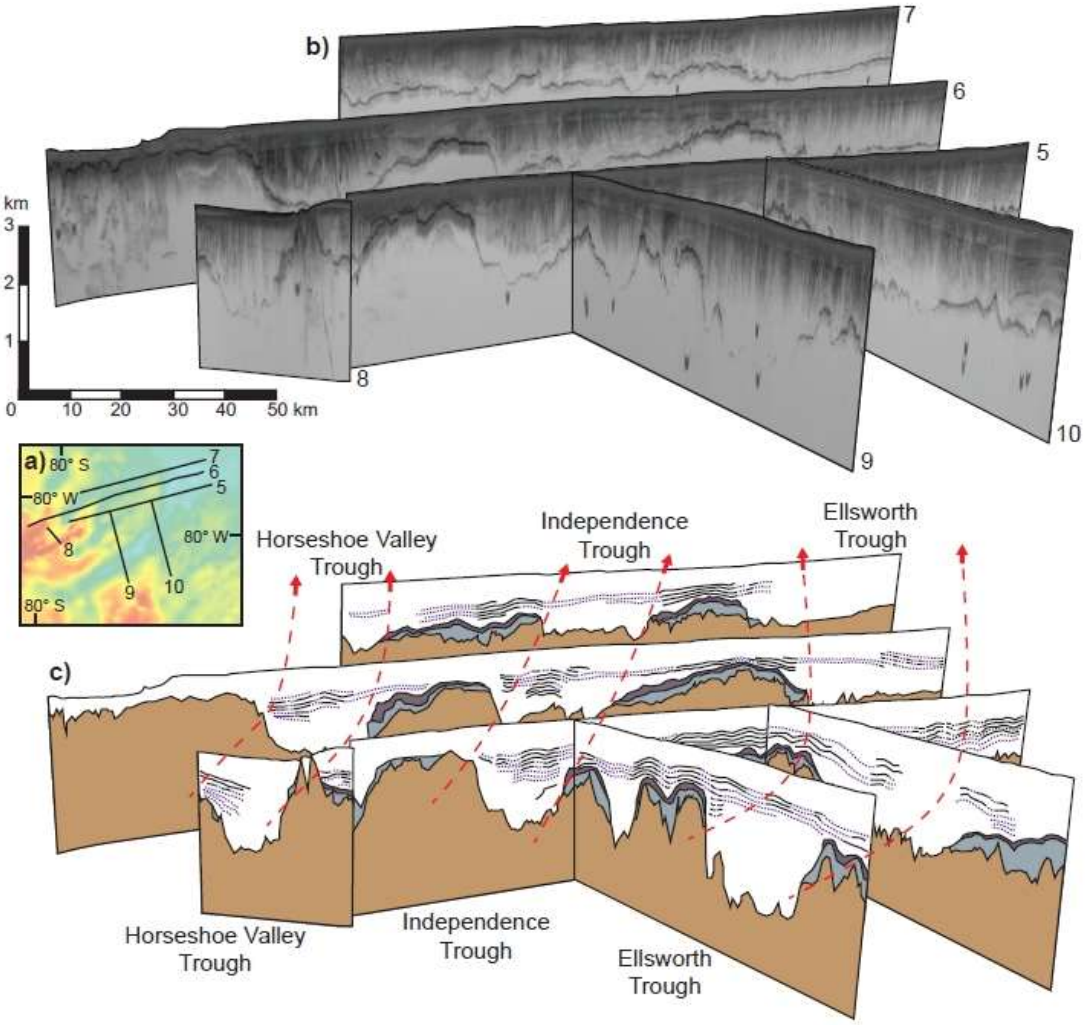

Figure 6.11. (a) Location of lines 5–10 in relation to the bed topography, derived from Bedmap2 [*Fretwell et al*., 2013]. (b) Three-dimensional schematic diagram to highlight the morphology of Horseshoe Valley, Independence and Ellsworth Troughs in the upper Institute Ice Stream catchment, as well as the development of internal stratigraphy down flow. (c) Interpreted gross-scale structure of the three troughs approximately marked by the red dashed lines and flow direction arrows. Conformable layering is present above the highland plateaus which define the troughs and in the upper 500 m of ice within Horseshoe Valley Trough. Disrupted isochrones are restricted to the deeper ice of Horseshoe Valley Trough and within Independence and Ellsworth Troughs.

mountain ranges that delimit the trough. These units can be traced down flow on the south-western side of the trough for at least 110 km where they are clearly visible at a maximum depth of 500 m below sea level, but they cannot be found any more centrally or deeper inside the trough itself.

Within the trough, discontinuous ice layers dominate the mid to lower ice column, where the most disturbed and buckled englacial layers - with an ILCI value of 0 - 0.06 are found down the north east flank of the trough (Figure 6.6, Figure 6.12) (as discussed in section 6.1, internal layers cannot be resolved within the south-western side of the trough, as the aircraft took off and/or landed at this locality). Continuous and parallel isochrones sit conformably above these deeper, more disrupted and buckled ice layers, where a 500 m thick sequential ice package, ~20 km wide is recorded in the upper 20% of the ice column (Figure 6.6, 6.13). These continuous layers can be traced down flow in numerous radargrams, and through ILCI analysis, for at least 90 km, where the layers become increasingly apparent and numerous as the basal topography becomes elevated and the trough margins widen (Figures 6.10 - 6.13).

Although hard to distinguish precisely in all RES transects due to the scale at which they are presented in Figures 6.6 and 6.11 largely vertical 'whirlwind' features are also visible within the ice flow of Horseshoe Valley Trough. Within the better resolved northern side of the ice flow, the 'whirlwinds' appear to span the entire height of the ice sheet column (although processing steps largely prevent the upper 200 samples (top ~500 m) from being imaged), where they cut through discontinuous internal layering. These 'whirlwinds' generally tend to extend vertically downwards from the surface or near-surface, where they are sometimes curved or sub vertical (see Figure 6.9 for a detailed example). A similar morphology is recorded on a smaller scale where the 'whirlwinds' interface with the upper boundary of the basal ice units, for example on the flanks of Horseshoe Valley Trough [*Ross and Siegert*, 2014].

Independence Trough

RES of Independence Trough has revealed strong radar returns within the top 50% (800 m) of the ice column, where ice within the trough is dominated by disrupted englacial stratigraphy

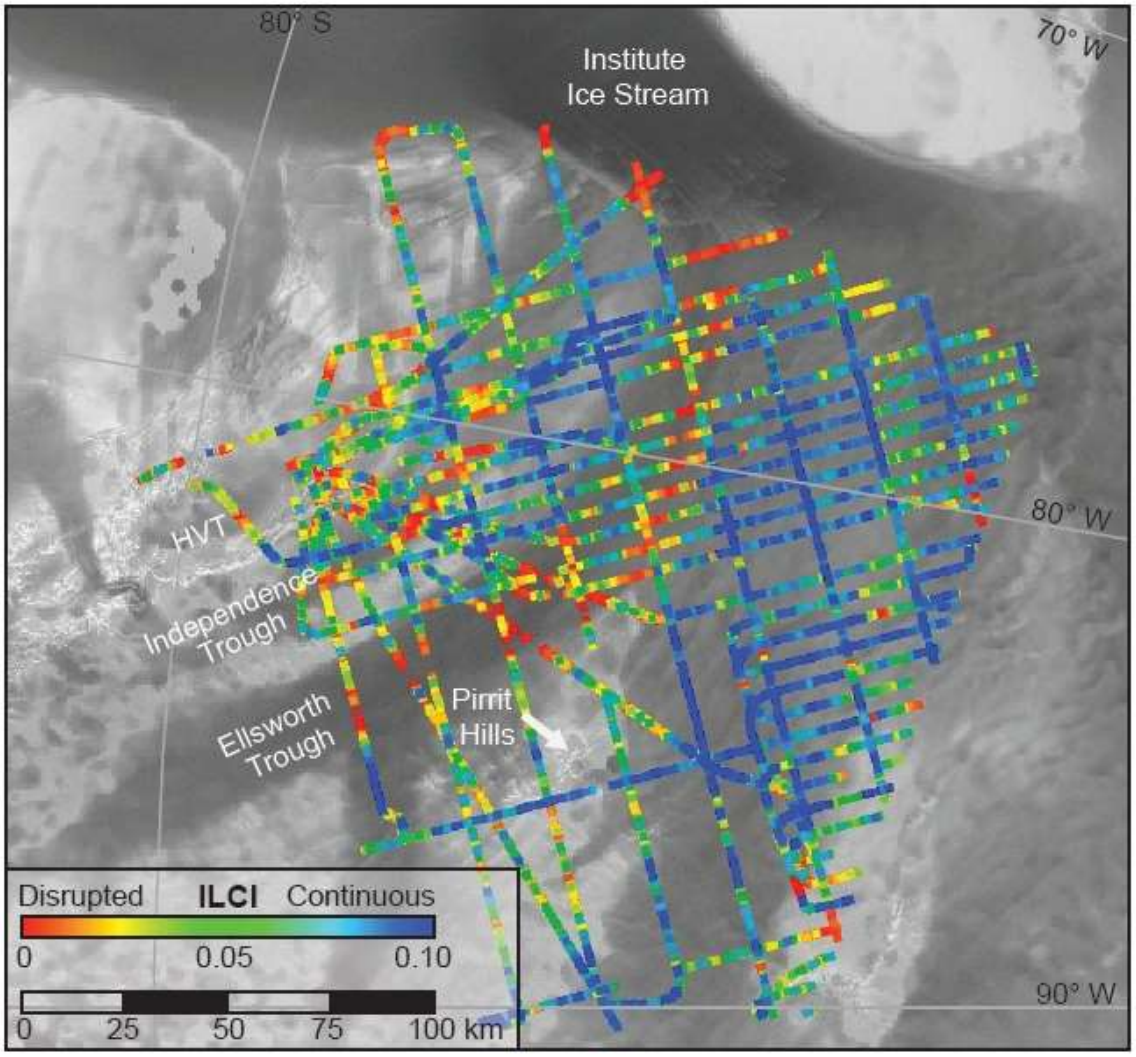

Figure 6.12. Results of the full-depth Internal Layer Continuity Index (ILCI) from several flight lines over the Institute Ice Stream upper catchment near the Ellsworth Mountains. Background shows surface ice-flow velocity from MEaSUREs [*Rignot et al*., 2011a] in grey scale, superimposed onto RADARSAT mosaic [*Haran et al*., 2006]. Low ILCI values (<0.06), representing disrupted englacial layering, dominate ice flows within Horseshoe Valley Trough (HVT), Independence Trough, and Ellsworth Trough as well as the Institute Ice Stream. High ILCI values (>0.06), representing continuous layering, are located above the subglacial highlands which delimit the three troughs.

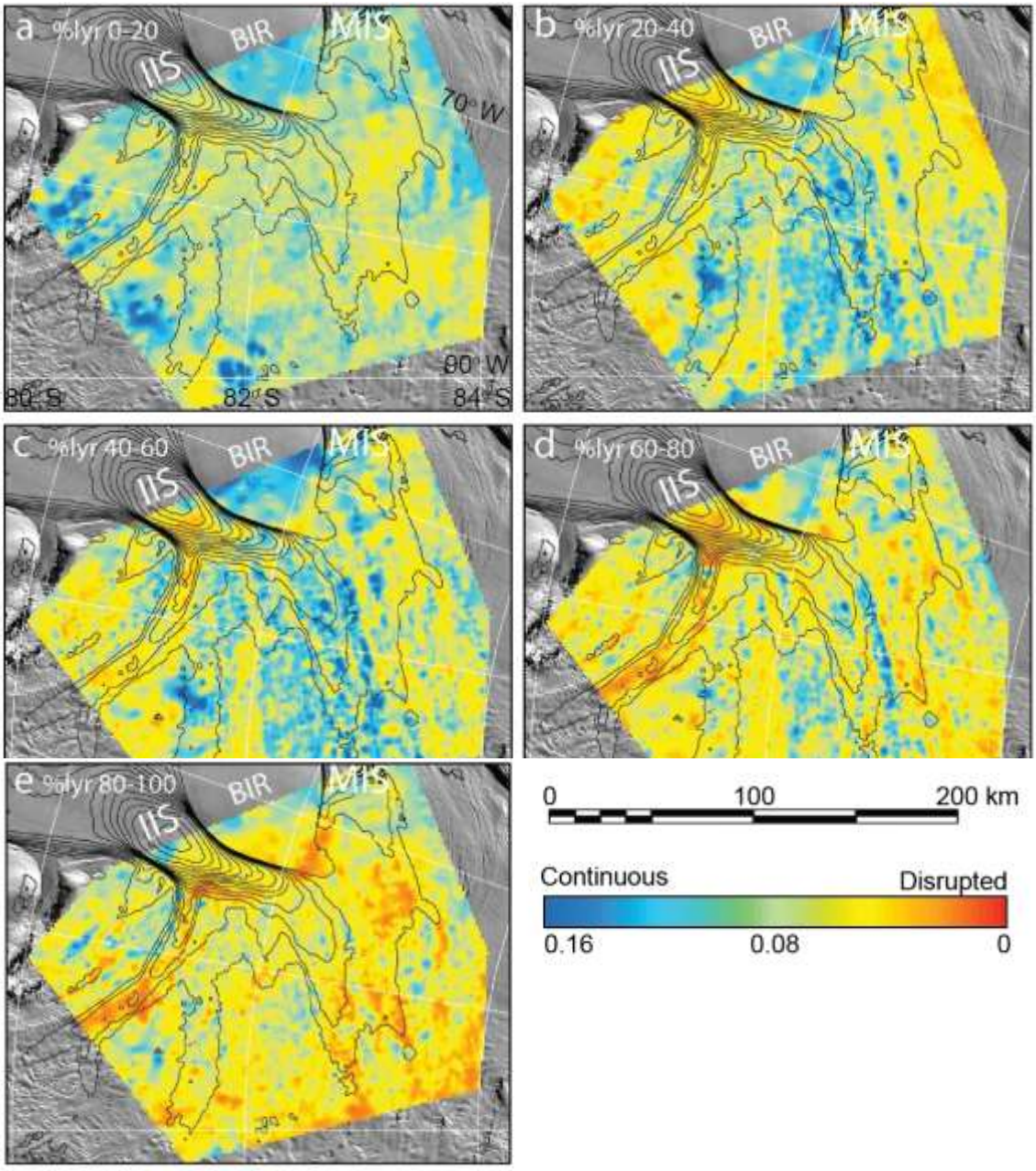

Figure 6.13. Internal Layer Continuity Index (ILCI) results from 100 trace moving windows, partitioned by depth ranges (or "layers", abbreviated as "lyr") progressively downward through fifths of the ice column. Background shows surface ice-flow velocity from MEaSUREs [*Rignot et al*., 2011a] in grey scale, superimposed onto RADARSAT mosaic [*Haran et al*., 2006]. IIS = Institute Ice Stream, BIR = Bungenstock Ice Rise, and MIS = Möller Ice Stream. Figure adapted from *Bingham et al*. [2015].

(Figure 6.7) which repeatedly exhibits an ILCI index <0.06 (Figure 6.13). Figures 6.7, 6.10 and 6.11 demonstrate the abundance of this stratified englacial layer buckling across flight lines of all orientations. These figures also show that the buckled ice layers become progressively less discernible down valley, presumably as a function of enhanced ice flow and associated intense disruption of englacial stratigraphy on approach to the fast-flowing IIS trunk. Although low ILCI values dominate the majority of the ice flow within Independence Trough, ILCI values in excess of 0.06 (reflecting continuous layering) are recorded within the upper reaches of the trough, where they are often co-incident with the subglacial plateaus which have a relatively smooth basal topography (Figures 6.10, 6.11 and 6.12).

Although basal ice units are not found within the centre of the Independence Trough, they have been recorded at the trough margins, where the ~100 m thick packages drape over the subglacial highlands, spanning an elevation range of 1250 m. Similar to Horseshoe Valley Trough, a dense network of 'whirlwinds' is also observed in the ice flow contained within Independence Trough. These 'whirlwinds' are found above the higher elevation subglacial mountain ranges and associated basal ice units, where they have been located in ice as thin as 600 m, and in ice as thick as 1500 m.

Ellsworth Trough and Pirrit Highlands

The length of the Ellsworth Trough is dominated by sub-parallel, buckled isochrones which are visible within the uppermost 1000 m of the ice column, to a maximum depth of 250 m below current sea level, beneath which the radar did not resolve internal layering due to signal attenuation (a function of the 2600 m+ ice thickness and the likely existence of warm ice within the lower ice column). ILCI results reveal the greatest percentage of low to intermediate ILCI values (0 – 0.6) within the ice flows of Ellsworth Trough (Figures 6.12 and 6.13). This quantitatively confirms that the Ellsworth Trough contains the most abundant unresolved and disrupted internal stratigraphy of all the south-western IIS tributaries. Although continuous layering is clearly distinguishable above the highland plateau of the Pirrit Highlands (Figures 6.8, 6.11 and 6.12), which delimit the south-western extent of the trough, very few continuous

layers are found within the Ellsworth Trough itself. This is particularly evident from the full-depth ILCI results (Figure 6.12), where values <0.6, representing disrupted englacial layering are found down the centre of the trough, whilst intermediate to high ILCI values (0.6 – 0.10) are recorded near the trough margins.

Beneath the surface-conformable layers of the Pirrit Subglacial Highlands basal ice units are clearly visible down the length of mountainous ridges (Figure 6.11), where they typically reach thicknesses in excess of 200 m, with a maximum thickness of 850 m (recorded in a small trough within the upper reaches of the highland area). The most frequent and elongate 'whirlwinds' of the entire airborne RES study are also found in Ellsworth Trough, where the nearly-vertical 'whirlwind' features display longitudinal continuity down flow. Although smaller, more infrequent and less distinctive, 'whirlwind' features are also resolved over some areas of the Pirrit Highlands.

6.2.4 Surface velocity and surface features

Satellite remotely-sensed ice velocity data [*Rignot et al.*, 2011a] reveal spatially variable ice flow speeds within the upper catchment of the IIS tributaries, in and around the Ellsworth Mountains (Figure 6.2c). The slowest ice flow speeds of <9 m a^{-1} are recorded above high elevation subglacial plateaus and subglacial mountain ranges, whilst faster ice flow is recorded within the deep subglacial troughs which feed the IIS trunk, where current flow speeds reach 415 m a^{-1}. Ice within Horseshoe Valley Trough maintains the slowest average flow speeds of 12 m a^{-1} (Figure 6.6), permitting the preservation of early-mid Holocene ice. Ages quoted here and henceforth are approximate and estimated using age-depth modelling calculations from the Bungenstock Ice Rise, which suggest that ice at 40% ice thickness is ~4000 years old [*Siegert et al.*, 2013], as there is currently no dating control across the upper IIS catchment. Ice in Independence Trough currently reaches flow speeds of up to 35 m a^{-1} (Figure 6.7). Assuming average flow speeds ≥35 m a^{-1} it can be deduced that ice in Independence Trough is unlikely to contain ice deposited earlier than the mid-Holocene. Even greater advection of early to mid-Holocene ice is expected within Ellsworth Trough where tributary flow speeds of ~70 - 130 m

a^{-1} are currently recorded. Here, distinctive surface flow stripes, orientated parallel to ice flow, are clearly identified on satellite imagery and ice velocity maps (Figure 6.7c, 6.7d) Recent investigations by *Glasser and Gudmundsson*, [2012] and *Glasser et al*. [2015] suggest that these longitudinal features are likely to be the surface expression of simple shear and lateral compression, in this case originating from the confluence point of tributary flows entering Ellsworth Trough. Fast flow speeds of 38-129 m a^{-1} are also recorded throughout the Pirrit Lowlands where ice streams over thick basal ice sequences (Figure 6.8).

6.3 Discussion

6.3.1 Current configuration of the Institute Ice Stream and its tributaries

In its present configuration, two main tributaries feed the upper catchment of the IIS; these tributaries carry ice along the Independence and Ellsworth troughs to the main trunk of the IIS and ultimately the FRIS, entraining the flow of smaller tributaries, including ice that has originated from Horseshoe Valley.

Horseshoe Valley Trough is characterised at its upper end by the Horseshoe Valley overdeepened basin, where maximum measured ice thickness is in excess of 2000 m. This ice thickness is not maintained down valley, reducing to ~1400 m, and later ~750 m, when the ice is driven up topographic steps in the bed near the valley mouth (Figure 6.6). Surface-conformable ice layers dominate the upper 20% of the ice column in all transects; this continuity reflects the current slow flow speeds within Horseshoe Valley Trough which amount to ~12 m a^{-1}. However, disrupted internal layers visible within RES transects displayed in Figure 6.6 and 6.11 and in the % layer ILCI plot (Figure 6.13) imply former enhanced ice flow within the trough. As surface-conformable stratigraphy blankets the buckled ice layers it can be deduced that at some time the faster-than-present ice flow experienced a switch-off, fossilising the enhanced-flow features (buckled layers). The continuous isochrones beneath the surface of Horseshoe Valley Trough, combined with the preservation of conformable stratigraphy and basal ice zones above the subglacial mountains that delimit the trough, provide evidence for topographically confined, and relatively stagnant isolated ice flow throughout the Holocene. RES evidence from

Horseshoe Valley Trough therefore suggests that the switch from enhanced to stagnant flow occurred pre-Holocene, and that enhanced ice flow in this system is likely to pre-date the major changes in regional ice flow associated with the shutdown of ice streaming across the Bungenstock Ice Rise [*Siegert et al*., 2013].

Confined by steep mountain ranges along its length, the ~2200 m thick ice flow within Independence Trough is dominated by buckled ice layers which are visible in the top 50% of the ice column, within flight lines of all orientations (Figures 6.10, 6.11 and 6.11). These buckled layers become less discernible on approach to the main IIS trunk (Figures 6.10 and 6.11), as a function of enhanced ice flow speeds and increased strain rates. Unlike the ice within Horseshoe Valley Trough, there is no evidence for recent continuous englacial layering within Independence Trough, even though similar flow speeds of 15 m a^{-1} are recorded within the upper reaches of the trough. This suggests that the buckled ice layers within Independence Trough are younger than those in Horseshoe Valley Trough, implying a more recent slow-down of ice flow here.

Low ILCI values are recorded throughout the topographically constrained Ellsworth Trough, where discontinuous and buckled ice layers dominate the uppermost 1000 m of the ice column (note that detailed internal layering is poorly resolved at greater depths). These disrupted layers can be found in radargrams of all orientations (Figures 6.7, 6.10, 6.11 and 6.12). This extensive deformation is largely attributed to the relatively high ice surface flow speeds of 70 - 130 m a^{-1} (calculated from *Rignot et al*. [2011a]). Surface flow stripes correlate well to ILCI values, where the lowest ICLI values and surface flow stripes are recorded near the ice stream margin (Figures 6.7. and 6.12) where shear stress is high. A similar phenomenon is found in Whillans and the Carlson Inlet Ice Stream [*Raymond et al*., 2006; *King*, 2011], as well as the IIS towards its upper confluence with the MIS [*Bingham et al*., 2015] where the greatest disruption of internal layering is found along the lateral shear margins. These features define a constant direction of shear within the ice of Ellsworth Trough, which, given the topographic confinement of the ice [*Ross et al*., 2014], is likely to have existed over significant intervals of geological time.

The Pirrit Lowlands represent an ice tributary which is sufficiently wide to be relatively unconstrained by the subglacial topography. This allows ice from the upper IIS catchment to flow along a more or less straight flow path towards the local grounding line of the Filchner-Ronne Ice Shelf, which enables the internal layering and basal ice packages in the centre of the ice flow to remain relatively undisturbed over long distances. Higher ILCI values are recorded at the margins of the ice flow, where increased longitudinal strain is exerted by the more elevated subglacial topography bordering the Ellsworth Mountains and Pirrit Hills. The nature of ice flow through the Pirrit Lowlands indicates stable flow conditions throughout the Holocene, where high flux rates have consistently contributed to the main flow of IIS.

6.3.2 Evidence for former enhanced ice flow

Satellite-derived ice flow velocity measurements of the upper IIS catchment by *Rignot et al*. [2011a] reveal that enhanced ice flow conditions are only currently recorded within the largest tributary ice stream, which flows through the Ellsworth Trough. Here, airborne RES surveys have recorded fast flow features throughout the entire ice column, which include intensely buckled and discontinuous ice layers as well as 'whirlwinds'. Combined, these features strongly suggest that enhanced ice flow conditions have existed in the Ellsworth Trough since at least the mid-Holocene (as older ice is likely to have been advected towards the grounding line by fast ice flow). Similarly buckled and disrupted isochrones in the Independence Trough ice flow also suggest former enhanced ice flow conditions in the upper IIS tributary. However, as the present day ice flow speeds are much slower than those supported by the larger Ellsworth Trough and indeed too slow to produce such disrupted and discontinuous internal layering it is expected that the ice flow in Independence Trough has recently began to slow down.

6.3.3 Evidence for ice flow reorganisation

Although ice flowing through the Ellsworth and Independence troughs provide evidence for former enhanced ice flow, regional airborne RES analysis provides no evidence for former ice flow reorganisation. Continuous stratigraphy and thick basal ice zones above neighbouring

subglacial mountain ranges suggest that both ice flows have remained topographically constrained to the present day, during periods of both slower and more enhanced ice flow. This unique topographic confinement limits the potential for water piracy or ice-flow reorganisation in the upper IIS catchment, as has been speculated in other ice streams, most notably for the currently stagnant Kamb Ice Stream [*Jacobel et al*., 1996; *Anandakrishnan and Alley*, 1997] (see Chapter 2, section 2.6.2), though it does permit on-and-off streaming of tributary flow through the Independence and Ellsworth Troughs.

Although disrupted isochrones are qualitatively and quantitatively recorded in the ice flows of Horseshoe Valley Trough, the presence of a 500 m thick sequence of surface conformable stratigraphy beneath the ice surface implies that the ice has not experienced enhanced flow for some time. Current ice flow speeds of 7 m a^{-1} - 16 m a^{-1}, combined with the thick conformable ice sequence suggest that the ice in Horseshoe Valley has remained slow flowing since at least the mid-Holocene, allowing the preservation of much older, buckled and disrupted isochrones at depth. As Horseshoe Valley ice flow is topographically confined by a number of nunataks and mountain ranges it is unlikely that the ice flow in the upper reaches of Horseshoe Valley migrated during this time.

6.3.4 Former ice-sheet configuration, with respect to the Bungenstock Ice Rise

Tectonically-controlled bedrock folds beneath the IIS catchment [*Jordan et al*., 2013] govern the location of deep trough systems and high mountain ranges in and around the Ellsworth Mountains, which facilitate channelised ice flow from the WAIS interior to the FRIS in the Weddell Sea. *Bingham et al*. [2015] suggested that the current configuration of topographically-confined IIS tributary flows also reflects the spatial configuration of ice flow throughout the Holocene (and possibly earlier). Although the topographic constraints of the IIS tributaries mean that they are unable to migrate, buckled isochrones and ‘whirlwind’ features within ice flows of the Horseshoe Valley and Independence troughs evidence former enhanced ice flow in presently slow-flowing tributaries, indicating a switch-off of past enhanced ice flow. Enhanced ice flow through Independence and Ellsworth troughs during the mid- to late-Holocene would

have been conducive to driving ice flow across the IIS and the region now covered by Bungenstock Ice Rise (Figure 6.14), making these troughs strong candidates for contributing the ice flux necessary to facilitate paleo-ice streaming across what is currently a slow flowing ice rise [*Siegert et al*., 2013]. The occurrence of buckled and disrupted layering at depth in Independence Trough supports this suggestion by providing evidence for former enhanced flow in a trough where ice flow is now much slower.

As surface-conformable stratigraphy dominates the upper ice column within Horseshoe Valley it is unlikely that flow from Horseshoe Valley Trough contributed significantly to the streaming flow over the Bungenstock Ice Rise. This is likely to be a function of the topographically constrained nature of Horseshoe Valley Trough, as the high Ellsworth Mountains to the south east largely block the ingress of the WAIS in this area, and subglacial topography at the trough mouth encourages the diversion of flow into Hercules Inlet (Figure 6.14b). However, as buckled ice layers have been preserved in the mid to lower half of the ice column in Horseshoe Valley Trough, it is proposed that changes within the flow of this tributary may have occurred earlier than the mid-Holocene. Assuming advection of the buckled englacial layers at a current average velocity of 12 m a^{-1}, early Holocene buckles would still be present in Horseshoe Valley Trough. The late-Holocene deceleration of flow across the Bungenstock Ice Rise, previously inferred by *Siegert et al.* [2013], may therefore represent just one relatively local component of wider regional changes to ice flow that have occurred across the IIS and MIS catchments as the WAIS thinned after the LGM. Stagnation of Bungenstock Ice Rise is the main hypothesis for the present-day configuration of IIS [*Bingham et al.*, 2015]. The resultant reorganisation of flow and switch-on of the main IIS trunk would have re-routed and/or switched off ice flow exiting the deep trough systems of the IIS upper catchment (e.g. Independence Trough), and led to grounding line migration and the diversion of flow across the FRIS, in an ice flow configuration akin to that we see today (Figure 6.14).

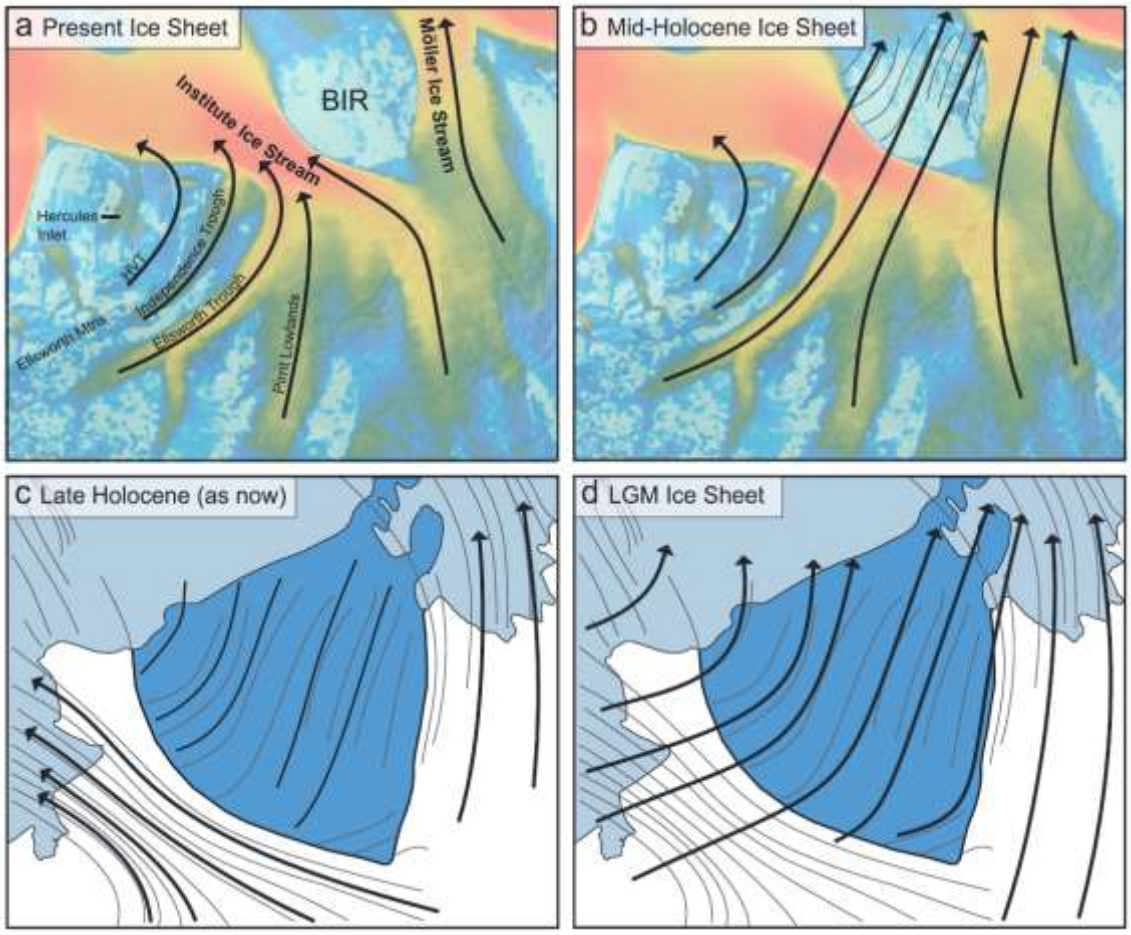

Figure 6.14. Schematic model of ice sheet change with respect to the Bungenstock Ice Rise (BIR). (a) The current glaciological situation with ice flow indicated by arrows. (b) Mid-Holocene ice sheet, where north-eastward ice flow dominates the region, crosscutting the present-day trunk of the Institute Ice Stream. (c) Late Holocene (as now) ice sheet flow described by *Siegert et al.* [2013] in which ice flow over Bungenstock Ice Rise becomes stagnant, thus leading to the present-day ice sheet configuration. (d) Last Glacial Maximum ice sheet hypothesised by *Siegert et al*. [2013]. The interpretation in Figure 6.14b refines flow paths and their relative ages (mid-Holocene instead of LGM), as well as indicating minimal flow from Horseshoe Valley Trough towards the Bungenstock Ice Rise.

6.4 Summary

This chapter defines the current configuration of the IIS and its tributaries and provides evidence for former enhanced ice flow and ice flow reorganisation in the Weddell Sea Sector of Antarctica. Airborne RES investigations of the internal stratigraphy of three tributaries of the IIS sourced from and transecting the Ellsworth Subglacial Highlands provide evidence for heterogeneous ice stream behaviour and Holocene flow dynamics. It is likely that the Independence and Ellsworth troughs acted as source areas for the mid- to late-Holocene enhanced flow recorded in flow stripes across the Bungenstock Ice Rise [*Siegert et al*., 2013]. The internal stratigraphy of ice flowing along Independence and Ellsworth troughs suggests that they may have acted independently of one another, undergoing asynchronous enhanced ice flow or a slow-down in ice streaming. The earliest evidence for enhanced ice flow, believed to have occurred ~4000 years ago [*Siegert et al*., 2013] is found in Horseshoe Valley Trough, where buckled and discontinuous isochrones are surveyed beneath a 500 m thick sequence of parallel, surface conformable isochrones. Evidence for changing ice flow velocities, possibly occurring more than ~400 years before present [*Siegert et al*., 2013], can be found within the topographically-confined Independence and Ellsworth troughs where strongly-deformed isochrones represent former enhanced ice flow through each trough, which would have allowed ice to traverse the main trunk of the IIS and flow over the region now covered by Bungenstock Ice Rise.

These observations are consistent with the hypothesis that the LGM and Holocene drainage pathways within the Weddell Sea sector of the WAIS were different from those of the present-day [*Larter et al*., 2012; *Siegert et al*., 2013] and that they indicate dynamic changes in ice flow velocity, which affected the interior parts of the Weddell Sea sector.

CHAPTER 7

Radar detected englacial debris

In this chapter strong englacial reflectors identified in GPR, airborne RES and ground RES will be mapped and analysed in 2D and 3D to constrain the location, form and approximate volume of englacial debris in and around Horseshoe Valley. Transects will be compared to pre-existing datasets to determine debris source areas as well as processes of debris entrainment. Implications for englacial debris transportation in the Weddell Sea sector of West Antarctica will also be discussed.

Radar detected englacial debris objective

Investigate debris entrainment mechanisms in the Weddell Sea sector of the West Antarctic Ice Sheet.

Research questions

1) Can geophysical methods detect debris in ice in and around Horseshoe Valley?
2) How much englacial debris is contained within Horseshoe Glacier?
3) What are the controls on debris entrainment and transportation in Antarctica?

7.1 Introduction

Although recent advances in ice penetrating radar data acquisition and processing have enabled englacial sedimentary structures to be identified in alpine-type glaciers [*Goodsell et al*., 2005; *Dunning et al*., 2015] and surge-type glaciers (characteristic of the Svalbard archipelago [*Boulton*, 1970; *Woodward et al*., 2003a; *Hambrey et al*., 2005; *Murray and Booth*, 2010; *Sevestre et al*., 2015]), very few studies have documented englacial debris in Antarctica. Whilst this is largely a function of radar resolution, and field site accessibility, a lack of detailed surveys has suppressed our understanding of debris sources and debris entrainment mechanisms beneath large ice sheets, as well as debris transport pathways through the ice. As debris sources

can alter frictional stress at the glacial bed and modify ice flow speeds [*Bell et al*., 1998], change ice flow direction through long-term erosive processes [*Harbor et al*., 1988] and transfer essential nutrients from continental sources to the Southern Ocean [*Death et al*., 2014; *Hawkings et al*., 2014] (Chapter 2) it is now critical to examine the controls on englacial sediments in West Antarctica.

In order to analyse englacial debris reflectors on both local and regional scales, this chapter will examine airborne and ground RES data, collected in and around Horseshoe Valley, as well as detailed step-and-collect mode GPR returns, surveyed in front of Patriot and Independence Hills. Figure 7.1 details the location of these survey lines where strong englacial reflectors within RES transects have been marked by black circles. A further airborne RES profile, collected across the Evans Ice Stream will also be examined to determine the wider controls on debris sources, entrainment mechanisms and debris transport pathways in the Weddell Sea sector of West Antarctica.

7.2 Results

7.2.1 Airborne radio-echo sounding of Horseshoe Valley

Pulse and SAR processed radargrams (collected by Dr. Neil Ross from the University of Newcastle and collaborators during a traverse of the IIS and MIS in 2010/2011), displayed in Figures 7.2, 7.3 and 7.4, detail a number of distinct englacial reflectors above basal topographic features. Two of these highly reflective, upwards dipping englacial structures, termed R1 and R2 are highlighted in Figure 7.2, where each reflector is distinct from the largely echo-free ice that surrounds them. R1 denotes the smaller of the two reflectors (which is only visible in flight line 14, as the other flight lines did not extend across Horseshoe Valley), where the strong reflector extends over 500 m through the ice column. This reflector dips at an angle of 35 - 40° from vertical, where the englacial structure stops short of the glacier surface by ~390 m. Although R2 exhibits similar reflection characteristics to R1, this second reflector represents a much larger englacial feature, where several steeply dipping diffractors (with a dip angle of ~60 - 65° from vertical) extend from the subglacial bed towards the ice surface, where the reflector

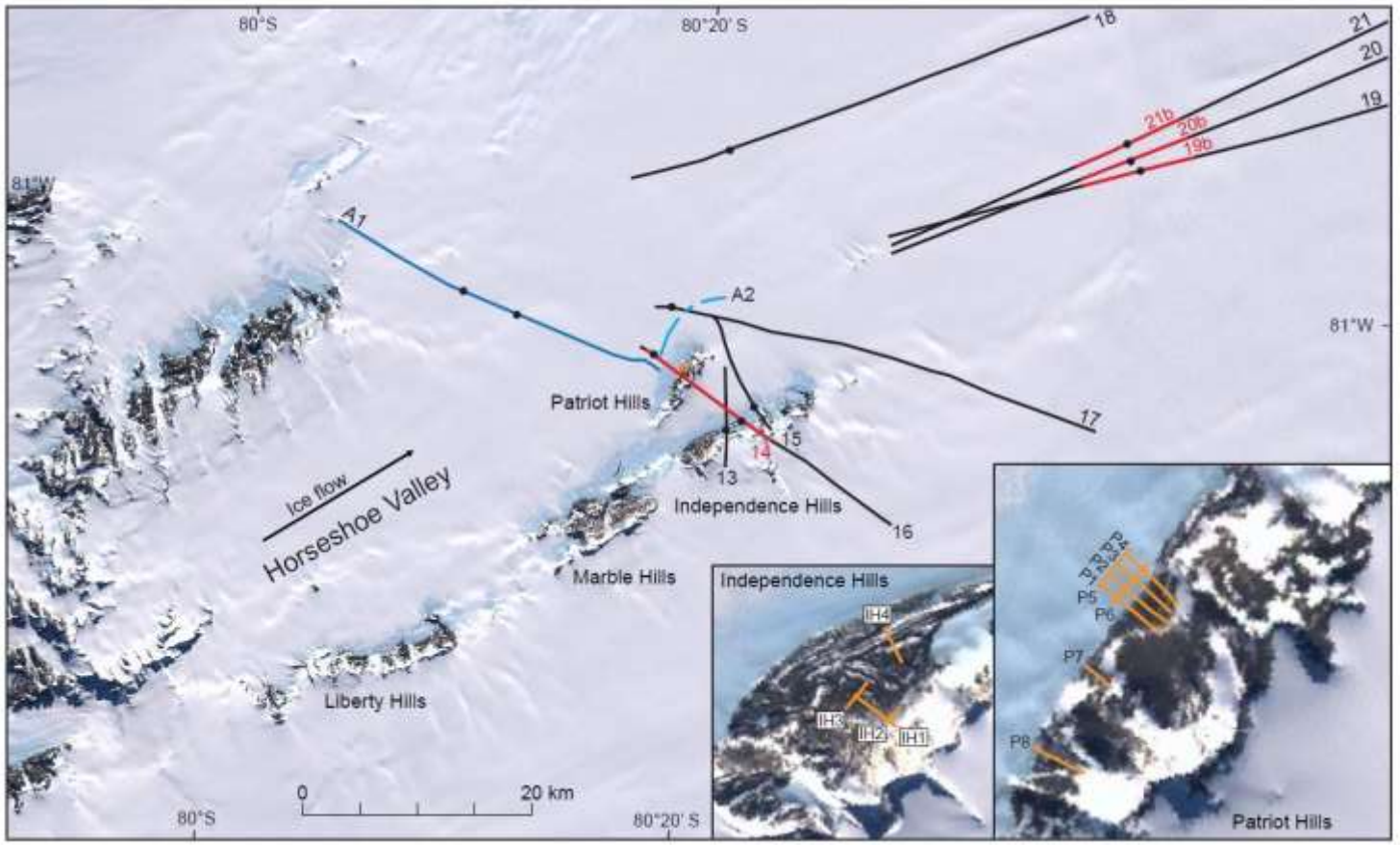

Figure 7.1. Geophysical transect lines examined in this chapter. Each profile contains strong englacial reflectors, where the strongest reflectors have been marked by a black circle. Black and red lines detail airborne RES flight lines, collected by Dr. Neil Ross (Newcastle University) and collaborators, blue lines indicate ground RES transects surveyed by Dr. Andrés Rivera (Centro de Estudios Científicos, Chile) and orange lines mark the location of GPR surveys across the main embayment of Patriot Hills, and along moraine sequences in front of Independence Hills. These GPR lines have been magnified in the two inset boxes.

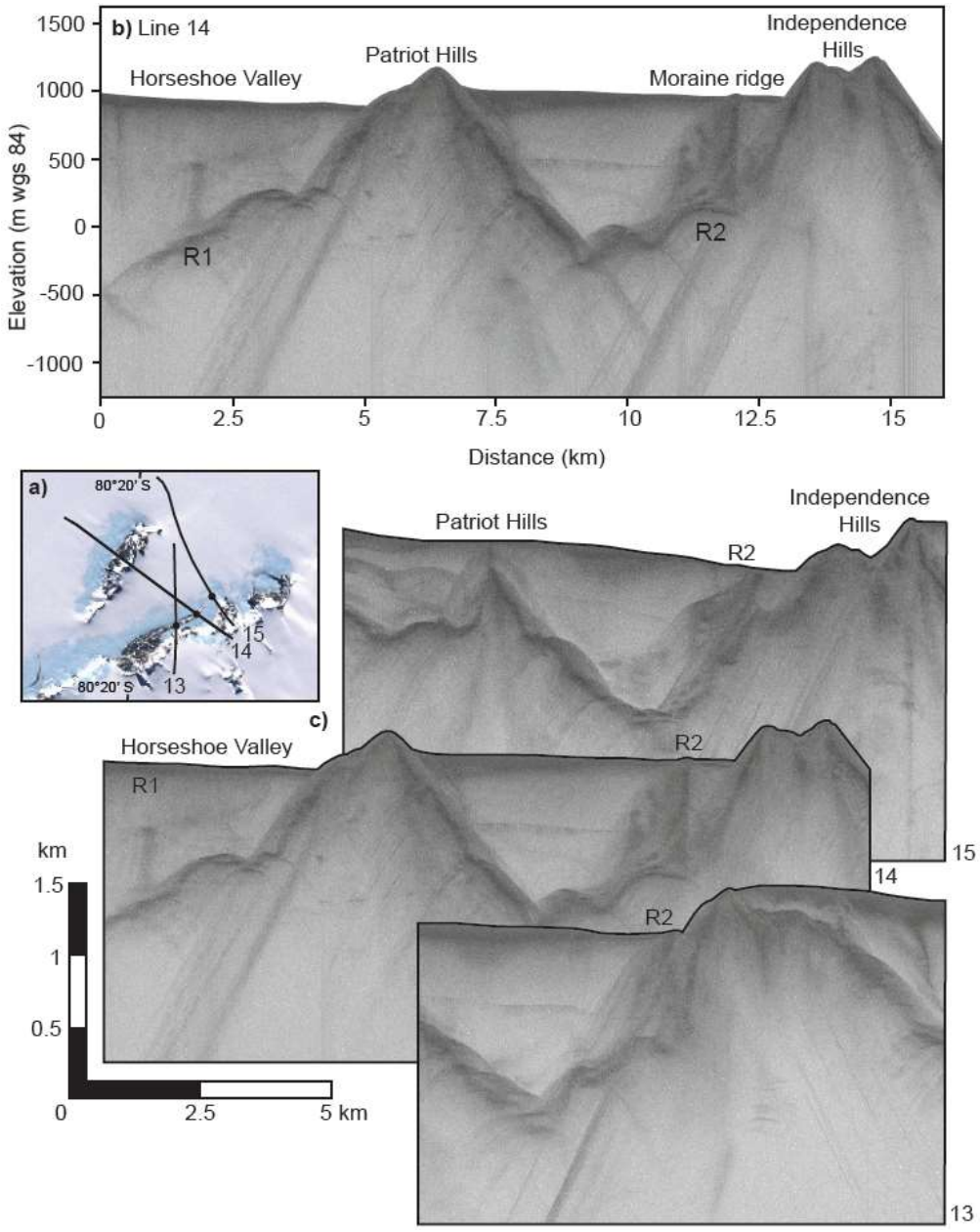

Figure 7.2. Englacial reflectors recorded in pulse-processed airborne RES transects across Horseshoe Valley. R1 is situated in front of Patriot Hills, where the reflector extends from the bed, but fails to reach the ice surface, whilst R2 is recorded in front of Independence Hills, where reflectors can be traced from the bed up towards the BIA surface, where moraine ridges elevate the surface topography.

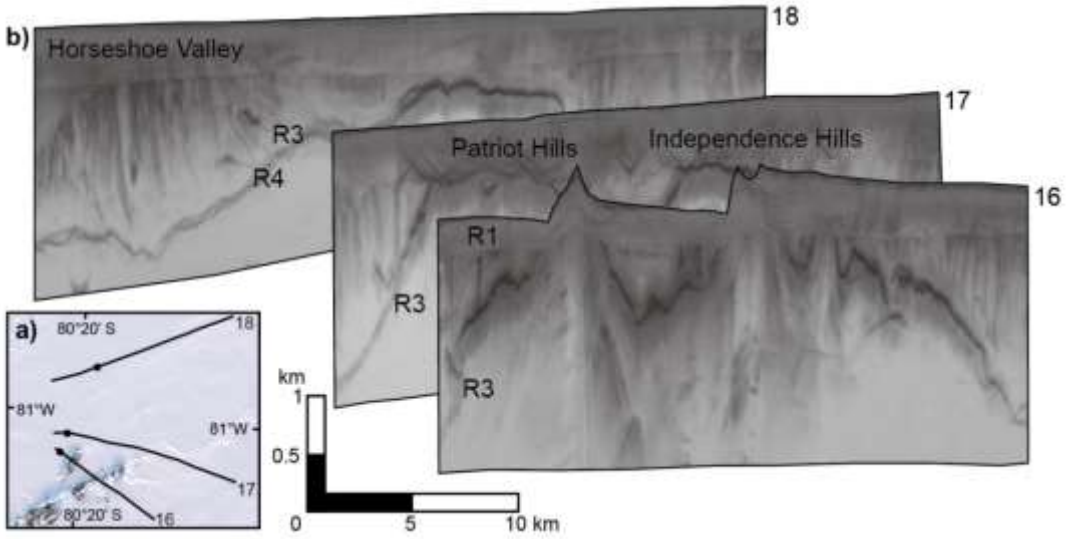

Figure 7.3. Englacial reflectors R3 and R4 recorded in front of Patriot Hills in three SAR-processed airborne RES flight lines, where ice flows through Horseshoe Valley, towards the local grounding line. Note that this processing technique fails to resolve the upper ~200 m of the ice column and nunataks.

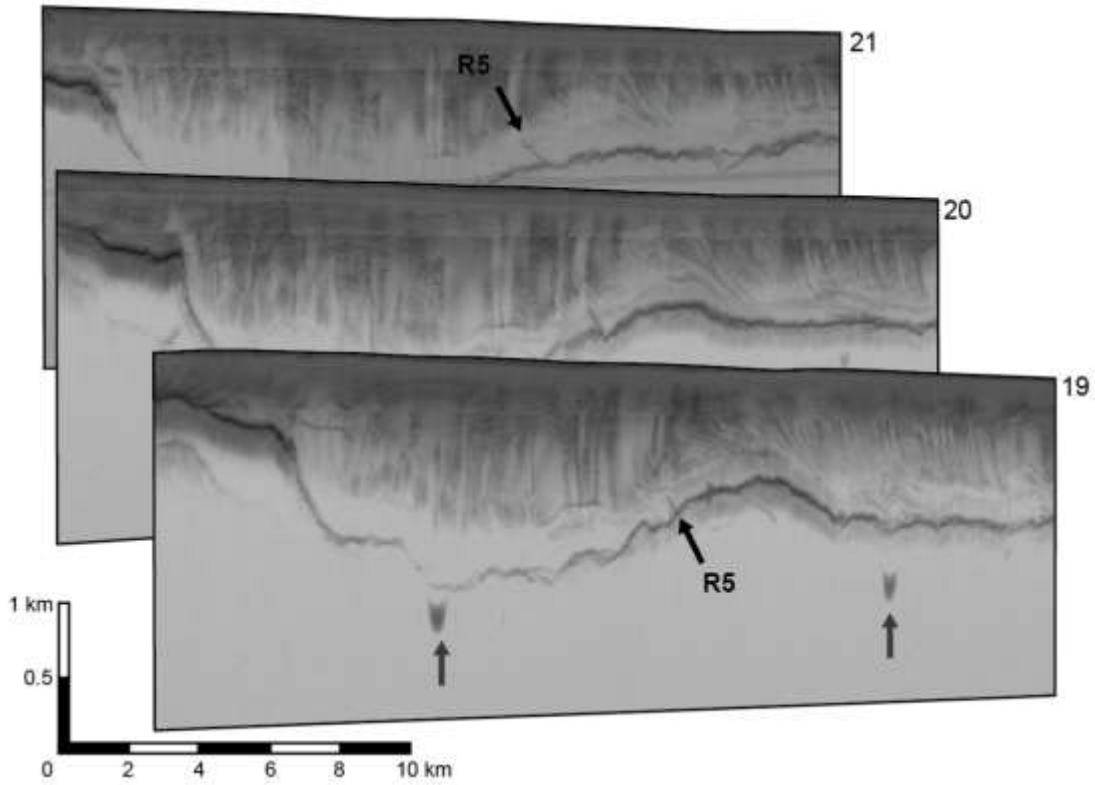

Figure 7.4. Distinct englacial features in SAR processed airborne RES flight lines 19, 20 and 21 (location has been marked in Figure 7.1), where ice flow is into the page. Grey arrows indicate processing artefacts. R5 represents a distinct englacial feature that extends from the bed in each radargram.

intersects a 22 m high moraine ridge in front of Independence Hills (annotated in Figure 7.2b). Whilst adjacent radargrams reveal that the steep angle of R2 is preserved down-flow, Figure 7.2 also demonstrates how the reflector geometry varies with depth through the ice column, and with distance from the exposed nunataks that define Independence Hills.

Although R1 and R2 document upwards dipping englacial reflectors near the ice sheet surface, Figure 7.3 reveals strong englacial reflectors further down the ice column, ~1.4 km below the surface of Horseshoe Glacier, and over 750 m below present day sea level. In this figure, a third highly reflective englacial feature, termed R3, extends over 200 m from the glacial bed; towards the centre of Horseshoe Glacier in three airborne RES transect lines. Although the reflector remains a similar shape and size down flow, Figure 7.3 shows how the reflector dip angle changes from ~65° to 75° (from vertical) over 4.5 km (between lines 16 and 17). In the last airborne RES flight, line 18, R3 dips at ~86° (from vertical), where R3 is now disconnected from the ice/bed interface. A fourth distinctive englacial reflector is also recorded in flight line 18 (Figure 7.3), where R4 extends over 300 m through the ice, at a dip angle of ~87° from vertical.

Figure 7.4 details the last group of strong englacial reflectors to be recorded within airborne RES traverses of Horseshoe Valley Trough (Figure 7.1). These radargrams reveal a fifth set of strong englacial reflectors, which extend from a subglacial bedrock bump, towards the centre of the ice flow at angles of ~55° - 63° from vertical. Whilst Figure 7.4 documents the down-ice persistence of R5 (where the reflector varies in shape and size with distance down valley), Figure 7.5 highlights the relationship between R5, the subglacial bed and numerous weak internal reflectors that represent isochronal layers and whirlwind features. This figure shows how R5 extends beneath buckled and disrupted englacial stratigraphic layers in flight lines 19b and 20b, where folded isochrones are recorded above the strong englacial reflector. Whilst these two radargrams reveal similar features, flight line 21b (traversed ~2500 m from the first transect line – 19b) records nearly straight and parallel internal stratigraphic layers, which are more conformable with the subglacial bed topography. In this last flight line R5 appears to be disconnected from the ice/bed interface (Figures 7.5c and 7.5f).

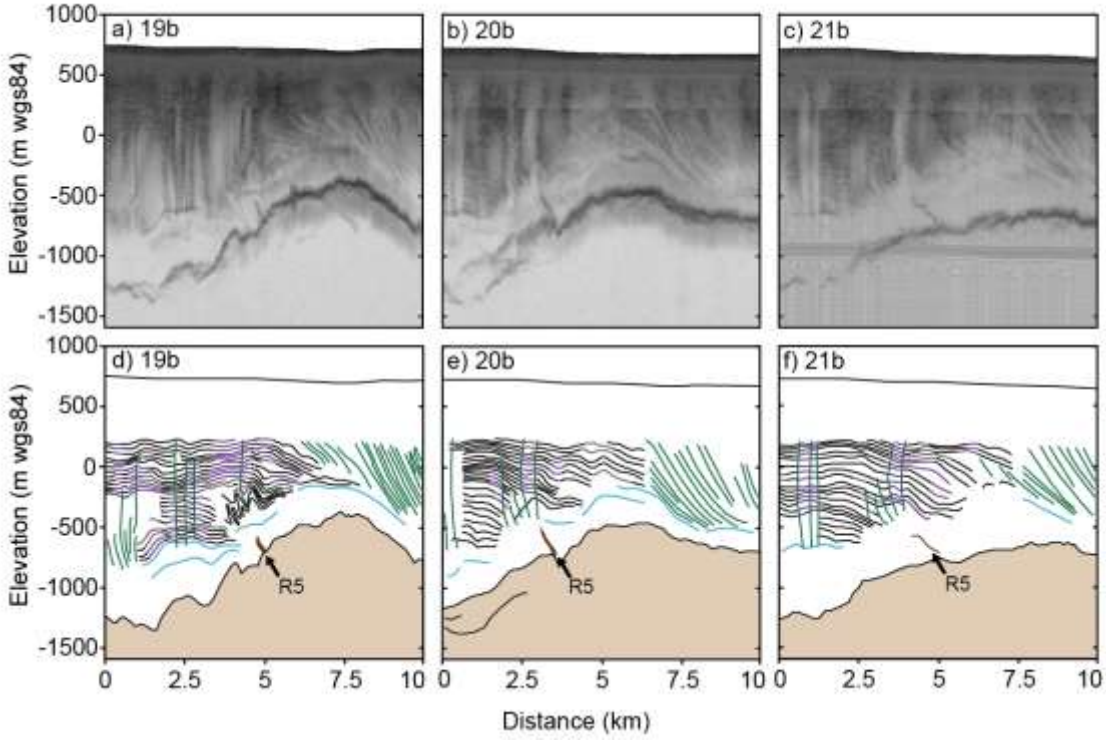

Figure 7.5. Detailed investigations of englacial reflector R5 in 2D radargrams. Boxes a-c reveal SAR-processed airborne RES transects (visualised in full in Figure 7.4), which are digitised in d-f to show prominent englacial features (black for observed, dashed for inferred and purple for best estimate), the basal topography (brown), strong englacial reflector R5 (dark brown) and englacial whirlwind features (green).

7.2.2 Ground penetrating radar surveys of Horseshoe Valley

Detailed, high-resolution step-and-collect mode GPR transects, collected during the austral summer of 2012/2013 have also revealed a number of distinct englacial features beneath BIAs and their associated moraine sequences in Horseshoe Valley. Figure 7.1 shows the geographic location of these survey lines, where the PulseEKKO system (detailed in Chapter 4) collected radar returns within Patriot Hills main embayment, and along the moraine system in front of Independence Hills.

Patriot Hills main embayment

Figure 7.6 details a number of GPR lines, surveyed across Patriot Hills main embayment. These transects reveal the surface of Horseshoe Glacier, and the sloping bed topography that extends away from Patriot Hills, as well a number of englacial stratigraphic features and hyperbolic radar returns. Although stacked and inclined isochrones, representing former ice sheet surfaces [*Turney et al*., 2013] are visible at the start of each transect line (Figure 7.6), where dip angles record BI flow trajectories (see Chapters 2 and 5), it is difficult to trace englacial stratigraphic layers near the mountain front, where the surface is covered by BI moraine accumulations (detailed in Chapter 3). Hyperbolic radar returns dominate this section of the radargram, where the returns represent point-like objects imaged by the radar at different angles [*Daniels*, 2004]. Figure 7.7b shows how these returns are often grouped into near vertical bands, which extend from the subglacial bed, all the way up to the surface, where BI moraine systems elevate the local topography.

Independence Hills moraine system

During the austral summer of 2012/2013 four GPR transects were also surveyed across the distinctive hooked moraine systems which lie at the foot of Independence Hills (see Chapter 3, section 3.6.2 for an introduction to Independence Hills moraine system). Figure 7.8 documents the subglacial topography and englacial stratigraphy of the largest transect line (IH3) – where the PulseEKKO system was manually towed over the debris-covered surface, in a survey line

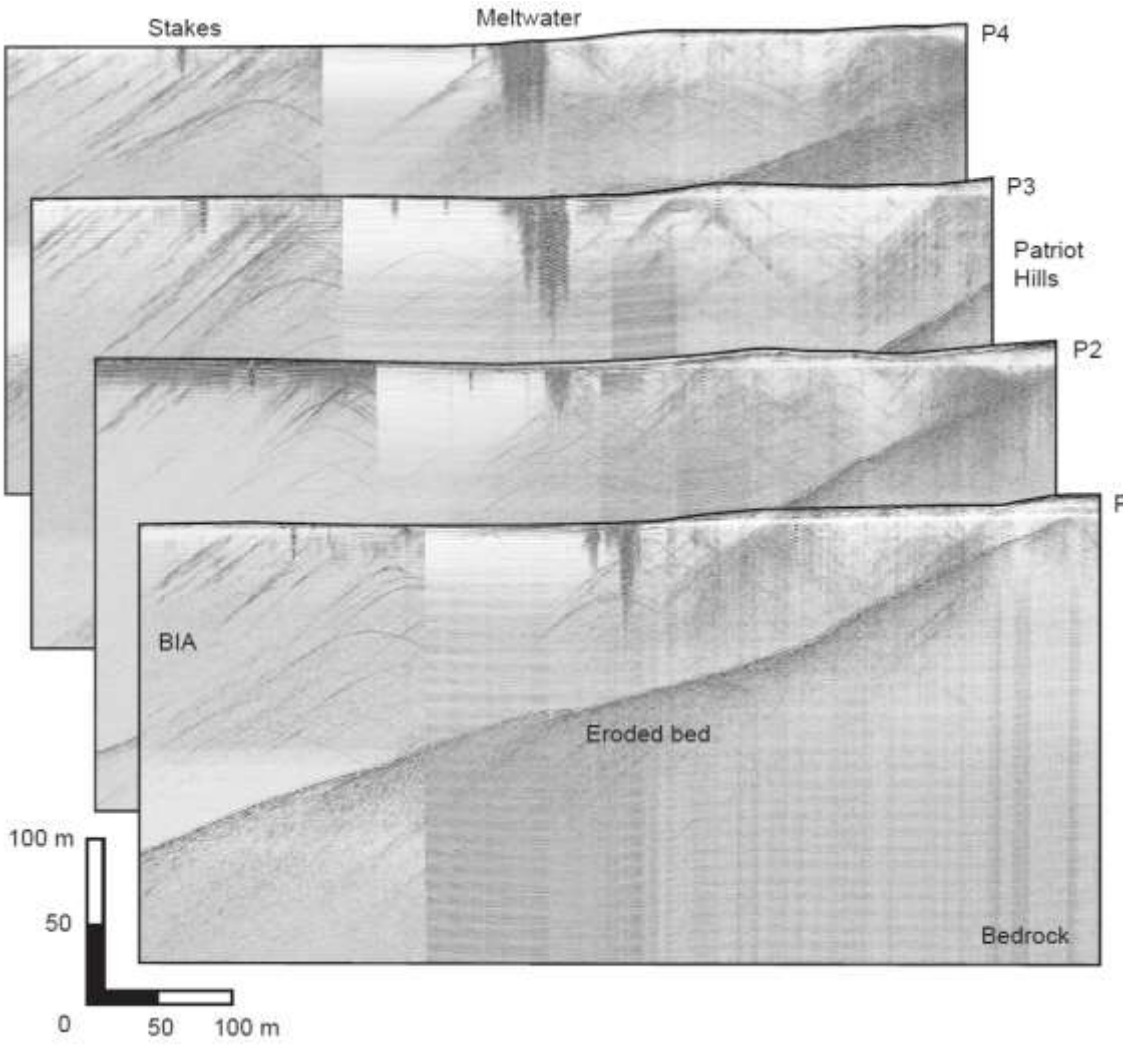

Figure 7.6. GPR transects collected in step-and-collect mode across Patriot Hills main embayment. A glacially eroded ice/bed interface is recorded beneath moraine sequences in front of Patriot Hills.

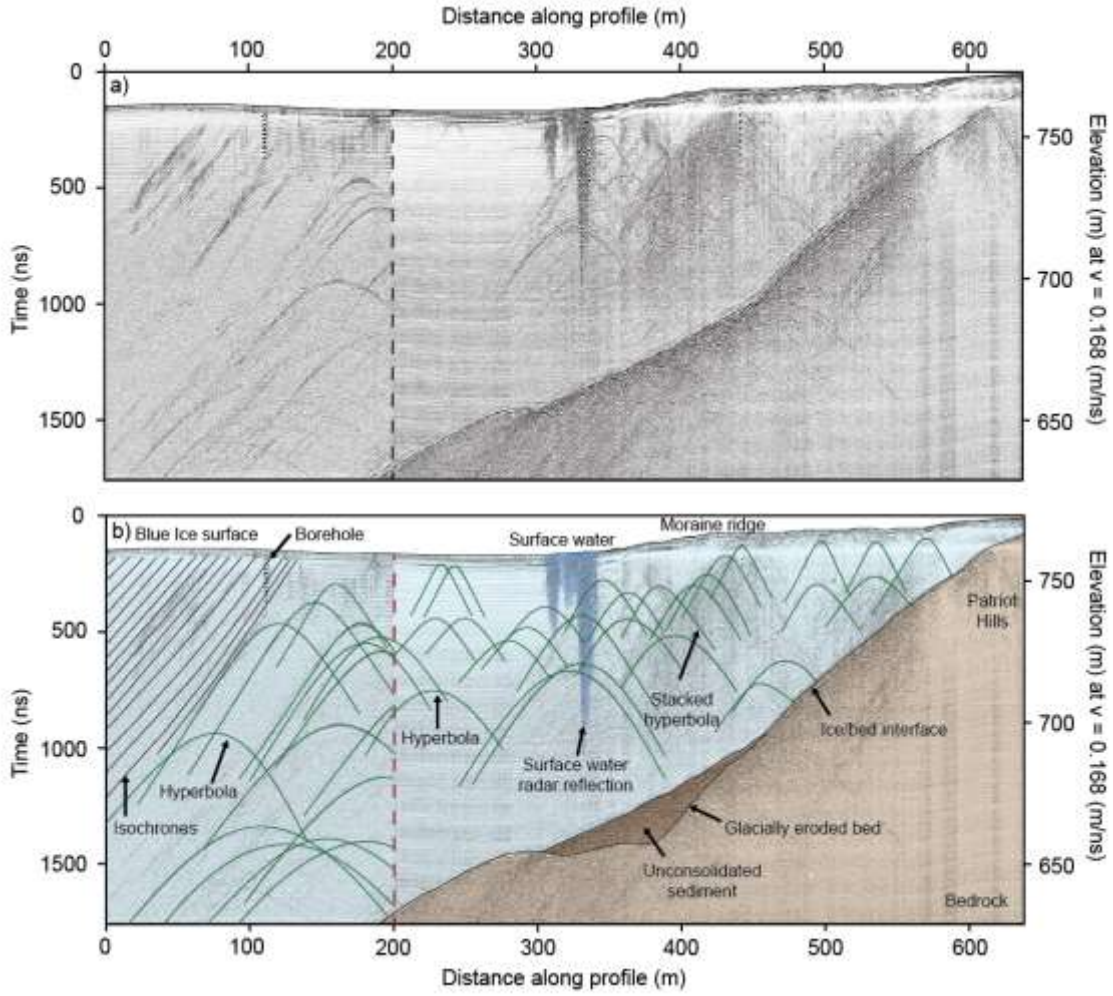

Figure 7.7. GPR transect line P1, surveyed across Patriot Hills BIA and Patriot Hills BI moraine sequences (a), and annotated in (b) to highlight prominent features (where hyperbolic reflectors are coloured green, isochrones are coloured black and radar reflections from surface water are coloured blue). Brown polygons define bedrock and unconsolidated sediment whilst the dashed line in a) and b) represents the junction between two radargrams.

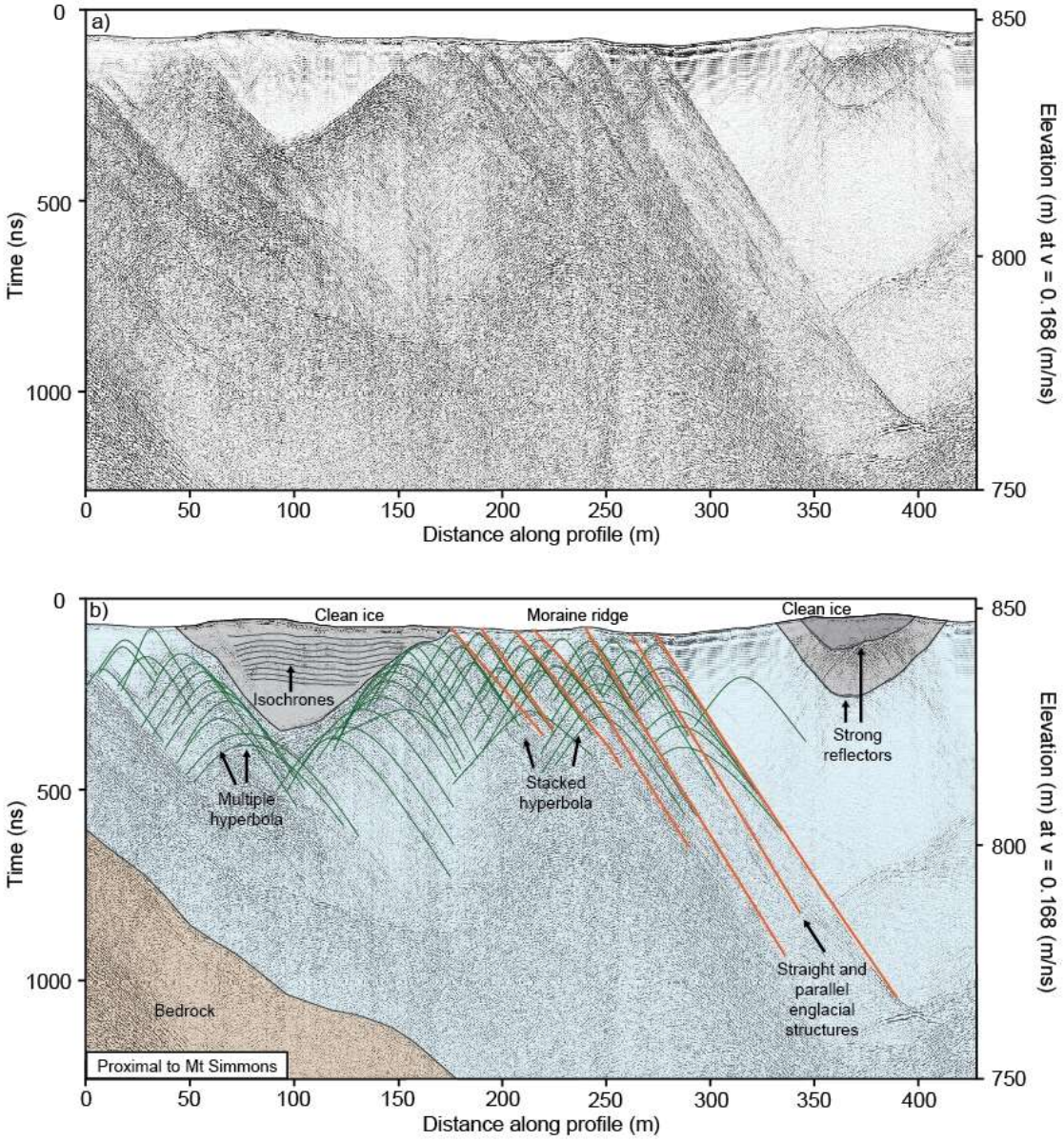

Figure 7.8. GPR transect IH3, collected along BI moraine sequences in front of Independence Hills (a), and annotated in (b) to highlight prominent features, where radar returns are coloured green if they are hyperbolic, black when they represent continuous isochrones and orange when they reveal straight and parallel englacial structures. Grey polygons reflect clean ice incursions, whilst bedrock is highlighted by a brown polygon.

orientated approximately parallel to the main mountain ridge (see Figure 7.1). Hyperbolic radar returns and the point sources that they represent dominate this transect line, where these distinctive subsurface features help to reveal straight and parallel englacial structures, that extend from the ice/bed interface, towards elevated BI moraine sequences. Although it is difficult to detect and trace englacial stratigraphic layers beneath the thick BI moraine accumulations, a set of straight and parallel isochronal layers are recorded just beneath the surface, approximately 100 m along transect IH3 (Figure 7.8b). As these layers are recorded within a zone of clean ice, which is separated from the main flow of ice (which contains a number of steeply dipping structures and point-like reflectors), it is likely that this zone of ice, and indeed another region of clean ice (located ~350 m along the transect line) evidence exotic ice flows. By analysing geomorphological features along Independence Hills it is suggested that these ice flows are derived from hanging valleys near Mount Simmons, where the local clean ice flows cut across the main flow of debris-rich ice, which is being driven towards the steep ridge of Independence Hills by compressive BI flow.

7.2.3 Other geophysical surveys

Horseshoe Valley ground and airborne RES

In order to understand the regional occurrence of strong englacial reflectors in Horseshoe Valley, Figures 7.9 and 7.10 document ground RES surveys across Horseshoe Glacier, which were originally collected by Dr. Andrés Rivera (Centro de Estudios Científicos, Chile) to detect and image basal topographic features. Two strong internal reflectors are recorded near the ice/bed interface in Profile A1 (Figure 7.9), where the reflectors are located approximately 1180 m and 1690 m along the transect, at depths of ~1300 m and ~1000 m below the ice sheet surface. Just like the deep englacial features recorded in airborne RES transects, these strong internal features also exhibit similar reflection strengths to the bed, where the reflectors are angled upwards, and towards the centre of Horseshoe Valley. In a similar manner to R3 (Figure 7.3), Figure 7.9 reveals that the reflector with the highest dip angle is connected to the bed whilst the more horizontal reflector (detected further up the ice column) is not connected to the

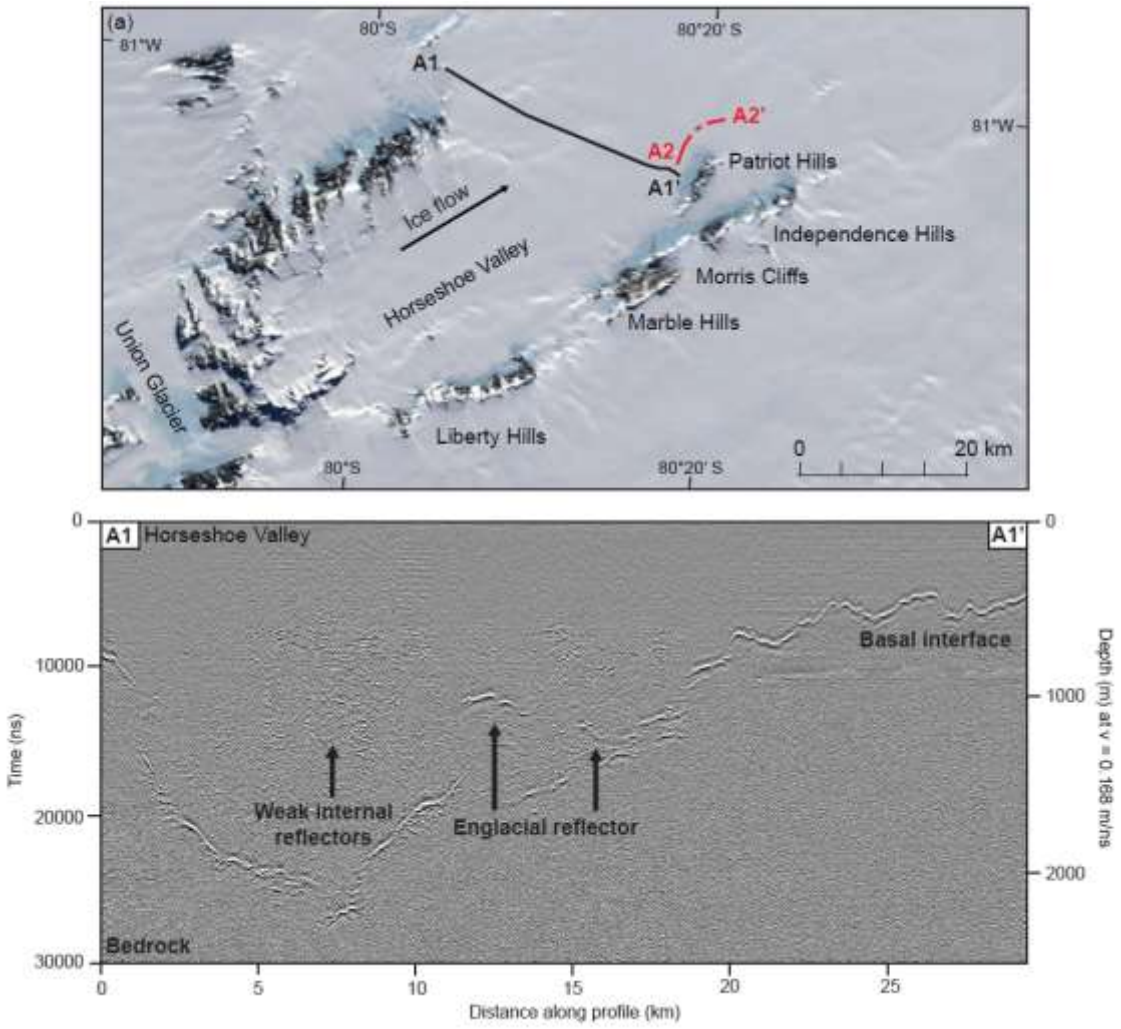

Figure 7.9. Ground RES transect A1, collected across Horseshoe Valley by Dr. Andrés Rivera (Centro de Estudios Científicos). The radargram resolves the complex basal topography as well as two distinct englacial reflectors ~1180 – 1690 m along the transect, at depths of 1300 – 100 m below the ice surface, where ice flows through Horseshoe Valley towards the local grounding line of the FRIS.

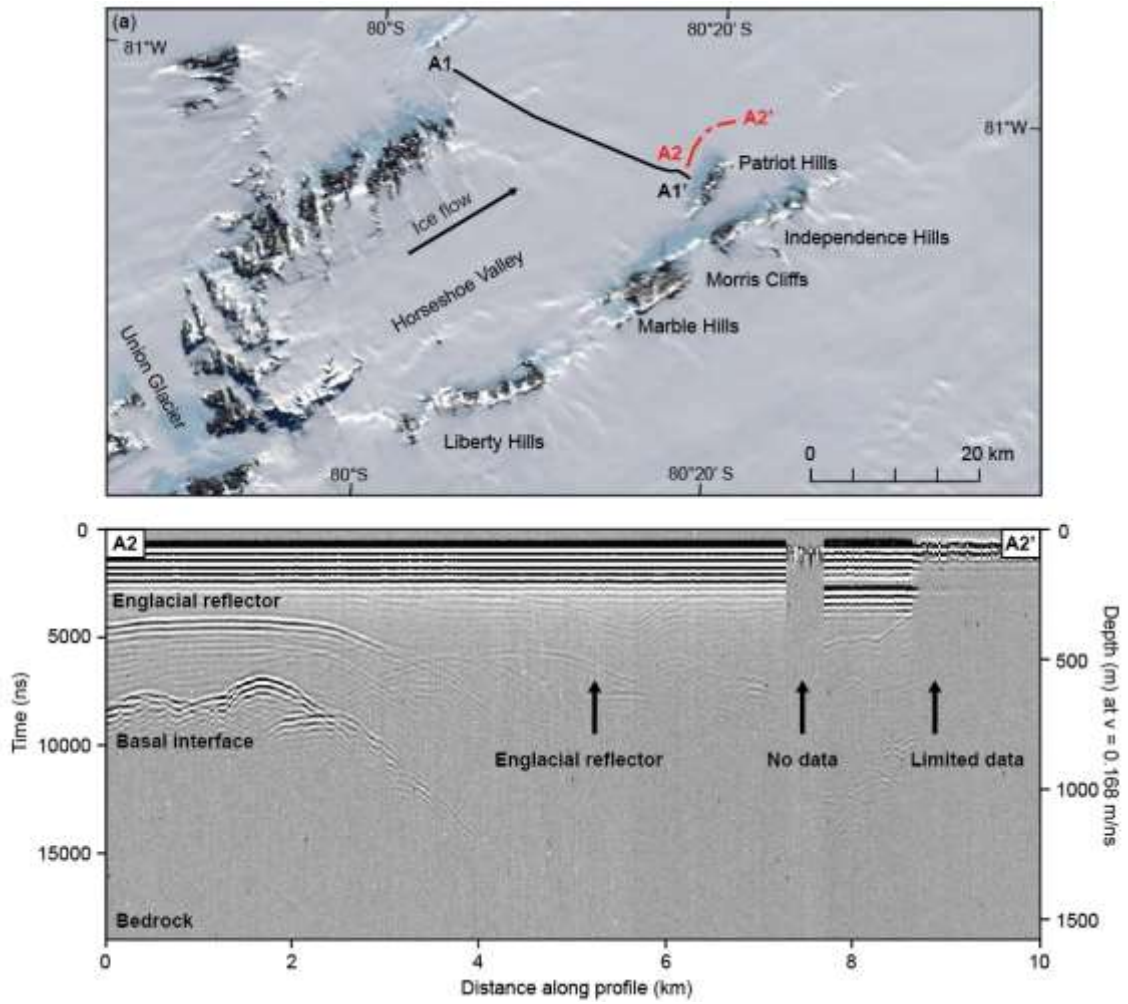

Figure 7.10. Ground RES transect A2, collected in front of Patriot Hills by Dr. Andrés Rivera (Centro de Estudios Científicos). This radargram records the basal interface near Patriot Hills BIA, as well as a number of englacial reflectors. As the radar system failed twice during the traverse, two sections of the radargram contain limited or no data.

bed. In this radargram numerous weak reflectors are also recorded in the mid- to lower ice column, where echoes cross cut internal stratigraphic features.

The second ground RES profile, line A2, imaged in Figure 7.10, reveals a new perspective of Horseshoe Glacier as the transect line was surveyed down flow, rather than across it. This radargram reveals a number of strong, near-horizontal englacial reflectors, which exhibit similar reflections to the bed. Although these straight and parallel englacial features can be traced along the front of Patriot Hills for over 3 km, more diffuse and disturbed layers feature when the survey line traverses the perimeter of Patriot Hills.

Airborne RES of the Evans Ice Stream

In order to appreciate the continent-wide occurrence of strong englacial reflectors near the ice/bed interface, Dr. David Ashmore from the University of Aberystwyth has allowed this thesis to examine an airborne RES transect across the Evans Ice Stream (Figure 7.11), where data were collected by the same British Antarctic Survey PASIN system described in Chapter 4. Although the radargram in Figure 7.11c reveals a number of subsurface features, related to differential ice flow velocities between the fast flowing Evans Ice Stream (where isochronal layers are disrupted and discontinuous), and slow-flowing upland catchment (where stratigraphic layers are often conformable with the subglacial topography) (Figure 7.11b), three distinct reflectors (E1-E3) are also recorded at the ice/bed interface. These reflectors extend into gently folded basal ice, where the boundary of the basal ice zone changes shape, and increases in thickness in conjunction with the occurrence of E1-E3.

7.3 Interpretation

7.3.1 Englacial reflectors

This chapter has documented a number of highly reflective englacial structures, in a variety of ice penetrating radar surveys in and around Horseshoe Valley and the Evans Ice Stream. In each case, the radar system has recorded englacial bands or hyperbola (depending on scale) near the ice/bed interface; where the reflectors are recorded at a number of elevations (and depths below

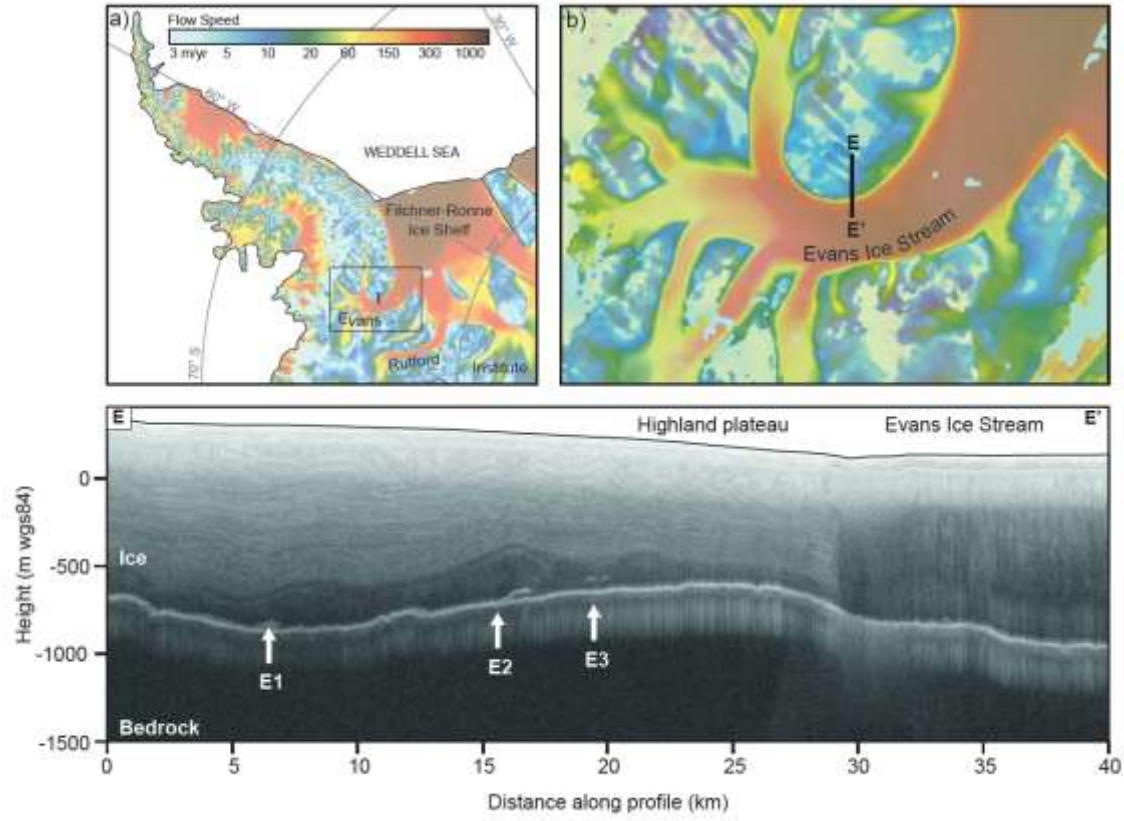

Figure 7.11. Airborne RES transect line across the Evans Ice Stream (processed by Dr. David Ashmore from the University of Aberystwyth). a) shows the location of the Evans Ice Stream in relation to the Institute Ice Stream and the Antarctic Peninsula (background imagery details surface ice-flow velocity from MEaSUREs [*Rignot et al*., 2011a]). The black box marks the location of b) which details the position of the airborne RES flight line in more detail. The radargram in c) reveals continuous and parallel isochrones above the highland plateau and much more disturbed and discontinuous layering within the Evans Ice Stream. Three strong englacial reflectors, E1 – E3 are also highlighted, where the features record similar reflection strengths to the bed. These strong reflectors are co-incident with englacial stratigraphic folds near the bed.

sea level); along transect lines of various orientations. Although the englacial features display similar reflection characteristics to the bed, two distinct forms exist; (1) reflectors that typically extend up to BI moraine sequences, on the leeward foreground of nunataks and (2), strong reflectors that are found at depth (beneath a thicker ice sheet), where reflectors do not reach the ice sheet surface. As all of the reflectors vary in size, shape and reflectivity with depth and distance from valley side walls, multiple reflection origins from the mountain front can be eliminated [*Daniels*, 2004; *Cuffey and Patterson*, 2010]. These findings reveal that the strong englacial reflectors documented throughout this chapter must evidence debris clasts/particles within the ice.

7.3.2 Approximating englacial debris in and around Horseshoe Valley

In order to approximate the area, volume and mass of englacial debris in and around Horseshoe Valley, polygons were used to define the perimeter of debris reflector bands within zones of offline reflectors and hyperbolic radar returns in various airborne RES transects (see Figure 7.12). Approximate area calculations for each group of debris reflectors have been detailed in Table 7.1, which reveals a total debris area of approximately 14 million m^2 within airborne RES detected debris bands. To convert area to volume, known distances between transect lines were fed into equation 7.1, which denotes a standard equation, developed to calculate the volume of a frustum (V_f).

$$V_f = (\text{distance between transects}/3) * (A_1+A_2 + \sqrt{(A_1 * A_2)} \quad (7.1)$$

This calculation reveals over 18 billion m^3 of debris-rich ice in and around Horseshoe Valley, and over 14 billion m^3 in front of Independence Hills alone (between transect lines 13-15). By converting volume to mass, using a standard high limestone density of 2560 kg/m^3 [*Ingham*, 2010], Table 7.1 shows how debris bands in the upper IIS catchment (in and around the Ellsworth subglacial highlands) amount to over 46 tera tonnes of debris. Whilst this total mass assumes that debris-band reflectors evidence large debris blocks within the ice, more realistic

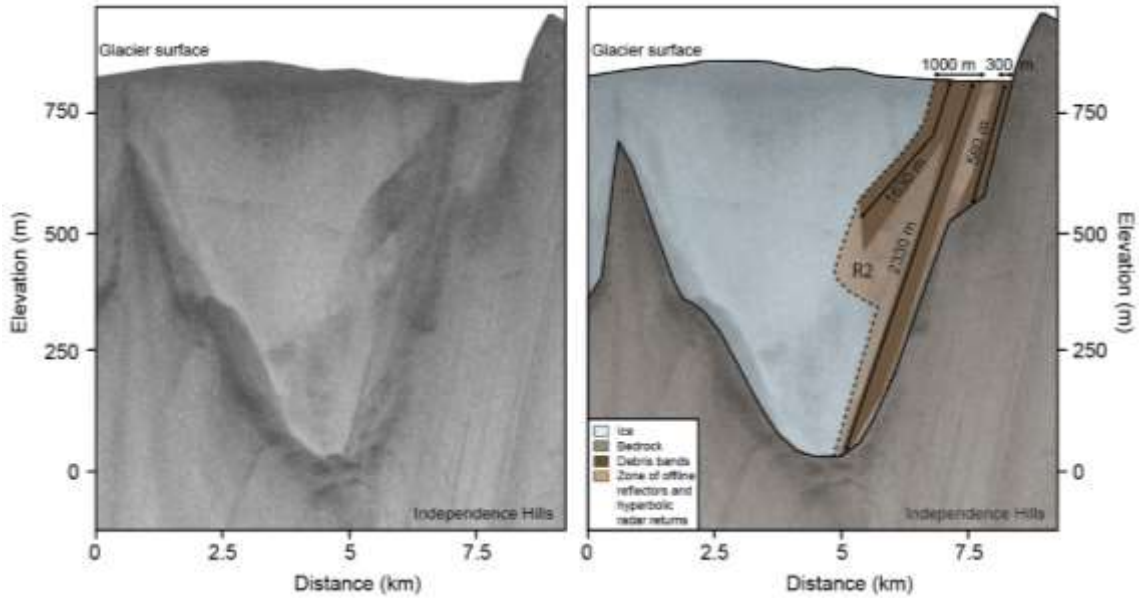

Figure 7.12. Airborne RES transect line 15, annotated in b) to show the perimeter of debris reflector bands within zones of offline reflectors and hyperbolic radar returns (R2) in airborne RES transects.

Table 7.1 Approximate debris calculations

Debris Calculations	Area (m^2 x10^5)	Distance between lines (m)	Debris volume (x10^7 m^3)	Mass 100% (x10^{11} T)	Mass 10% (x10^{11}T)	Mass 20% (x10^{11} T)	Mass 30% (x10^{11} T)
R2 - Line 13	49	-	-	-	-	-	-
R2 - Line 14	55	1,690	878	225	22	45	67
R2 - Line 15	21	1,596	585	150	15	30	45
R2 total	125		1463	375	37	75	112
R3 - Line 16	0.8	-	-	-	-	-	-
R3 - Line 17	0.8	3,426	27	7	0.7	1.4	2.1
R3 - Line 18	1.5	12,611	143	37	3.7	7.3	11
R3 total	3.1		170	44	4.4	8.7	13.1
R5 - Line 19b	0.2	-	-	-	-	-	-
R5 - Line 20b	0.3	1,104	2.7	0.7	0.07	0.14	0.21
R5 - Line 21b	0.1	1,396	2.7	0.7	0.07	0.14	0.21
R5 total	0.6		5.4	1.4	0.14	0.28	0.42
R1 - Line 14	1	-	-	-	-	-	-
R1 - Estimate	1*	5,000*	50	13	1	3	4
R1 total	2		50	13	1	3	4
R4 - Line 18	2.6	-	-	-	-	-	-
R4 - Estimate	2.6*	5,000*	130	33	3.3	6.7	10
R4 total	5.2		130	33	3.3	6.7	10
R1-R5 total	**136 x10^5 m^2**		**18 x10^9 m^3**	**466 x10^{11} T**	**46 ± 23 x10^{11} T**	**94 ± 48 x10^{11} T**	**140 ± 46 x10^{11} T**

*Estimated area or distance due to lack of 3D data
T = metric tonnes
Mass of debris = total volume of debris*2560 (limestone density in kg/m^3)
Mass 100% assumes 100% debris block, Mass 10% assumes 90% ice, 10% rock etc.

estimates of ice/debris ratios have also been provided in Table 7.1, where mass 10% documents debris-rich ice with a ratio of 90% ice, and 10% debris within the reflectors, and mass 20% details an ice/debris ratio of 80:20 etc. Whilst further investigations are required to determine exact ice/debris ratios, a conservative estimate of debris-rich ice concentrations of mass 20% reveals over 9 tera tonnes of debris-rich ice in Horseshoe Valley Trough using airborne RES methods alone. Although this value approximates the mass of over 28 million Empire State Buildings (each weighing 331,122 metric tonnes), estimates in terms of Horseshoe Valley reveal that this equates to a layer of less than 1 mm of sediment across the entirety of Horseshoe Glacier surface. As this value is derived from a small number of surveyed lines, this low coverage indicates that ice flows in the Weddell Sea sector of the WAIS are capable of entraining and transporting large volumes of debris.

7.4 Discussion

Following discussions of debris entrainment mechanisms in Chapter 2 (section 2.7.2) this section will focus on the specific controls that regulate debris entrainment processes in Horseshoe Valley, where commentary on debris entrainment mechanisms in the Weddell Sea sector of the WAIS will also be provided. As debris entrainment is governed by a variety of processes including sediment availability, ice flow and ice temperature (see Chapter 2, section 2.7.3) - which are often associated with ice thickness, debris entrainment mechanisms will be examined in terms of near-surface debris incorporation (in thin ice flows near nunataks), and then debris entrainment at depth (beneath thick ice accumulations).

7.4.1 Near-surface debris entrainment

Englacial layer folding, crevasse filling, thrust faulting and regelation process can all facilitate near-surface debris entrainment (section 2.7.2). By analysing the relationship between englacial stratigraphic features and the hyperbolic radar returns that represent englacial debris clasts/particles in thin ice flows near nunataks (e.g. Figures 7.6 and 7.8), it is possible to eliminate two of these near-surface debris entrainment mechanisms in Horseshoe Valley. As

detailed step-and-collect mode radargrams reveal that isochronal layers beneath BI moraine deposits in front of Patriot and Independence Hills are continuous and parallel (Figure 7.7), where there is no evidence of englacial layer folding or basal crevassing, near-surface debris entrainment through compressive folding or basal crevassing can be ruled out. Following literature reviews in Chapter 2, these findings imply that clasts must be entrained through thrust faulting and/or regelation processes at the ice/bed interface (Figure 7.13). Although most studies regard debris incorporation through regelation as a self-limiting process - as regelation into the bed eventually slows itself as the debris layer thickens [*Alley et al.*, 1997], BI flows will suppress this condition, as compressive ice flows with upwards trajectories will help to elevate previously entrained clasts through the ice column, and expose new sediments at the glacial bed. These processes can account for some of the hyperbolic radar returns within Patriot and Independence Hills BIAs, as well as extensive surface moraine deposits (reported by *Fogwill et al*. [2012] and *Westoby et al*. [2015]).

Whilst regelation processes can enhance debris entrainment mechanisms beneath BIAs in Antarctica, it is also anticipated that the characteristically compressive flow regimes of BIAs associated with nunataks could promote debris entrainment through the initiation and development of thrust faults. In order to investigate this assertion, detailed step-and-collect mode GPR returns have been examined beneath Independence Hills moraine system in Figure 7.8. Here, transect line IH3 reveals a series of stacked hyperbolic radar returns which frequently reveal one dominant limb which tends to vertical when migrated (although the complex 3-D nature of the features, recorded within 2-D transect lines prevents full migration). The crests of these hyperbolic features and their steepened limbs help to reveal seven linear features that cross-cut dipping isochrones as they extend from the subglacial bed, to the moraine surface. These features are interpreted as faults, which must develop in response to compression as BI flows are driven towards the ~14 km long mountain front of Independence Hills, which stands at a maximum elevation of 1670 m above sea level. Unconsolidated sediments will be entrained near the glacial beds as these thrust faults open and slip, which will allow the debris-rich ice to

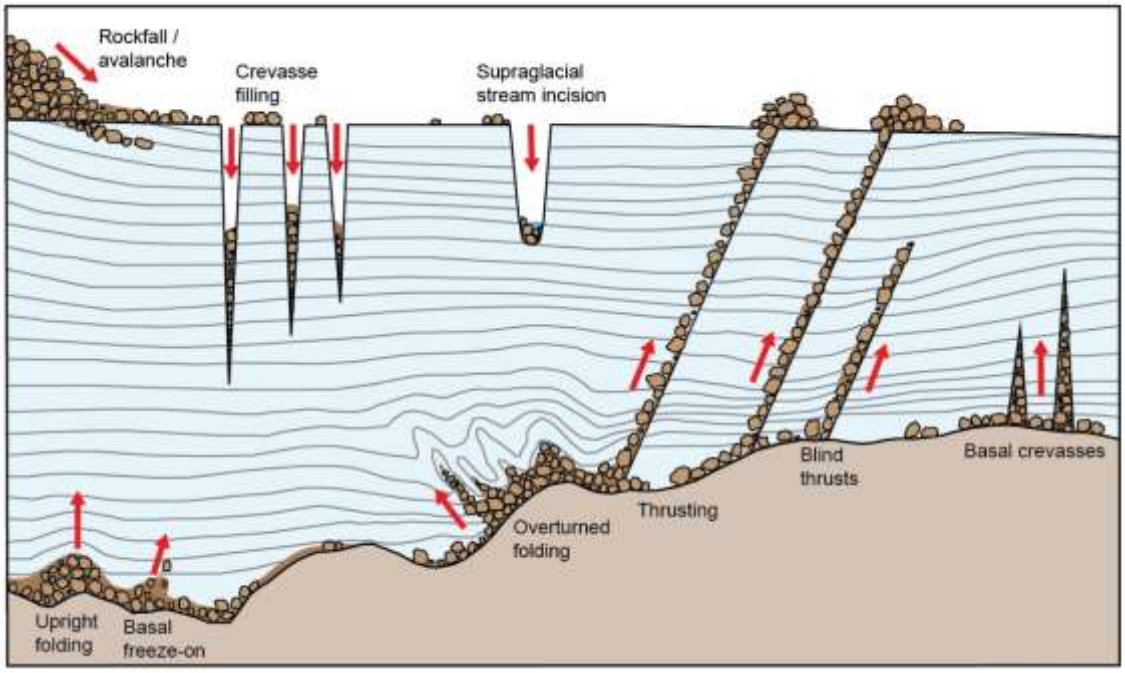

Figure 7.13. Possible debris entrainment mechanisms in ice sheets (repeat of Figure 2.17). Supraglacial debris can be incorporated into ice flows through successive snow deposition in the accumulation zone, through crevasse filling or supraglacial stream incision. Basal debris can be entrained through a variety of processes linked to internal ice deformation. This includes folding, thrusting, freeze-on and crevasse-filling.

be transported through the ice column, towards surface moraine deposits [*Hambrey and Glasser,* 2011].

Overall, these findings reveal that near-surface debris entrainment processes in the vicinity of nunataks are facilitated by the regelation of ice around debris clasts at the ice/bed interface and through thrust faulting mechanisms, where favourable conditions beneath BIAs allow large volumes of sediment to be entrained and transported towards the glacier surface. Spatial variations in debris entrainment mechanisms in Horseshoe Valley suggests that near-surface debris incorporation throughout the EAIS and WAIS must be governed by local ice flow conditions (e.g. flow direction, velocity and internal stresses), debris availability at the ice/bed interface and ice thickness, where the point of entrainment will depend on ice temperature (and therefore the local thermal regime).

7.4.2 Debris entrainment at depth

Debris reflectors deep within the ice column are very different from the stacked hyperbolic radar returns described above. Figures 7.3 – 7.4 describe how debris reflectors at depth are always angled away from the mountain front, rather than towards it, where steeply dipping debris bands are often co-incident with elevated basal topography and englacial stratigraphic folds. In Horseshoe Valley, airborne RES transects reveal a number of englacial debris bands that extend from valley side walls or bedrock obstacles. The relationship between these debris bands and stratigraphic folds in several radargrams in Figure 7.5 indicates that debris entrainment at depth must be facilitated by englacial layer folding. As field work by *Boulton* [1979] and many others have revealed that folds associated with compressive stress regimes around bedrock obstacles can remain stationary over time, this method of debris entrainment can account for the large volume of englacial debris clasts entrained at depth in this study, where sediment must be sourced from erosion along the ice stream margin. Following reviews by *Stokes and Clark* [2002] it is expected that stationary folds are maintained by stable ice flow conditions, where faster (and warmer) ice flow around a bedrock obstacle and slower (and colder) ice flow above the obstacle can create compressive conditions near the interface. This

compressive environment between warm and cold ice can account for the shearing and folding of ice near the ice/bed interface in transect lines 19b-21b, where sediment is entrained at the exact point at which the thermal boundary intersects the bedrock obstacle [*Hindmarsh and Stokes*, 2008]. Given that ice stream shear margins are highly dynamic features that are susceptible to migration [*Jacobel et al*., 1996; *Smith et al*., 2007], Figure 7.14 schematically represents the sensitivity of debris entrainment through englacial layer folding beneath thick ice sheets, where it is evident that debris incorporation at depth must rely upon debris availability, ice flow conditions, basal topography and ice temperature.

7.4.3 Debris transport

Processes of englacial debris transport beneath thick ice sheets are recorded by successive ice penetrating radar transects in and around Horseshoe Valley. These radargrams document the persistence and development of englacial debris bands, as ice flows from upland areas towards the local grounding line, where ice sheet conditions, sediment availability and bedrock conditions change spatially and temporally. At the point of entrainment, debris clasts beneath thick ice sheets can be moved vertically through the ice column as englacial layers fold in response to changes in the local thermal regime, and by successive debris entrainment at the ice/bed interface, where newly entrained clasts elevate previously incorporated clasts through the ice column. As *Stokes and Clark* [2002] discovered that sediment will be 'smeared out' in the downstream direction by passive transport when conditions are no longer met for entrainment (e.g. R3 in transect line 18 and R5 in transect line 21b), compression and extension regimes must govern sediment transportation in Antarctica. Figure 7.15 demonstrates this assertion by showing how debris is actively transported through compressive ice flows near bedrock obstacles, and passively transported when ice flows past the obstacle (where ice experiences extensional flow). These processes allow debris to be entrained and transported through the WAIS, where sediment can be efficiently transported from continental sources to the local grounding line, and ultimately the Southern Ocean.

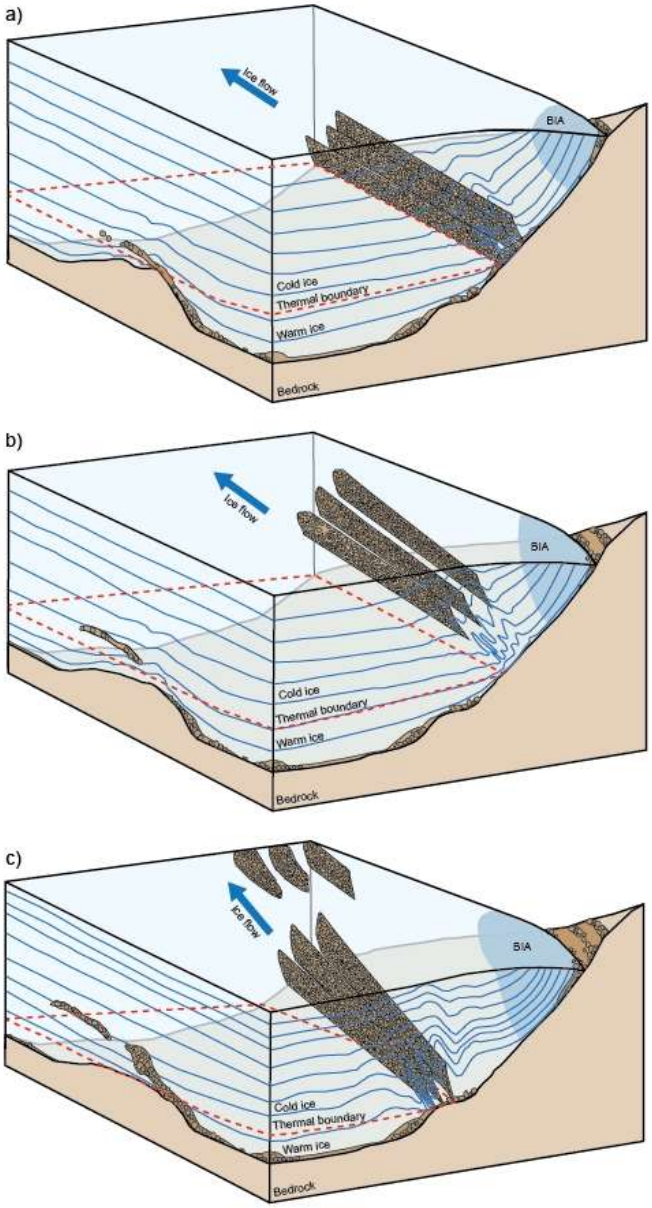

Figure 7.14. Investigations of debris entrainment at the glacial thermal boundary. In a) debris is excavated at the thermal boundary, at the junction between fast flow (warm-based ice) and slow flow (cold-based ice). This process will continue until sediment sources are exhausted at the interface e.g. in b), when previously entrained clasts are passively transported down flow, through the ice. If the thermal boundary were to move in response to ice thickness changes (e.g. in c), new sediment sources could be exploited. Passively transported clasts could still be present in the regional ice flow in this scenario.

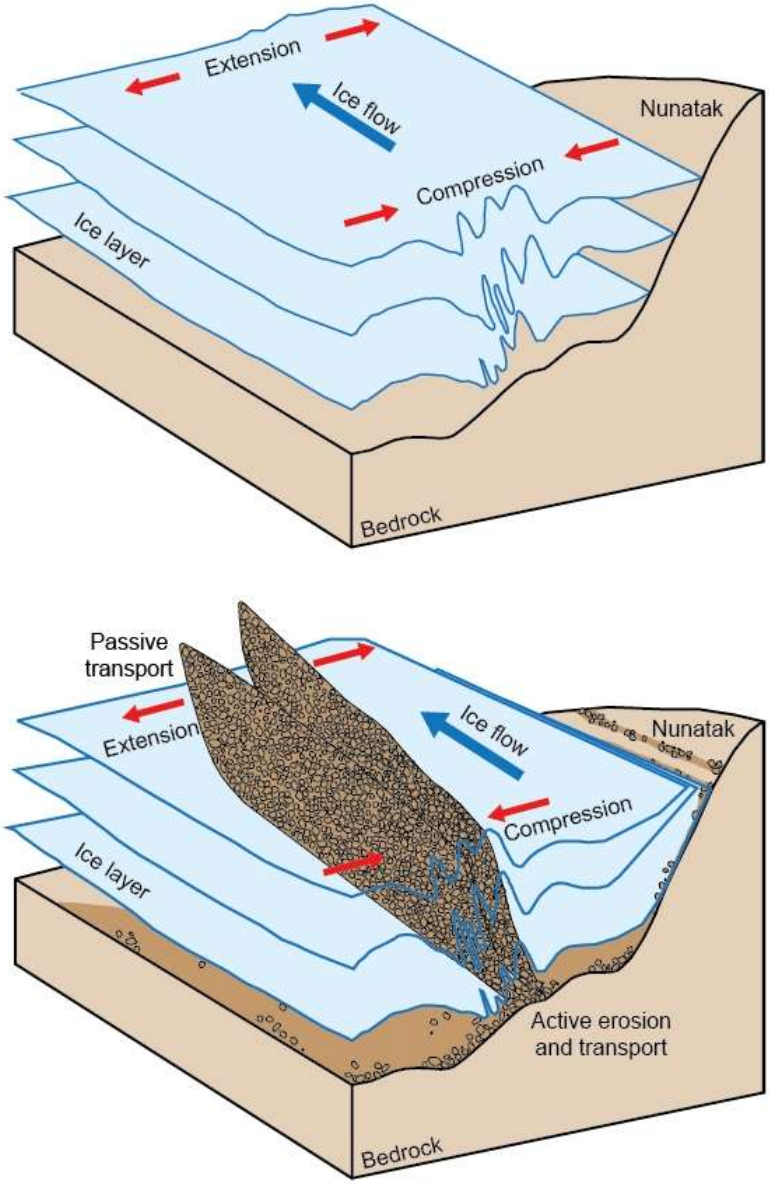

Figure 7.15. Extension and compression of ice layers and associated debris sequences, as ice flows past a bedrock obstacle like a nunatak. Active erosion and transportation will occur under compressive flow regimes near the mountain front, whilst more passive debris transport will dominate under extensional flow.

Whilst many studies also recognise the importance of near-surface debris transportation through BIA systems, particularly because of their rare ability to bring old ice and meteorite deposits to the glacial surface [*Whillans and Cassidy*, 1983; *Bintanja*, 1999], traditional ice penetrating radar surveys have failed to resolve the detailed internal stratigraphy, and distribution of debris clasts within BIAs. Although this has hindered our understanding of near-surface debris entrainment and transportation processes until now, detailed step-and-collect mode radar surveys across Patriot Hills BIA and the BI moraine sequences in front of Independence Hills have allowed debris clasts to be traced through the ice column, where it is evident that clasts are transported by compressive ice flow and thrust faulting. These mechanisms have allowed over 3.7 ± 3 tera tonnes of material (assuming an ice/debris ratio of approximately 80:20) to be transported from the subglacial bed to BI moraine surfaces in front of Independence Hills. However, *Westoby et al.* [2016] stress that transportation does not cease once clasts are deposited at the surface, as BI flow beneath the moraine continues to elevate exposed sediments, and push them in towards the mountain front (see Chapter 3, section 3.6.1 and Figure 3.9). At the same time, sublimation from katabatic winds will also elevate moraine clasts relative to the exposed ice surface [*Westoby et al*., 2016].

7.5 Summary

Ice penetrating radargrams reveal that airborne RES, ground RES and detailed step-and-collect mode GPR surveys can be used to image and trace englacial debris accumulations in Antarctica at a variety of scales, depths and orientations. By investigating englacial debris reflectors in and around Horseshoe Valley and the Evans Ice Stream this study has revealed that debris sources are abundant in the Weddell Sea sector of West Antarctica, where over 9 ± 5 tera tonnes of englacial debris clasts (assuming an ice/debris ratio of 80:20) have been approximated in airborne RES traverses across Horseshoe Valley Trough alone. Although these clasts and particles are entrained at a variety of elevations and depths beneath the ice surface, all debris entrainment mechanisms rely upon sediment availability and ice flow, where ice temperatures regulate the exact point of entrainment. In Horseshoe Valley debris is frequently excavated

when the thermal boundary intersects bedrock obstacles. This allows available debris clasts and particles to be entrained through regelation processes and compressive faulting and folding, where successive debris entrainment at the ice/bed interface and debris transportation through the ice column is encouraged by local ice flow conditions.

As debris sources, entrainment mechanisms and transportation routes are sensitive to a number of controls related to sediment availability, ice flow and ice temperature, englacial debris accumulations in Antarctica will be spatially variable, and subject to temporal changes associated with both internal and external forcings. This finding is particularly important for predictive forecasting, as surface warming in Antarctica could de-buttress rock walls and alter glacial thermal regimes through ice elevation and topographic changes. These modifications to ice temperatures or debris availability would alter frictional stress at the glacial bed, which could modify ice flow speeds [*Bell et al*., 1998], change ice flow direction through long-term erosive processes [*Harbor et al*., 1988] and influence the abundance of essential nutrients like BioFe in the Southern Ocean [*Death et al*., 2014; *Hawkings et al*., 2014]. This work suggests that it is now critical to assess continental debris sources from the extraglacial and subglacial environment.

CHAPTER 8

Snow drift modelling for Blue Ice Areas

As BIAs have the ability to bring large quantities of ice and sediment to the glacial surface, numerous studies have used BIAs to infer the history of the Antarctic Ice Sheet, where cosmogenic nuclide and climate investigations typically assume stability in katabatic winds and BIAs. In order to determine the conditions necessary to initiate and maintain BIAs in Horseshoe Valley, this chapter will utilise a rule-based snow-drift model, termed *Snow_Blow* which was recently coded by Dr. Stephanie Mills from Plymouth University and collaborators. A variety of model runs will be presented and analysed to validate *Snow_Blow* and simulate conditions across the Southern Heritage Range ~10 ka ago.

Snow drift modelling objective

Model the transport of snow by wind in Horseshoe Valley and compile a sensitivity analysis to determine the conditions necessary to initiate and maintain Blue Ice Areas in front of the Patriot, Independence and Marble Hills.

Research questions

1) Can the *Snow_Blow* model define the current spatial variability and extent of snow accumulation/erosion patterns in Horseshoe Valley?
2) How sensitive are BIAs to changes in wind direction?
3) How do *Snow_Blow* model outputs respond to changes in ice surface elevation?
4) What was the spatial distribution of BIAs in Horseshoe Valley through the Holocene?
5) What are the implications for debris/BI moraines?

8.1 Introduction

The uplift and horizontal transport of snow by wind, henceforth referred to as drifting snow, is an important process in Antarctica, due to the nature of topography, wind flow (Figure 8.1) and

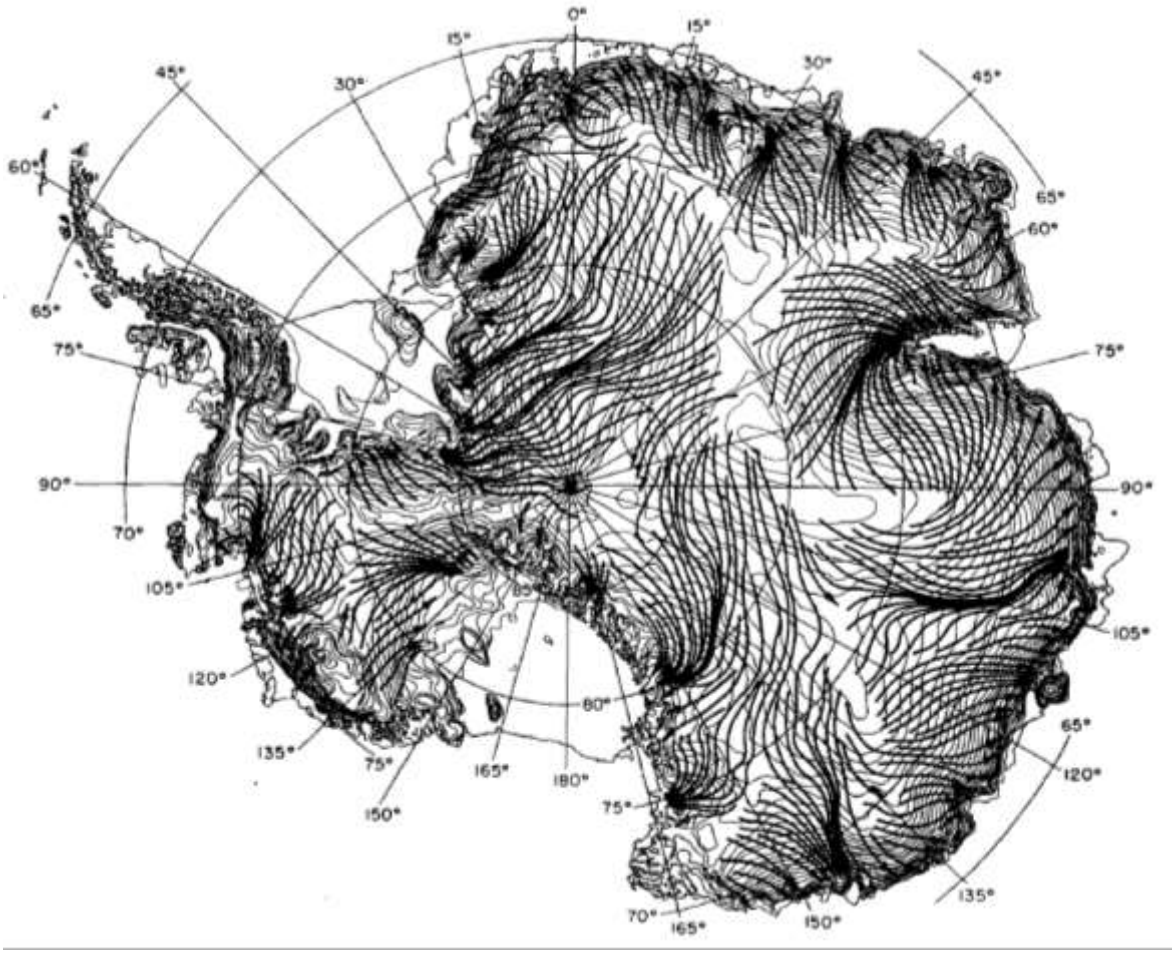

Figure 8.1. Surface airflow over Antarctica, marked by black arrows (downloaded from *Bromwich et al.* [1994]). Thin solid lines show ice surface elevation contours in 100 m increments (after *Parish and Bromwich* [1987]).

snow accumulation patterns (Figure 8.2) [*Metvold et al*., 1998]. Drifting snow represents a coupled system between the cryosphere and the atmosphere, where snow has shaped the topography in Antarctica, and consequently altered the wind field, which modifies drifting snow [*Frezzotti et al*., 2002]. As such, snow drift has important hydrological implications, related to differential distribution across catchments. Whilst snow accumulation in Antarctica is generally regarded as quite low, snow falls over the entire ice surface, at a mean accumulation rate of approximately 15 cm a^{-1} (water equivalent) [*Genthon et al*., 2007] (although Figure 8.2 shows how many areas experience much lower accumulation rates). The net surface accumulation is the sum of precipitation, surface sublimation, accumulation or erosion by drifting snow and melt with associated runoff although typically ice surfaces greater than 1000 m a.s.l. do not experience melt in Antarctica [*Bintanja*, 1999]. These processes can result in either a positive or negative surface mass balance. However, net mean ablation does not always result in a region of negative mass balance, as compensating ice flow from surrounding areas can often counteract ablation and create a relatively stable mean surface elevation. Areas such as these tend to exist at high elevations (up to 2500 m a.s.l. [*Bintanja*, 1999]) where orographic features favour strong and persistent katabatic wind flow. These winds evolve high on the Antarctic plateau (Figure 8.2) where net long-wave radiation losses cool the near-surface air [*Nylen et al*., 2004]. This allows the cold dense air to flow downslope to replace the less dense air at lower elevations [*Hoinkes*, 1960; *Ishkawa et al*., 1982]. The resultant wind scour and surface ablation favour compressive ice flow and produce BIAs, which cover 0.8 – 1.6 % of the Antarctic continent [*Winther et al*., 2001] (section 2.5.6, Chapter 2). These BIAs, typically in the lee of nunataks have the ability to bring large quantities of ice and debris to the surface by compressive, upwards ice flow (Chapters 5 and 7). BIAs have therefore been used to infer the history of the Antarctic Ice Sheets, where horizontal isotopic climate record interpretations (e.g. *Turney et al.* [2013]) and studies such as that by *Hein et al.* [2016a] have inferred stability in katabatic winds in order to suggest unbroken ice sheet conditions in West Antarctica for 1.4 million years. In order to determine the sensitivity of BIAs in Horseshoe Valley to changes in ice sheet elevation and prevailing katabatic wind direction this chapter will use a novel snow drift model, termed

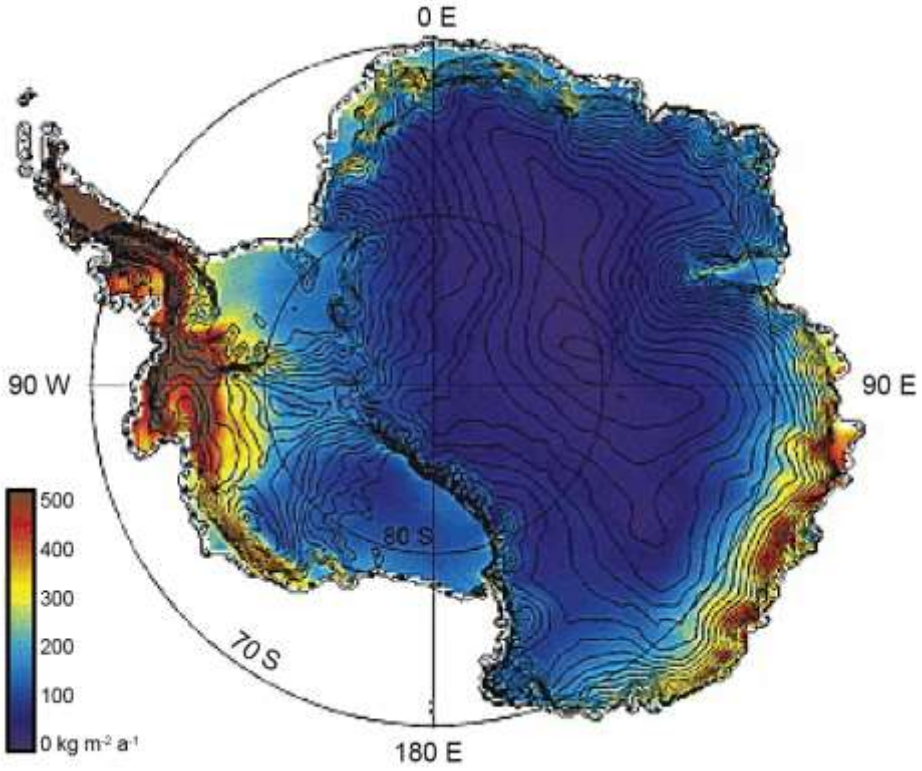

Figure 8.2. Antarctic snow accumulation mapped using polarisation of 4.3 cm wavelength microwave emission. Image downloaded from *Arthern* [2006].

Snow_Blow, to assess the main controls on BIA formation and preservation in front of the Patriot, Independence and Marble Hills (Figure 8.3).

8.2 Methodology

A simple qualitative snow drift model (*Snow_Blow)* developed by *Mills et al*. [Submitted] has been employed to derive spatial variations in the redistribution of snow over irregular topography in and around the Southern Heritage Range. The snow drift model requires two primary inputs to determine the local wind vector field: wind data (speed and direction) and a high resolution Digital Elevation Model (DEM) of the study site.

8.2.1 Snow_Blow model specifications, developed by Mills et al. [Submitted].

In order to create a local wind vector field (to derive the spatial variations in the relative accumulation of snow at various locations), the initial average wind direction (Θ) (the direction the wind is coming from) and average wind speed (*F*) from the field site were used to calculate the deflection of wind around the topography (Figure 8.4) using an empirical equation developed by *Ryan* [1977] (equation 8.1).

$$F_d = -0.225 * S_d * \sin(2(A - \Theta)) \quad (8.1)$$

Where: F_d is the wind diversion factor (°), S_d is the slope to the horizon in the downwind direction (%), A is the slope aspect (°) and Θ is the initial average wind direction (°) [*Purves et al*., 1999b].

Using this vector field, the sheltering effect of the terrain was computed for every cell using the slope index (S_i) (equation 8.2) and shelter index (T_i) (equation 8.3), to produce a modified wind speed (F_m) (equation 8.4).

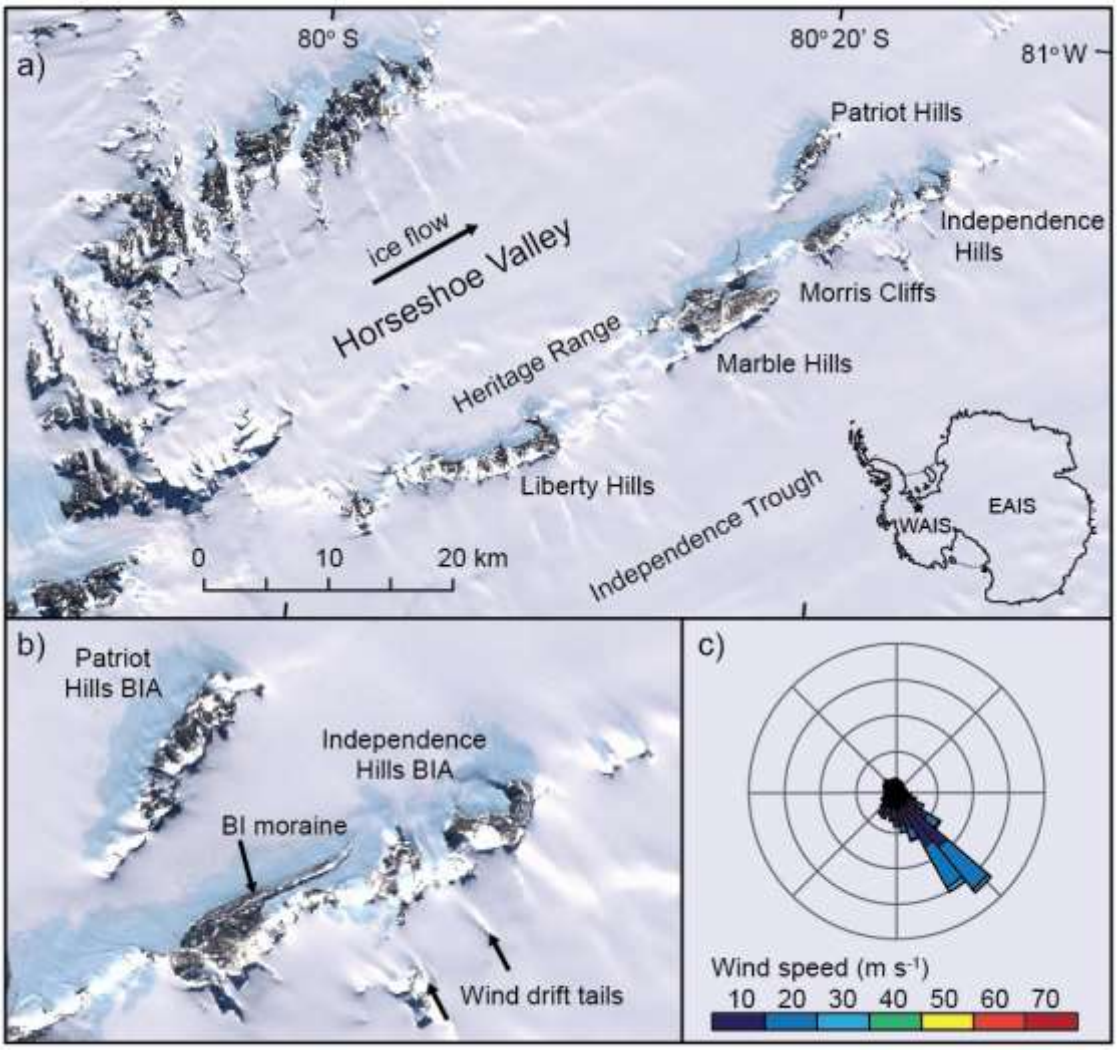

Figure 8.3. Landsat Image Mosaic of Antarctica showing the location of Patriot, Marble and Independence Hills. Panel b) highlights wind drift tails, BI moraine sequences and BIAs in front of nunataks in the Southern Heritage Range. The rose diagram (projected in polar stereographic) in c) shows persistent katabatic winds from the southwest, recorded hourly from an AWS at Patriot Hills blue-ice aircraft runway throughout 2009.

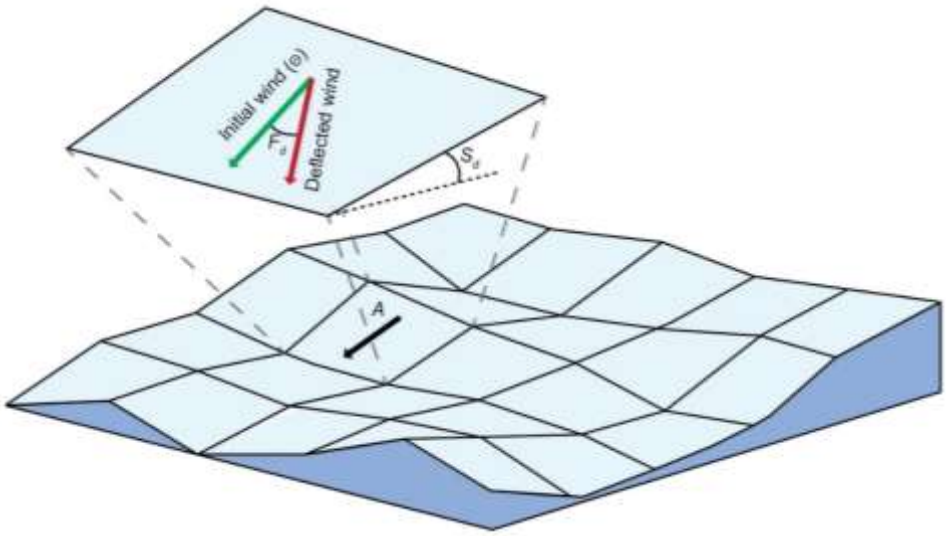

Figure 8.4. Schematic diagram, adapted from *Purves et al*. [1998] to show modified wind deflection (F_d) for each individual cell, based upon slope aspect (A) and slope to the horizon downwind (S_d) relative to the initial wind direction (Θ).

$$S_i = \frac{S_d - 5}{S_{max}} \tag{8.2}$$

Where S_{max} is the maximum slope angle.

$$T_i = A_i * S_i \tag{8.3}$$

$$F_m = F - (F * T_i) \tag{8.4}$$

Once the wind direction and speed have been modified, snow transport from cell to cell is calculated before the full movement of snow is modelled. The amount of material eroded from a cell by the wind factor within a cell is calculated using equation 8.5 which ultimately controls the number of model iterations required. This equation is based on an empirically derived relationship by *Pomeroy* [1993]. Depositional distance is then calculated using equations 8.6 and 8.7.

$$Q = k * (F^3 - F_t^3) \tag{8.5}$$

Where Q is the amount of snow eroded from a cell, k is a constant, F is the wind velocity and F_t is the threshold wind velocity.

$$L = \frac{1}{md} \tag{8.6}$$

$$mxd = log \frac{1 - 0.99}{-L} \tag{8.7}$$

Where L is Lamba, *md* is the mean depositional distance and *mxd* is the maximum depositional distance.

The final model component involves moving snow from cell to cell relative to the wind direction. The cells which can contribute to snow transport are selected based on the *Tarboton*

[1997] multiple-flow direction routing algorithm, which shows the least dispersion compared to other multiple-flow direction routing algorithms [*Le Brocq et al.*, 2006] (Figure 8.5). As a result, the model can determine the locations most likely to experience erosion and accumulation. More specific details on the *Snow_Blow* model can be found in *Mills et al.* [Submitted].

8.2.2 Digital elevation model selection

Due to the complex mountainous topography in Horseshoe Valley only two DEMs contained suitable resolutions and time stamps for the *Snow_Blow* model; these included an Advanced Spaceborne Thermal Emission and Reflection Radiometer (ASTER) 30 m resolution DEM (collected in 2011 and available to download from *Earth Explorer*) and a Satellite Pour l'Observation (SPOT) 40 m resolution DEM (collected by SPOT5-HRS images in 2008 [*Korona et al.*, 2009] and available to download from the *Theia Land Data Centre*). Although the ASTER DEM possesses the greater resolution, false spikes in the dataset (most likely caused by scattering from clouds above nunataks [*Eckert et al.*, 2005]) have resulted in unrealistic surface topography in Horseshoe Valley (Figure 8.6a, 8.6b). Methods to remove these spikes were explored using 3D Structure-from-Motion software packages such as Quick Terrain Modeller (QTM) where a site-scale and peak-scale smoothing algorithm were applied to the DEM (Figure 8.6c – 8.6f) and MeshLab software [*Meshlab*, 2014], where applications were employed to remove spikes in the data by gridding the entire surface topography (Figure 8.6g, 8.6h). As none of these methods could accurately replicate the surface topography in and around Horseshoe Valley, particularly behind Patriot and Independence Hills, a second DEM, this time a SPOT 40 m resolution DEM, was explored. A visual comparison between these DEMs has been provided in Figure 8.7. This figure shows that the false spikes recorded in the ASTER 30 m resolution DEM do not exist in the SPOT 40 m resolution DEM, which accurately depicts the surface topography of Horseshoe Valley. As a result, all model simulations in this chapter have been run on the SPOT DEM.

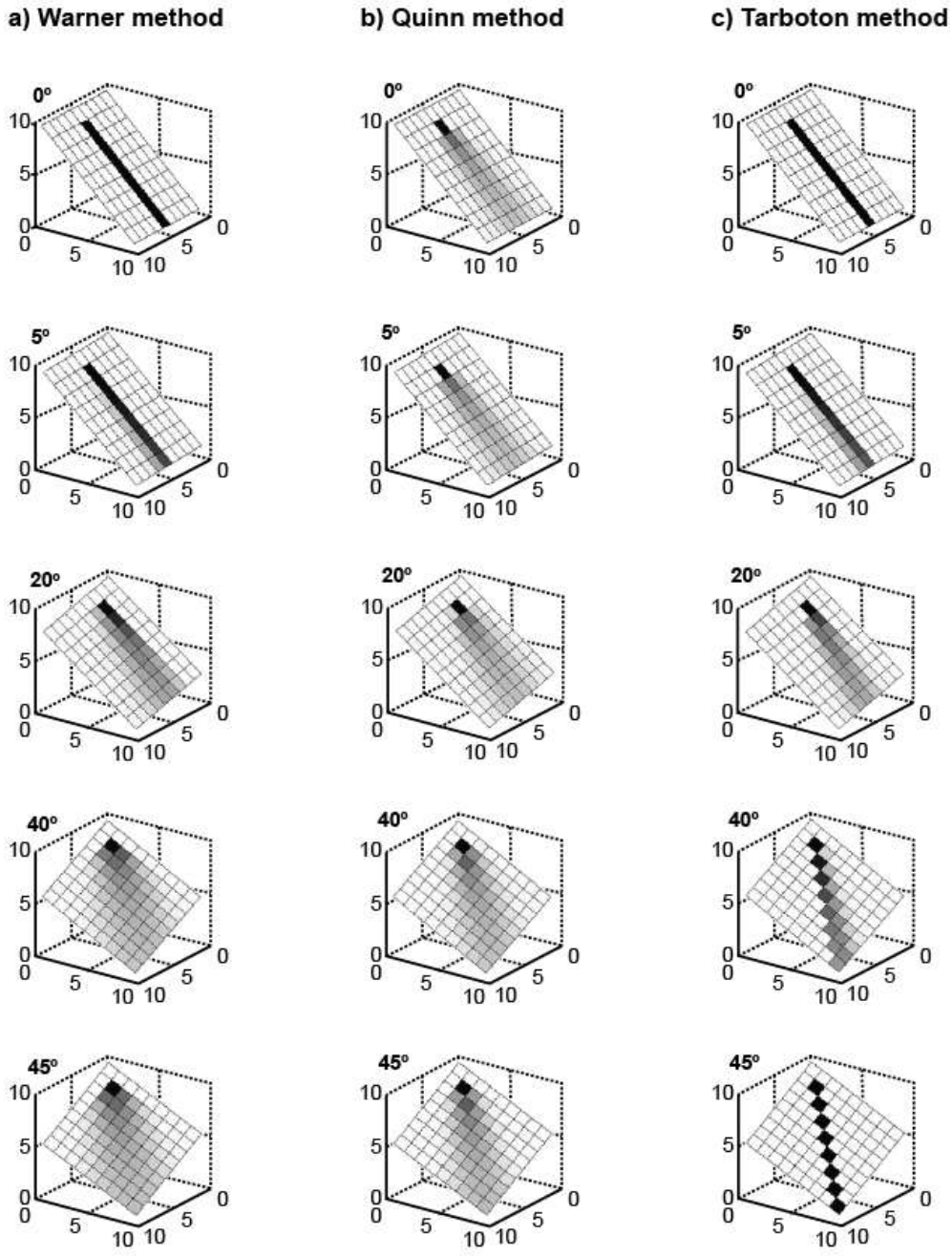

Figure 8.5. Comparisons between three widely used multiple-flow routing methods; Warner, Quinn and Tarboton. In each case influence maps for 1 unit of accumulation (m^3 yr^{-1}; scale 1 (black) to 0 (white)) have been added at the top of a planar surface orientated at various angles to the grid (x, y and z are arbitrary units and represent the number of cells). The Tarboton method shows the least dispersion of the three algorithms. This figure has been modified from *Le Brocq et al*. [2006].

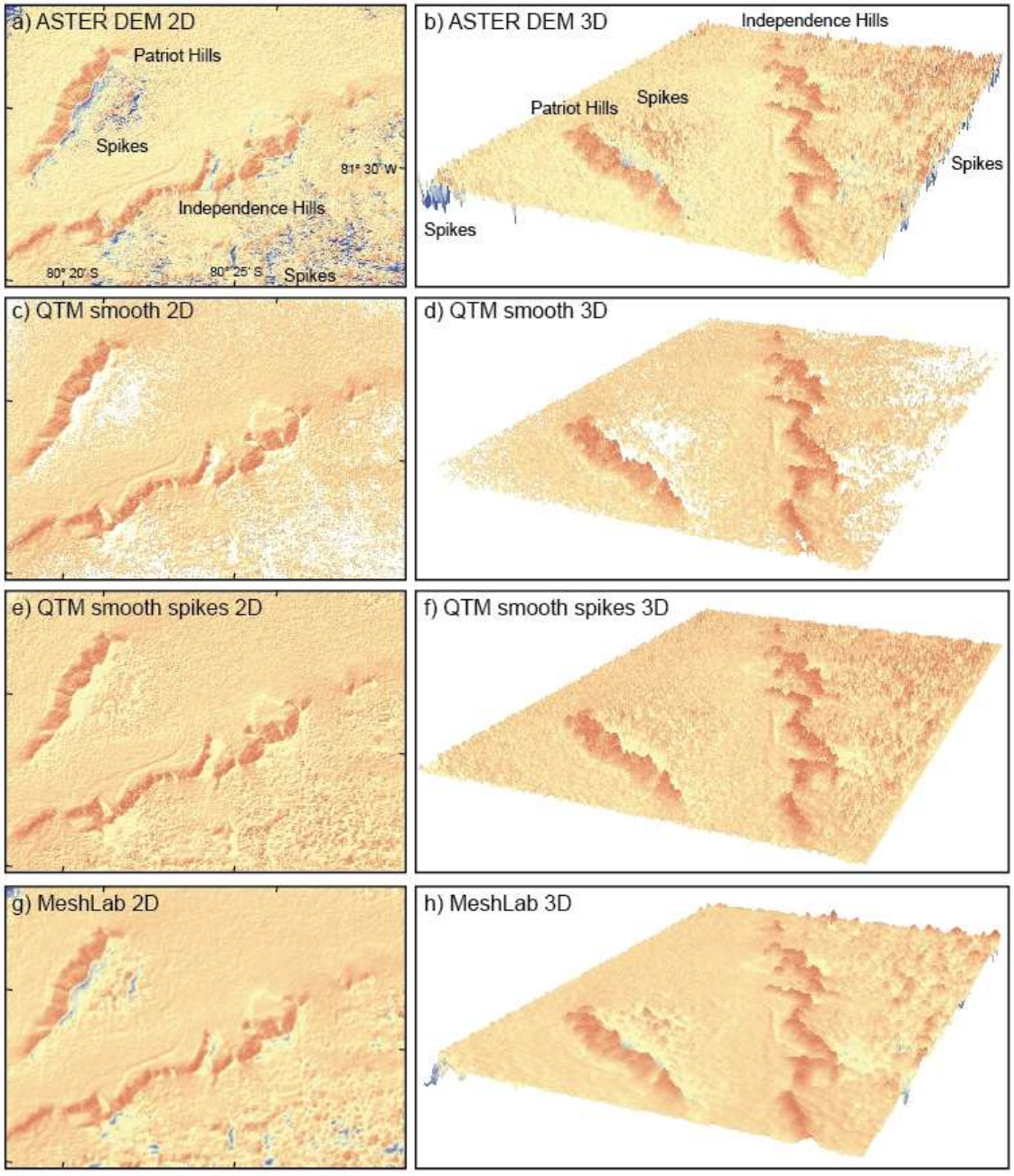

Figure 8.6. Various methods applied to remove spikes in a 30 m resolution ASTER DEM across Horseshoe Valley. a) and b) show false spikes in the DEM behind Patriot and Independence Hills. The entire DEM surface was smoothed in panels c) and d) to try and remove the spikes in Quick Terrain Modeller (QTM) but this resulted in large data gaps. Smoothing of the spikes only in e) to f) was much more effective, but still produced an un-representative topography, particularly behind Independence Hills. MeshLab software was employed in g) and h) to grid the entire surface of the study site. This smoothed false spikes but did not eradicate them.

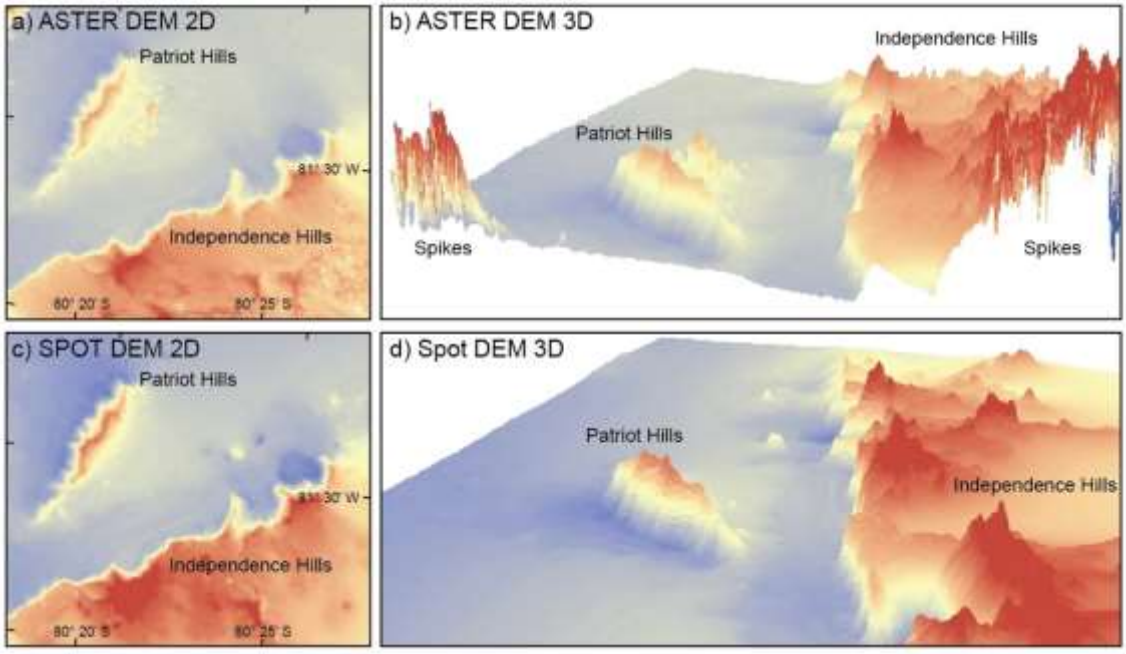

Figure 8.7. Comparisons between an ASTER 30 m resolution DEM and a SPOT 40 m resolution DEM, collected across Patriot and Independence Hills, Horseshoe Valley. Numerous false spikes are recorded behind the Patriot and Independence Hills and towards the centre of Horseshoe valley in a) and b) which detail the ASTER DEM. These large areas of unrepresentative topography are not recorded in the SPOT DEM in panels c) and d).

8.2.3 Site specific inputs

Once the DEM was selected, the *Snow_Blow* model was initialised assuming an equal distribution of snow over the whole topography, although a constant flux was set at the boundaries, so that the rate of surface snow drift erosion equalled the rate of snow accumulation at the boundary of the SPOT 40 m resolution DEM. This condition allows material to drift into the model in subsequent iterations, so long as conditions for drifting snow are met at the boundaries. An initial wind direction of 135° (polar stereographic) and wind speed of 15 m s^{-1} were used for most model runs (unless specified), based on average hourly weather station data from Patriot Hills blue-ice aircraft runway in 2009 (displayed as a rose diagram in Figure 8.3c). Threshold wind speed to initiate snow drift was defined as 5 m s^{-1} following *Frezzotti et al*., [2004] and references therein, whilst the mean depositional distance of snow was set to 150 m, with a maximum depositional distance of 690 m (further details on the derivation of these values can be found in *Mills et al*. [Submitted]). Each model was run for a sample of 20 iterations (see Figure 8.8) to simulate the repetition, and therefore the evolution of snow transport over time. It should be noted that the qualitative *Snow_Blow* model does not take into account any feedback mechanisms to stop the transportation of snow over subsequent iterations, such as the further state of metamorphism in the snow pack, sublimation or complex ice sheet flow.

8.3 Results

8.3.1 Model validation

Initial model runs (displayed in Figure 8.9), using the SPOT 40 m resolution DEM and locally derived wind data from Patriot Hills BIA reveal consistently strong surface snow drift erosion on the downwind side of Patriot, Independence and Marble Hills, where the locally derived wind vector field approximates katabatic wind flow over the nunataks and down gullies. Moderate surface snow drift erosion is simulated in the cells behind outcrops with less topographic relief, for example, at the eastern end of Independence Trough. The exact position of snow accumulation varies throughout subsequent iterations. During initial model runs

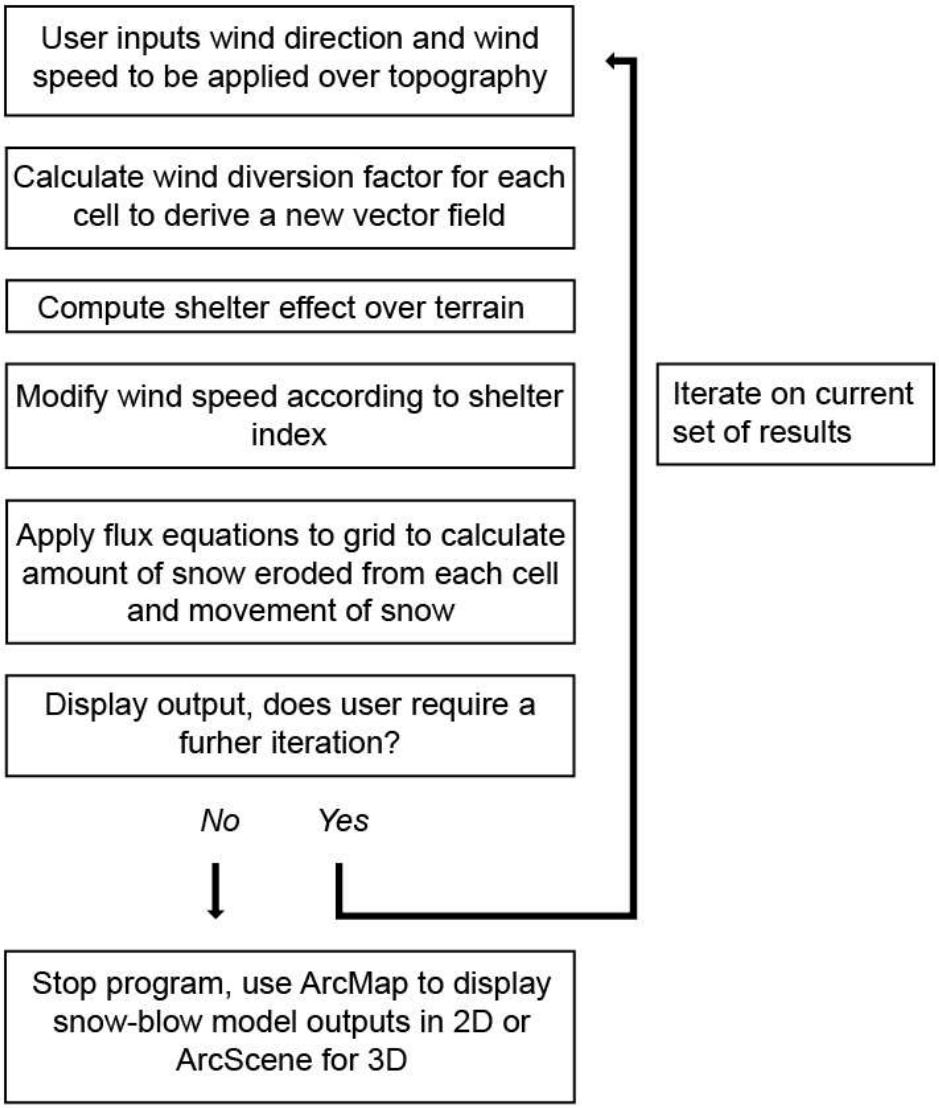

Figure 8.8. Iterative path applied to the *Snow_Blow* model.

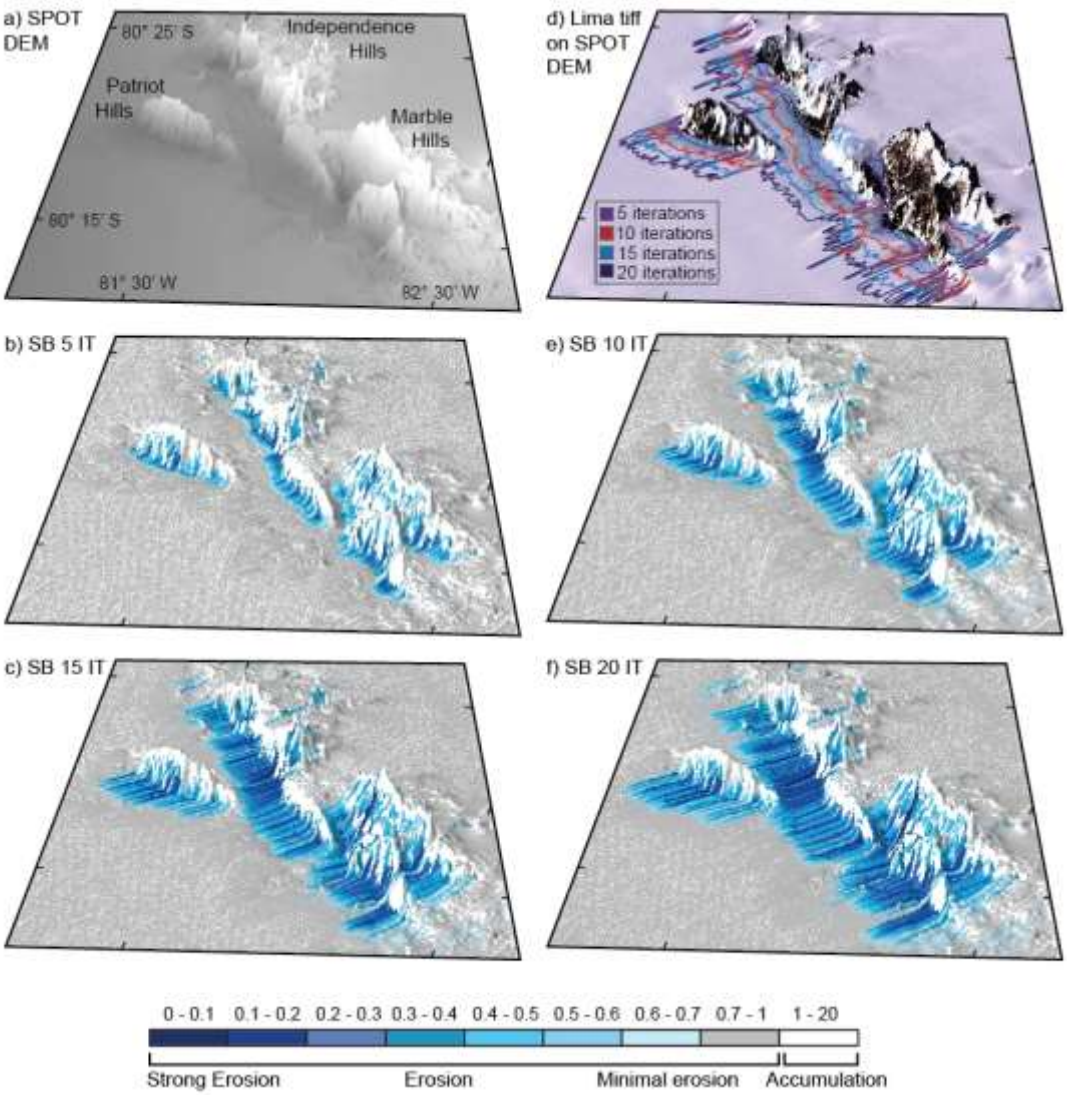

Figure 8.9. *Snow_Blow* model outputs from the SPOT 40 m resolution DEM. a) original DEM, b) *Snow_Blow* run over 5 iterations, c) *Snow_Blow* run over 15 iterations, d) Lima tiff on SPOT DEM to compare current Blue Ice Area extent with *Snow_Blow* iterations, to show that the 10th iteration, modelled in e) provides the most representative snow drift output. Finally, f) shows the output of the *Snow_Blow* model run over 20 iterations.

(1-5 iterations) snow accumulates on surfaces which are upwind of obstacles which have low-to-high topographic relief. These include individual massifs and rock outcrops as well as a distinct 10 m high moraine ridge in front of Independence Hills (Figure 8.9b). However, as snow transportation evolves through subsequent iterations (10-20 iterations), snow accumulation becomes restricted to cells with more moderate to high topographic relief, as surface snow drift erosion begins to dominate areas of lower relief, such as the moraine ridge on the leeward side of Independence Hills. Moving away from the nunataks of the Heritage Range, there is very little modification to surface snow redistribution over the relatively flat ice surface that extends across Horseshoe Valley and Independence Trough during the 20 model iterations, representing a constant flux into and out of the cells (Figure 8.9).

In order to determine the most representative number of iterations required to simulate the current spatial extent of surface snow drift erosion in front of Patriot, Marble and Independence Hills, each model iteration was compared to LIMA satellite imagery, collected in 2008 (Figure 8.9d). This assessment revealed that the modelled surface snow drift erosional extent in the 10th iteration best reproduced the current, observed BIA extent (Figure 8.9d), where qualitative analysis reveals that 93% of the area is correctly modelled (Figure 8.9). This demonstrates that the present day prevailing wind direction of 135° polar stereographic allows contemporary snow drift conditions to be simulated effectively. As the *Snow_Blow* model does not contain any feedback mechanisms to stop the progressive expansion of snow drift erosion and accumulation through subsequent iterations, all model runs are analysed on the 10th iteration.

8.3.2 Changing prevailing wind direction

In order to determine the impact that wind direction has on the areal extent of surface snow drift erosion, and therefore the location and extent of BIAs in Horseshoe Valley, slight changes in the prevailing wind direction were corded in three further *Snow_Blow* model runs. By altering the current prevailing wind direction of 135° in 10° increments, to 95°, 115° and 155° (to simulate

wind flow forced by morphological changes in the ice sheet) Figure 8.10 shows the modelled output for each hypothetical wind direction. Although the severity of surface snow drift erosion remains similar in all model runs the exact position, orientation and extent of snow drift erosion differs in each simulation (Figure 8.10b, 8.10c and 8.10d). The least extent of surface snow drift erosion is simulated when winds approach Horseshoe Valley from 95° polar stereographic, when the model only predicts 36% of the eroded BI surface. A general increase in surface snow drift erosional extent is recorded when the dominant wind direction is simulated from 115° (63% success rate) and then from 155° when the model predicts 74% of the eroded BI surface. Subtle changes in the snow accumulation field are recorded over each model run, as snow continues to accumulate on the upwind side of exposed outcrops.

8.3.3 Historic ice surface elevation

To determine snow drift conditions in Horseshoe Valley through the Holocene, a variety of former ice surface elevations were also simulated in accordance with recently published cosmogenic nuclide exposure age dating of glacial debris on mountain slopes within the field site [*Hein et al*., 2016b]. Dated erratics suggest that during the LGM and until 10 ka ago the ice-sheet surface was ~400 m thicker than present. Thus, the original SPOT 40 m resolution DEM was modified to simulate conditions 10 ka ago. The new DEMs, representing thicker ice-sheet surfaces were generated using ESRI ArcMap 'raster calculator', which was employed to increase the present ice surface elevation by 100 m increments (whilst preserving the current topography), without altering the elevation of the three nunataks and Morris Cliffs. A simple horizontal extrapolation was used to fill any voids between the raised ice sheet surface and the unmodified rock outcrops. These new DEMs can be viewed in Figure 8.11, where the approximate extent of exposed bedrock is highlighted, along with a cross sectional profile through Patriot and Independence Hills.

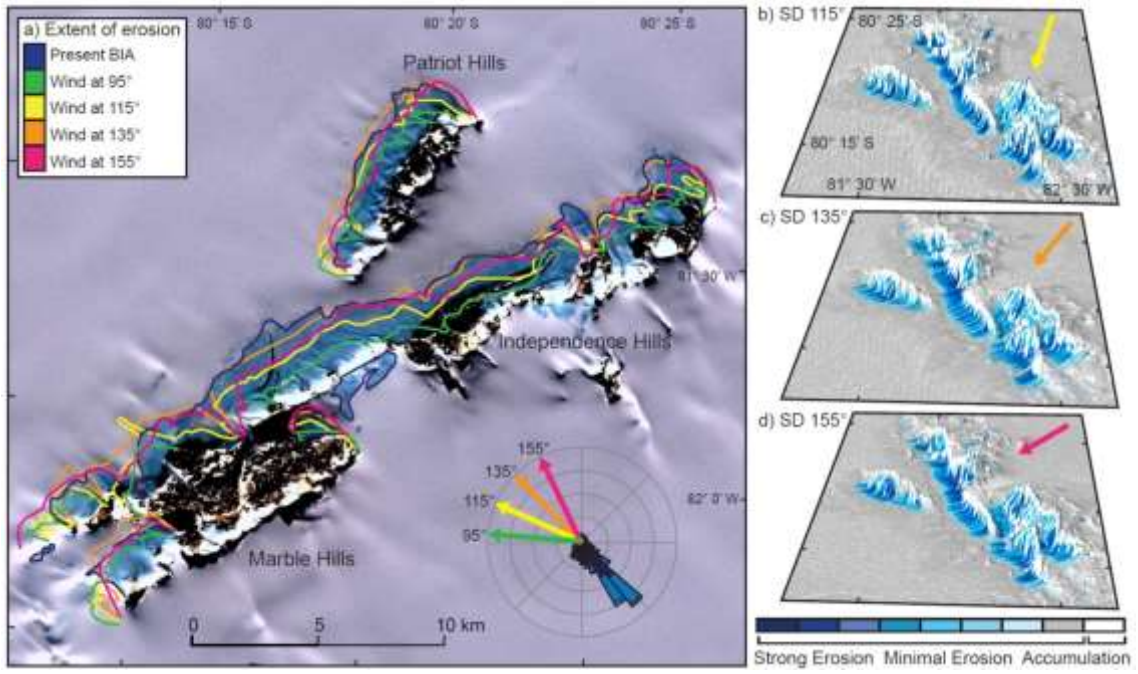

Figure 8.10. Wind-driven snow erosion simulations, a) extent of erosion in front of Patriot, Independence and Marble Hills under a variety of modelled polar stereographic wind directions: 95°, 115°, 135° and 155°, as indicated by the wind rose. The *Snow_Blow* model outputs from 115°, 135° and 155° are shown in 3D in figures b-d.

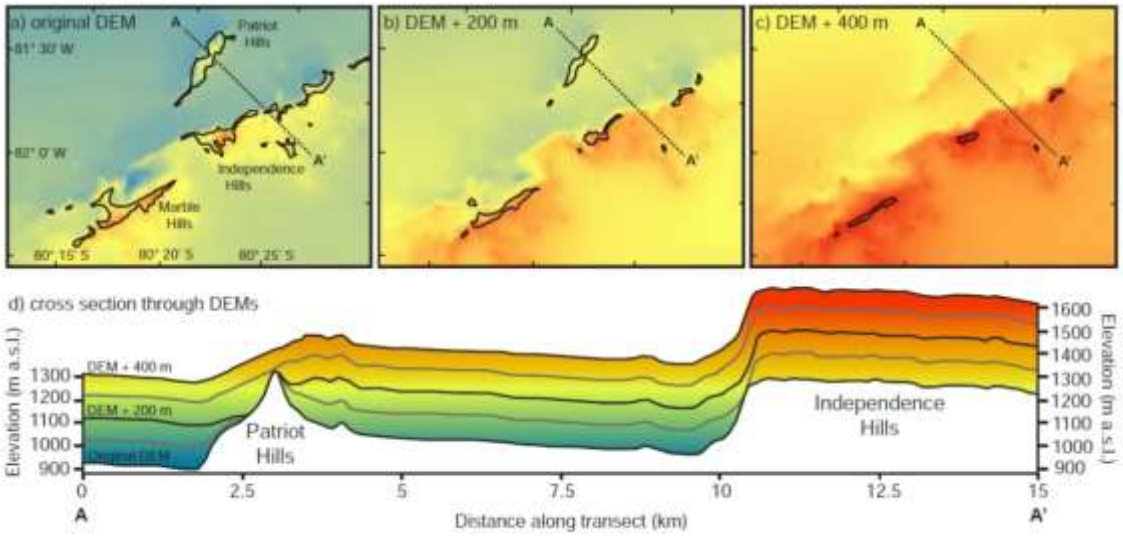

Figure 8.11. Original and modified SPOT 40 m resolution DEMs to show a) the present ice surface elevation as well as modified DEMs, where the ice elevation was increased by b) 200 m and c) 400 m. Black lines indicate the approximate extent of exposed bedrock, d) shows a cross section (A-A') through Patriot and Independence Hills.

Direct comparisons from each *Snow_Blow* simulation, run over former ice surface elevations can be seen in Figures 8.12 and 8.13, where each model was run for 10 iterations, with a prevailing wind direction of 135° polar stereographic. Panel A documents the difference between surface snow drift erosion, modelled on present day ice sheet surfaces, and snow drift conditions simulated on the DEM modified to represent an ice surface elevation increase of 100 m. Although these panels reflect minimal changes in surface snow drift erosion close to Patriot Hills, the spatial extent of surface snow drift erosion decreases as the nunatak relief is effectively lowered by the ice elevation increase. Along the leeward slopes of Independence and Marble Hills there is an overall decrease in erosion between the two model runs. However, some areas with lower topographic relief do experience considerably less snow drift erosion when the ice surface is raised, relative to the height of the nunataks. Panels 8.12a and 8.13a also show an increase in snow accumulation on each of the massifs when the ice surface is raised by 100 m.

A comparison between *Snow_Blow* model outputs from DEMs modified to represent increased ice sheet elevations of 200 m and 100 m above present (Figure 8.13b) reveals very little change in the spatial extent and intensity of surface snow drift erosion across the study site, although a slight increase in accumulation is still recorded on the upwind side of major slopes. However, Panel 8.13c reflects another important shift in the *Snow_Blow* model output when the initial ice level is raised by 300 m, causing Patriot Hills and a number of other, previously exposed outcrops behind Independence and Marble Hills to be effectively buried (this can also be seen in Figure 8.12c, where the *Snow_Blow* model records significantly less erosion than previous model runs). This burial dramatically reduces wind scour in front of Patriot Hills, causing model outputs to simulate considerably less snow drift erosion. When the ice surface is raised by 300 m snow accumulation is also more spatially variable. The final panel, Figure 8.13d, shows a result much more similar to 8.13b than 8.13c, representing another shift in ice surface conditions, as snow drift erosion rates begin to stabilise between the *Snow_Blow* model run on an ice sheet elevation of 300 m and 400 m. Again, more snow accumulation is simulated on the upwind side of areas with high relief, which include the now buried Patriot Hills as well

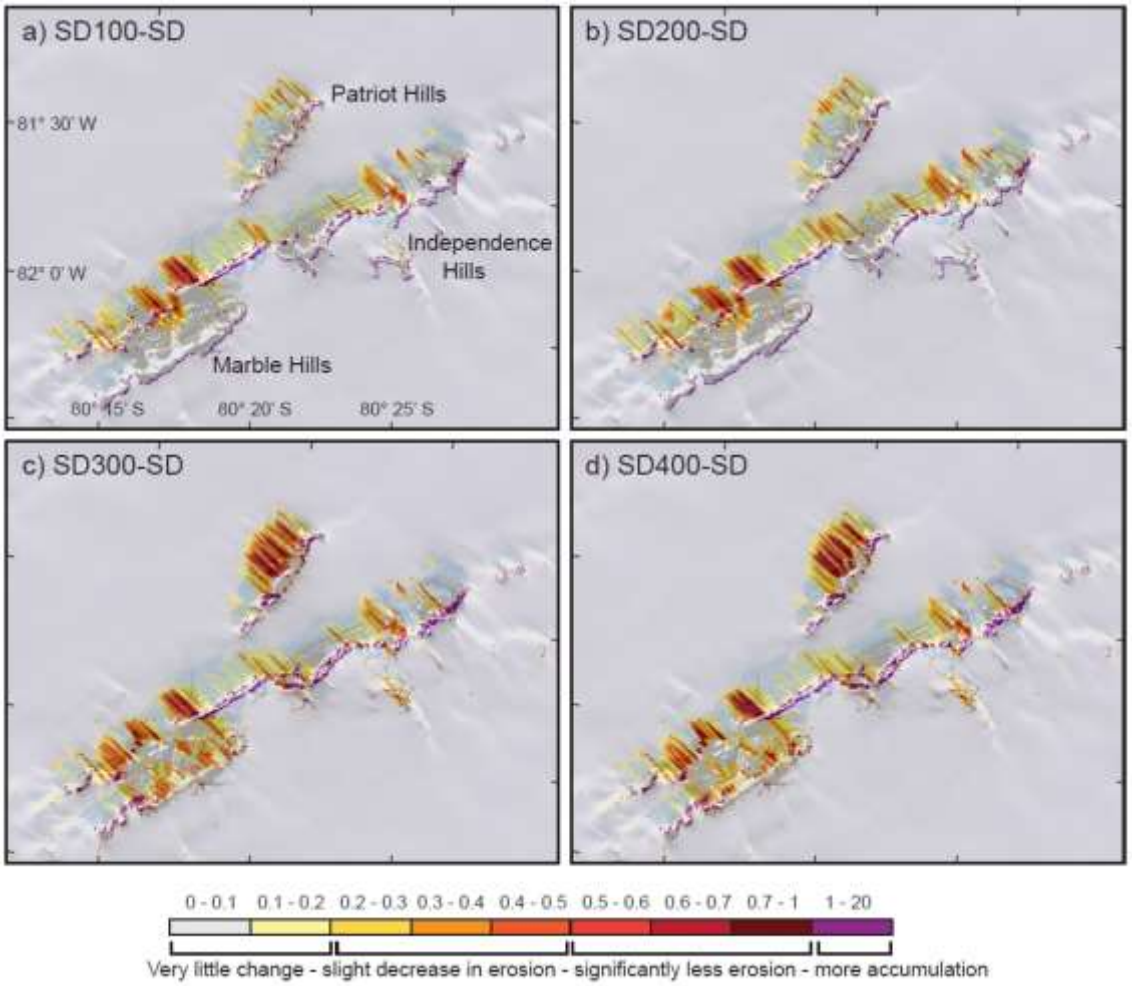

Figure 8.12. Quantified changes in snow drift conditions as the ice elevation is raised to simulate past ice sheet conditions. Each model was run over 10 iterations with an incoming wind direction of 135°. Simulated outputs for each new DEM, raised by a) 100m, b) 200 m, c) 300 m and d) 400 m have been subtracted from the original *Snow_Blow* model output, which was run on an ice surface elevation representative of present day conditions.

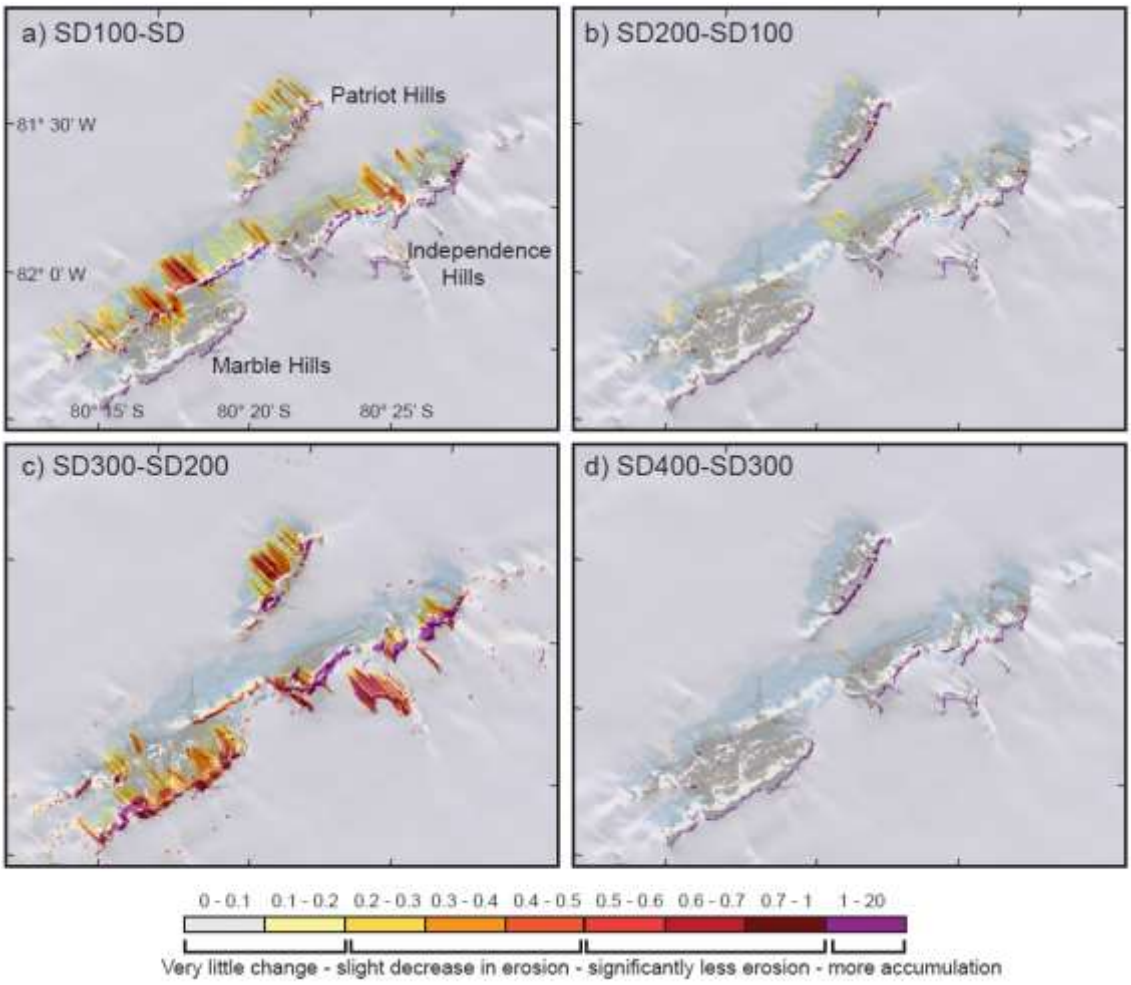

Figure 8.13. Quantified changes in snow drift conditions as the ice elevation is raised in 100 m increments to simulate past ice sheet conditions. Each *Snow_Blow* simulation (run over 10 iterations, with an incoming wind direction of 135°) has been subtracted from the previous *Snow_Blow* model output (which was run on a DEM with an ice surface 100 m lower).

as remaining outcrops, which largely comprise of the high elevation peaks of Independence and Marble Hills (Figure 8.11c).

8.4 Discussion

8.4.1 Model validation

By comparing snow drift features identified in satellite imagery, such as wind drift tails and BIAs in Figure 8.3 to initial model outputs in Figure 8.9, it is evident that the *Snow_Blow* model (which utilises basic meteorological parameters and a 40 m resolution DEM) can accurately identify sheltered snow accumulation zones and areas of surface snow drift erosion in the southernmost Heritage Range at the north-eastern flank of Horseshoe Valley. Outputs from the simple, qualitative model mimic the irregular surface topography captured by satellite imagery and DEMs. Nunataks and their upwind slopes are regions capable of capturing snow whilst surface snow drift erosion is simulated when the modelled wind vector field approximates katabatic wind flow on the downwind side of uplands where the modelled wind vector field simulates katabatic wind flow. BIAs are located in such leeside locations and act as a unique form of model validation. Comparisons between modelled and observed BIA extent reveals that the *Snow_Blow* model can simulate surface snow drift erosion in areas with complex topography. Indeed, model simulations reveal that the location of BIAs and their orientation is governed by the local wind vector field, which is influenced by topography (Figure 8.10). These findings confirm results from numerical model simulations (using meteorological data and a finite element code in Elmer) in Scharffenbergbotnen BIA, Dronning Maud Land, East Antarctica by *Bintanja and Reijmer* [2001] and *Zwinger et al*. [2015], which find that katabatic winds are required to initiate and maintain BIAs and associated moraine sequences in Antarctica.

Although the large BIAs in Horseshoe Valley reflect persistent wind scour in front of nunataks in the southern Heritage Range it is worth noting that the snow drift model is also capable of capturing real-world processes acting on hourly-to-daily timescales. Initial model simulations reflect the gradual build-up of snow on topographic ridges like the BI moraine ridge

in front of Independence Hills (Figure 8.3b), before erosion begins to dominate in subsequent iterations without the additional input of snow. These processes, combined with other factors not considered by the *Snow_Blow* model, such as local ice flow (see chapters 2 and 5) and snow metamorphism control a variety of feedback mechanisms which regulate BIA extents in Antarctica [*Bintanja and Reijmer*, 2001].

8.4.2 Changing meteorological conditions

Although relatively consistent wind directions have been recorded at Patriot Hills BIA on short timescales by AWS data and on longer timescales of several thousand years through analysis of GPR transects (see chapter 5 and resultant paper *Winter et al*. [2016]), *Snow_Blow* simulations reveal that any future change in the prevailing wind direction would reduce surface snow drift erosion in Horseshoe Valley (Figure 8.10). Each of the hypothetical wind directions simulated in Figure 8.10 show a reduction in the areal extent of surface snow drift erosion in front of the nunataks when compared to simulations run under present conditions. These findings reveal that even a slight change in wind direction caused, for example by a change in the morphology of the ice sheet would reduce the size of BIAs in Horseshoe Valley. In turn this would alter local ice-flow dynamics and sediment transfer in BIAs as well as the hydrological regime.

Although the *Snow_Blow* model shows that the current prevailing wind direction across Horseshoe Valley permits the greatest surface snow drift erosion, and therefore the greatest BIA extents, this study has also discovered that the orientation of the mountain range, relative to the prevailing wind direction plays an important role in the location and size of BIAs. For example, the BIA in front of Morris Cliffs is nearly twice as large as the BIA in front of the northern extremity of Patriot Hills. As the prevailing wind direction is nearly perpendicular to Morris Cliffs, katabatic wind flow can easily stream over the long, thin mountain chain and erode a large area in the lee. In comparison, the katabatic winds flowing over Patriot Hills, where the wind fetch is limited by the complex topography of Independence Hills, is less extensive. This has important implications for ice flow and debris transport in Horseshoe Valley, as the larger

BIAs in front of Independence Hills, Morris Cliffs and Marble Hills can encourage more ice and debris to reach the surface than the neighbouring, and smaller Patriot Hills BIA.

8.4.3 Past snow drift conditions

By simulating former ice sheet conditions in Horseshoe Valley, patterns of surface snow drift have been explored under a variety of former ice sheet elevations. Simulating a thicker ice sheet, akin to ~10 ka ago, has revealed that the height of an outcrop, relative to the ice surface elevation, has a strong influence on the intensity and areal extent of surface snow drift erosion, transportation and accumulation. For example, an ice elevation just 100 m thicker than present simulated less surface snow drift erosion on the downwind slopes of the Heritage Range (Figures 8.12 and 8.13) than models run on current ice sheet elevations. This finding can be accounted for by weakened air turbulence; a direct result of reduced nunatak to ice surface relief [*Bintanja*, 1999] (e.g. Figure 8.14). Whilst sublimation is not accounted for in the *Snow_Blow* model it is worth noting that this weakened air turbulence will also reduce rates of sublimation, which will promote a positive feedback loop that will encourage the ice sheet to thicken (see *Bintanja* [1999]).

Although Figure 8.13a reveals the influence that ice surface elevation has on snow drift conditions, further simulations (run on increasingly thicker ice) reveal that there is not a linear relationship between ice elevation changes and snow drift erosion/accumulation at the ice surface. By comparing Figure 8.13a to other panels in the same figure it is evident that surface snow drift erosion must sometimes surpass thresholds that initiate system reorganisation. In Horseshoe Valley thresholds are reached when the ice sheet surface is raised by 100 m and then by 300 m. When the present day ice sheet surface is increased by 300 m, Patriot Hills and numerous other lower elevation nunataks and outcrops are buried. This allows snow to drift over the now raised ice sheet surface, which impacts simulated snow drift conditions in Horseshoe Valley. Although studies, such as that by *Zwinger et al*. [2015], have documented similar reductions in katabatic winds and surface snow drift erosion under thicker ice sheets, the continued snow accumulation above Patriot Hills in Figures 8.13c and 8.13d represent DEM

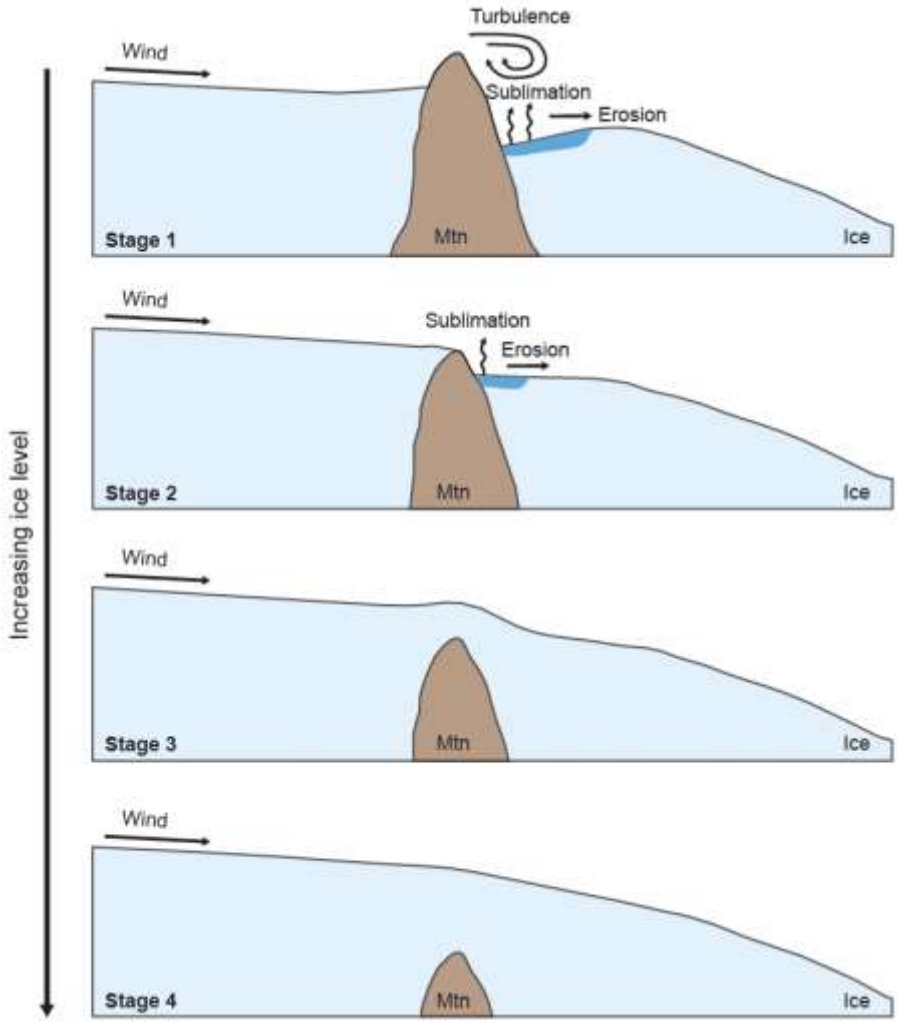

Figure 8.14. Schematic illustration of BIA decline during periods of increasing ice thickness (adapted from *Bintanja* [1999]). When mountains are exposed above an ice sheet (like Stage 1) increased turbulence from katabatic wind flow will promote sublimation of the ice surface and contribute to the surface lowering of the BIA. If meteorological or ice flow conditions change and the mountains become less exposed, like Stage 2, there will be a lower ice surface to mountain top relief, which will reduce air turbulence, limiting surface erosion and sublimation. This will act to decrease the size and extent of BIAs associated with nunataks. Once the mountain is buried by ice, leeward wind erosion will reduce dramatically (e.g. Stage 3), to the point at which wind will flow freely over the smooth, sloping surface topography (Stage 4).

modifications, rather than real-world processes, as the original ice sheet surface was raised without accounting for any glaciological changes in ice surface morphology or ice flow modifications, which would smooth the surface over Patriot Hills and limit snow accumulation.

As Independence and Marble Hills protrude up to 500 m above the present ice sheet surface, the tops of these mountains would have been ice-free when the ice sheet was approximately 400 m thicker, during the LGM and up to 10 ka ago [*Hein et al*., 2016b] (Figure 8.11). The consequence of this is reflected in the *Snow_Blow* output, as surface snow drift erosion still dominates the downwind slopes of the massifs, albeit at a reduced spatial coverage and intensity. Whilst the modified DEMs cannot emulate exact ice surface conditions at the LGM and ~10 ka ago, the *Snow_Blow* model outputs suggest that BIAs in front of Independence and Marble Hills, and indeed BIAs in front of other local mountain ranges at similar elevations (including Liberty Hills) have existed for at least the last glacial cycle and that lower elevation nunataks, like Patriot Hills only emerged from a thinning ice sheet ~6.5 ka ago. These findings capture spatial changes in BIA formation and evolution, where the shape and form of individual BIAs will have varied as the ice sheet elevation fluctuated in response to internal and external forcings.

These results help explain elevated glacial trimlines and BI moraine deposits in the Southern Heritage Range and substantiate work published by *Hein et al*. [2016b], as katabatic wind flow has been stable for long periods of time. Since simulations also reveal that BIAs would have existed in front of the highest nunataks in Horseshoe Valley during the LGM and until 10 ka ago, zones of previously scoured BI must have been transported along the length of Horseshoe Glacier for thousands of years. These results agree with local GPR investigations detailed in Chapter 5 and the resultant paper by *Winter et al*. [2016], by confirming that the two unconformities in Patriot Hills BIA sequence can indeed be attributed to paleo katabatic wind scour further up valley, as ice flowed through BIAs in front of Liberty and Marble Hills (Figure 5.10).

Snow_Blow investigations also highlight the sensitivity of katabatic wind scour (and therefore BIA erosion) to ice sheet elevation changes. Findings have revealed that snow

transport, erosion and deposition in Antarctica can experience dramatic changes as a result of small adjustments in ice sheet thickness or prevailing wind directions. This allows BIAs to initiate, grow, shrink, migrate, stagnate and re-initiate over both short and long time periods. As simulations of recent ice sheet surface lowering in Horseshoe Valley and Scharffenbergbotnen Valley [*Zwinger et al*., 2015] have documented the initiation and growth of BIAs in recent years it is expected that the number (and size) of BIAs in Antarctica could increase as feedbacks associated with warmer surface temperatures lower ice sheet elevations further (see Chapter 2, section 2.4).

8.5 Summary

Snow_Blow model runs accurately identify surfaces of accumulation and snow drift erosion in Horseshoe Valley, West Antarctica. The location and extent of BIAs and snow drift tails help to validate the simple qualitative model, showing how the *Snow_Blow* model can simulate areas of surface snow drift erosion and accumulation using basic AWS measurements and a local DEM. The snow drift simulations show that BIAs in Horseshoe Valley are currently maintained by stable meteorological conditions, where surface winds are influenced by the complex topography to create spatially variable surface snow drift erosion and accumulation patterns. These investigations support previous views of persistent katabatic wind flow in Horseshoe Valley by *Hein et al*. [2016b], and the assertion that BI moraine formation requires these unrelenting winds. By simulating a variety of prevailing wind directions and past ice sheet elevations, use of the *Snow_Blow* model has discovered that even modest changes in prevailing katabatic wind flow or ice thickness will greatly alter the location and size of BIAs. Model outputs suggest that thresholds to initiate system reorganisation must exist in areas of complex topography, in mountainous regions. In Horseshoe Valley the greatest change in the extent of surface snow drift erosion is simulated when Patriot Hills was largely buried by an ice sheet 300 m thicker than present, when katabatic wind strength is reduced. These findings have profound implications for the understanding of ice flow in Horseshoe Valley, as taller nunataks, including the Independence, Marble and Liberty Hills would have retained their BIAs ~10 ka ago,

allowing older packets of ice and entrained debris, and indeed previously scoured BI to travel through Horseshoe Glacier, and associated BIA systems for a long time. As Patriot Hills BIA is much younger, and smaller as a result of nunatak orientation and elevation (relative to the ice sheet surface), old packages of ice are just emerging at the ice surface, and as such, they represent considerable opportunity for investigating historic ice sheet flow and past climatic conditions (through isotope analysis) in West Antarctica. As BIAs help to bring sediment up to the surface (Chapter 7), these findings also provide support for blue ice moraine investigations in Horseshoe Valley. Critically, the *Snow_Blow* model outputs reveal that snow drift conditions in Horseshoe Valley have transformed over time and that present snow accumulation and snow drift erosion patterns would be affected by any future changes in ice sheet elevation or prevailing wind direction. This study therefore highlights the sensitivity of BIAs to changing meteorological conditions, whilst revealing that nunatak elevation (relative to the ice surface) and nunatak orientation (relative to the prevailing wind direction) are critical to BIA stability and subsequent ice flow phenomenon.

CHAPTER 9

Discussion

9.1 Introduction

This thesis has used ice penetrating radar to investigate englacial stratigraphy in order to determine BIA stability (Chapter 5), Holocene flow reconfigurations of the IIS catchment (Chapter 6) and debris entrainment mechanisms in Horseshoe Valley and the wider Weddell Sea sector of the WAIS (Chapter 7). Snow drift simulations have also been employed to investigate past and present katabatic wind scour and snow accumulation patterns (Chapter 8). In this chapter these findings will be combined to review historic ice flow conditions in Horseshoe Valley (section 9.2) and to discuss the stability of the upper IIS catchment, in and around the Ellsworth Mountains (section 9.3). Section 9.4 will then address the significance of detecting englacial debris by geophysical means, as well as the importance of tracing debris accumulations from continental sources to Southern Ocean delivery. Finally, section 9.5 will review the advantages and disadvantages of using the novel snow drift model *Snow_Blow* (detailed in Chapter 8) and suggest considerations for future model simulations.

9.2 Historic ice flow conditions in and around Horseshoe Valley

Although advances in satellite technology have recently allowed the current ice flow trajectory and velocity of remote areas of the WAIS, such as Horseshoe Glacier to be determined (e.g. *Rignot et al*. [2011a]), the geophysical investigations documented in this thesis provide the first account of former ice flow conditions in Horseshoe Valley in the Southern Heritage Range. In order to approximately date surface and subsurface features, a number of published datasets have been consulted. These local datasets include age-depth modelling calculations at the BIR [*Siegert et al*., 2013], deuterium isotope climate reconstructions from Patriot Hills BIA [*Turney et al*., 2013] and cosmogenic nuclide dating of boulders along the Southern Heritage Range [*Hein et al*., 2016a, 2016b]. As a result of these investigations, a time line of ice flow changes in and around Horseshoe Valley has been compiled to produce Table 9.1.

Date	Horseshoe Glacier	BIAs in Horseshoe Valley	Independence Trough ice flow	Ellsworth Trough ice flow
Present conditions	• Ice flowing <16 m a^{-1} * • Stable mass balance conditions †	• Large BIAs in front of Liberty, Marble, Patriot and Independence Hills • Stable BIA extents◊ • Active BIA moraine systems Δ	• Ice flowing at 35 m a^{-1} * • No BIAs along trough as nunataks only exposed on stoss side	• Ice flowing at 70 – 130 m a^{-1} * • No BIAs as no exposed nunataks
~400 years before present	• Ice flowing <30 m a^{-1} * • Stable mass balance conditions	• Large BIAs in front of Liberty, Marble, Patriot and Independence Hills • Stable BIA extents◊ • Active BIA moraine systems Δ	• Ice flowing at >35 m a^{-1} * • No BIAs along trough as nunataks only exposed on stoss side	• Ice flowing >70 m a^{-1} * • No BIAs as no exposed nunataks
~4,000 years before present	• Ice flowing ≥ 30 m a^{-1} * • Ice sheet elevations similar to present day conditions +	• BIAs in front of Liberty, Marble, Patriot and Independence Hills • Each BIA was smaller than present day extents • Active BIA moraine systems	• Conditions unknown as old ice has been advected out of trough and there are no dating controls for former ice sheet elevations	• Conditions unknown as old ice has been advected out of trough and there are no dating controls for former ice sheet elevations
~10,000 years before present	• Ice flowing > 30 m a^{-1} * • Ice sheet ~400 m thicker than present +	• BIAs in front of Liberty, Marble and Independence Hills • Each BIA was smaller than present • Patriot Hills was buried, so BIA in leeward foreground became stagnant	• Conditions unknown as old ice has been advected out of trough and there are no dating controls for former ice sheet elevations	• Conditions unknown as old ice has been advected out of trough and there are no dating controls for former ice sheet elevations

Table 9.1. A summary of ice flow conditions in and around Horseshoe Valley during the Holocene from work pertained in this thesis, and acknowledged literature sources: **Rignot et al.* [2011a], †*Casassa et al.* [2004], ◊*Rivera et al.* [2014] Δ*Westoby et al.* [2016], +*Hein et al.* [2016b].

In Chapters 5 and 6 ice penetrating radar returns revealed that ice in Horseshoe Valley has been relatively slow flowing and isolated for at least the last ~4 ka. Continuous, conformable and parallel englacial stratigraphic features in the upper ice column of Horseshoe Glacier indicate that layers of snow and ice have steadily accumulated at the head of Horseshoe Valley during this time, where PISM perturbations suggest that ice has continuously migrated through the over-deepened trough, towards the local grounding line of the FRIS at Hercules Inlet. Although the majority of ice flow in Horseshoe Valley Trough has followed this well-established route-way, GPR investigations and snow drift simulations reveal that some of the ice in Horseshoe Valley has been deflected upwards to compensate for katabatic wind erosion and sublimation of the ice surface on the leeward side of nunataks. Recent dating of ice along Patriot Hills BIA has revealed that this steady upwards flow phenomenon has encouraged ice as old as 30 ka to emerge at the surface [*Turney et al*., 2013]. As this old ice reaches the fresh BIA surface, previously entrained debris clasts are released through sublimation. This process has allowed thick BI moraines to accumulate along the leeward slopes of nunataks which define the Southern Heritage Range [*Fogwill et al*., 2012; *Westoby et al*., 2015, 2016].

Whilst airborne RES transects reveal continuous internal stratigraphy in the upper ice column of Horseshoe Glacier (representative of steady snow accumulations and ice flow conditions over the past ~4 ka), discontinuous and buckled layers were found to dominate the lower ice column (see Chapter 6). These layers would have been deformed during a period of enhanced ice flow 'switch on' in response to external forcings. By reviewing relevant literature, it is suggested that this enhanced ice flow (occurring more than 4 ka ago) could have been promoted by increased ice surface elevations in Horseshoe Valley between ~3.5 ka ago and ~10 ka ago, when ice was approximately 400 m thicker than present [*Hein et al*., 2016b]. This increased ice thickness would have amplified the gravitational acceleration of the ice flow, and altered basal conditions, which would have temporarily modified the internal flow dynamics of Horseshoe Glacier. Due to the topographic confinement of Horseshoe Glacier (which has been revealed by long cosmogenic nuclide exposure dates along nunataks [*Hein et al*., 2016a, 2016b], and thick basal ice units along highland plateaus – documented in Chapter 6), it is now

understood that Horseshoe Glacier must have 'switched on' and 'off' in response to local ice accumulation changes (instigated by external forcings) during the Holocene.

Even when ice in Horseshoe Valley was thicker, and flowing much faster, around 10 ka ago, snow drift simulations on former ice surface elevations (explored in Chapter 8) reveal that upwards ice flow in the vicinity of nunataks would have continued to maintain several BIAs in Horseshoe Valley throughout the Holocene (see Table 9.1). Although BIAs in front of the Liberty, Marble and Independence Hills would have been much smaller during this period (as a result of a reduced ice surface to nunatak elevation ratio and therefore limited katabatic wind scour on the leeward slopes), englacial debris would have continuously been released in front of the exposed mountain chains. The continual exposure of the tallest nunataks in Horseshoe Valley throughout the Holocene would therefore have contributed to long-term debris availability, entrainment, transportation and deposition processes in the Weddell Sea sector of the WAIS. However, whilst BIAs and associated BI moraine sequences were sustained in front of the tallest nunataks during the Holocene, it is important to recognise that smaller mountain chains like Patriot Hills would have been buried by the thicker ice accumulations ~10 ka ago. This would have altered local ice flow dynamics, as ice and entrained debris accumulations would have traversed the front of the buried mountain chain, on route to the local grounding line, and eventually the Southern Ocean (as opposed to flowing up towards a BIA surface).

To conclude this section, this thesis has found that ice in Horseshoe Valley has been topographically confined, and therefore relatively isolated throughout the Holocene, at least. This has allowed Horseshoe Glacier to 'switch on' and 'off' independently of neighbouring ice flows, as each tributary flow adapts to external forcings and internal ice dynamical changes independently. These findings show intermittent ice streaming in Horseshoe Valley, as well as the relative stability of BIAs and BI moraine systems in front of the tallest nunataks over long periods of time.

9.3 Stability of the upper Institute Ice Stream catchment

Throughout this study, geophysical investigations and snow drift simulations have been employed to better understand the nature of ice flow in and around the Southern Heritage Range in the Ellsworth Mountains, in order to determine the stability of the upper IIS catchment and the Weddell Sea sector of the WAIS. By analysing the complex subglacial topography in and around Horseshoe Valley, this study has confirmed that tributary flows sourced near the Ellsworth Mountains rest on bedrock well below sea level, where geophysical returns have revealed even lower bed elevations than those published in Bedmap2 by *Fretwell et al*. [2013]. This low basal topography greatly increases the possibility of future unstable retreat of the grounding line in the Weddell Sea sector of the WAIS, should the grounding line position change in response to predicted climatic and/or oceanic forcing (detailed in Chapter 2). Whilst these fears have already been hypothesised by a number of authors who have investigated the main ice flows draining into the FRIS (e.g. *Siegert et al.* [2013]; *Ross et al.* [2014]; *Bingham et al.* [2015]), this thesis provides the first conclusive evidence for former ice flow reorganisation of the upper IIS catchment, when ice flows dramatically changed speed and direction in response to external forcings.

Complete re-organisation of the main IIS trunk ~400 years ago is now understood to have resulted from enhanced ice flow through the Independence and Ellsworth troughs, when thick, topographically confined ice flows began to spill out of their deep channelised systems and stream across the region now covered by the BIR (Table 9.1). As geophysical analysis has revealed slow and stable ice flow in Horseshoe Valley during this time, it is evident that each tributary flow in the upper IIS acts largely independently of one another. This exemplifies theoretical assumptions detailed in Chapter 2, which stress that internal flow controls in each ice stream will allow similar external forcings to be addressed in a number of ways.

In the Weddell Sea Sector of the WAIS, the exact timings of enhanced ice flow ‘switch on’ and ‘off’ can be attributed to a number of local factors, including, but not limited to ice sheet dynamics, basal hydrology, sediment availability and trough morphology. So far, this discussion has shown how ice in Horseshoe Valley is largely protected from the main WAIS ice

flow by high nunataks on three sides. This makes Horseshoe Glacier much more stable than neighbouring ice flows, as ice can slowly accumulate or thin in the wide trough in response to external forcings without draining large proportions of the inland ice sheet or influencing neighbouring tributary flows. However, as adjacent troughs are only confined on two sides - often by subglacial highlands and basal ice sequences rather than nunataks, it is expected that external forcings will have a greater impact on the ice flows supported by the Independence and Ellsworth Troughs. Although the Independence and Ellsworth Troughs are more similar to one another, than to Horseshoe Valley, ice in the Ellsworth Trough currently flows at a much faster rate. By reviewing relevant literature, it is suggested that the fast ice flow speeds in the Ellsworth Trough could be promoted by enhanced basal lubrication, resulting from subglacial drainage into and out of the upstream Subglacial Lake Ellsworth [*Vaughan et al*., 2007] (introduced in Chapter 2, section 2.6). Combined with reduced frictional resistance along valley side walls from the buried highland plateaus which define the Ellsworth Trough, this study concludes that ice in Ellsworth Trough will be the first to react to changes in internal or external forcings. This makes ice in Ellsworth Trough the most unstable of all IIS tributary flows (sourced in and around the Ellsworth Mountains).

These findings suggest that ice flows in the Weddell Sea Sector of Antarctica are acutely sensitive to both external forcings and changes in internal ice sheet dynamics. Whilst external forcings (e.g. atmospheric and oceanic) are known to trigger and pace changes in ice sheet dynamics, this thesis has shown that a multitude of factors govern the location and flow regime of ice streams in this area of Antarctica, as well as the precise rate and timings of changes in ice flow dynamics. These differences have allowed ice streams in the upper IIS to 'switch on' and 'off' independently of one another, where enhanced ice flow through deep trough systems has facilitated complete re-organisation of the main IIS trunk. These findings suggest that periods of enhanced ice flow, in conjunction with mass changes may have been regular during the Holocene and that recent ice stream switching in the Siple Coast and Amundsen Sea sectors are not unique in Antarctica, and could in fact characterise the decline of

the WAIS. As a result, these discussions are particularly relevant to the ice sheet modelling, climate and sea level communities.

9.4 Significance of englacial debris detection

Although englacial debris clasts have been detected in a number of alpine glacier systems, Chapter 7 provides the first detailed account of large debris concentrations within the WAIS, where over 9 ± 5 tera tonnes of debris has been approximated in Horseshoe Valley Trough (assuming an ice/debris ration of 80:20), through airborne RES analysis. This study exemplifies recent successes in ice penetrating radar data acquisition and processing, where debris clasts and particles in compressive BIAs and thick ice flows have been detected by a number of ice penetrating radar systems. Whilst this study has focussed on debris sources, and methods of debris entrainment in the Weddell Sea sector of the WAIS, it is expected that debris sources and englacial sediment incorporation in other areas of Antarctica will also vary spatially and temporally as a result of ice flow conditions, ice temperature, ice thickness, sediment availability and basal topography.

As glaciers adjust to a changing climate, these controls will impact sediment availability, debris entrainment and debris transport routes through the glacial system. Should extraglacial debris volumes increase, as exposed rock-walls are de-buttressed by a thinning ice sheet, increased sediment availability and transfer could alter frictional stress at the glacial bed and modify ice flow speeds [*Bell et al*., 1998], change ice flow direction through long-term erosive processes [*Harbor et al*., 1988] and enhance sediment flux from continental sources to Southern Ocean delivery [*Death et al*., 2014; *Hawkings et al*., 2014]. This would increase the abundance of sediment-derived nutrients like bio-available iron (BioFe) in the Southern Ocean, which could enhance primary productivity and ultimately result in the drawdown of atmospheric CO_2 in the southern hemisphere. Whilst coastal sediments [*Tagliabue et al*., 2009], dust [*Jickells et al*., 2005], sea ice [*Edwards and Sedwick*, 2001] and iceberg rafted debris [*Raiswell and Canfield*., 2012] are all well-established sources of BioFe (Figure 9.1), the transportation and deposition of BioFe-rich sediments from the Antarctic continent have yet to

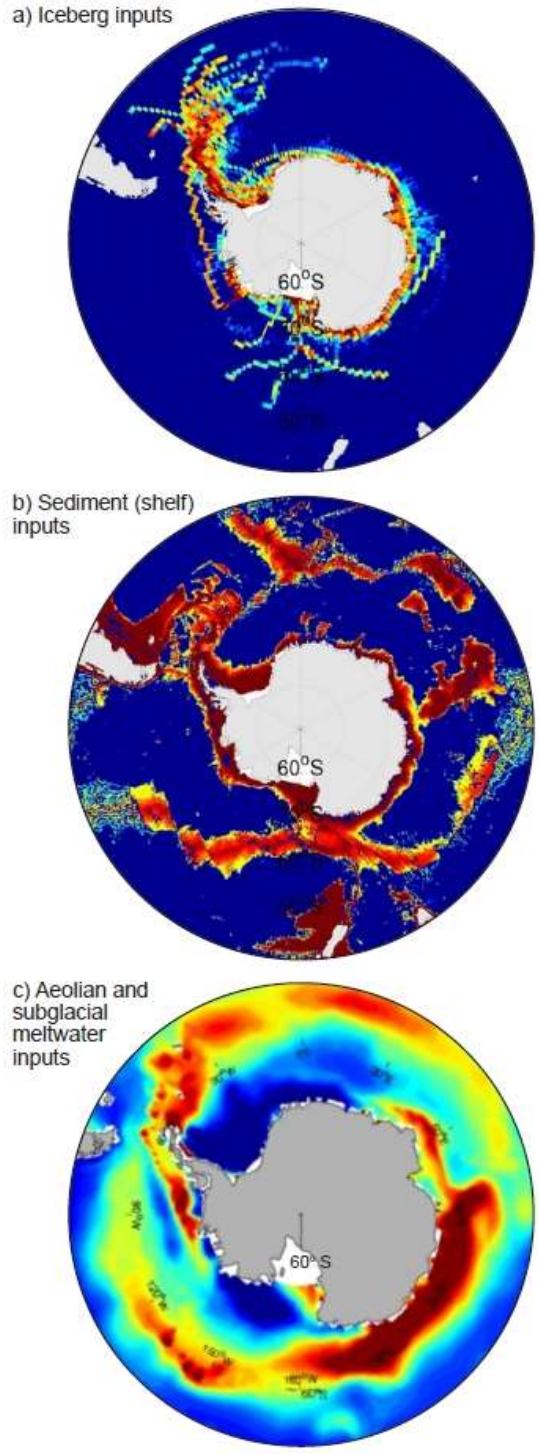

Figure 9.1. Known sources and modelled spatial variability of Fe delivery to the Southern Ocean through a) iceberg inputs [*Wadley et al*., 2014], b) sediments (shelf) [*Wadley et al*., 2014] and c) aeolian and subglacial meltwater altered primary productivity [*Death et al*., 2014]. In each case, red colouration represents high Fe, while blue represents low Fe.

be considered in scientific literature or IPCC reports. As englacial debris transportation could play an important role in the negative climate feedback loop known as the 'FE hypothesis', it is imperative that continental debris sources in Antarctica are better understood and quantified. This is particularly important when other sources of BioFe are known to be decreasing, global temperatures are warming, and CO_2 levels are rising at glacial terminations [*Watson et al*., 2000]. Whilst these investigations are beyond the scope of this PhD it is suggested that future studies should use recent advancements in Terrestrial Laser Scanning and Structure-from-Motion DEM differencing to quantify hillslope processes in Antarctica (e.g. *Westoby et al*. [2012, 2015]). This will improve magnitude/frequency curves of rock failures in Antarctica, and allow debris flux to be calculated from continental sources. Ice penetrating radar techniques should then be employed to detect and trace sediments through the glacial system, from continental source areas to the coastal shelf (e.g. Figure 9.2).

9.5 Reviewing the *Snow_Blow* model

As *Mills et al.* [Submitted] have recently coded *Snow_Blow* the discussion chapter of this thesis poses an appropriate location to assess the merits and pitfalls of the *Snow_Blow* model, particularly when simulations are run over complex mountainous topography. The main advantages and disadvantages of *Snow_Blow* will be presented before considerations for future investigations are discussed.

9.5.1 Advantages of the Snow_Blow model

- User-friendly interface – the model can run through an ArcGIS toolbox
- The model requires limited data input (a DEM and local meteorological data)
- Once the code has been modified in Python to include model inputs and user specifications simulations are quick to run
- Outputs are automatically saved after each iteration
- Katabatic wind erosion can be simulated over complex topography

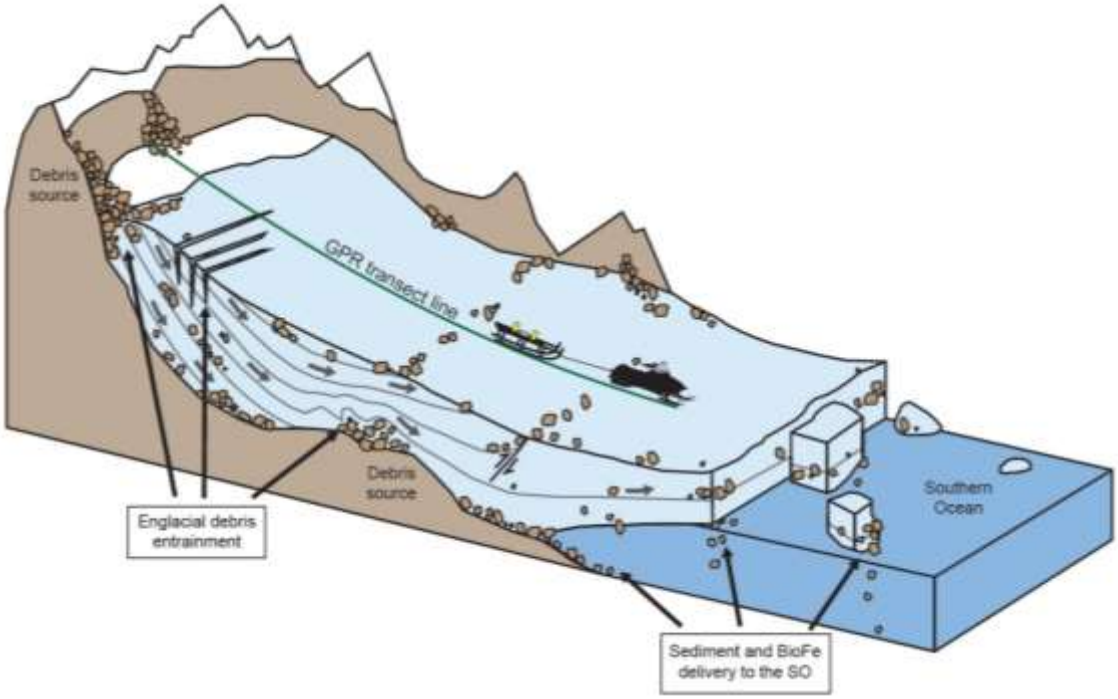

Figure 9.2. Schematic diagram depicting how GPR systems could detect and trace sediments (as well as associated nutrients like BioFe) from continental sources to Southern Ocean delivery.

- The model can simulate accumulation on, and behind a variety of topographic features, including low elevation moraine ridges and boulders resting on the ice surface
- Outputs define variations in the erosive strength of snow drift over the study site

9.5.2 Disadvantages of the Snow_Blow model

- Metamorphism of the snow pack is not included in the model
- No feedback mechanisms are included, to stop the progressive erosion of BIA surfaces
- The number of iterations required will vary depending on the study site. This will be difficult to determine in areas where snow accumulation and erosional extents are not known
- As *Snow_Blow* simulations mimic the user-defined wind direction and surface topography from the DEM, it is difficult to accurately simulate historic snow drift, and/or predict future snow drift conditions
- Surface elevation changes as a result of progressive snow drift accumulation or erosion are not accounted for in the model

9.5.3 Considerations for future investigations

Chapter 8 has detailed how the *Snow_Blow* model, initially designed to interpret historic snow drift conditions in the Scottish Highlands (e.g. *Purves et al.* [1999a, 199b] and *Mills et al.* [Submitted]) has been successfully employed to determine the controls on katabatic wind erosion and snow accumulation in Horseshoe Valley, West Antarctica. The simple, qualitative *Snow_Blow* model has highlighted the relatively simplistic processes behind BIA formation and evolution, without the need for numerous user-inputs or complex and time-consuming algorithms. It is therefore suggested that future studies use the outputs from the *Snow_Blow* model as a guide, to explain local glaciological features like BIA moraine deposits and paleo BIA wind scour events. More complex flow models, like those developed by *Grinsted et al.*

[2003] can then be employed to quantify rates of upwards ice flow or BI moraine deposition. This limits the need to make the simple, qualitative model more complex.

9.6 Summary

This thesis has combined a number of ice penetrating radar surveys and BIA simulations to review historic ice flow conditions in Horseshoe Valley, and other upper IIS tributary flows. By comparing radar returns to published data sets, this thesis has refined age-estimates for ice streaming, tributary flow stagnation, ice stream reconfiguration, BIA formation and BIA evolution in the upper IIS catchment, in and around the Ellsworth Mountains. Dynamic changes in ice flow velocity have also been recorded within three distinct tributaries of the IIS, where results are consistent with the hypothesis that the LGM and Holocene drainage pathways within the Weddell Sea sector of the WAIS were different from those of the present-day [*Larter et al*., 2012; *Siegert et al*., 2013], and that ice streams in this area are susceptible to changes associated with both internal and external forcings. These findings suggest that ice stream switching and mass changes in the Siple Coast and Amundsen Sea sectors of Antarctica are not unique to these sectors, and that the dynamic nature of ice flow in the IIS and its tributaries may have been regular during the Holocene and may characterise the decline of the WAIS.

During these investigations, innovative snow drift simulations have refined the controls on BIA formation and evolution and stressed the importance of analysing the detailed internal stratigraphy of BIAs when assessing the continuity of horizontal climate records. Improvements in ice penetrating radar acquisition and processing have also improved our understanding of ice flow processes in West Antarctica, as well as the controls on debris entrainment mechanisms within the Weddell Sea sector of the WAIS. These findings have opened up new possibilities for investigating potentially rich sources of BioFe within glacial systems, and ultimately CO_2 drawdown in the Southern Ocean.

CHAPTER 10

Conclusions

10.1 Introduction

This concluding chapter will document the main findings from the thesis (section 10.2), before outlining how each of the objectives introduced in Chapter 1, section 1.2 have been met (section 10.2). A brief summary of ice flow and ice sheet stability in and around Horseshoe Valley will then be provided in section 10.4, whilst section 10.5 will detail inherent limitations of the project. Finally, suggestions for future work, beyond the scope of this PhD will be outlined in section 10.5.

10.2 Main findings

This thesis has used a number of techniques to investigate the past and present behaviour of the West Antarctic Ice Sheet in and around Horseshoe Valley and the upper Institute Ice Stream catchment. In order to determine changes due to grounding line migration, ice streaming and ice accumulation under a changing climate this project has:

1) Investigated the internal annual layers of Patriot Hills BIA, where it was noted that stable ice sheet flow and accumulation has been interrupted by two periods of erosion, indicative of paleo katabatic wind scour.

2) Utilised numerical ice sheet models, ILCI plots and geophysical datasets to establish paleo ice flow direction in Horseshoe Valley.

3) Examined airborne RES transects to establish that ice in Horseshoe Valley has remained slow-flowing and isolated for at least the past 4000 years.

4) Analysed airborne RES transects from the Independence and Ellsworth Troughs, where buckled layers throughout the ice column document enhanced ice flow ~400 years ago,

revealing the source of paleo ice streaming over the region now covered by the Bungenstock Ice Rise.

5) Re-created Holocene flow trajectories in the upper IIS catchment to reveal that ice in topographically confined tributaries has 'switched on' and 'off' in response to external forcings, associated with climate change.

6) Used airborne RES to locate and trace over 9 ± 5 tera tonnes of englacial debris in Horseshoe Valley Trough (assuming an ice/debris ratio of 80:20).

7) Established that debris in the Weddell Sea sector of the WAIS is entrained into local ice flows by folding, shearing, faulting and regelation processes, which are ultimately controlled by debris availability, ice flow, ice temperature and basal topography.

8) Determined the sensitivity of katabatic wind driven snow erosion and accumulation to changes in ice sheet thickness and the prevailing wind direction using *Snow_Blow*.

9) Outlined the controls on BIA formation and evolution in Horseshoe Valley.

10.3 Reviewing objectives introduced in Chapter 1

Objective 1: Analyse englacial stratigraphy within the Blue Ice Area at Patriot Hills to determine historic changes in ice flow and/or accumulation

High resolution step-and-collect mode GPR data, collected by the Northumbria PulseEKKO system in 2013/2014 was used to determine the englacial stratigraphy of Patriot Hills BIA and to assess the continuity of a local BIA horizontal climate record (collected by *Turney et al.* [2013] in 2012). All radargrams were processed in ReflexW and examined in MATLAB and Opendtect to highlight prominent internal GPR reflectors within the BIA in 2D and 3D. Digitisation of the main transect line revealed numerous continuous and conformable dipping isochrones, separated by two discontinuities in the isochrone layers, where internal layers displayed divergence and truncation. By comparing geophysical returns to cosmogenic nuclide derived ice thickness measurements, PISM perturbations, surface velocity measurements and

ILCI plots it was evident that these discontinuities must represent unconformities in the stratigraphic record, caused by paleo katabatic wind scour in front of the Liberty and Marble Hills. Combined with more regional GPR returns, these findings reveal that the ice flow direction in Horseshoe Valley has remained unchanged since the LGM, even as the ice sheet thickness fluctuated in response to external forcings associated with climate change.

Objective 2: Determine the internal structure of the West Antarctic Ice Sheet in the upper Institute Ice Stream catchment to establish historic changes in regional ice streaming

Airborne RES data collected in and around the Ellsworth Mountains by Dr. Neil Ross (Newcastle University) and collaborators during an aero geophysical investigation of the IIS and MIS in 2011/2012 was collated to investigate the subsurface structure of the WAIS in the upper IIS catchment. Radargrams were imaged in 2D and 3D (in MATLAB and Opendtect respectively), before internal layers were manually digitised in Adobe Illustrator and automatically classified, using an ILCI developed by *Karlsson et al.* [2009]. Internal layer buckling within the topographically confined Independence and Ellsworth troughs provided the first evidence for former enhanced ice flow in the upper IIS tributaries, during the mid- to late-Holocene. These enhanced ice flows dramatically altered the configuration of the main IIS trunk by sourcing ice flows which streamed across the region now covered by the Bungenstock Ice Rise. Although buckled layers were also detected within the slow-flowing ice of Horseshoe Valley Trough, a thick sequence of surface-conformable layers in the upper ice column revealed slowdown more than ~4000 years ago and as such, enhanced flow switch-off here was not attributed to late Holocene ice flow reorganisation. The dynamic nature of the IIS and its tributaries suggests that ice stream ‘switch on’ and ‘off’ may have been cyclical during the Holocene as a result of ice thickness changes, and that these fluctuations may characterise the decline of the WAIS in this area.

Objective 3: Investigate debris entrainment mechanisms in the Weddell Sea sector of the West Antarctic Ice Sheet

In order to investigate debris entrainment mechanisms in Horseshoe Valley, highly reflective, steeply dipping englacial debris bands and hyperbolic radar returns - detected in previously analysed GPR and airborne RES transects (collected to fulfil objectives 1 and 2) were imaged in 2D and 3D using Reflexw and Opendtect respectively. Similar features in ground RES profiles across Horseshoe Valley (collected by Andrés Rivera from the Centro de Estudios Científicos) and an airborne RES survey of the Evans Ice Stream (and proximal upland catchment) (processed by Dr. David Ashmore from the University of Aberystwyth) were also analysed to investigate the spatial variability of debris sources and debris entrainment mechanisms in the Weddell Sea sector of the WAIS. By comparing radar detected debris reflectors to the subglacial bed and internal stratigraphic features, this thesis has recognised a number of debris entrainment mechanisms. Whilst thin and compressive BI flows on the leeward side of nunataks promote debris entrainment through regelation processes at the ice/bed interface and thrust faulting, more regional surveys evidence debris entrainment at depth, along englacial layer folds at the glacial margin. This latter debris entrainment mechanism allows debris clasts to be incorporated at the local thermal boundary by shearing and englacial layer folding, which occurs in response to the compressive conditions imposed at the interface between faster and warmer ice flow around bedrock obstacles, and slower, colder ice flow above obstacles. As regelation processes, faulting and folding are all controlled by ice flow, ice temperature, ice thickness, sediment availability and bedrock topography, internal and external forcings modulate these controls, where changes can alter ice flow routes and velocities as well as debris entrainment mechanisms and sediment transport fluxes from continental sources to Southern Ocean delivery. These findings indicate that it is now critical to detect and trace englacial sediments through the Antarctic Ice Sheets, as ice flows and topographic features respond to a changing climate.

Objective 4: Model the transport of snow by wind in Horseshoe Valley and compile a sensitivity analysis to determine the conditions necessary to initiate and maintain Blue Ice Areas in front of the Patriot, Independence and Marble Hills.

Dr. Stephanie Mills (Plymouth University) and collaborators novel *Snow_Blow* model was employed to improve the understanding of surface snow drift conditions and blue ice erosion in Horseshoe Valley, using a 40 m resolution SPOT DEM, and local wind data from an automatic weather station situated at Patriot Hills BIA. Initial simulations validated the simple, qualitative model, where results showed that *Snow_Blow* could accurately identify sheltered zones and areas of surface erosion in Horseshoe Valley. The *Snow_Blow* model revealed that BIAs in Horseshoe Valley are currently maintained by stable conditions, where strong and persistent katabatic wind flows are re-routed over the surface by the complex topography, resulting in spatially variable snow erosion and accumulation patterns. By simulating a variety of prevailing hypothetical wind directions and past ice sheet elevations (constrained by cosmogenic nuclide dating of exposed nunataks [*Hein et al*., 2016b] and deuterium isotope analysis of paleo ice surfaces [*Turney et al*., 2013]), the *Snow_Blow* model has revealed that even modest changes in the prevailing wind direction or ice sheet elevation would greatly alter the location, size and orientation of BIAs. Model outputs suggest that thicker ice accumulations <10 ka ago would have resulted in stepped changes in the spatial extent of BIAs in Horseshoe Valley, where simulations reveal that only the tallest nunataks could have supported BIAs ~10 ka ago, when ice in Horseshoe Valley was approximately 400 m thicker than present. This investigation has highlighted the sensitivity of BIAs to changes in ice sheet elevations and the prevailing wind direction, whilst discovering that BIAs accompanying the highest nunataks are the most stable and that mountain orientation, relative to the prevailing wind direction has a strong control on the location, orientation and extent of wind-driven snow erosion, and therefore BIAs.

10.4 Ice flow and ice sheet stability in and around Horseshoe Valley

This thesis has established that ice flow in Horseshoe Valley has remained relatively slow flowing and stable for at least the last ~4000 years. The topographic confinement of Horseshoe

Valley has largely suppressed the ingress of the main WAIS flow during this time, allowing local snow and ice accumulations (and associated englacial debris) to be directed through the over deepened valley, towards the local grounding line of the FRIS at Hercules Inlet. Although the majority of ice in Horseshoe Valley flows towards the Weddell Sea, some ice and debris is deflected upwards, to compensate for the sublimation and erosion of the ice surface at BIAs. This ice flow phenomenon has enabled so-called 'horizontal climate records' to be collected across Patriot Hills BIA, where paleo katabatic wind scour from BIAs further up valley has resulted in unconformities in the paleo climate record. Upward ice flow has also allowed debris clasts to be entrained and transported through the ice and towards the BIA surface, generating extensive debris accumulations in front of the nunataks that delimit Horseshoe Valley. The existence of thick moraine sequences in front of the tallest nunataks, combined with katabatic wind simulations over paleo ice surfaces (defined by [*Hein et al*., 2016b]) reveal that BIAs have been relatively consistent features in Horseshoe Valley, although BIAs accompanying smaller nunataks, like Patriot Hills, would have been buried ~10 ka ago, when the ice in Horseshoe Valley was ~400 m thicker [*Hein et al*., 2016b].

Although ice flow in Horseshoe Valley has remained relatively stable over the past ~4000 years, the occurrence of buckled ice layers deep within Horseshoe Glacier has revealed former, enhanced ice streaming which would have occurred in response to changes in the climate. Similar enhanced ice flow, representing the 'switch-on' of IIS tributary flow has been found in neighbouring Independence and Ellsworth Troughs, where buckled ice layers throughout the ice column reveal the source for Holocene ice flow reconfigurations of the main IIS trunk. Combined, these findings reveal that ice flows draining into the FRIS are sensitive to changes in the climate, where geophysical investigations have revealed that adjustments in the position of the grounding line, ice accumulation and/or ice streaming have allowed ice flows to 'switch on' and 'off' independently of one another. This has permitted resultant changes in ice flow patterns in the Weddell Sea Sector of West Antarctica. Although the topographically confined tributaries of the upper IIS largely prevent flow switching and water piracy, typical of ice flows in the Ross sea sector of the WAIS [*Anandakrishnan and Alley*, 1997], there is now a

growing concern that enhanced ice flow could quickly transform tributary flows of the IIS into discrete ice stream outlets. As the subglacial topography in the upper IIS lies well below sea level, enhanced ice flow would greatly increase the potential for more widespread and possibly irreversible ice sheet drawdown (as previously suggested by *Ross et al*. [2014]). The findings of this thesis are therefore significant for the ice sheet modelling, climate and sea level communities as results and discussions can inform users about paleo ice flow configurations and former ice sheet conditions in the Weddell Sea sector of West Antarctica.

10.5 Limitations of this research

Although geophysical methods have allowed the englacial stratigraphy and internal structure of Horseshoe Valley and the upper IIS catchment to be determined there are some inherent limitations related to geophysical data collection and analysis and snow drift model simulations. As these restrictions are common in remote areas of Antarctica, most of the limitations listed below could be remedied by further research.

1. As areas suitable for landing aircraft are limited in the vicinity of the Ellsworth Mountains, aircraft equipped with RES systems often had to take off and/or land in front of Patriot Hills, and consequently some internal features cannot be discerned from radargrams traversed in this area. To eliminate this concern in the future, fly overs should be made across aircraft runways when the RES system is warm and fully operational.

2. Although this study has provided a unique insight into Holocene ice flow configurations, the exact timing of events is restricted by a lack of precise dating in the IIS catchment. In order to constrain the timings of events a wider variety of dating methods (e.g. tephrochronology) needs to be performed on the horizontal climate record which was sampled across Patriot Hills BIA in 2012. Deep, vertical borehole extraction and analysis of the Bungenstock Ice Rise would also be helpful.

3. As airborne geophysical surveys were not designed to source and detect englacial debris at depth, there are only a few locations where englacial debris can be imaged in 3D. In order to fully understand the source and entrainment mechanisms of debris entrainment in Antarctica more radar survey lines need to be collected and analysed across the continent.

4. Although the *Snow_Blow* model can determine areas which are susceptible to surface erosion and accumulation in areas of complex surface topography, it is difficult to recreate former ice surface conditions so care must be taken when model outputs are used to investigate past ice sheet configurations. A lack of feedback mechanisms in the model also limits its use for understanding the evolution of BIAs.

10.6 Suggestions for further work

Recent advances in ice penetrating radar data acquisition and processing have enhanced our ability to detect englacial features and understand ice sheet stability. As a direct result of this increased resolution and efficiency a number of suggestions can be made for further work;

1. More BIAs should be examined with step-and-collect mode GPR as traditional continuous surveying speeds cannot capture the detailed internal stratigraphy of BIAs.

2. More radargrams need to be collected and analysed throughout the WAIS and EAIS to determine the regional controls on debris availability and entrainment in Antarctica.

Although both of these suggestions are important, the last point provides the greatest scope for further work. In order to quantify englacial debris accumulations and fully appreciate the controls on debris entrainment in Antarctica it is critical to investigate the movement of debris through the glacial system in more detail. It is therefore suggested that future studies quantify landslide hillslope processes using novel Structure-from-Motion photographic surveying [*Westoby et al*., 2012] or more conventional terrestrial laser scanning (e.g. *Westoby et al.*,

[2015]) to allow DEM differencing of surfaces. GPR in step-and-collect mode should then be employed to investigate englacial debris entrainment mechanisms in other mountainous areas of Antarctica, whilst continuous GPR surveying or RES should be used to detect and trace the transportation of debris through the glacial system, from continental sources to the coastal shelf. Results will improve magnitude-frequency curves of rock failures in Antarctica and increase our understanding of landscape development and evolution in Antarctica. It will also allow debris transport routes through the Antarctic glacier system to be quantified. This is particularly relevant under a changing climate, where it is expected that surface warming could alter glacial thermal regimes and trigger slope instability in Antarctica, allowing more debris to move from continental sources to the coastal shelf, and ultimately the Southern Ocean. As continental sediments are released into the Southern Ocean, essential nutrients will also be deposited, where it is anticipated that essential nutrients like BioFe could enhance primary productivity in the ocean, and, ultimately, improve the drawdown of atmospheric CO_2. As englacial sediment transportation could play an important role in the negative climate feedback loop known as the 'FE hypothesis', it is imperative that continental debris sources are better understood and quantified, particularly as other sources of BioFe are decreasing, global temperatures are warming, and CO_2 levels are rising at glacial terminations.

REFERENCES

Alley, R. B., D. D. Blankenship, C. R. Bentley, and S. T. Rooney (1986), Deformation of till beneath ice stream B, West Antarctica, *Nature*, 322, 57-59, doi:10.1038/322057a0.

Alley, R. B., D. D. Blankenship, S. T. Rooney, and C. R. Bentley (1987), Till beneath ice stream B:4, A coupled ice-till flow model, *Journal of Geophysical Research*, 92, 8931-8940, doi: 10.1029/JB092iB09p08931.

Alley, R. B. (1993), In search of ice stream sticky spots, *Journal of Glaciology*, 39, 447–454, doi:10.3198/1993JoG39-133-447-454.

Alley, R. B., S. Anandakrishnan, C. R. Bentley, and N. Lord (1994), A water-piracy hypothesis for the stagnation of ice stream C, *Annals of Glaciology*, 20, 187-194, doi:10.3189/172756494794587032.

Alley, R. B., K. M. Cuffey, E. B. Evenson, J. C. Strasser, D. E. Lawson, and G. J. Larson (1997), How glaciers entrain and transport basal sediment: physical constraints, *Quaternary Science Reviews*, 16, 1017-1038, doi:10.1016/S0277-3791(97)00034-6.

Anandakrishnan, S., and R. B. Alley (1997), Stagnation of ice stream C, West Antarctica by water piracy, *Geophysical Research Letters*, 24, 265-268, doi:10.1029/96GL04016.

Anandakrishnan, S., D. D. Blankenship, R. B. Alley, and P. L. Stoffa (1998), Influence of subglacial geology on the position of a West Antarctic ice stream from seismic observations, *Nature*, 394, 62-65, doi:10.1038/27889.

Andersen, M. L., M. Nettles, P. Elosegui, T. B. Larsen, G. S. Hamilton, and L. A. Strearns (2011), Quantitative estimates of velocity sensitivity to surface melt variations at a large Greenland outlet glacier, *Journal of Glaciology*, 57 (204), 609-620, doi:10.3189/002214311797409785.

Arthern, R. J., D. P. Winebrenner, and D. G. Vaughan (2006), Antarctic snow accumulation mapped using polarization of 4.3-cm wavelength microwave emission, *Journal of Geophysical Research*, 111, D06107, doi:10.1029/2004JD005667.

Ashmore, D. W., and R. G. Bingham (2014), Antarctic subglacial hydrology: an overview of current knowledge and forthcoming scientific challenges, *Antarctic Science*, 26 (6), 758-773, doi:10.1017/S0954102014000546.

Bamber, J. L., R. E. M. Riva, B. L. A. Vermeersen, and A. M. Le Brocq (2009), Reassessment of the potential sea-level rise from a collapse of the West Antarctic Ice Sheet, *Science*, 324, 901-903, doi:10.1126/science.1169335.

Bartholomew, I., P. Nienow, D. Mair, A. Hubbard, M. A. King, and A. Sole (2010), Seasonal evolution of subglacial drainage and acceleration in a Greenland outlet glacier, *Nature Geoscience*, 3, 408-411, doi:10.1038/ngeo863.

Bell, R. E., D. D. Blankenship, C. A. Finn, D. L. Morse, T. A. Scambos, J. M. Brozena, and S. M. Hodge (1998), Influence of subglacial geology on the onset of a West Antarctic ice stream from aerogeophysical observations, *Nature*, 394, 58-62, doi:10.1038/27883.

Benn, D. I., and D. J. A. Evans (2010), *Glaciers and Glaciation* (2nd ed.), Hodder Education, England.

Bennett, M. (2003), Ice streams as the arteries of an ice sheet; their mechanics, stability and significance, *Earth Science Reviews*, 61, 309-339, doi:10.1016/S0012-8252(02)00130-7.

Bennett, M., and N. Glasser (2009), *Glacial Geology: Ice sheets and landforms*, Wiley Blackwell, Sussex.

Bentley, M.J., C. J. Fogwill, A. M. Le Brocq, A. L. Hubbard, D. E. Sugden, T. J. Dunai, and S. P. H. T. Freeman (2010), Deglacial history of the West Antarctic Ice Sheet in the Weddell Sea embayment: Constraints on past ice volume change, *Geology*, 38, 411-414, doi:10.1130/G30754.1.

Berthling, I., B. Etzelmüller, K. Isaksen, and J. Sollid (2000), Rock glaciers on Prins Karls Forland II: GPR soundings and the development of internal structures, *Permafrost Periglacial Process*es, 11(4), 357–369, doi:10.1002/1099-1530.

Bindschadler, R., and T.A. Scambos (1991), Satellite-Image-Derived Velocity Field of an Antarctic Ice Stream, *Science*, 252, 242-246, doi:10.1126/science.252.5003.242.

Bindschadler, R., J. Bamber, and S. Anandakrishnan (2001), Onset of Streaming Flow in the Siple Coast Region, West Antarctica, In: Alley, R. B., and R. A. Binschadler (ed.), *West Antarctic Ice Sheet: Behavior and Environment*, American Geophysical Union, Washington, D. C., doi:10.1029/AR077p0123.

Bindschadler, R. A. (2006), Hitting the ice sheets where it hurts, *Science*, 311 (5768), 1720-1721, doi:10.1126/science.1125226.

Bindschadler, R., and H. Choi (2007), Increased water storage at ice stream onsets: a critical mechanism?, *Journal of Glaciology*, 53 (181), 163–171, doi:10.3189/172756507782202793.

Bindschadler, R. A., D. G. Vaughan, and P. Vornberger (2011), Variability of basal melt beneath the Pine Island Glacier ice shelf, West Antarctica, *Journal of Glaciology*, 57, 581-595, doi:10.3189/002214311797409802.

Bingham, R. G., and M. J. Siegert (2007), Radio-echo sounding over polar ice masses, *Journal of Environmental and Engineering Geophysics*, 12 (1), 47-62, doi:10.2113/JEEG12.1.47.

Bingham, R. G., E. C. King, A. M. Smith, and H. D. Pritchard (2010), Glacial Geomorphology: towards a convergence of glaciology and geomorphology, *Progress in Physical Geography*, 34 (3), 327-355, doi:10.1177/0309133309360631.

Bingham, R. G., D. M. Rippin, N. B. Karlsson, H. F. J. Corr, F. Ferraccioli, T. A. Jordan, A. M. Le Brocq, K. C. Rose, N. Ross, and M. J. Siegert (2015), Ice-flow structure and ice-dynamic

changes in the Weddell Sea sector of West Antarctica from radar images internal layering, *Journal of Geophysical Research*, 120, 655-670, doi:10.1002/204JF003291.

Bintanja, R. (1999), On the glaciological, meteorological, and climatological significance of Antarctic blue ice areas, *Reviews of Geophysics*, 37(3), 337–359, doi:10.1029/1999RG900007.

Bintanja, R., and C. H. Reijmer (2001), Meteorological conditions over Antarctic blue-ice areas and their influence on the local surface mass balance, *Journal of Glaciology*, 47 (156), 37-50, doi:10.3189/172756501781832557.

Blankenship, D. D., C. R. Bentley, S. T. Rooney, and R. B. Alley (1986), Seismic measurements reveal a saturated porous layer beneath an active Antarctic ice stream, *Nature*, 322, 54-57, doi:10.1038/322054a0.

Blankenship, D. D., C. R. Bentley, S. T. Rooney, and R. B. Alley (1987), Till beneath ice stream B: 1. Properties derived from seismic travel times, *Journal of Geophysical Research*, 92 (B), 8903-8911, doi:10.1029/JB092iB09p08903.

Boulton, G. S. (1970), On the origin and transport of englacial debris in Svalbard Glaciers, *Journal of Glaciology*, 9 (56), 213-229, doi:10.3198/1970JoG9-56-213-229.

Boulton, G. S. (1972), The role of thermal regime in glacial sedimentation, In: *Polar Geomorphology*, Institute of British Geographers, Special Publication, 4, 1-19.

Boulton, G. S. (1978), Boulder shapes and grain-size distributions of debris as indicators of transport paths through a glacier and till genesis, *Sedimentology*, 25, 773-799, doi:10.1111/j.1365-3091.1978.tb00329.x.

Boulton, G. S. (1979), Processes of glacier erosion on different substrata, *Journal of Glaciology*, 23 (89), 15-38, doi:10.3198/1979JoG23-89-15-38.

Boulton, G. S., and R. C. A. Hindmarsh (1987), Sediment deformation beneath glaciers: rheology and geological consequences, *Journal of Geophysical Research*, 92 (B9), 9059-9082, doi:10.1029/JB092iB09p09059.

Boulton, G. S. (1993), Ice ages and climate change, In: Duff, P. McL.D (ed.), *Holmes Principle of Physical Geography*, 4th ed. (1998), Stanley Thornes Ltd, United Kingdom.

Boulton, G. S., J. D. Peacock, and D. G. Sutherland (2003), Quaternary, In: Trewin, N. H (ed.), *Geology of Scotland,* Geological Society of London, London, 409-430.

Bromwich, D. H., Y. Du, and T. R. Parish (1994), Numerical simulation of winter katabatic winds from West Antarctica crossing Siple Coast and the Ross Ice Shelf, *American Meteorological Society*, 122, 1417-1435, doi:10.1175/1520-0493.

Campbell, S., G. Balco, C. Todd, H. Conway, K. Huybers, C. Simmons, and M. Vermeulen (2013), Radar detected englacial stratigraphy in the Pensacola Mountains, Antarctica: implications for recent changes in ice flow and accumulation, *Annals of Glaciology*, 54 (63), 91–100, doi:10.3189/2013AoG63A371.

Carrasco, J. F., G. Casassa, and A. Rivera (2000), A warm event at Patriot Hills, Antarctica: an ENSO related phenomenon? In: Carrasco, J. F., G. Casassa, and A. Rivera (ed.), *Sixth International Conference on Southern Hemisphere Meteorology and Oceanography*, 3–7 April 2000, Santiago, Chile, Proceedings, Boston, American Meteorological Society, 240–241.

Carter, S. P., D. D. Blankenship, M. E. Peters, D. A. Young, J. W. Holt, and D. L. Morse (2007), Radar-based subglacial lake classification in Antarctica, *Geochemistry, Geophysics, Geosystems*, 8 (3), Q03016, doi:10.1029/2006GC001408.

Casassa, G., H. H. Brecher, C. Cárdenas, and A. Rivera (1998), Mass balance of the Antarctic ice sheet at Patriot Hills, *Annals of Glaciology*, 27, 130-134, doi:10.3198/1998AoG27-1-130-134.

Casassa, G., A. Rivera, C. Acuña, H. Brecher, and H. Lange (2004), Elevation change and ice flow at Horseshoe Valley, Patriot Hills, West Antarctica, *Annals of Glaciology*, 39 (1), 20-28, doi:10.3189/172756404781814564.

Cavitte, M. G. P., D. D. Blankenship, D. A. Young, M. J. Siegert, and E. Le Meur (2013), Radar stratigraphy connecting Lake Vostok and Dome C, East Antarctica, constrains the EPICA/DMC ice core time scale, *The Cryosphere*, 7, 321–342, doi:10.5194/tcd-7-321-2013.

Christoffersen, P., M. Bougamont, S. P. Carter, H. A. Fricker, S. Tulaczyk (2014), Significant groundwater contribution to Antarctic ice streams hydrologic budget, *Geophysical Research Letters*, 41 (6), 2003–2010, doi:10.1002/2014GL059250.

Chu, V. W. (2013), Greenland ice sheet hydrology: A review, *Progress in Physical Geography*, 38 (1), 19-54, doi:10.1177/0309133313507075.

Clark, P. U., A. S. Dyke, J. D. Shakun, A. E. Carlson, J. Clark, B. Wohlfarth, J. X. Mitrovica, S. W. Hostetler, and A. M. McCabe (2009), The last glacial maximum, *Science*, 325, 710-714, doi:10.1126/science.1172973.

Clarke, G. K., U. Nitsan, and W. S. B. Paterson (1977), Strain heating and creep instability in glaciers and ice sheets, *Reviews of Geophysics and Space Physics*, 15 (2), 235-247, doi:10.1029/RG015i002p00235.

Collins, M., and 13 others (2013), Long-term Climate Change: Projections, Commitments and Irreversibility, In: Stocker, T. F., D. Qin, G.-K. Plattner, M. Tignor, S. K. Allen, J. Boschung, A. Nauels, Y. Xia, V. Bex, and P. M. Midgley (ed.), *Climate Change 2013: The Physical Science Basis, Contribution of Working Group I to the Fifth Assessment Report of the Intergovernmental Panel on Climate Change*, Cambridge University Press, Cambridge, United Kingdom and New York, NY, USA, 1029–1136, doi:10.1017/CBO9781107415324.024.

Conway, H., B. L. Hall, G. H. Denton, A. M. Gades, and E. D. Waddington (1999), Past and future grounding-line retreat of the West Antarctic Ice Sheet, *Science*, 286, 280-283, doi:10.1126/science.286.5438.280.

Corr, H., F. Ferraccioli, N. Frearson, T. A. Jordan, C. Robinson, A. Armadillo, G. Caneva, E. Bozzo, and I. E. Tabacco (2007), Airborne radio-echo sounding of the Wilkes Subglacial Basin, the Transantarctic Mountains, and the Dome C Region, *Terra Antartica Reports*, 13, 55-63.

Cuffey, K. M., and W. S. B. Patterson (2010), *The Physics of Glaciers*, 3rd ed., Butterworth Heinemann, Oxford.

Dahe, Q., J. R. Petit, J. Jouzel, and M. Stievenard (1994), Distribution of stable isotopes in surface snow along the route of the 1990 International Trans-Antarctica Expedition, *Journal of Glaciology*, 40 (134), 107-118, doi:10.3198/1994JoG40-134-107-118.

Daniels, D. J., D. J. Guton, and H. F. Scott (1988), Introduction to subsurface radar, *IEEE Proceedings*, 135 (F4), 278-305, doi:10.1049/ip-f-1:19880038.

Daniels, D. J. (1996), Surface-penetrating radar, *Electronics and Communication Engineering Journal*, 8 (4), 165-182, doi:10.1049/ecej:19960402.

Daniels, D. J. (1998), Surface penetrating radar image quality, In: *Detection of abandoned land mines*, Oct 12-14, IEEE Conference Publication, 458, 68-72.

Daniels, D. J. (2004), *Ground Penetrating Radar*, 2nd ed., The Institute of Engineering and Technology, London.

Davis, J. L., and A. P. Annan (1989), Ground Penetrating radar for high resolution mapping of soil and rock stratigraphy, *Geophysical Prospecting*, 37, 531-551, doi:10.1111/j.1365-2478.1989.tb02221.x.

Davis, C. H., Y. Li, J. R. McConnell, M. M. Frey, and E. Hanna (2005), Snowfall-driven growth in East Antarctic Ice Sheet mitigates recent sea-level rise, *Science*, 308, 1898-1901, doi:10.1126/science.1110662.

Death, R., J. L. Wadham, F. Monteiro, A. M. Le Brocq, M. Tranter, A. Ridgwell, S. Dutkiewicz, and R. Raiswell (2014), Antarctic ice sheet fertilises the Southern Ocean, *Biogeosciences*, 11, 2635-2643, doi:10.5194/bg-11-2635-2014.

Degenhardt, J. J., and J. R. Giardino (2003), Subsurface investigation of a rock glacier using ground-penetrating radar: Implications for locating stored water on Mars, *Journal of Geophysical Research*, 108 (E4), 8036, doi:10.1029/2002JE001888.

Degenhardt, J. J. (2009), Development of tongue-shaped and multilobate rock glaciers in alpine Environments - Interpretations from ground penetrating radar surveys, *Geomorphology*, 109 (3–4), 94–107, doi:10.1016/j.geomorph.2009.02.020.

Deline, P., K. Hewitt, N. Reznichenko, and D. Shugar (2014), Rock avalanches onto glaciers, In: Davies, T., *Landslide Hazards, Risks, and Disasters*, 263–320, doi:10.1016/B978-0-12-396452-6.00009-4.

Denton, G.H., J. G. Bockheim, R. H. Rutford, and B. G. Andersen (1992), Glacial history of the Ellsworth Mountains, West Antarctica. *Geological Society of America Memoir*, 170, 403-432, doi:10.1130/MEM170.

Doake, C.S.M. (1981), Tracing particle paths in the Antarctic Ice Sheet, *Journal of Glaciology*, 27 (97), 483-486.

Dunning S. A., N. J. Rosser, S. T. McColl, and N. V. Reznichenko (2015), Rapid sequestration of rock avalanche deposits within glaciers, *Nature Communications*, 6, 7964, doi:10.1038/ncomms8964.

Earth Explorer, Digital elevation model data sets, [Available to download from http://earthexplorer.usgs.gov/].

Eckert, S., T. Kellenberger, and K. Itten (2005), Accuracy assessment of automatically derived digital elevation models from aster data in mountainous terrain, *International Journal of Remote Sensing*, 26 (9), 1943-1957, doi:10.1080/0143116042000298306.

Edwards, R., and P. Sedwick (2001), Iron in East Antarctic snow: Implications for atmospheric iron deposition and algal production in Antarctic waters, *Geophysical Research Letters*, 28, 3907–3910, doi:10.1029/2001GL012867.

Eisen, O. (2008), Inference of velocity pattern from isochronous layers in firn, using an inverse method, *Journal of Glaciology*, 54 (187), 613–630, doi:10.3189/002214308776570818.

EPICA Community Members, and 86 others (2006), One-to-one coupling of glacial climate variability in Greenland and Antarctica, *Nature*, 444, 195–198, doi:10.1038/nature05301.

Fahnestock M., W. Abdalati, S. Luo, and S. Gogineni (2001a), Internal layer tracing and age depth-accumulation relationships for the northern Greenland ice sheet, *Journal of Geophysical Research*, 106 (D24), 33789–33798, doi:10.1029/2001JD900200.

Fahnestock M., W. Abdalati, I. Joughin, J. Brozena, and P. Gogineni (2001b), High geothermal heat flow, basal melt and the origin of rapid ice flow in central Greenland, *Science*, 294, 2338–2342, doi:10.1126/science.1065370.

Fettweis X, M. Tedesco, M. van den Broeke, and J. Ettema (2011), Melting trends over the Greenland ice sheet (1958–2009) from spaceborne microwave data and regional climate models, *The Cryosphere*, 5, 359-375, doi:10.5194/tc-5-359-2011

Fisher, D. A., N. Reeh, and K. Langley (1985), Objective Reconstructions of the Late Wisconsinan Laurentide Ice Sheet and the Significance of Deformable Beds, *Géographie Physique et Quaternaire*, 39 (3), 229-238, doi:10.7202/032605ar.

Flowers G. E., and G. K. C. Clarke (2002), A multicomponent coupled model of glacier hydrology, 2, Application to Trapridge Glacier, Yukon, Canada, *Journal of Geophysical Research*, 107, 2288, doi:10.1029/2001JB001124.

Flowers G. E., S. Marshall, H. Björnsson, and G. Clarke (2005), Sensitivity of Vatnajökull ice cap hydrology and dynamics to climate warming over the next 2 centuries, *Journal of Geophysical Research*, 110, F02011, doi:10.1029/2004JF000200.

Fogwill, C. J., A. S. Hein, M. J. Bentley, and D. E. Sugden (2012), Do blue-ice moraines in the Heritage Range show the West Antarctic ice sheet survived the last interglacial?, *Palaeogeography, Palaeoclimatology, Palaeoecology*, 335-336, 61–70, doi:10.1016/j.palaeo.2011.01.027.

Fossen, H. (2010), *Structural Geology*, Cambridge University Press, New York.

Fowler, A. C. (2003), On the rheology of till, *Annals of Glaciology*, 37, 55-59, doi:10.3189/172756403781815951.

Fretwell, P., and 59 others (2013), Bedmap2: improved ice bed, surface and thickness datasets for Antarctica, *The Cryosphere*, 7, 375-393, doi:10.5194/tc-7-375-2013.

Frezzotti, M., S. Gandolfi, and S. Urbini (2002), Snow megadunes in Antarctica: Sedimentary structure and genesis, *Journal of Geophysical Research*, 107 (D18), 4344, doi:10.1029/2001JD000673.

Frezzotti, M., and 13 others (2004), New estimations of precipitation and surface sublimation in East Antarctica from snow accumulation measurements, *Climate Dynamics*, 23 (7), 803-813, doi:10.1007/s00382-004-0462-5.

Fujita, S., H. Maeno, S. Uratsuka, T. Furukawa, S. Mae, Y. Fujii, and O. Watanabe (1999), Nature of radio echo layering in the Antarctic Ice Sheet detected by a two-frequency experiment, *Journal of Geophysical Research*, 104 (B6), 13013-13024, doi:10.1029/1999JB900034.

Gabler, R. E., J. F. Petersen, L. M. Trapasso, and D. Sack (2009), *Physical Geography* (9th ed.), Brooks/Cole: Canada.

Genthon, C., and A. Braun (1995), ECMWF analyses and predictions of the surface climate of Greenland and Antarctica, *Journal of Climatology*, 8, 2324-2332, doi:10.1175/1520-0442(1995)008<2324:EAAPOT>2.0.CO;2.

Genthon, C., P. Lardeux, and G. Krinner (2007), The surface accumulation and ablation of a coastal blue-ice areanear Cap Prudhomme, Terre Adélie, Antarctica, *Journal of Glaciology* 53 (183), 635-645, doi:10.3189/002214307784409333.

Gladstone, R. M., V. Lee, J. Rougier, A. J. Payne, H. Hellmer, A. Le Brocq, A. Shepherd, T. L. Edwards, J. Gregory and S. L. Cornford (2012), Calibrated prediction of Pine Island Glacier retreat during the 21st and 22nd centuries with a coupled flowline model, *Earth and Planetary Science Letters*, 333-334, 191-199, doi:10.1016/j.epsl.2012.04.022.

Glasser, N. F., and G. H. Gudmundsson (2012), Longitudinal surface structures (flowstripes) on Antarctic glaciers, *The Cryosphere*, 6, 383-391, doi:10.5194/tc-6-383-2012.

Glasser, N.F., S. J. A. Jennings, M. J. Hambrey, and B. Hubbard (2015), Origin and dynamic significance of longitudinal structures ("flow stripes") in the Antarctic Ice Sheet, *Earth Surface Dynamics*, 3, 239-249, doi:10.5194/esurf-3-239-2015.

Golledge, N. R., C. J. Fogwill, A. N. Mackintosh, and K. M. Buckley (2012), Dynamics of the Last Glacial Maximum Antarctic ice-sheet and its response to ocean forcing, *Proceedings of the National Academy of Science*, 109 (40), 16052-16056, doi:10.1073/pnas.1205385109.

Golledge, N. R., and 12 others (2013), Glaciology and geological signature of the Last Glacial Maximum Antarctic ice sheet, *Quaternary Science Reviews*, 78, 225-247, doi:10.1016/j.quascirev.2013.08.011.

Goodsell, B., M. J. Hambrey, and N. F. Glasser (2005), Debris transport in a temperate valley glacier: Haur Glacier d'Arolla, Valais, Switzerland, *Journal of Glaciology*, 51 (172), 139-146, doi:10.3189/172756505781829647.

Grinsted, A., J. Moore, V. B. Spikes, and A. Sinisalo (2003), Dating Antarctiuce blue ice sreas using a novel ice flow model, *Geophysical Research Letters*, 30 (19), doi:10.1029/2003GL017957.

Grossman, J., and J. Zipfel (2001), The Meteoritical Bulletin, No. 85, *Meteoritics and Planetary Science*, 36, A293–A322.

Hagen, J. O., O. Liestøl, E. Roland, and T. Jørgensen (1993), *Glacier atlas of Svalbard and Jan Mayen*, Norsk Polarinstitutt Meddelelser: Oslo.

Hambrey, M. J., T. Murray, N. F. Glasser, A. Hubbard, B. Hubbard, G. Stuart, S. Hansen, and J. Kohler (2005), Structure and changing dynamics of a polythermal valley glacier on a centennial timescale: Midre Lovénbreen, Svalbard, *Journal of Geophysical Research: Earth Surface*, 110, F01006, doi:10.1029/2004JF000128.

Hambrey, M. J., and N. F. Glasser (2011), Sediment entrainment, transport and deposition, 984-1003, In: Singh, V. P., P. Singh, and U. K. Haritashya (ed.), *Encyclopaedia of Snow, Ice and Glaciers*, Springer, Netherlands, doi:10.1007/978-90-481-2642-2_475.

Haran, T., J. Bohlander, T. Scambos, T. Painter, and M. Fahnestock (2006), MODIS mosaic image of Antarctica, *National Snow and Ice Data Center*, Digital media, Boulder, Colorado, USA.

Harbor, J. M., B. Hallet, and C. F. Raymond (1988), A numerical model of land-form development by glacial erosion, *Nature*, 333, 347-349, doi:10.1038/333347a0.

Harrington, J. A., N. F. Humphrey, and J. T. Harper (2015), Temperature distribution and thermal anomalies along a flowline of the Greenland ice sheet, *Annals of Glaciology*, 56 (70), doi:10.3189/2015AoG70A945.

Hawkings, J. R., J. L. Wadham, M. Tranter, R. Raiswell, L. G. Benning, P. J. Statham, A. Tedstone, P. Nienow, K. Lee, and J. Telling (2014), Ice sheets as a significant source of highly reactive nanoparticulate iron to the oceans, *Nature Communications*, 5, 3929, doi:10.1038/ncomms4929.

Hein, A. S., C. J. Fogwill, D. E. Sugden, and S. Xu (2011), Glacial/interglacial ice-stream stability in the Weddell Sea embayment, Antarctica, *Earth Planetary Science Letters*, 307, 211-221, doi:10.1016/j.epsl.2011.04.037.

Hein, A. S., J. Woodward, S. M. Marrero, S. A. Dunning, E. J. Steig, S. P. H. T. Freeman, F. M. Stuart, K. Winter, M. J. Westoby, and D. E. Sugden (2016a), Evidence for the stability of the West Antarctic Ice Sheet divide for 1.4 million years, *Nature Communications*, 7:10325, doi:10.1038/ncomms10325.

Hein, A. S., S. M. Marrero, J. Woodward, S. A. Dunning, K. Winter, M. J. Westoby, S. P. H. T. Freeman, R. Shanks and D. E. Sugden (2016b), Mid-Holocene pulse of thinning in the Weddell Sea sector of the West Antarctic Ice Sheet, *Nature Communications*, 7:12511 doi:10.1038/ncomms12511.

Hemming, S. R. (2004), Heinrich events: massive late Pleistocene detritus layers of the North Atlantic and their global imprint, *Reviews of Geophysics*, 42, RG1005, doi:10.1029/2003RG000128.

Hindmarsh, R. C. A. (2009), Consistent generation of ice-streams via thermo-viscous instabilities modulated by membrane stresses, *Geophysical Research Letters*, 36 (6), L06502, doi:10.1029/2008GL036877.

Hindmarsh, R. C. A., and C. R. Stokes (2008), Formation mechanisms for ice-stream margin moraines, *Earth Surface Processes and Landforms*, 33 (4), 610-626, doi:10.1002/esp.1665.

Hoinkes, H. (1960), Studies of solar radiation and net radiation in the Antarctic, *Theoretical and Applied Climatology*, 10(2), 175-181, doi:10.1007/BF02246563.

Holschuh, N., K. Christianson, and S. Anandakrishnan (2014), Power loss in dipping internal reflectors, imaged using ice-penetrating radar, *Annals of Glaciology*, 55, 49-56, doi:10.3189/2014AoG67A005.

Hooke, R. L. (2005), *Principles of Glacier Mechanics* (2nd ed.), Cambridge University Press, Cambridge, U.K.

Hubbard, B., and N. Glasser (2005), *Field techniques in glaciology and glacial geomorphology*, Wiley, England.

Hughes, O. L., C. R. Harington, J. A. Janssens, J. V. Matthews, R. E. Morlan, N. W. Rutter, and C. E. Schweger (1981), Upper Pleistocene stratigraphy, paleoecology, and archaeology of the northern Yukon interior, eastern Beringia, 1. Bonnet Plume Basin, *Arctic*, 34 (4), 329-365, doi:10.14430/arctic2538.

Hulton, N. R. J., and M. J. Mineter (2000), Modelling Self-Organisation in Ice Streams, *Annals of Glaciology*, 30, 127-136, doi:10.3189/172756400781820561.

Ingham, J. (2010), *Geomaterials under the microscope*, Manson Publishing, CRC Press, Chapter 2: Building Stone, 21-50, doi:10.1016/B978-0-12-407230-5.50010-8.

Ishikawa, N., S. Kobayashi, T. Ohtake, and S. Kawaguchi (1982), Some radiation properties at Mizuhu Station, East Antarctica in 1980, *Memoirs of National Institute of Polar Research*, 24, 19-31.

Iverson, N. R., T. S. Hooyer, and R. W. Baker (1998), Ring-shear studies of till deformation: Coulomb-plastic behavior and distributed strain in glacier beds, *Journal of Glaciology*, 44 (148), 634-642, doi:10.3198/1998JoG44-148-634-642.

Jacobel, R. W., T. A. Scambos, C. F. Raymond, and A. M. Gades (1996), Changes in the configuration of ice stream flow from the West Antarctic Ice Sheet, *Journal of Geophysical Research*, 101, 5499-5504, doi:10.1029/95JB03735.

Jennings, S. J. A., M. J. Hambrey, and N. F. Glasser (2014), Ice flow-unit influence on glacier structure, debris entrainment and transport, *Earth Surface Processes and Landforms*, 10, 1279-1292, doi:10.1002/esp.3521.

Jickells, T. D., and 18 others (2005), Global iron connections between desert dust, ocean biogeochemistry and climate, *Science*, 308, 67-71, doi:10.1126/science.1105959.

Jiskoot, H. (2011), Dynamics of Glaciers, In: Singh, V. P., P. Singh, and U. K. Haritashya (ed.), *Encyclopedia of snow, ice and glaciers*, Springer: Dordrecht, The Netherlands, 245-256.

Jol, H. M. (2009), *Ground Penetrating Radar – Theory and Applications*, Elsevier, Oxford.

Jonsson, S. (1990), Local climate and mass balance of a blue-ice area in western Dronning Maud Land, Antarctica, *Zeitschrift für Gletscherkunde und Glazialgeologie*, 26 (1), 11-29.

Jordan, T. A., F. Ferraccioli, N. Ross, H. F. J. Corr, P. T. Leat, R. G. Bingham, D. M. Rippin, A. M. Le Brocq, and M. J. Siegert (2013), Inland extent of the Weddell Sea Rift imaged by new aerogeophysical data, *Tectonophysics*, 585, 137-160, doi:10.1016/j.tecto.2012.09.010.

Joughin, I., and J. L. Bamber (2005), Thickening of the ice stream catchments feeding the Filchner-Ronne Ice Shelf, Antarctica, *Geophysical Research Letters*, 32, L17503, doi:10.1029/2005GL023844.

Joughin, I., and 10 others (2005), Continued deceleration of Whillans Ice Stream, West Antarctica, *Geophysical Research Letters*, 32, L22501, doi:10.1029/2005GL024319.

Joughin, I., S. B. Das, M. A. King, B. E. Smith, I. M. Howat, and T. Moon (2008), Seasonal speedup along the western flank of the Greenland ice sheet, *Science*, 320, 781–783, doi:10.1126/science.1153288.

Joughin, I., B. E. Smith, and D. M. Holland (2010), Sensitivity of 21st century sea level to ocean-induced thinning of Pine Island Glacier, Antarctica, *Geophysical Research Letters*, 37, L20502, doi:10.1029/2010GL044819.

Kahn, S. A., A. Aschwanden, A. A. Bjørk, J. Wahr, K. K. Kjeldsen, and K. H. Kjær (2015), Greenland ice sheet mass balance: a review, *Reports on Progress in Physics*, 78, 046801, doi:10.1088/0034-4885/78/4/046801.

Karlsson, N. B., D. M. Rippin, D. G. Vaughan, and H. F. J. Corr (2009), The internal layering of Pine Island Glacier, West Antarctica, from airborne radar-sounding data, *Annals of Glaciology*, 50, 141-146.

Karlsson, N. B., D. M. Rippin, R. G. Bingham, and D. G. Vaughan (2012), A 'continuity index' for assessing ice-sheet dynamics from radar-sounded internal layers, *Earth Planetary Science Letters*, 335-336, 88-94, doi:10.1016/j.epsl.2012.04.034, doi:10.1016/j.epsl.2012.04.034.

King, E. C., J. Woodward, and A. M. Smith (2004), Seismic evidence for a water-filled canal in deforming till beneath Rutford Ice Stream, West Antarctica, *Geophysical Research Letters*, 31 (20), L20401, doi:10.1029/2004GL020379.

King, E. C., J. Woodward, and A. M. Smith (2007), Seismic and radar observations of subglacial bed forms beneath the onset zone of Rutford Ice Stream Antarctica, *Journal of Glaciology*, 53, 665–672, doi:10.3189/002214307784409216.

King, E. C., R. C. A. Hindmarsh, and C. R. Stokes (2009), Formation of mega-scale glacial lineations observed beneath a West Antarctic ice stream, *Nature Geoscience*, 2, 585–588, doi:10.1038/ngeo581.

King, E. C. (2011), Ice stream or not? Radio-echo sounding of the Carlson Inlet, West Antarctica, *The Cryosphere*, 5, 907-916, doi:10.5194/tc-5-907-2011.

King, E. C., H. D. Pritchard, and A. M. Smith (2016), Subglacial landforms beneath Rutford Ice Stream, Antarctica: detailed bed topography from ice-penetrating radar, *Earth Systems Science Data*, 8, 151-158, doi:10.5194/essd-8-151-2016.

Kjær, K. H., N. J. Korsgaard and A. Schomacker (2008), Impact of multiple glacier surges – a geomorphological map from Brúarjöjull, East Iceland, *Journal of Maps*, 4 (1), 5-20, doi:10.4113/jom.2008.91.

Knight, P. G. (1997), The basal ice layer of glaciers and ice sheets, *Quaternary Science Reviews*, 16, 975-993, doi:10.1016/S0277-3791(97)00033-4.

Knight, P. G. (1999), *Glaciers*, Nelson Thornes, Cheltenham.

Korona J., E. Berthier, M. Bernard, F. Rémy and E. Thouvenot (2009), SPIRIT, SPOT 5 Stereoscopic survey of Polar Ice: Reference Images and Topographies during the fourth International Polar Year (2007-2009), ISPRS, *Journal of Photogrammetry & Remote Sensing*, 64, 204-212, doi:10.1016/j.isprsjprs.2008.10.005.

Kulessa, B. (2007), A critical review of the low-frequency electrical properties of ice sheets and glaciers, *Journal of Environmental and Engineering Geophysics*, 12 (1), 23-36, doi:10.2113/JEEG12.1.23.

Larter, R. D., A. G. C. Graham, C. -D. Hillenbrand, J. A. Smith, and J. A. Gales (2012), Late Quaternary grounded ice extent in the Filchner Trough, Weddell Sea, Antarctica: new marine geophysical evidence, *Quaternary Science Reviews*, 53, 111-122, doi:10.1016/j.quascirev.2012.08.006.

Le Brocq, A. M., A. J. Payne, and M. J. Siegert (2006), West Antarctic balance calculations: Impact of flux-routing algorithm, smoothing algorithm and topography, *Computers and Geosciences*, 32, 1780-1795, doi:10.1016/j.cageo.2006.05.003.

Lee, P., W. A. Cassidy, D. Apostolopoulos, M. Deans, A. Foessel, C. Krause, J. Parra, L. Pedersen, K. Schwehr, and W. L. Whittaker (1998), Search for Meteorites in the Patriot Hills Area, Ellsworth Mountains, West Antarctica, *Meteorites and Planetary Science*, 33, A92-A93.

Lemke, P., and 10 others (2007), Observations: changes in snow, ice and frozen ground, In: Solomon, S., D. Qin, M. Manning, Z. Chen, M. Marquis, K. B. Averyt, M. Tignor, and H. L. Miller (ed.), *Climate Change 2007: The Physical Science Basis. Contribution of Working Group I to the Fourth Assessment Report of the Intergovernmental Panel on Climate Change*, Cambridge University Press, Cambridge, 337-384.

Livingstone, S. J., C. O. Cofaigh, C. R. Stokes, C-D. Hillenbrand, A. Vieli, and S. S. R. Jamieson (2012), Antarctic paleo-ice streams, *Earth Science Reviews*, 111, 90-128, doi:10.1016/j.earscirev.2011.10.003.

Lythe, M. B., Vaughan, D. G., and the BEDMAP Consortium (2001), BEDMAP: a new ice thickness and subglacial topographic model of Antarctica, *Journal of Geophysical Research*, 106 (B6), 11335-11351, doi:10.1029/2000JB900449.

Martin, C., R. C. A. Hindmarsh, and F. J. Navarro (2006), Dating ice flow change near the flow divide at Roosevelt Island, Antarctica, by using a thermomechanical model to predict radar stratigraphy, *Journal of Geophysical Research: Earth Surface*, 111 (F1), F01011, doi:10.1029/2005jf000326.

Martin, C., R. C. A. Hindmarsh, and F. J. Navarro (2009), On the effects of divide migration, along ridge flow, and basal sliding on isochrones near an ice divide, *Journal of Geophysical Research: Oceans*, 114 (F2), F02006, doi:10.1029/2008jf001025.

Masson-Delmotte, V., and 16 others (2013), Information from Paleoclimate Archives, In: Stocker, T. F., D. Qin, G. -K. Plattner, M. Tignor, S.K. Allen, J. Boschung, A. Nauels, Y. Xia, V. Bex, and P. M. Midgley (ed.), *Climate Change 2013: The Physical Science Basis, Contribution of Working Group I to the Fifth Assessment Report of the Intergovernmental Panel on Climate Change*, Cambridge University Press, Cambridge, United Kingdom and New York, NY, USA, 383–464, doi:10.1017/CBO9781107415324.013.

McIntyre, N. F. (1985), Antarctic ice-sheet topography and surface-bedrock relationships, *Annals of Glaciology*, 8, 124-128, doi:10.3198/1986AoG8-1-124-128.

Melvold, K., J. O. Hagen, J. F. Pinglot, and N. Gunderstrup (1998), Large spatial variation in accumulation rate in Jutulstraumen ice stream, Dronning Maud Land, Antarctica, *Annals of Glaciology*, 27, 231-238, doi:10.3198/1998AoG27-1-231-238.

Mercer, J. H. (1978), West Antarctic ice sheet and CO2 greenhouse effect: a threat of disaster, *Nature*, 271, 321-325, doi:10.1038/271321a0.

Meredith, M. P., and J. C. King (2005), Rapid climate change in the ocean west of the Antarctic Peninsula during the second half of the 20th century, *Geophysical Research Letters*, 32 (19), L19604, doi:10.1029/2005GL024042.

MeshLab (2014), visual computing lab for core mesh processing tasks, [Available at: http://meshlab.sourceforge.net/].

Mills, S. C., M. Smith, A. M. Le Brocq, J. Hillier, E. Ardakova, and C. Boston (Submitted), *Snow_Blow*: quantifying enhanced snow accumulation in areas of former glaciation. *Submitted to Journal of Quaternary Science,* August 2016.

Monnier, S., C. Camerlynck, and F. Rejiba (2008), Ground penetrating radar survey and stratigraphic interpretation of the Plan du Lac rock glaciers, Vanoise Massif, northern French Alps, *Permafrost Periglacial Processes*, 19 (1), 19–30, doi:10.1002/ppp.610.

Murray, T., H. Corr, A. Forieri, and A. M. Smith (2008), Contrasts in hydrology between regions of basal deformation and sliding beneath Rutford Ice Stream, West Antarctica, mapped using radar and seismic data, *Geophysical Research Letters*, 35, L12504, doi:10.1029/2008GL033681.

Murray, T., and A. D. Booth (2010), Imaging glacial sediment inclusions in 3-D using ground penetrating radar at Kongsvegen, Svalbard, *Journal of Quaternary Science*, 25 (5), 754-761, doi:10.1002/jqs.1351.

Neal, A. (2004), Ground-penetrating radar and its use in sedimentology: Principles, problems and progress, *Earth-Science Reviews*, 66, 261–330, doi:10.1016/j.earscirev.2004.01.004.

Nylen, T. H., A. G. Fountain, and P. T. Doran (2004), Climatology of katabatic winds in the McMurdo dry valleys, southern Victoria Land, Antarctica, *Journal of Geophysical Research*: *Atmospheres*, 109: D03114, doi:10.1029/2003JD003937.

Opendtect (2015), *Three-dimensional seismic interpretation software*, version 4.6.0, dGB Earth Sciences, [Available to download from www.opendtect.org/index.php/products/download].

Orheim, O., and B. Lucchitta (1990), Investigating climate change by digital analysis of blue ice extent on satellite images of Antarctica, *Annals of Glaciology*, 14, 211–215, doi:10.3198/1990AoG14-1-211-215.

Palmer, S., A. Shepherd, P. Nienow, and I. Joughin (2011), Seasonal speedup of the Greenland Ice Sheet linked to routing of surface water, *Earth and Planetary Science Letters*, 302 (3-4), 423-428, doi:10.1016/j.epsl.2010.12.037.

Parish, T. R. and D. H. Bromwich (1987), The inversion wind pattern over West Antarctica, *Monthly Weather Review*, 114, 849-860, doi:10.1175/1520-0493(1986)114<0849: TIWPOW>2.0.CO;2.

Parrenin, F., and R. Hindmarsh (2007), Influence of a non-uniform velocity field on isochrone geometry along a steady flowline of an ice sheet, *Journal of Glaciology,* 53 (183), 612-622, doi:10.3189/002214307784409298.

Payne, A. J., and P. W. Dongelmans (1997), Self-organization in the thermomechanical flow of ice sheets, *Journal of Geophysical Research: Solid Earth*, 102 (B6), 12219-12233, doi:10.1029/97JB00513.

Pomeroy, J. W., D. M. Gray, and P. D. Landine (1993), The Prairie blowing snow model: characteristics, validation and operation, *Journal of Hydrology*, 144, 165-192, doi:10.1016/0022-1694(93)90171-5.

Price, S. F., R. A. Bindschadler, C. L. Hulbe, and I. R. Joughin (2001), Post-stagnation behaviour in the upstream regions of Ice Stream C, West Antarctica, *Journal of Glaciology*, 47 (157), 283-293, doi:10.3189/172756501781832232.

Pritchard, H. D., S. R. M. Ligtenberg, H. A. Fricker, D. G. Vaughan, M. R. van den Broeke, and L. Padman (2012), Antarctic ice-sheet loss driven by basal melting of ice shelves, *Nature*, 484. 502-505, doi:10.1038/nature10968.

Purves, R. S., J. S. Barton, W. A. Mackaness, and D. E. Sugden (1998), The development of a rule-based spatial model of wind transport and deposition of snow, *Annals of Glaciology*, 26, 197-202, doi:10.3198/1998AoG26-1-197-202.

Purves, R., J. Barton, W. Mackaness, and D. Sugden (1999a), The application of GIS to the modelling of snow drift, 243-254 In: B. M. Gittings (ed.), *Innovations in GIS 6-Integrating Information Infrastructures with Geographical Information Technology*, Taylor & Francis, London.

Purves, R. S., W. A. Mackaness, and D. E. Sugden, (1999b), An approach to modelling the impact of snow drift on glaciation in the Cairngorm Mountains, Scotland, *Journal of Quaternary Science*, 14 (4), 313-321, doi:10.1002/(SICI)1099-1417(199907)14:4<313::AID-JQS457>3.0.CO;2-M.

Raiswell, R., and D. E. Canfield (2012), The iron biogeochemical cycle past and present, *Geochemical Perspectives*, 1, 1–220, doi:10.7185/geochempersp.1.1.

Rasmussen, S. O., and 15 others (2006), A new Greenland ice core chronology for the Last glacial termination, *Journal of Geophysical Research*, 111, 1-46, doi:10.1029/2005JD006079.

Raymond, C. F., G. A. Catania, N. Nereson, and C. J. van der Veen (2006), Bed radar reflectivity across the north margin of the Whillans Ice Stream, West Antarctica, and

implications for margin processes, *Journal of Glaciology*, 52, 3-10, doi:10.3189/172756506781828890.

Rea, B. R., and D. J. A. Evans (2011), An assessment of surge-induced crevassing and the formation of crevasse squeeze ridges, *Journal of Geophysical Research*, 116, F04005, doi:10.1029/2011JF001970.

ReflexW (2012), version 6.1.1, *Sandmeier scientific software*, [available to download from http://www.sandmeier-geo.de/download.html].

Retzlaff, R., and C. R. Bentley (1993), Timing of stagnation of Ice Stream C, West Antarctica, from short-pulse radar studies of buried surface crevasses, *Journal of Glaciology*, 39 (133), 553-561, doi:10.3198/1993JoG39-133-553-561.

Reynolds, J. M. (2011), *An Introduction to Applied and Environmental Geophysics* (2nd ed.), Wiley and Sons, Chichester.

Rignot, E., and S. S. Jacobs (2002), Rapid bottom melting widespread near Antarctic Ice Sheet grounding lines, *Science*, 296 (5575), 2020-2023, doi:1 0.1126/science.1070942.

Rignot, E., and P. Kanagaratnam (2006), Changes in the velocity structure of the Greenland Ice Sheet, *Science*, 311 (5763), 986-990, doi:10.1126/science.1121381.

Rignot, E., J. Mouginot, and B. Scheuchl (2011a), MEaSUREs InSAR-Based Antarctica Ice Velocity Map, *NASA DAAC* at the National Snow and Ice Data Centre, Boulder, Colorado, doi:10.5067/MEASURES/CRYOSPHERE/nsidc-0484.001.

Rignot, E., J. Mouginot, and B. Scheuchl (2011b), Ice flow of the Antarctic Ice Sheet, *Science*, 333, 1427–1430, doi:10.1126/science.1208336.

Rignot, E., J. Mouginot, M. Morlighem, H. Seroussi, and B. Scheuchl (2014), Widespread, rapid grounding line retreat of Pine Island, Thwaites, Smith, and Kohler glaciers, West Antarctica, from 1992 to 2011, *Geophysical Research Letters*, 41 (10), 3502-3509, doi:10.1002/2014GL060140.

Rippin, D. M., M. J. Siegert, and J. L. Bamber (2003), The englacial stratigraphy of Wilkes Land, East Antarctica, as revealed by internal radio-echo sounding layering, and its relationship with balance velocities, *Annals of Glaciology*, 36, 189-196, doi:10.3189/172756403781816356.

Rippin, D. M., M. J. Siegert, J. L. Bamber, D. G. Vaughan, and H. F. J. Corr (2006), Switch-off of a major enhanced ice flow unit in East Antarctica, *Geophysical Research Letters*, 33, L15501, doi:10.1029/2006GL026648.

Rivera, A., F. Cawkwell, A. Wendt, and R. Zamora (2014), Mapping blue-ice areas and crevasses in West Antarctica using ASTER images, GPS and radar measurements, In: J. S. Kargel, G. J. Leonard, M. P. Bishop, A. Kääb, and B. H. Raup (ed.), *Global Land Ice Measurements from Space*, Chapter 31, Springer Praxis Books, doi: 10.1007/978-3-540-79818-7_31.

Robin, G. DE Q., C. W. M. Swithenbank, and B. M. E. Smith (1970), Radio echo exploration of the Antarctic ice sheet, *International symposium on Antarctic glaciological exploration*, Hanover, New Hampshire, USA, 3–7 September, 1968.

Roe, G. H., and R. S. Lindzen (2001), The mutual interaction between continental-scale ice sheets and atmospheric stationary waves, *Climate Dynamics*, 17, 479–87, doi:10.1175/1520-0442(2001)014<1450:TMIBCS>2.0.CO;2.

Ross, N., R. G. Bingham, H. F. J. Corr, F. Ferraccioli, T. A. Jordan, A. Le Brocq, D. M. Rippin, D. Young, D. D. Blankenship, and M. J. Siegert (2012), Steep reverse bed slope at the grounding line of the Weddell Sea sector in West Antarctica, *Nature Geoscience*, 5, 393-396, doi:10.1038/NGEO1468.

Ross, N., T. A. Jordan, R. G. Bingham, H. F. J. Corr, F. Ferraccioli, A. Le Brocq, D. M. Rippin, A. P. Wright, and M. J. Siegert (2014), The Ellsworth Subglacial Highlands: inception and retreat of the West Antarctic Ice Sheet, *Geological Society of America Bulletin*, 126, 3-15, doi:10.1130/B30794.1.

Ross, N., and M. Siegert (2014), Concentrated englacial shear over rigid basal ice, West Antarctica: implications for modelling and ice sheet flow, *Geophysical Research Abstracts*, 16, EGU2014-5568.

Rutford, R.H. (1972), Glacial geomorphology of the Ellsworth Mountains, In: Adie, R.J., (ed.) *Antarctic Geology and Geophysics*, Universitetsforlaget, Oslo, 225-232.

Ryan, B. C. (1977), A mathematical model for diagnosis and prediction of surface winds in mountainous terrain, *Journal of Applied Meteorology*, 16 (6), 571-584, doi:10.1175/1520-0450(1977)016<0571:AMMFDA>2.0.CO;2.

Schoof, C. (2007), Ice sheet grounding line dynamics: steady states, stability, and hysteresis, *Journal of Geophysical Research: Earth Surface*, 112, F3, doi:10.1029/2006JF000664.

Sevestre, H., D. I. Benn, N. R. J. Hulton, and K. Bælum (2015), Thermal structure of Svalbard glaciers and implications for thermal switch models of glacier surging, *Journal of Geophysical Research: Earth Surface*, 120, 220-2236, doi:10.1002/2015JF003517.

Shabtaie, S., and C. R. Bentley (1987), West Antarctic ice streams draining into the Ross Ice Shelf: Configuration and mass balance, *Journal of Geophysical Research*, 92, 2156-2202, doi:10.1029/JB092iB02p01311.

Sharp, M. (2005), Subglacial Drainage, *Encyclopedia of Hydrological Sciences*, John Wiley & Sons, Ltd.

Shepherd, A., D. Wingman, and E. Rignot (2004), Warm ocean is eroding West Antarctic Ice Sheet, *Geophysical Research Letters*, 31, L23402, doi:10.1029/2004GL021106.

Shepherd, A., A. Hubbard, P. Nienow, M. King, M. McMillan, and I. Joughin (2009), Greenland Ice Sheet motion coupled with daily melting in late summer, *Geophysical Research Letters*, 36, L01501, doi:10.1029/2008GL035758.

Shepherd, A., D. Wingham, D. Wallis, K. Giles, S. Laxon, and A. V. Sundal (2010), Recent loss of floating ice and the consequent sea level contribution, *Geophysical Research Letters*, 37, L13503, doi:10.1029/2010GL042496.

Shepherd A., E. R. Ivins, A. Geruo, V. R. Barletta, M. J. Bentley, S. Bettadpur, K. H. Briggs, D. H. Bromwich, R. Forsberg, and N. Galin (2012), A reconciled estimate of ice-sheet mass balance, *Science*, 338, 1183-1189, doi:10.1126/science.1228102.

Siegert, M. J. (2003), Glacial-interglacial variations in central East Antarctic ice accumulation rates, *Quaternary Science Reviews*, 22 (5-7), 741-750, doi:10.1016/S0277-3791(02)00191-9.

Siegert, M. J., A .J. Payne, and I. Joughin (2003), Spatial stability of Ice Stream D and its tributaries, West Antarctica, revealed by radio-echo sounding and interferometry, *Annals of Glaciology*, 37, 377-382, doi:10.3189/172756403781816022.

Siegert, M. J., B. Welch, D. Morse, A. Vieli, D. D. Blankenship, I. Joughin, E. C. King, G. J. M.C. Leysinger Vieli, A. J. Payne, and R. Jacobel (2004), Ice flow direction change in interior West Antarctica, *Science*, 305, 1948-1951, doi:10.1126/science.1101072.

Siegert, M. J., and A. J. Payne (2004), Past rates of accumulation in central West Antarctica, *Geophysical Research Letters*, 31 (12), L12403, doi:10.1029/2004GL020290.

Siegert, M. J., S. Carter, I. Tobacco, S. Popov, and D. D. Blankenship (2005a), A revised inventory of Antarctic subglacial lakes, *Antarctic Science*, 17 (3), 453-460, doi:10.1017/S0954102005002889.

Siegert M. J., M. Pokar, J. A. Dowdeswell, and T. Benham (2005b), Radio-echo layering in West Antarctica: a spreadsheet dataset, *Earth Surface processes and Landforms*, 30, 1583-1591, doi:10.1002/esp.1238.

Siegert, M. J., N. Ross, H. F. J. Corr, J. Kingslake, and R. C. Hindmarsh (2013), Late Holocene ice flow reconfiguration in the Weddell Sea sector of West Antarctica, *Quaternary Science Reviews*, 78, 98-107, doi:10.1016/j.quascirev.2013.08.003.

Siegert, M. J., N. Ross, J. Li, D. M. Schroeder, D. Rippin, D. Ashmore, R. Bingham, and P. Gogineni (2016), Subglacial controls on the flow of Institute Ice Stream, West Antarctica, *Annals of Glaciology*, 57 (73), 19-24, doi:10.1017/aog.2016.17.

Sime, L. C., R. C. Hindmarsh, and H. F. J. Corr (2011), Instruments and Methods: Automated processing to derive dip angles of englacial radar reflectors in ice sheets, *Journal of Glaciol*ogy, 57, 260-266, doi:10.3189/002214311796405870.

Sinisalo, A., and J. C. Moore (2010), Antarctic blue ice areas – towards extracting paleoclimate information, *Antarctic Science*, 22 (02), 99-115, doi:10.1017/S0954102009990691.

Smith, A. M. (2006), Microearthquakes and subglacial conditions, *Geophysical Research Letters*, 33, L24501, doi:10.1029/2006GL028207.

Smith, A. M., T. Murray, K. W. Nicholls, K. Makinson, G. Aðalgeirsdóttir, A. E. Behar, and D. G. Vaughan (2007), Rapid erosion, drumlin formation, and changing hydrology beneath an Antarctic ice stream, *Geology*, 35 (2), 127-130, doi:10.1130/G23036A.1.

Smith, B. E., H. A. Fricker, I. R. Joughin and S. Tulaczyk (2009), An inventory of active subglacial lakes in Antarctica detected by ICESat (2003-3008), *Journal of Glaciology*, 55 (192), 573-595, doi:10.3189/002214309789470879.

Solomon S., D. Qin, M. Manning, M. Marquis, K. Averyt, M. Tignor, and H. L. Miller (ed.) (2007), *Climate Change 2007: The Physical Science Basis*, Contribution of Working Group I to the Fourth Assessment Report of the Intergovernmental Panel on Climate Change, Cambridge University Press, Cambridge, 337-384.

Spörli, K.B., and C. Craddock (1992), Stratigraphy and structure of the Marble, Independence and Patriot Hills, Heritage Range, Ellsworth Mountains, West Antarctica, *Geological Society of America Memoir*, 170, 375-392, doi:10.1130/MEM170.

Stillman, D. E., J. A. MacGregor, and R. E. Grimm (2013), The role of acids in electrical conduction through ice, *Journal of Geophysical Research: Earth Surface*, 118, 1-16, doi:10.1029/2012JF002603.

Stokes, C. R., and C. D. Clark (2002), Ice stream shear margin moraines, *Earth Surface Processes and Landforms*, 27, 547-558, doi:10.1002/esp.326.

Studinger, M., R. E. Bell, and A. A. Tikku (2004), Estimating the depth and shape of subglacial Lake Vostok's water cavity from aerogravity data, *Geophysical Research Letters*, 31, L12401, doi:10.1029/2004GL019801.

Sugden, D. E. (1977), Reconstruction of the morphology, dynamics, and thermal characteristics of the Laurentide ice sheet at its maximum, *Arctic and Alpine Research*, 9 (1), 21-47, doi:10.2307/1550407.

Swithinbank, C. W. M. (1954), Ice streams, *Polar Record*, 7 (48), 185-186, doi:10.1017/S0032247400043746.

Tagliabue, A., L. Bopp and O. Aumont (2009), Evaluating the importance of atmospheric and sedimentary iron sources to Southern Ocean biogeochemistry, *Geophysical Research Letters*, 36, L13601, doi:10.1029/2009GL038914.

Tarboton, D. G. (1997), A new method for the determination of flow directions and upslope areas in grid digital elevation models, *Water Resources Research*, 33 (2), 309–319, doi:10.1029/96WR03137.

Theia Land Data Centre, SPOT 5 stereoscopic survey of Polar Ice, [Available to download at: https://theia.cnes.fr/rocket/#/search?collection=Spirit&view=default].

Thorarinsson, S. (2011), Glacier surges in Iceland, with special references to surges of Brúarjökull, *Canadian Journal of Earth Sciences*, 6 (4), 875-88, doi:10.1139/e69-089.

Tulaczyk, S., K. B. Kamb, and H. F. Engelhardt (2000), Basal mechanics of ice stream B, West Antarctica I. Till mechanics, *Journal of Geophysical Research*, 105, 463–481, doi:10.1029/1999JB90032.

Turney, C., C. Fogwill, T. D. Van Ommen, A. D. Moy, D. Etheridge, M. Rubino, and A. Rivera (2013), Late Pleistocene and early Holocene change in the Weddell Sea a new climate record from the Patriot Hills, Ellsworth Mountains, West Antarctica, *Journal of Quaternary Science*, 28 (7), 697–704, doi:10.1002/jqs.2668.

van den Broeke, M., and R. Bintanja (1995), The interaction of katabatic winds and the formation of blue-ice areas in East Antarctica, *Journal of Glaciology*, 41 (138), 395-407, doi:10.3198/1995JoG41-138-395-407.

Vaughan, D. G., G. J. Marshall, W. M. Connolley, C. Parkinson, R. Mulvaney, D. A. Hodgson, J. C. King, C. J., Pudsey, and J. Turner (2003), Recent rapid regional climate warming on the Antarctic Peninsula, *Climatic Change*, 60, 243-374, doi:10.1023/A:1026021217991.

Vaughan, D. G., A. Rivera, J. Woodward, H. F. J. Corr, J. Wendt, and R. Zamora (2007), Topographic and hydrological controls on Subglacial Lake Ellsworth, West Antarctica, *Geophysical Research Letters*, 34 (18), L18501, doi:10.1029/2007GL030769.

Waddington, E. D., T. A. Neumann, M. R. Koutnik, H.-P. Marshall, and D. L. Morse (2007), Inference of accumulation-rate patterns from deep radar layers in glaciers and ice sheets, *Journal of Glaciol*ogy, 53, 694–712, doi:10.3189/002214307784409351.

Wadley, M. R., T. D. Jickells, and K. J. Heywood (2014), The role of iron sources and transport for Southern Ocean productivity, *Deep-Sea Research Part 1: Oceonographic Research Papers*, 87, 82-94, doi: 10.1016/j/dsr.2014.02.003.

Watson, A. J., D. C. E. Bakker, A. J. Ridgwell, P. W. Boyd and C. S. Law (2000), Ocean CO_2 uptake and implications for glacial atmospheric CO_2, *Nature*, 407, 730-733, doi:10.1038/35037561.

Webers, G.F., C. Craddock, and J. F. Splettstoesser (1992), Geologic History of the Ellsworth Mountains, West Antarctica, *Geological Society of America Memoir*, 170, 1-8, doi:10.1130/MEM170-p1.

Weertman, J. (1961), Stability of ice-age ice sheets, *Journal of Geophysical Research*, 66 (11), 3783-3792, doi:10.1029/JZ066i011p03783.

Weertman, J. (1974), Stability of the junction of an ice sheet and ice shelf, *Journal of Glaciology*, 13, 3–11, doi:10.3198/1974JoG13-67-3-11.

Welch, B. C., and R.W. Jacobel (2005), Bedrock topography and wind erosion sites in East Antarctica: observations from the 2002 US-ITASE traverse, *Annals of Glaciology*, 41, 92–96, doi:10.3189/172756405781813258.

Wendt, A., G. Casassa, A. Rivera, and J. Wendt (2009), Reassessment of ice mass balance at Horseshoe Valley, Antarctica, *Antarctic Science*, 21, 505–513, doi:10.1017/S0954102009002053.

Westoby, M. J., J. Brasington, N. F. Glasser, M. J. Hambrey, and J. M. Reynolds (2012), 'Structure-from-Motion' photogrammetry: A low-cost, effective tool for geoscience applications', *Geomorphology*, 179, 300-314, doi:10.1016/j.geomorph.2012.08.021.

Westoby, M. J., S. A. Dunning, J. Woodward, A. S. Hein, S. M. Marrero, K. Winter, and D. E. Sugden (2015), Sedimentological characterization of Antarctic moraines using UAVs and Structure-from-Motion photogrammetry, *Journal of Glaciology*, 61 (230), 1088-1102, doi:10.3189/2015JoG15J086.

Westoby, M. J., S. A. Dunning, J. Woodward, A. S. Hein, S. M. Marrero, K. Winter, and D. E. Sugden (2016), Interannual surface evolution of an Antarctic blue-ice moraine using multi-temporal DEMs, *Earth Surface Dynamics*, 4, 515-529, doi:10.5194/esurf-4-515-2016.

Whillans, I. M., and W. A. Cassidy (1983), Catch a falling star: meteorites and old ice, *Science*, 222, 55–57, doi:10.1126/science.222.4619.55.

Whillans, I. M., and C. J. van der Veen (1993), The role of lateral drag in the dynamics of Ice Stream B, Antarctica, *Journal of Glaciology*, 43 (144), 231-237, doi:10.3198/1997JoG43-144-231-237.

Wingham, D. J., D. W. Wallis, and A. Shepherd (2009), Spatial and temporal evolution of Pine Island Glacier thinning, 1995-2006, *Geophysical Research Letters*, 36, L17501, doi:10.1029/2009GL039126.

Winsborrow, M. C. M., C. D. Clark, and C. R. Stokes (2010), What controls the location of ice streams?, *Earth-Science Reviews*, 103 (1-2), 45-59, doi:10.1016/j.earscirev.2010.07.003.

Winter, K., J. Woodward, N. Ross, S. A. Dunning, R. G. Bingham, H. F. J. Corr, and M. J. Siegert (2015), Airborne radar evidence for tributary flow switching in Institute Ice Stream, West Antarctica: Implications for ice sheet configuration and dynamics, *Journal of Geophysical Research: Earth Surface*, 120, 1611-1625, doi:10.1002/2015JF003518.

Winter, K. J. Woodward, S. A. Dunning, C. S. M. Turney, C. J. Fogwill, A. S. Hein, N. R. Golledge, R. G. Bingham, S. M. Marrero, D. E. Sugden, and N. Ross (2016), Assessing the continuity of the blue ice climate record at Patriot Hills, Horseshoe Valley, West Antarctica, *Geophysical Research Letters*, 43 (5), 2019-2026, doi:10.1002/2015GL066476.

Winther, J. -G., M. Jespersen, and G. Liston (2001), Blue-ice areas in Antarctica derived from NOAA AVHRR satellite data, *Journal of Glaciology*, 47 (157), 325-334, doi:10.3189/172756501781832386.

Wolovick, M. J., R. E. Bell, T. T. Creyts, and N. Frearson (2013), Identification and control of subglacial water networks under Dome A, Antarctica, *Journal of Geophysical Research: Earth Surface*, 118, 140–154, doi:10.1029/2012JF002555.

Woodward, J., T. Murray, R. A. Clarke, and G. W. Stuart (2003a), Glacier surge mechanisms inferred from ground-penetrating radar: Kongsvegen, Svalbard, *Journal of Glaciology*, 49 (167), 473-480, doi:10.3189/172756503781830458.

Woodward, J., P. J. Ashworth, J. L. Best, G. H. Sambrook Smith, and C. J. Simpson (2003b), The use and application of GPR in sandy fluvial environments: methodological considerations, In: C. S. Bristow, and H. M. Jol (ed.) *Ground Penetrating Radar in Sediments*, Geological Society Special Publication, 211, 127-142, Geological Society, London, doi:10.1144/GSL.SP.2001.211.01.11.

Woodward, J., and E. C. King (2009), Radar surveys of the Rutford Ice Stream onset zone, West Antarctica: indications of flow (in)stability?, *Annals of Glaciol*ogy, 50 (51), 57-62, doi:10.3189/172756409789097469.

Woodward, J., A. M. Smith, N. Ross, M. Thoma, H. F. J. Corr, E. C. King, M. A. King, K. Grosfeld, M. Tranter, and M. J. Siegert (2010), Location for direct access to subglacial Lake Ellsworth: An assessment of geophysical data and modeling, *Geophysical Research Letters*, 37 (11), L11501, doi:10.1029/2010GL042884.

Wright, A., and M. J. Siegert (2012), A fourth inventory of Antarctic subglacial lakes, *Antarctic Science*, 24 (6), 659-664, doi:10.1017/S095410201200048X.

Wright, A. P., and 10 others (2014), Sensitivity of the Weddell Sea sector ice streams to sub shelf melting and surface accumulation, *The Cryosphere*, 8, 2119–2134, doi:10.5194/tc-8-2119-2014.

Yu, J. (2011), Temporal variations of Antarctic blue ice extent: a possible mass balance indicator, *Polar Record*, 47 (243), 348-255, doi:10.1017/S0032247411000131.

Zwally, H. J., W. Abdalati, T. Herring, K. Larson, J. Saba, and K. Steffen (2002), Surface melt induced acceleration of Greenland ice-sheet flow, *Science*, 297, 218-222, doi:10.1126/science.1072708.

Zwinger, T., T. Malm, M. Schäfer, R. Stenberg, and J. C. Moore (2015), Numerical simulations and observations of the role of katabatic winds in the creation and maintenance of Scharffenbergbotnen blue ice area, Antarctica, *The Cryosphere*, 9, 1415-1426, doi:10.5194/tc-9-1415-2015.

Appendix 1

Published Papers by K. Winter Based on the Findings of this Thesis

Co-authors' involvement with publications pertaining to this project

Below are details of the role of each author in the research and publication of papers associated with this research. Articles are listed in chronological order.

Winter, K., J. Woodward, N. Ross, S. A. Dunning, R. G. Bingham, H. F. Corr, and M. J. Siegert (2015), Airborne radar evidence for tributary flow switching in Institute Ice Stream, West Antarctica: implications for ice sheet configuration and dynamics, *Journal of Geophysical Research: Earth Surface*, 120, 1-15, doi:10.1002/2015JF003518.

Winter, K.

- Designed the project
- Responsible for reviewing relevant literature
- Led data processing and interpretation
- Responsible for writing the manuscript and liaising with the journal editor

Woodward, J.

- Principal supervisor of research
- Helped to devise the concept behind the article
- Assisted with data interpretation, article structure and editing

Ross, N.

- Responsible for data collection
- Assisted with data processing and interpretation
- Assisted with article structure and editing

Dunning, S. A.

- Secondary supervisor of research
- Assisted with article structure and editing

Bingham, R. G.

- Responsible for data analysis in figure 8
- Assisted with article editing

Corr, H. F.

- Responsible for preliminary data processing
- Assisted with article editing

Siegert, M.J.

- Principal investigator for Institute and Möller Ice Stream radio-echo sounding project
- Assisted with article structure and editing

Westoby, M. J., S. A. Dunning, J. Woodward, A. S. Hein, S. M. Marrero, **K. Winter**, and D. E. Sugden (2015), Sedimentological characterization of Antarctic moraines using UAVs and Structure-from-Motion photogrammetry, *Journal of Glaciology*, 61 (230), 1088-1102, doi: 10.3189/2015JoG15J086.

Westoby, M. J.

- Designed the project
- Responsible for reviewing relevant literature
- Led data processing and interpretation
- Responsible for writing the manuscript and liaising with the journal editor

Dunning, S. A.

- Responsible for data collection in the first field season
- Assisted with data processing and interpretation
- Assisted with article structure and editing

Woodward, J.

- Responsible for data collection in the second field season
- Aided data interpretation
- Assisted with article structure and editing

Hein, A. S.

- Provided field assistance
- Assisted with article editing

Marrero, S. M.

- Provided field assistance
- Assisted with article editing

Winter, K.

- Helped to collect terrestrial laser scanning data in the second field season
- Assisted with article editing

Sugden, D. E.

- Provided field assistance
- Provided discussions that were helpful to initial data interpretation
- Assisted with article structure and editing

Hein, A. S., Woodward, J., S. M. Marrero, S. A. Dunning, E. J. Steig, S. P. H. T. Freeman, F. M. Stuart, **K. Winter**, M. J. Westoby, and D. E. Sugden, (2016), Evidence for the stability of the West Antarctic Ice Sheet divide for 1.4 million years, *Nature Communications*, 7:10325 doi:10.1038/ncomms10325.

Hein, A. S.

- Designed the project
- Responsible for reviewing relevant literature and identifying the research gap
- Led data collection and analysis
- Responsible for writing the manuscript and liaising with the journal editor

Woodward, J.

- Helped to devise the concept behind the article
- Provided field assistance
- Assisted with article structure and editing

Marrero, S. M.

- Supported data collection in the field
- Assisted with data processing and interpretation
- Provided assistance with article structure and editing

Dunning, S. A.

- Provided field assistance
- Provided discussions that were helpful to data interpretation
- Assisted with article structure and editing

Steig, E. J.

- Created ice-sheet model (Figure 5a)
- Assisted with article structure and editing

Freeman, S. P. H. T.

- Assisted with cosmogenic nuclide analysis
- Provided discussions that were helpful to data interpretation

Stuart, F. M.

- Contributed to the analysis of ice-sheet model results
- Provided discussions that were helpful to data interpretation

Winter, K.

- Created location map (Figure 1)
- Processed and analysed radio-echo sounding profile to create Figure 2
- Produced Figure 5b
- Assisted with article editing

Westoby, M. J.

- Provided discussions that were helpful to data interpretation
- Assisted with article editing

Sugden, D. E.

- Helped to devise the concept behind the article
- Produced initial draft of manuscript figures
- Assisted with article structure and editing

Winter, K. J. Woodward, S. A. Dunning, C. S. M. Turney, C. J. Fogwill, A. S. Hein, N. R. Golledge, R. G. Bingham, S. M. Marrero, D. E. Sugden, and N. Ross (2016), Assessing the continuity of the blue ice climate record at Patriot Hills, Horseshoe Valley, West Antarctica, *Geophysical Research Letters*, 43 (5), 2019-2026, doi:10.1002/2015GL066476.

Winter, K.

- Responsible for reviewing relevant literature and identifying the research gap
- Led snowmobile-towed GPR data collection
- Led data processing and interpretation
- Responsible for writing the manuscript and liaising with the journal editor

Woodward, J.

- Principal Supervisor of research
- Led Blue Ice GPR data collection
- Aided snowmobile-towed GPR data collection
- Assisted with data processing and interpretation
- Provided assistance with article structure and editing

Dunning, S. A.

- Secondary supervisor of research
- Aided Blue Ice GPR data collection
- Assisted with article structure and editing

Turney, C.

- Principal Investigator of Patriot Hills Blue Ice Area Climate Record
- Jointly responsible for deuterium isotope concentration graph (Figure 2d)
- Assisted with article structure and editing

Fogwill, C.

- Jointly responsible for deuterium isotope concentration graph (Figure 2d)
- Assisted with article structure and editing

Hein, A. S.

- Provided field assistance
- Assisted with article editing

Golledge, N.

- Created the Parallel Ice Sheet Model (Figure 4)
- Assisted with text related to the Parallel Ice Sheet Model

Bingham, R. G.

- Created the Internal Layer Continuity Index plot (Figure 5)

Marrero, S.

- Provided field assistance
- Assisted with article editing

Sugden, D. E.

- Provided field assistance
- Provided discussions that were helpful to data interpretation
- Assisted with article structure and editing

Ross, N.

- Tertiary supervisor of research
- Assisted with article structure and editing

Westoby, M. J., S. A. Dunning, J. Woodward, A. S. Hein, S. M. Marrero, **K. Winter**, and D. E. Sugden (2016), Interannual surface evolution of an Antarctic blue-ice moraine using multi-temporal DEMs, *Earth Surface Dynamics*, 4, 515-529, doi:10.5194/esurf-4-515-2016.

Westoby, M. J.

- Designed the project
- Responsible for reviewing relevant literature
- Led data processing and interpretation
- Responsible for writing the manuscript and liaising with the journal editor

Dunning, S. A.

- Responsible for data collection in the first field season
- Assisted with data processing and interpretation
- Assisted with article structure and editing

Woodward, J.

- Responsible for data collection in the second field season
- Provided discussions that were helpful to data interpretation
- Assisted with article structure and editing

Hein, A. S.

- Provided field assistance
- Assisted with article editing

Marrero, S. M.

- Provided field assistance
- Assisted with article editing

Winter, K.

- Assisted with terrestrial laser scanning data collection in the second field season
- Provided assistance with article editing

Sugden, D. E.

- Provided discussions that were helpful to initial data interpretation
- Assisted with article structure and editing

Hein, A. S., S. M. Marrero, J. Woodward, S. A. Dunning, **K. Winter**, M. J. Westoby, S. P. H. T. Freeman, and D. E. Sugden (2016), Mid-Holocene pulse of thinning in the Weddell Sea sector of the West Antarctic Ice Sheet, *Nature Communications*, 7, 12511, doi:10.1038/ncomms12511.

Hein, A. S.

- Designed the project
- Responsible for reviewing relevant literature and identifying the research gap
- Led data collection and analysis
- Responsible for the writing the manuscript and liaising with the journal editor

Marrero, S. M.

- Helped to design the project
- Supported data collection in the field
- Assisted with data processing and interpretation
- Assisted with article structure and editing

Woodward, J.

- Helped to devise the concept behind the article
- Provided field assistance
- Assisted with article structure and editing

Dunning, S. A.

- Provided field assistance
- Provided discussions that were helpful to data interpretation
- Assisted with article structure and editing

Winter, K.

- Created location map (Figure 1)
- Collected DGPS measurements (mapped and graphed in Figure 2c)
- Assisted with article editing

Westoby, M. J.

- Provided discussions that were helpful to data interpretation
- Assisted with article editing

Freeman, S. P. H. T.

- Assisted with cosmogenic nuclide analysis
- Provided discussions that were helpful to data interpretation

Sugden, D. E.

- Helped to devise the concept behind the article
- Assisted with article structure and editing